Geometry, Topology, and Dynamics of Many-Body Systems: Quantum and Classical Perspectives

(Article begins on next page)

28 December 2024

UNIVERSITÀ DI SIENA 1240

Aix∗Marseille
université
Socialement engagée

Dipartimento di Scienze fisiche, della Terra e dell'ambiente

Doctoral thesis in physics

XXXVI° Ciclo

Coordinatore: Prof. Riccardo Paoletti

Geometry, Topology, and Dynamics of Many-Body Systems:

Quantum and Classical Perspectives

Settore scientifico disciplinare: FIS/02

Candidate
Arthur Vesperini
Università di Siena
Aix Marseille Univ

Supervisor
Roberto Franzosi
University of Siena

Co-supervisor
Marco Pettini
University of Aix-Marseille

Academic year
2020/2023

Affidavit

I, undersigned, Arthur Vesperini, hereby declare that the work presented in this manuscript is my own work, carried out under the scientific supervision of Roberto Franzosi and Marco Pettini, in accordance with the principles of honesty, integrity and responsibility inherent to the research mission. The research work and the writing of this manuscript have been carried out in compliance with both the french national charter for Research Integrity and the Aix-Marseille University charter on the fight against plagiarism.

This work has not been submitted previously either in this country or in another country in the same or in a similar version to any other examination body.

Marseille, 15/10/2023

List of publications and participation to conferences

List of publications submitted during doctorate studies

1. A. Vesperini, R. Franzosi, S. Ruffo, A. Trombettoni, and X. Leoncini, "Fast collective oscillations and clustering phenomena in an antiferromagnetic mean-field model," *Chaos, Solitons & Fractals*, vol. 153, p. 111 487, Dec. 2021, ISSN: 0960-0779. DOI: 10.1016/j.chaos.2021.111487

2. A. Vesperini, G. Bel-Hadj-Aissa, and R. Franzosi, "Entanglement and quantum correlation measures for quantum multipartite mixed states," *Scientific Reports*, vol. 13, no. 1, p. 2852, Feb. 2023. DOI: 10.1038/s41598-023-29438-7

3. A. Vesperini and R. Franzosi, *Entanglement, quantum correlators and connectivity in graph states*, arXiv:2308.07690 [quant-ph], Aug. 2023. DOI: 10.48550/arXiv.2308.07690

4. A. Vesperini, "Correlations and projective measurements in maximally entangled multipartite states," *Annals of Physics*, p. 169 406, 2023, ISSN: 0003-4916. DOI: https://doi.org/10.1016/j.aop.2023.169406

5. A. Vesperini, G. Bel-Hadj-Aissa, L. Capra, and R. Franzosi, *Unveiling the geometric meaning of quantum entanglement*, arXiv:2307.16835 [quant-ph], Jul. 2023. DOI: 10.48550/arXiv.2307.16835

Participation aux conférences et écoles d'été au cours de la période de thèse:

1. December 2021, Winter School - *Analytical Methods in Quantum and Continuum Mechanics*, Politecnico di Torino, Italy.

2. February 2022 - *Winter PhD school on statistical field theories*, Galileo Galilei Institute for Theoretical Physics, Arcetri, Firenze

3. May- June 2023, Workshop *chats2023 : Trends in Hamiltonian systems, chaos and its applications*, Luminy, Marseille (France)

Abstract

In the present thesis, we study various instances of many-body systems, both quantum and classical, adopting an overall geometrical and topological perspective. Systems with many degrees of freedom can exhibit a great variety of emergent phenomena, from metastability to dynamical or thermodynamic phase transitions, and their intricate properties often elude our full understanding. Through careful inspection of the underlying geometrical structures behind these complex objects, and using diverse mathematical tools, some of which are borrowed from the field of Riemannian geometry and topology, we try to characterize their most prominent aspects.

The first part of this thesis focuses on the field of quantum information, exploring in particular the notions of entanglement and correlations in discrete quantum systems, first in pure and then in mixed states. We propose a novel measure of entanglement for pure quantum states, the entanglement distance, and discuss and test it using various examples. We then study maximally entangled pure states, revealing in part their internal structures, using the intuitive notion of correlations and projective measurements. Doing so, we are able to show simple relations between pre-measurement correlations and post-measurement expectation values and provide an upper bound to the persistency of entanglement of such states. We further demonstrate how the connectivity properties of a paradigmatic model for quantum computing, the celebrated graph state, can be probed through the proper use of quantum correlators. Our study is then extended to the framework of mixed quantum states. We infer from the pure state entanglement distance, the induced measures of quantum correlations, on the one hand, and of mixed state entanglement, on the other hand. We emphasize the strengths and limitations of the latter, in particular the heavy optimization procedure it implies, for which we propose a workaround. Finally, we investigate the superradiant transition present in the Tavis–Cummings model and reveal that it is accompanied by a jump in the quantum correlation and entanglement between the atoms.

In the second part of our work, we tackle two classical models, both possessing ergodicity-breaking and strongly non-linear behaviours. We first present a comprehensive numerical and analytical investigation of a toy model, which is a prototypical example of a long-range interacting, strongly non-additive model: the Hamiltonian Mean Field (HMF). At low energy in the microcanonical ensemble, a metastable state may arise, coined as a bicluster. By inspecting the dynamics of a macroscopic quantity, the magnetization, and by observing the occurrence of two distinct timescales in the system, we provide a quite intuitive and self-consistent

scenario accounting for the great stability of biclusters, which sustain themselves for extensive amounts of time. Finally, we present the results of an extensive numerical study, applying the topological theory of phase transition to a model of glass-forming material. Such systems are notoriously difficult to simulate and equilibrate, because of the very slow dynamics, characteristic of the glass phase, yielding a tendency to remain stuck in small regions of phase space. Within a microcanonical framework, a Monte Carlo algorithm was developed, for which various numerical methods were implemented, such as parallel tempering and particle swapping. Our results, though preliminary, are encouraging: the heat capacity is found to exhibit clear peaks for two values of the energy, indicating a two-step second order transition, in correspondence with topological changes of the equipotential level sets on which the system is confined. We conclude by a thorough discussion of our findings, and by a proposition of a promising follow-up research, that would top off the bridge between our diverse finding: namely, applying the topological theory to quantum phase transitions, possibly drawing a further link with the creation of entanglement in these processes.

Aknowledgements

I want to thank Marco Pettini and Roberto Franzosi, who supervised my work; the former encouraged me since my graduate studies, and the latter promptly granted his trust.

I thank my parents, who raised me to be curious and to believe in myself; they always supported me, whatever choices I made.

I thank all of my undergrad teachers from Sciences et Humanités; their patience and dedication allowed me and many others to discover and glance at so many corners of knowledge. I am grateful to all of them, but I have to mention Marie, Jean-Yves, Olivier, Gaetan, Simona and Anne-Marie, who introduced me to, and nourished my enthusiasm towards mathematics and physics, and convinced me of my abilities; nothing would have been possible without them.

I thank Matteo, Ghofrane and Valentin for the inspired discussions and for their help; I thank also to Salvatore, whose reassuring voice helped me stay on track.

Finally, I thank all my friends, my dear cousins and the many people who supported and accompanied me in both the nice and difficult times.

Contents

Contents

Introduction

The study of many-body systems, as it ultimately tackles our daily experience of reality, constitutes one of the most important aspects of modern physics. Statistical physics and complex systems draw the link between our ever-increasing knowledge of fundamental physics and the observation of *emergent behaviour*, ubiquitous in nature. Indeed, from the intricate interplay and interactions among the many constituents of physical systems emerge phenomena that do not find any counterpart in individual dynamics, such as self-organization, pattern formation, synchronization and phase transitions.

Evidently, owing to the computational inaccessibility of their microscopic dynamics, the study of many-body systems requires the use of elaborate mathematical tools. Within this framework, and despite its numerous limitations, the conventional methodology of statistical physics, which is devoted to the study of systems at thermodynamic equilibrium, holds a position of utmost significance. One of its prominent features, of great interest to us, is the *state space representation* of the evolution of a system; it considers the state of the system as a point in a $6N$-dimensional space, rather than a collection of $2N$ vectors describing the position and momenta of the N individual particles that it contains. This elegant viewpoint allows, in particular, the interpretation of constraints such as conservation of macroscopic quantities as a loss of dimensionality of the accessible state space. For instance, Hamiltonian systems, in which energy is conserved, evolve on $6N - 1$-dimensional hypersurfaces embedded in the global $6N$-dimensional state space.

It has been shown in pioneer works [1] that the geometric properties of these accessible hypersurfaces, envisioned as Riemannian manifolds, can account for many phenomena such as Hamiltonian chaos, phase transitions, and metastability.

In this thesis, we thus adopt an overall geometrical and topological perspective to explore the structure of state space in both quantum and classical systems.

The Part I of this thesis focuses on the field of quantum information, and specifically on the characterization of entanglement and quantum correlations, leaning on the equivalence between classes of states, that can be encoded in the construction of *projective spaces*.

Quantum entanglement is one of the most prominent nonclassical properties that a quantum system can exhibit. While relatively well understood in the simple case of bipartite pure states, its characterization in the general case of mixed, multipartite states remains an open problem. Deciding whether a multipartite

Contents

state is separable, exploring its network-like correlation structure, or asserting its k-separability are very difficult tasks that are of critical importance in the development of quantum technologies. We develop a novel measure of entanglement in pure quantum states using the metric of a projective Hilbert space. Remarking that quantum states can be seen as statistical distributions, we attempt to deepen our understanding of entanglement structures by applying the intuitive notion of correlations and projective measurements to maximally entangled states. In this spirit, we demonstrate how the connectivity properties of a paradigmatic model for quantum computing, the celebrated graph state, can be probed through the proper use of quantum correlators. We then infer from the entanglement distance a measure of quantum correlations, and a measure of mixed state entanglement. We emphasize the strengths and limitations of the latter, in particular the heavy optimization procedure on which it relies, and for which we propose a workaround. Finally, we investigate the superradiant transition present in the Tavis–Cummings model and reveal that it is accompanied by a jump in the quantum correlation and entanglement between the atoms.

In Part II, we tackle with classical systems, employing a dynamical perspective by considering the properties of the Hamiltonian flow and of the space on which it evolves. More specifically, claiming that all of the information is contained in the potential function, we study its behaviour and the landscape it shapes, depending on the constraints and parameters of the model. The two classical models we studied both present ergodicity-breaking, strongly non-linear behaviours. We first present a comprehensive numerical and analytical investigation of a toy model, which is a prototypical example of a long-range interacting, strongly non-additive model: the Hamiltonian Mean Field (HMF). At low energy in the microcanonical ensemble, a metastable state may arise, coined as a bicluster. By inspecting the dynamics of a macroscopic quantity, the magnetization, and by observing the occurrence of two distinct timescales in the system, we provide a quite intuitive and self-consistent scenario accounting for the great stability of biclusters, which sustain themselves for extensive amounts of time. In a second chapter, we present the results of an extensive numerical study, with the aim of applying the topological theory of phase transition to a model of glass-forming material. Such systems are notoriously difficult to simulate and equilibrate, because of the very slow dynamics of the glassy phase and their tendency to remain stuck in small regions of phase space. Within a microcanonical framework, a Monte Carlo algorithm was developed, for which various numerical methods were implemented, such as parallel tempering and particle swapping algorithms. Our results, though preliminary, are encouraging: the heat capacity is found to exhibit clear peaks for two values of energy, in correspondence with topological changes of the equipotential level sets on which the system is confined.

Through the combination of our work on quantum states and their statistical

Contents

properties and that on the topological theory of phase transitions, we aim to provide tools that allow the study of quantum phase transitions from this double perspective. As we exemplify in the case of the Tavis-Cummings model, quantum phase transitions may be accompanied by a jump of entanglement, which can thus be considered an order parameter in this context. Further study of the topological properties of the accessible state space of the associated quantum dynamics might improve our understanding of these phenomena and open new research perspectives.

Part I.

Quantum correlations and entanglement

Introduction of part I

The concept of entanglement emerged in the first half of the 20th century from the seminal article of A. Einstein, B. Podolsky, and N. Rosen (EPR), who first pointed out the existence of this seemingly paradoxical type of correlation naturally arises from quantum theory [2], soon follow by E. Schrödinger [3, 4].

Today widely considered as an essential aspect of the quantum realm, it was at the time deemed by many to be a paradox, because it implies instantaneous action at a distance, thus breaking the causal principle. Baptized *EPR paradox* in reference to the latter authors, it was thought by them to be an indication of the incompleteness of the theory; EPR postulated that a more fundamental theory, yet to be discovered, should be at the root of the quantum formalism, namely, a *hidden variable theory.* In other words, the indetermination of the properties of quantum objects would be a mere consequence of our ignorance of deeper deterministic phenomena [5].

Later on, J. Bell formulated a set of inequalities that should be fulfilled by any local realistic hidden variable theory [6], and further showed that they theoretically can be violated in a quantum mechanical framework.

Finally, A. Aspect proposed [7] and performed [8] a series of experiments, definitively proving the Bell's inequalities were indeed violated by some quantum systems.

It is worth noting that causality is nevertheless preserved, as no information can be sent instantaneously using entanglement alone, due to the *no-communication theorem* [9].

Entanglement and quantum correlations play an essential role in quantum information theory and in the development of the quantum technologies. It stems as the key resource at the foundation of the promising fields of quantum cryptography, quantum computation, quantum teleportation, quantum batteries and quantum metrology [10, 11, 12]. To fully exploit the quantum advantages of the involved systems, a full and detailed quantification of entanglement is required [13].

However, despite its importance, entanglement remains an elusive and challenging concept, and the problem of its quantification in the most general case is still open [14, 15].

Over the past few decades, several approaches and an extensive literature have been developed address the problem of measuring and characterizing entanglement for the wide variety of quantum states . However, the rigorous achievements in the explicit quantification of entanglement are mostly limited to the case of bipartite systems [13], and a computationally affordable measure valid in the most general

case is still lacking, up to our best knowledge.

Entropy of entanglement is widely accepted as the paradigmatic measure of entanglement for pure states of bipartite systems [16, 17], while entanglement of formation [18], entanglement distillation [19, 20, 21] and relative entropy of entanglement [22] are widely acknowledged as faithful measures for bipartite mixed systems [23].

A vast body of literature is further devoted to the study of entanglement in multipartite systems. Over time, different approaches have been proposed including, e.g. in the case of pure states, the study of the equivalence classes in the set of multipartite entangled states [24, 25], whereas, the study of entanglement in mixed multipartite states have been addressed, e.g., with a Schmidt measure [26] or with a generalization of the Concurrence [27, 28].

In the last years, have been proposed entanglement estimation-oriented approaches and derived from a statistical distance [29] concept, as, for instance, the quantum Fisher information [30, 31, 32, 33].

In this first Part, we will address a number of these issues, resorting to a abstract geometric framework and to somewhat more intuitive notions such as correlators and expectation values, while drawing links between these mathematical concepts. We start in Chapter 1 by introducing the general framework of multi-qubit quantum states, recalling the concepts of pure and mixed quantum states, and the various formulations that can be employed to describe them; we further discuss and recall the definition of *quantum entanglement* and *quantum correlations*, and the requirements that should be met by a measure of these properties. In Chapter 2, we focus on the characterization of entanglement in pure states of many qubits, introducing the *Entanglement Distance*, a novel entanglement measure, and by further exploring correlations patterns and their implications in maximally entangled cases. In Chapter 3, we expand our analysis to mixed states, adapting the entanglement distance to define both a measure of quantum correlations, the *Quantum Correlation Distance*, and an extension of the *Entanglement Distance* to entanglement for mixed states. Chapter 4 is devoted to the study, through the computation of correlators, of the connectivity properties of *Graph States*, a particular instance of quantum states useful to quantum computation. Finally, in Chapter 5, we study the superradiant phase transition exhibited by the Tavis-Cummings model, applying the Quantum Correlation Distance and entanglement criteria to show that it is accompanied by a Quantum Correlation transition, and that entanglement is most likely extensive at the critical crossing point.

Chapters 2 and 3 mainly depict the work we published in [34, 35, 36], while Chapter 4 refers to [37] and Chapter 5 to [38].

1. Preliminary statements

Notoriously, Pierre-Simon de Laplace, one of the founding fathers of probability theory, believed in absolute determinism. In the introduction of his book on probability theory [39], he thus wrote:

> *"La probabilité est relative en partie à [notre] ignorance, en partie à nos connaissances."[1]*

That is, randomness is to be understood as the mere result of our lack of knowledge of some links in a causal chain, i.e. of the exact initial conditions of the considered system.

Quantum theory, at least in its standard interpretation, contradicts this point of view. The EPR paradox [2], mentioned in Section I, is in fact representative of this contradiction: during the dawn of quantum mechanics, many scientists, amongst which EPR, were very strong advocates of Laplace's deterministic worldview, hence the century-old dispute about the essence of quantum indetermination.

In the following, we call *classical* the probabilities and indetermination due to the incompleteness of the available information, that is Laplace's definition of probability; conversely, we call *quantum* the probabilities that are quantum in nature and, according to the standard interpretation of quantum mechanics, due to an essential indetermination.

The most general quantum systems contain, of course, both.

Yet, our understanding of the quantum realm can benefit greatly from the study of *pure* quantum states, that is, states that contain only quantum indetermination; as unrealistic as it may be, this a theoretical framework sometimes allows to isolate, to some extent, the "truly" quantum phenomena at stake.

In contrast with pure states, mixed states, other than quantum indetermination, hold *classical* uncertainty, and stem as the formal expression of our incomplete knowledge of the state of the system.

1.1. Two-level quantum systems: generalities and notations

Throughout this thesis, we focus on two-level quantum systems, called qubits in the language of quantum information theory.

---

[1]*"Probability is relative in part to our ignorance, in part to our knowledge."*

1. Preliminary statements

Qubits, being the simplest possible quantum systems, constitute the preferred basic unit in the field of quantum information. Owing to their binary nature, they are simpler to understand and manipulate than higher dimensional systems, and further allow ease of comparison of computing powers of quantum computers and classical computers.

The most obvious examples of qubits are spin-$\frac{1}{2}$ particles and photon polarization states; they can, however, be experimentally implemented using a great variety of physical supports, e.g. superconducting qubits, such as Cooper boxes or Transmon qubits [40, 41, 42, 43, 44, 45]. Note, however, that the latter, like most qubit realizations intended as building blocks of quantum computers, constitute in fact many-level systems, for which the energy gap between the first and second excited state is large enough to approximate them as two-level systems.

Formally, a qubit μ is described in a 2-dimensional complex Hilbert space that we denote $\mathcal{H}^\mu$, spanned by the basis state vectors $|0\rangle$, $|1\rangle$.

The set of all observables acting on $\mathcal{H}^\mu$ is spanned by σ_k^μ, with $k = x, y, z$ the Pauli matrices acting on qubit μ. We denote $\boldsymbol{\sigma}^\mu = \left(\sigma_x^\mu, \sigma_y^\mu, \sigma_z^\mu\right)$ the Pauli vector acting on μ, and $\sigma_{\boldsymbol{v}}^\mu = \boldsymbol{v}^\mu \cdot \boldsymbol{\sigma}^\mu = \sum_{k=x,y,z} v_k^\mu \sigma_k^\mu$ the Pauli observable acting on μ oriented in the direction $\boldsymbol{v}^\mu$. We call Pauli observable any operator that can be written as a tensor product of Pauli matrices, i.e. tensor products of 2×2 traceless hermitian matrices.

Given set Q of M qubits, and any operator, vector or subspace A^μ, we will hereafter abbreviate $\bigotimes_{\nu \in Q} A^\nu = A^Q$. Identity operators $\mathbb{I}^\mu$ will be implicit from now on.

The order in which tensor products are shown is irrelevant: we simply keep track of the subsystems operators apply on, by using our superscript notation. If the algebra is to be made explicit, one can simply choose a conventional ordering of the subsystems, and then reorder every tensor products using these superscripts.

We occasionally drop the superscript μ when we clearly refer to single-qubit systems.

In the following, all of the vectors denoted by a lower-case bold letter belong to $\mathbb{R}^3$, and are in general distinct from each other, if their indices do not match.

The state of any single qubit μ is fully described by a 2×2 density matrix, conventionally denoted ρ, which is simply an operator acting on $\mathcal{H}^\mu$. This corresponds to a set of two complex numbers, hence four real numbers, along with the constraint coming from the hermiticity of ρ: a qubit can therefore be represented in a 3-dimensional space.

A pure state can also be expressed as a unit vector $|s\rangle$ such that $\rho = |s\rangle \langle s|$.

More precisely, a generic single-qubit density matrix writes

$$\rho = \frac{1}{2} \begin{pmatrix} 1 + n_z & n_x - in_y \\ n_x + in_y & 1 - n_z \end{pmatrix} = \frac{1}{2} \left(\mathbb{I} + \boldsymbol{n} \cdot \boldsymbol{\sigma} \right), \tag{1.1}$$

where $|\boldsymbol{n}| \leq 1$, owing to the fact that physically meaningful density matrices are positive semi-definite, since their eigenvalues can be interpreted as probability weights.

This yields a considerable advantage in visualization, as the state of a single qubit is therefore uniquely determined by $\boldsymbol{n}$, and can hence be represented as a point in the unit ball, called in this context the Bloch ball.

$|\boldsymbol{n}| = 1$, i.e. the state belongs to the Bloch sphere, if and only if the considered qubit is in a pure state. The outcome of a measurement along the $\boldsymbol{n}$ direction (and only along this direction) is then 1 with certainty.

Pure quantum states are indeed, by definition, states of which we have complete knowledge. Their indetermination, i.e. the uncertainty of some measurement outcomes, thus solely arises from their quantum nature.

The purity of a state is defined as

$$P(\rho) = \mathrm{Tr}\left[\rho^2\right] = \sum_k p_k^2, \tag{1.2}$$

where $\{p_k\}_k$ is the set of eigenvalues of ρ. It accounts for the degree of mixedness, as its value ranges from 1, in the case of a pure state, to $1/2^M$ in the case of the maximally mixed state $\mathbb{I}/2^M$.

The von Neumann entropy [46, 47]

$$S(\rho) = -\mathrm{Tr}\left[\rho \log\left(\rho\right)\right] = -\sum_k p_k \log\left(p_k\right), \tag{1.3}$$

can also be interpreted as another measure of mixedness, as can be seen by the similarity of Eqs. (1.2) and (1.3). In fact, the *linear entropy*, derived considering the first term of the Mercator series, can be expressed as a function of the purity

$$S_L(\rho) = -\mathrm{Tr}\left[\rho\left(\rho - 1\right)\right] = 1 - P(\rho). \tag{1.4}$$

Remark. *Pure quantum states are nothing but a theoretical idealization, as it is impossible to perfectly reconstruct such states from experimental data, using quantum state tomography. This is due to the fact that, if a state lies on the Bloch sphere, there exists a measurement axis for which the outcome is $+1$ with probability 1, and -1 with probability 0; yet, it is in principle impossible to determine that a given outcome is certain (or impossible) given a finite statistical sample.*

In other words, experimentalists should never be able to determine that a quantum state is pure, because frequency equates probability only if the statistical sample is

infinite.

The most general situation can be described as follows: a quantum apparatus generates quantum states $|k\rangle$, with some associated probability weights p_k, accounting for the imperfect knowledge we have of the underlying process. The whole statistics is then described by a mixed state, formally expressed through a density matrix ρ, including both quantum and classical uncertainties. It consists of a linear combination of the form

$$\rho = \sum_k p_k |k\rangle \langle k|, \tag{1.5}$$

where the $|k\rangle$ are normalized quantum pure state, and the p_k are probability weights, such that $\forall k$, $0 \leq p_k \leq 1$ and $\sum_k p_k = 1$.

Hereafter, we call such sets of couples $\{p_k, |k\rangle\}_k$ *realizations* or *decompositions* of ρ. Interestingly, the realization of a given ρ is not unique, and there actually exist an infinite number of such ways to produce a given ρ. In other words, there exists an infinite number of distinct apparatuses generating a given statistics.

As a prototypical example of this ambiguity, consider an even-weighted mixture of the two Bell states $|\psi_\pm\rangle = \frac{1}{\sqrt{2}} (|00\rangle \pm |11\rangle)$; it is easy to verify that

$$\frac{1}{2} (|\psi_+\rangle \langle \psi_+| + |\psi_-\rangle \langle \psi_-|) = \frac{1}{2} (|00\rangle \langle 00| + |11\rangle \langle 11|). \tag{1.6}$$

This emphasizes how a quantum apparatus that produces, with some classical uncertainty, an entangled state or another, may yet yield statistics equivalent to that of an apparatus that produces product states. It results that the entanglement of a mixed state cannot be simply defined as the sum of the entanglement of the pure states composing it.

While this ambiguity may seem rather counter-intuitive, it is in fact a reminder that quantum theory is, over all, a theory of measurements, and that density matrices ρ are in fact the quantum equivalent of statistical distributions, not describing reality as it is, but rather as we experiment it; from this point of view, it appears on the contrary quite natural to identify as completely equivalent, states that yields the exact same statistical properties.

One could naively argue that since, in reality, there exists only pure states, in some sense mixed states should not be essential to quantum theory, and that the statistical ambiguity they highlight emphasizes its incompleteness. Yet, on the contrary, the concept of mixed states is an essential ingredient of the quantum formalism, as they encompass, with the maximal attainable precision, the reality accessible to experiments.

Indeed, whereas in a classical world, the "true state" of the system (i.e. the pure state it is actually in) can always be distinguished by performing appropriate measurements, this does not hold in the quantum world: as measurements processes generally modify the state and henceforth destroy part of the information, and

no single measurement can allow to retrieve a complete information on quantum states, the "true state" cannot be known entirely.

The only available method to study quantum states is to perform the experiment many times, performing series of measurements on many instances of ρ. The statistical analysis of the outcomes is called quantum tomography, and allows to retrieve ρ within a given precision [48, 49, 50, 51].

This fact participate to the great difficulties encountered in experiments and applications involving entangled states: the mixture, practically almost unavoidable, tends to diminish or even erase the incidence of quantumness on measurements (that can for instance take the form of a violation of Bell's inequalities or quantum speedup for tasks).

It is sometimes useful to write general mixed states of M qubits in terms of Pauli matrices (see e.g. [52] or appendix A of [45])

$$\rho = \frac{1}{2^M} \left(\mathbb{I} + \sum_\mu \sum_{i=1,2,3} n_i^\mu \sigma_i^\mu + \sum_{\mu,\nu} \sum_{i,j=1,2,3} t_{ij}^{\mu\nu} \sigma_i^\mu \sigma_j^\nu + \sum_{\mu,\nu} \sum_{i,j,k=1,2,3} t_{ijk}^{\mu\nu\eta} \sigma_i^\mu \sigma_j^\nu \sigma_k^\eta + \cdots \right). \tag{1.7}$$

Notice that the tensors $\boldsymbol{n}^\mu$, $\boldsymbol{t}^{\mu\nu}$, $\boldsymbol{t}^{\mu\nu\eta}$ simply correspond to the expectation values of spin observable combinations, i.e.

$$\begin{aligned} n_i^\mu &= \langle \sigma_i^\mu \rangle_\rho = \mathrm{Tr}\left[\rho \sigma_i^\mu\right] \\ t_{ij}^{\mu\nu} &= \left\langle \sigma_i^\mu \sigma_j^\nu \right\rangle_\rho = \mathrm{Tr}\left[\rho \sigma_i^\mu \sigma_j^\nu\right] \\ t_{ijk}^{\mu\nu\eta} &= \left\langle \sigma_i^\mu \sigma_j^\nu \sigma_k^\eta \right\rangle_\rho = \mathrm{Tr}\left[\rho \sigma_i^\mu \sigma_j^\nu \sigma_k^\eta\right] \\ &\cdots, \end{aligned} \tag{1.8}$$

hence obey the constraint $|\boldsymbol{n}^\mu|, |\boldsymbol{t}^{\mu\nu}|, |\boldsymbol{t}^{\mu\nu\eta}|, \cdots \leq 1$. This particular formulation of density matrices highlights the fact that they stem as quantum statistical distributions, that can be written as the mere sum of their moments. Furthermore, it evidentiates how all operations that can be performed on ρ can be reduced to operations on Pauli matrices; recalling that the Pauli matrices are traceless, and that $\forall i, j = x, y, z$, and $\forall \mu, \nu \in Q$, we have $\sigma_i^\mu \sigma_j^\nu = \delta_{ij}\delta_{\mu\nu}$, this formulation greatly simplifies some computations.

In Appendix A, we provide an example depicting how, using formulation (1.7) to analyse the statistics of a (simple) mixed state, equivalent realizations such as (1.6) can be retrieved.

1.2. **Entanglement and quantum correlations**

1.2.1. **Definitions**

Definition 1. A pure state $|\psi\rangle$ is said to be separable in μ if and only if it can be expressed as a tensor product

$$|\psi\rangle = |\psi^\mu\rangle \otimes |\psi^{\mu^c}\rangle, \tag{1.9}$$

where μ^c is the complement of μ on the set Q of all qubits in the system. We can also say that μ is disentangled from μ^c. Conversely, a state which can't be written in the form (1.9) is said to be entangled in μ.

The reduced density matrix describing the state of a qubit μ is found by discarding the rest of the system, namely

$$\rho^\mu = \mathrm{Tr}_{\mu^c}\left[|\psi\rangle\langle\psi|\right] = \frac{1}{2}\left(\mathbb{I}^\mu + \boldsymbol{n}^\mu \cdot \boldsymbol{\sigma}^\mu\right), \tag{1.10}$$

where $\mathrm{Tr}_{\mu^c}[\cdot]$ is the partial trace over μ^c.

It is clear that, if Eq. (1.9) holds, we have $\rho^\mu = |\psi^\mu\rangle\langle\psi^\mu|$: the reduced state of a disentangled qubit is pure.

This also means that no information on μ is lost by discarding the rest of the system, i.e. $S(\rho^\mu) = 0$, and $|\boldsymbol{n}^\mu| = 1$. On the contrary, if μ is entangled with μ^c, ρ^μ is a mixed state, and there is some information loss, i.e. $S(\rho^\mu) > 0$, and $|\boldsymbol{n}^\mu| < 1$.

Thus $S(\rho^\mu)$, called in this context entropy of entanglement, stems as a valid measure of bipartite entanglement on pure states. It possesses, in contrast with $P(\rho^\mu)$, the desirable property of yielding the same value if computed on ρ^μ or on ρ^{μ^c}.

Proposition 1.2.1. *Given a multiqubit pure state $|\psi\rangle$, the following propositions are equivalent:*

- *μ is disentangled from the rest of the system.*

- *$S(\rho^\mu) = 0$*

- *$P(\rho^\mu) = 1$*

- *$\exists!\boldsymbol{n}^\mu$ such that $\langle\psi|\,\sigma^\mu_{\boldsymbol{n}}\,|\psi\rangle = 1$.*

- *The reduced state of μ can be represented as a point on the Bloch sphere, i.e. $\exists!\boldsymbol{n}^\mu$ such that $\rho^\mu = \left(\mathbb{I} + \boldsymbol{n}^\mu \cdot \boldsymbol{\sigma}\right)/2$, where $|\boldsymbol{n}| = 1$.*

On the other hand, while an entangled qubit μ might possess a unique axis maximizing the probability of a given outcome, this probability is always lesser than one.

Proposition 1.2.2. *Given a multiqubit pure state $|\psi\rangle$, the following propositions are equivalent:*

- *μ is maximally entangled with the rest of the system.*

- *$S(\rho^\mu) = \log(2)$*

- *$P(\rho^\mu) = 1/2$*

- *$\forall \boldsymbol{n}^\mu$, $\langle\psi|\,\sigma_{\boldsymbol{n}}^\mu\,|\psi\rangle = 0$.*

- *The reduced state of μ is the maximally mixed state $\rho^\mu = \mathbb{I}/2$.*

The only type of quantum correlation (QC) that a pure state can exhibit is entanglement. Therefore, a measure of QC is also a measure of entanglement for pure states.

On the contrary, in the case of mixed states, one can observe QC distinct from entanglement [53, 23], notably measured by *quantum discord*.

Let us recall the definitions for the various degrees of QCs[23].

Definition 2. Let $\rho^{AB} \in \mathcal{H}_{AB}$ be a state of a bipartite system, associated with the Hilbert space $\mathcal{H}_{AB} = \mathcal{H}_A \otimes \mathcal{H}_B$. The sets of product states $\mathcal{P}_A$, of separable states $\mathcal{S}_A$ and of classical states $\mathcal{C}_A$, with respect to the system A, are then defined as follows:

$$\mathcal{P}_A := \left\{ \rho^{AB} \,\middle|\, \rho^{AB} = \rho^A \otimes \rho^B \right\} = \mathcal{P}_B \tag{1.11}$$

$$\mathcal{C}_A := \left\{ \rho^{AB} \,\middle|\, \rho^{AB} = \sum_k p_k \,|k\rangle\,\langle k|^A \otimes \rho_k^B \right\} \neq \mathcal{C}_B \tag{1.12}$$

$$\mathcal{S}_A := \left\{ \rho^{AB} \,\middle|\, \rho^{AB} = \sum_k p_k \rho_k^A \otimes \rho_k^B \right\} = \mathcal{S}_B, \tag{1.13}$$

where we conventionally denote $\{|k\rangle^A\}_k$ a set of states forming an orthonormal basis in $\mathcal{H}_A$, while $\{\rho_k^A\}_k$ do not necessarily form an orthonormal basis, nor necessarily consist of pure states.

Less formally, $\mathcal{P}_A$ is the set of states for which there is no correlation (quantum of classical) between A and B; $\mathcal{C}_A$ is the set of states for which there is no QC with respect to the subsystem A; $\mathcal{S}_A$ is the set of states for which there is no *entanglement* between A and B.

We have $\mathcal{P}_A \subset \mathcal{C}_A \subset \mathcal{S}_A$.

Furthermore, in any Hilbert space $\mathcal{H} = \bigotimes_\mu \mathcal{H}_\mu$, where the $\mathcal{H}_\mu$ are irreducible, the set of genuine product states can be defined as $\mathcal{P} = \bigcap_\mu \mathcal{P}_\mu$, the set of fully separable states as $\mathcal{S} = \bigcap_\mu \mathcal{S}_\mu$, and the set of fully classical states (also called *pointer states*)

as $\mathcal{C} = \bigcap_A \mathcal{C}_A$.

If $\rho \in \mathcal{S}_A \setminus \mathcal{C}_A$, the subsystem A exhibits a kind of QC not linked to entanglement that we call quantum *dissonance*. This particular notion is an expression of the fact that distinct quantum states, at variance with classical states, are not necessarily orthogonal, that is, mutually exclusive; on the contrary, the former can overlap.

1.2.2. Quantum operations

CPTP maps

The most general quantum operations (also called *quantum channels*) can be seen as a map $\boldsymbol{\mathcal{M}} : \rho \longrightarrow \rho' = \sum_k \mathcal{M}_k [\rho]$, where each $\mathcal{M}_k$ is a trace non-increasing (i.e. *subnormalized*), completely positive map; they sum up to a completely positive trace preserving map (CPTP) $\mathcal{M} = \sum_k \mathcal{M}_k$. That is to say that a quantum operation must map density operators (positive semi-definite operators of trace unity) to density operators, although not necessarily defined on the same Hilbert space (as the addition or dismissal of new subsystems is a valid quantum operation). The $\mathcal{M}_k$ can be thought of as corresponding to specific measurement outcomes k, of probability

$$p_k = \text{Tr} \left[\mathcal{M}_k [\rho] \right] \tag{1.14}$$

and with resulting post-measurement state

$$\rho_k = \mathcal{M}_k [\rho] / p_k. \tag{1.15}$$

The dual of $\boldsymbol{\mathcal{M}}$ is normalized, that is $\sum_k \mathcal{M}_k^*[\mathbb{I}] = \mathbb{I}$. This is because we require it to be complete as a measurement, i.e.

$$
\begin{aligned}
\forall \rho, \ \sum_k \text{Tr} \left[\mathcal{M}_k [\rho] \right] &= \sum_k p_k = 1 \\
&= \sum_k \text{Tr} \left[\mathcal{M}_k [\rho] \, \mathbb{I} \right] = \sum_k \text{Tr} \left[\rho \mathcal{M}_k^* [\mathbb{I}] \right] \\
&= \text{Tr} \left[\rho \sum_k \mathcal{M}_k^* [\mathbb{I}] \right]
\end{aligned} \tag{1.16}
$$

The $\mathcal{M}_k^*[\mathbb{I}]$ thus form a positive operator valued measure (POVM). In contrast, since $\boldsymbol{\mathcal{M}}$ does not necessarily map an orthonormal basis into another, it does not have to be normalized, i.e. we can have

$$\sum_k \mathcal{M}_k [\mathbb{I}] \neq \mathbb{I}. \tag{1.17}$$

In general, the subnormalized completely positive maps can be written in matrix form as $\mathcal{M}_k [\rho] = M_k \rho M_k^\dagger$. To a given POVM correspond infinitely many different

CPTP maps.

Now, to better understand the above statements as to normalization conditions, consider the case of *generalized measurements*, i.e. $M_k = |\tilde{k}\rangle \langle k|$. Clearly, Eq. (1.16) implies that the set $\{|k\rangle\}_k$ forms an orthonormal basis, to translate the fact that, as a measurement, $\mathcal{M}$ must always yield an outcome, i.e. $\mathcal{M}[\rho] \neq 0$; this amount to satisfy Eq. (1.16). On the other hand, no condition is imposed on the $|\tilde{k}\rangle$: a general quantum operation may very well transform any ρ into a classical state (in which case $\{|\tilde{k}\rangle\}_k$ forms an orthonormal basis), or to a pure state (all the $|\tilde{k}\rangle$ are identical), or even generate quantum correlated states (in which case the $|\tilde{k}\rangle$ are not orthonormal). It is also possible to have a quantum channel with $M_k = \sqrt{q_k} |\tilde{k}\rangle \langle k|$, where q_k is the probability of performing this specific suboperation; with CPTP of the latter form, we can for instance write decohering channels, that is channels that decrease the purity of ρ.

Von Neumann Measurement

Formally, *von Neumann measurement*, also called projective measurements, are simply instances of CPTP maps, fulfilling the supplementary constraints $\mathcal{M}_k \mathcal{M}_l = \delta_{kl} \mathcal{M}_k$, i.e. they are orthogonal projectors; furthermore, they are of rank 1.

Unitary Operations

A unitary operation is a particular instance of CPTP map, that can be interpreted as a rotation, and expressed as a matrix U such that $UU^\dagger = \mathbb{I}$. Thus, their general form is

$$U(\xi, \boldsymbol{v}) = e^{-i\boldsymbol{v} \cdot G\xi}, \tag{1.18}$$

where $\xi \in \mathbb{R}$, $\boldsymbol{v}$ is a unit vector, and G is the generator of the transformation. In the case of a system of qubits, $G = \bigotimes_{\mu \in R \subseteq Q} \boldsymbol{\sigma}^\mu$, and $\boldsymbol{v}$ is of dimension $3|R|$.

Local and Unilocal Operations

In general, a quantum operation is said to be *local* if it can be written as products of operations acting on a single subsystem, i.e. $\mathcal{M} = \bigotimes_\mu \mathcal{M}^\mu$. It is said to be *unilocal* if it consists of a product of identity operators on all subsystems but one, i.e. $\mathcal{M} = \mathcal{M}^\mu \bigotimes_{\nu \neq \mu} \mathbb{I}$. Note the analogy between the structure of local operators, defined as products of single qubit operators, and product states, defined as products of single qubit states; in fact, non-local operations are sometimes referred to as *entangling* operations.

In particular, local unitary (LU) operations, are products of unilocal unitaries,

i.e. of the form $U = \bigotimes_{\mu \in Q} U^\mu(\xi^\mu, \boldsymbol{v}^\mu)$, with

$$U^\mu(\xi^\mu, \boldsymbol{v}^\mu) = e^{-i\sigma_v^\mu \xi^\mu}, \tag{1.19}$$

where $\xi^\mu \in \mathbb{R}$, and $\boldsymbol{v}^\mu$ is an arbitrary unit vectors of dimension 3.

1.2.3. Measures of entanglement

Vidal proposed, in a seminal work [54], that a reasonable measure of entanglement should be an entanglement monotone, that is

Condition 1. A magnitude $\mathcal{E}(\rho)$ is an entanglement monotone if it does not increase, in average, under *local operations and classical communications* (LOCC).

LOCC, i.e. the set of all operations that cannot generate entanglement, can simply be defined as the set of all *local CPTP operations.*

This condition quite naturally arises from the mere definition of entanglement, as a type of correlation that cannot be generated by classical operations alone. It results that any operation that can be classically performed, possibly generating classical correlation, should not increase entanglement, and the behaviour of a measure entanglement should reflect this fact.

Indeed, it is clear that local operations (such as local measurements, LU operations, the addition or dismissal of a local subsystem) cannot create entanglement, as they can always be decomposed into successive single qubit operations. On the other hand, classical communication evidently cannot create entanglement either.

Another requirement often encountered in the literature is the following

Condition 2. If $\rho \in \mathcal{S}$, then $\mathcal{E}(\rho) = 0$, i.e. an entanglement measure vanishes on the set of separable states.

Yet this condition amounts to a mere rescaling, as was noted in [17, 54]. In fact, by construction, LOCC is the set of free operation relative to entanglement; it results that any separable state can be transformed into any other by the means of LOCC alone. The definition 1 therefore implies that $\mathcal{E}(\rho)$ take a constant value $\mathcal{E}_0$ for any such states. The requirement that $\mathcal{E}$ should vanish for separable states can thus trivially be met by any LOCC monotone, simply by subtracting this constant term.

The reciprocal statement, that $\mathcal{E}(\rho)$ should vanish only on separable states, is a much stronger one, and arguably too restrictive in the case of mixed states. Indeed, it has been shown that the problem of deciding whether an arbitrary density matrix is separable or not is NP-hard [55]. Nevertheless, it can be met much more easily for pure state measures, as we will show in the case of the ED.

A variety of references have proposed sets of necessary conditions for a magnitude $\mathcal{E}$ to be an entanglement monotone [17, 22, 54]. Most of them are perfectly equivalent, and amount to the dissection of 1 into simpler and more practically tractable properties.

We now recall a set of necessary and sufficient conditions for a measure $\mathcal{E}$ to be an entanglement monotone, in the sense of Definition 1, drawn from [54]

E1 $\mathcal{E}$ is convex: let $\{p_k, \rho_k\}$ be a realization of ρ in terms of pure states, then

$$\mathcal{E}\left(\sum_k p_k \rho_k\right) \leq \sum_k p_k \mathcal{E}(\rho_k) \tag{1.20}$$

E2 $\mathcal{E}$ is monotonically decreasing in average, under unilocal quantum operations: let $\{L_k^\mu(\cdot)\}_k$ be a complete set of unilocal quantum operation performed on subsystem μ; then

$$\mathcal{E}(\rho) \geq \sum_k L_k^\mu(\rho) \tag{1.21}$$

The problem remains to fully characterize unilocal quantum operations. Condition **E2** can be decomposed as follows [54]:

E2.1 $\mathcal{E}$ is monotonically decreasing, in average, under unilocal unitary operations

E2.2 $\mathcal{E}$ is monotonically decreasing, in average, under unilocal von Neumann measurements

E2.3 $\mathcal{E}$ is monotonically decreasing, in average, under addition of an ancilla (i.e. tensor product with a new subsystem)

E2.4 $\mathcal{E}$ is monotonically decreasing, in average, under dismissal of an ancilla (i.e. partial trace over a subsystem)

The following is equivalent to Conditions **E1** and **E2**, and present the advantage of specifically addressing measures defined on pure states [54]

F A function $\mathcal{E}_\mu(|\psi\rangle)$ that can be expressed as $\mathcal{E}_\mu(|\psi\rangle) = f(\mathrm{Tr}_\mu(\psi))$, where $f(\rho)$ is concave and LU-invariant, is an entanglement monotone for pure states. In addition, the related mixed state measure obtained from $\mathcal{E}_\mu$ by convex roof extension is a LOCC-monotone on average, i.e. an entanglement monotone.

1.2.4. Measures of quantum correlations

Following [23] the requirements for a *one-sided measure of QCs* $\mathcal{Q}_A$ are the following

C1 $\mathcal{Q}_A(\rho^{AB}) = 0$ if $\rho \in \mathcal{C}_\mathcal{A}$.

C2 $\mathcal{Q}_A(U_A \rho^{AB} U_A^\dagger) = \mathcal{Q}_A(\rho^{AB})$, where U_A is a LU operation on A.

C3 $\mathcal{Q}_A(|\psi\rangle\langle\psi|) = E_A(|\psi\rangle)$

C4 $\mathcal{Q}_A(\mathbb{I}_A \otimes \Lambda_B^{CPTP}[\rho^{AB}]) \leq \mathcal{Q}_A(\rho^{AB})$, where Λ_B^{CPTP} is CPTP map on B.

Note that measures of QCs should not be concave nor convex. Indeed, the mixing of two maximally entangled pure states can result in a classical state[2], and the mixing of two non-entangled pure states can give rise to QCs [3].

For a comprehensive review on QCs and measures of QCs, we refer the reader to [23].

---

[2]See, for instance, Eq. (1.6).

[3]For instance, the mixing of two non orthogonal pure product state result in a quantum-correlated state: $x|00\rangle\langle00| + (1-x)|++\rangle\langle++|$.

2. Entanglement in pure states

In this chapter, we study entanglement and correlations in pure quantum states of many qubits.

In Section 2.1, we develop the construction of the Fubini-Study metric, natural feature of the space of physical quantum states defined on a projective Hilbert space. Section 2.2 depicts how this metric can be redefined by extending this projection to a stronger invariance requirement, hereby generating a measure of entanglement of pure states, the *Entanglement Distance*; these findings are drawn from the work published a few years back by our research group, in [56]. A proof of its monotonicity is then provided, relations to other quantities are discussed, and examples of applications are provided; the latter are original results we issued in [35]. Finally, Section 2.3 outlines our most recent contribution [36], where we explore the links between quantum correlators, expectation values and projective measurement processes, providing tools to investigate *k-separability* and *persistency of entanglement* in maximally entangled pure states, along with a procedure to find optimal entanglement breaking measurements.

2.1. Defining a projective Hilbert space: the Fubini-Study metric

Quantum mechanics can be understood as a geometric theory; in particular, the set of all quantum states forms a Riemannian manifold, thus endowed with a metric structure.

Hilbert spaces are indeed equipped with a Hermitian scalar product that naturally induces a distance between vectors. If $\mathcal{H}$ denotes a Hilbert space of a general quantum system, for given two close vectors in $\mathcal{H}$, $|\psi_1\rangle$ and $|\psi_2\rangle$, from the scalar product $\langle\psi_1|\psi_2\rangle$, one derives the norm $||$ and the (finite) distance between these two vectors as

$$D(|\psi_1\rangle, |\psi_2\rangle) = |||\psi_1\rangle - |\psi_2\rangle| = \langle\Delta\psi|\Delta\psi\rangle^{1/2}, \tag{2.1}$$

where $|\Delta\psi\rangle = |\psi_1\rangle - |\psi_2\rangle$. In the case of two normalized vectors $|\psi_1\rangle$ and $|\psi_2\rangle$, it results

$$D(|\psi_1\rangle, |\psi_2\rangle) = [2\,(1 - \mathrm{Re}(\langle\psi_1|\psi_2\rangle))]^{1/2}. \tag{2.2}$$

Furthermore, because Hilbert spaces are differentiable manifolds, it is possible, for any given state, to define a local chart on its neighbourhood in $\mathcal{H}$. This allows us to derive the metric tensor induced by the above-defined distance. Let $|\psi\rangle$ and

$|\psi\rangle + |d\psi\rangle$ be two arbitrarily close vectors. The squared infinitesimal distance between them writes

$$d^2(|\psi\rangle + |d\psi\rangle, |\psi\rangle) = \langle d\psi | d\psi \rangle. \tag{2.3}$$

By means of a local chart, the normalized vectors in $\mathcal{H}$ admit a smooth parametrization governed by a N-dimensional variable $\xi \in \mathbb{R}^N$ and we have

$$|d\psi\rangle = \sum_\mu |\partial_\mu \psi(\xi)\rangle d\xi^\mu, \tag{2.4}$$

where with $\partial_\mu(\cdot) := \partial/\partial\xi^\mu(\cdot)$. Thus we have

$$d^2(|\psi\rangle + |d\psi\rangle, |\psi\rangle) = \sum_{\mu\nu} \langle \partial_\mu \psi | \partial_\nu \psi \rangle d\xi^\nu d\xi^\mu. \tag{2.5}$$

Though the matrix of elements $g_{\mu\nu} = \langle \partial_\mu \psi | \partial_\nu \psi \rangle$ constitutes a valid Riemannian metric tensor for $\mathcal{H}$, the notion of distance it induces is unfit for the characterization of physical quantum states. This is because the latter are in fact defined *up to an irrelevant global phase*, and thus are not in one-to-one correspondence with the complex vectors of the Hilbert space. Quantum states are in fact associated with rays of the Hilbert space, and can be defined through equivalence classes of normalized vectors $|\psi\rangle \in \mathcal{H}$, for the relation $\underset{p}{\sim}$ on $\mathcal{H}$ given by

$$|\psi\rangle \underset{p}{\sim} |\phi\rangle \iff |\psi\rangle = e^{i\theta} |\phi\rangle, \tag{2.6}$$

with $\theta \in \mathbb{R}$.

Consistently, a physically meaningful metric must be defined so that the distance between $|\psi\rangle$ and $|\psi\rangle + |d\psi\rangle$, and the one between $|\psi'\rangle = e^{i\alpha} |\psi\rangle$ and $|\psi'\rangle + |d\psi'\rangle$ must be the same. An appropriate metric tensor for the state-space hence has to be invariant under gauge transformation $|\psi(\xi)\rangle \to e^{i\alpha(\xi)}|\psi(\xi)\rangle$. This is accomplished with the Fubini-Study metric, which gives the squared distance between two neighbouring rays

$$d_{FS}^2(|\psi\rangle + |d\psi\rangle, |\psi\rangle) = \langle d\psi | d\psi \rangle - \langle \psi | d\psi \rangle \langle d\psi | \psi \rangle, \tag{2.7}$$

from which we derive the metric tensor

$$g_{\mu\nu} = \langle \partial_\mu \psi | \partial_\nu \psi \rangle - \langle \partial_\mu \psi | \psi \rangle \langle \psi | \partial_\nu \psi \rangle. \tag{2.8}$$

The Fubini-Study metric (2.7) is therefore defined on the finite projective Hilbert-space $\mathcal{PH} := \mathcal{H}/\underset{p}{\sim}$ [57, 58].

It is worth noting that we can define the square of the finite distance between two rays $[|\phi_1\rangle]_p, [|\phi_2\rangle]_p \in \mathcal{PH}$, associated with the normalized states $e^{i\alpha_1}|\phi_1\rangle, e^{i\alpha_2}|\phi_2\rangle$,

respectively, as follows

$$D^2_{FS}(|\phi_1\rangle, |\phi_2\rangle) = \left(1 - |\langle\phi_1|\phi_2\rangle|^2\right), \tag{2.9}$$

which doesn't depend on the global phases α_1, α_2.

2.2. The Entanglement Distance

2.2.1. Construction

Following Ref. [56], we investigate here the deep link between the Riemannian metric structure associated with a projective Hilbert space and the entanglement properties of the states of this space. To this end, we consider another projection on the Hilbert space, and find its metric, adapted from the Fubini-Study metric. We consider the case of the Hilbert space $\mathcal{H} = \bigotimes_{\mu \in Q} \mathcal{H}^\mu$ that is, the tensor product of the Hilbert spaces of a set Q of M qubits.

A measure of entanglement (or of any type of correlation), is invariant under local unitary (LU) transformations: indeed, the choice of a local basis should not affect the amount of correlation between subsystems. Thus, given two normalized vectors $|\phi\rangle, |\psi\rangle \in \mathcal{H}$, we define the following additional equivalence relation between elements of the projective Hilbert space

$$[|\phi\rangle]_p \underset{LU}{\sim} [|\psi\rangle]_p \iff |\phi\rangle = e^{i\alpha} \prod_{\mu \in Q} U^\mu |\psi\rangle, \tag{2.10}$$

with $\alpha \in \mathbb{R}$ and where, for $\mu \in Q$, each U^μ is an arbitrary $SU(2)$ LU operator acting on the μth qubit.

With this equivalence relation, we define the quotient space $\mathcal{PH}/\underset{LU}{\sim}$. Thus, the entanglement measure E has to be a function $E : \mathcal{PH}/\underset{LU}{\sim} \to \mathbb{R}^+$, i.e. a function of the equivalence classes

$$[|\psi\rangle] = \left\{ [|\phi\rangle]_p \in \mathcal{PH} \,\middle|\, [|\phi\rangle]_p \underset{LU}{\sim} [|\psi\rangle]_p \right\}. \tag{2.11}$$

Any state in $[|\psi\rangle]$ has the same degree of entanglement as $|\psi\rangle$.

From now on, we neglect the global phase factor, as it is already discarded by construction of the Fubini-Study metric. Let us consider the equivalence classes

$$[|\psi\rangle]_{LU} = \left\{ |U, \psi\rangle = \prod_{\mu \in Q} U^\mu |\psi\rangle \right\}, \tag{2.12}$$

in which each state is parametrized by a set of variables $\{\xi^\mu, \boldsymbol{v}^\mu\}_{\mu \in Q}$. $[|\psi\rangle]_{LU}$ is a submanifold of $\mathcal{H}$, and we can thus build associated local charts, considering the

neighbouring states

$$|dU, \psi\rangle = \sum_{\mu \in Q} d\tilde{U}^{\mu} |\psi\rangle \ , \tag{2.13}$$

obtained by application of infinitesimal variations of the form

$$d\tilde{U}^{\mu} = -i\sigma_{\boldsymbol{v}}^{\mu} d\xi^{\mu} \tag{2.14}$$

which rotates the μth qubit by an infinitesimal angle $2d\xi^{\mu}$ around the unitary vector $\boldsymbol{v}^{\mu}$.

By substituting $|dU, \psi\rangle$ in place of $|d\psi\rangle$ in Eq. (2.7), we get

$$d_{FS}^2 \left(|\psi\rangle , |\psi\rangle + |dU, \psi\rangle, \{\boldsymbol{v}^{\mu}\}_{\mu \in Q} \right) = \sum_{\mu\nu \in Q} g_{\mu\nu} \left(|\psi\rangle , \{\boldsymbol{v}^{\mu}\}_{\mu \in Q} \right) d\xi^{\mu} d\xi^{\nu} \ . \tag{2.15}$$

The corresponding *projective Fubini-Study metric tensor* is

$$g_{\mu\nu}(|\psi\rangle , \{\boldsymbol{v}^{\mu}\}_{\mu \in Q}) = \langle\psi|\boldsymbol{\sigma}_{\boldsymbol{v}}^{\mu}\boldsymbol{\sigma}_{\boldsymbol{v}}^{\nu}|\psi\rangle - \langle\psi|\boldsymbol{\sigma}_{\boldsymbol{v}}^{\mu}|\psi\rangle \langle\psi|\boldsymbol{\sigma}_{\boldsymbol{v}}^{\nu}|\psi\rangle \ . \tag{2.16}$$

We shall from now on call the latter entanglement metric (EM), as it contains information on the entanglement structure of quantum states. Indeed, as will be discussed in chapter 2.3, the inspection of the block structure of the EM $g(|\psi\rangle)$ can be informative about the *k*-separability and the persistency of entanglement.

Clearly, the metric tensor $g_{\mu\nu}(|\psi\rangle , \{\boldsymbol{v}^{\mu}\}_{\mu \in Q})$ is not uniquely defined for each $|\psi\rangle$, as it depends on the unit vectors $\boldsymbol{v}^{\mu}$. We thus define the entanglement of $[|\psi\rangle]$, as the minimum of the trace of $g_{\mu\nu}(|\psi\rangle , \{\boldsymbol{v}^{\mu}\}_{\mu \in Q})$ taken over all the possible orientations of the unit vectors $\boldsymbol{v}^{\mu}$. Formally, the induced measure of entanglement, called entanglement distance (ED), writes

$$E(|\psi\rangle) = \inf_{\{\boldsymbol{v}^{\mu}\}_{\mu \in Q}} \mathrm{Tr}(g(|\psi\rangle , \{\boldsymbol{v}^{\mu}\}_{\mu \in Q})) \ , \tag{2.17}$$

where the inf operation, insures that the measure (2.17) is independent from the choice of the operators U^{μ}, and uniquely defined for each class (2.12). This is a necessary condition for a well-defined entanglement measure [22].

From Eq. (2.16) we derive

$$\mathrm{Tr}[g(|\psi\rangle , \{\boldsymbol{v}^{\mu}\}_{\mu \in Q})] = \sum_{\mu=0}^{M-1} \left[1 - (\boldsymbol{v}^{\mu} \cdot \langle\psi|\boldsymbol{\sigma}^{\mu}|\psi\rangle)^2 \right] \ , \tag{2.18}$$

that shows that the unit vectors

$$\tilde{\boldsymbol{v}}^{\mu} = \pm \langle\psi|\boldsymbol{\sigma}^{\mu}|\psi\rangle / |\langle\psi|\boldsymbol{\sigma}^{\mu}|\psi\rangle| \ , \tag{2.19}$$

provide the inf of $\mathrm{Tr}(g)$. Therefore, we obtain the following closed-form expression

for the ED

$$E(|\psi\rangle) = M - \sum_{\mu=0}^{M-1} |\langle\psi|\boldsymbol{\sigma}^\mu|\psi\rangle|^2. \tag{2.20}$$

Note that the latter equation can be seen as the sum of the M single-qubit EDs

$$E_\mu(|\psi\rangle) = 1 - |\langle\psi|\boldsymbol{\sigma}^\mu|\psi\rangle|^2. \tag{2.21}$$

$E_\mu(|\psi\rangle)$ is a measure of bipartite entanglement of μ with the rest of the system.

An entanglement monotone for mixed state is then obtained by straightforward convex roof construction

$$E_\mu(\rho) := \min_{\{p_j,\psi_j\}} \sum_j p_j E_\mu(|\psi_j\rangle), \tag{2.22}$$

where the minimization is carried over all of the possible realizations $\{p_j, \psi_j\}$ of ρ as a mixture of pure states.

As shown in our recent publication [35], the ED fulfils condition **F**, namely

Proposition 2.2.1. *The pure state ED defined in* (2.21)*, along with its convex roof extension to mixed states, is monotonically non-increasing under LOCC, hence is an entanglement monotone.*

Proof. First notice that the single-qubit measure (2.21) can be rewritten

$$E_\mu(|\psi\rangle) = 1 - |\langle\psi|\boldsymbol{\sigma}^\mu|\psi\rangle|^2 = 1 - |\boldsymbol{n}^\mu|^2, \tag{2.23}$$

where $\boldsymbol{n}^\mu$ is the 3 dimensional vector defining the reduced state ρ^μ obtained by tracing out the rest of the system μ^c, as in (1.10). Yet we have

$$\mathrm{Tr}\left[(\rho^\mu)^2\right] = \frac{1}{2}\left(1 + |\boldsymbol{n}^\mu|^2\right), \tag{2.24}$$

hence

$$\begin{aligned} E_\mu(|\psi\rangle) &= 2\left(1 - \mathrm{Tr}\left[(\mathrm{Tr}_{\mu^c}[|\psi\rangle\langle\psi|])^2\right]\right) \\ &= f(\mathrm{Tr}_{\mu^c}[\psi]), \end{aligned} \tag{2.25}$$

with $f(\boldsymbol{x}) = 2(1 - \mathrm{Tr}[\boldsymbol{x}^2])$.

f inherits the LU-invariance property of the trace. Let us now prove that f is concave. Consider $\rho_k = \frac{1}{2}(\mathbb{I} + \boldsymbol{n}_k \cdot \boldsymbol{\sigma})$, with $k = 1, 2$, two single-qubit density matrices, and $\lambda \in [0, 1]$. We have

$$f\left(\lambda\rho_1 + (1-\lambda)\rho_2\right) = 1 - |\lambda\boldsymbol{n}_1 + (1-\lambda)\boldsymbol{n}_2|^2 \tag{2.26}$$

and

$$\lambda f(\rho_1) + (1-\lambda)f(\rho_2) = 1 - \lambda|\boldsymbol{n}_1|^2 + (1-\lambda)|\boldsymbol{n}_2|^2, \tag{2.27}$$

and the convexity of the Euclidean squared norm implies

$$f\left(\lambda\rho_1 + (1-\lambda)\rho_2\right) \geq \lambda f(\rho_1) + (1-\lambda)f(\rho_2), \tag{2.28}$$

that is f is concave, which completes our proof that $E_\mu(|\psi\rangle)$ is a valid entanglement monotone for pure states. $\qquad\square$

The latter optimization procedure is notoriously hard to achieve, as it requires to explore a r-dimensional space, r being the rank of ρ, and in practice intractable for large systems. In fact, we were not able to find in the literature any example of entanglement measures applicable to mixed states of more than 3 qubits. On the other hand, criteria exist to assert for the separability of some states, in a boolean fashion [59, 52, 60].

For this reason, we propose in Section 3.2 an alternative definition for the ED, relying on an optimization trick.

2.2.2. Relation with other entanglement measures

2.2.2.1. Linear entropy

It is easy to see that the ED (2.21) of a qubit μ is related to the linear entropy (1.4) of the associated reduced state $\rho^\mu = \mathrm{Tr}_{\mu^c}[|\psi\rangle\langle\psi|]$. Indeed, inserting Eq. (1.10) in Eq. (1.4), we get

$$\begin{aligned}
S_L(\rho^\mu) &= 1 - \mathrm{Tr}\left[(\rho^\mu)^2\right] \\
&= 1 - \frac{1}{4}\mathrm{Tr}\left[(\mathbb{I} + \boldsymbol{n}^\mu \cdot \boldsymbol{\sigma}^\mu)^2\right] \\
&= 1 - \frac{1}{4}\mathrm{Tr}\left[(\mathbb{I} + |\boldsymbol{n}^\mu|^2\mathbb{I} + 2\boldsymbol{\sigma}^\mu)\right] \\
&= 1 - \frac{1}{2}\left(1 + |\boldsymbol{n}^\mu|^2\right) = \frac{1}{2}\left(1 - |\boldsymbol{n}^\mu|^2\right) = \frac{1}{2}E_\mu(|\psi\rangle)
\end{aligned} \tag{2.29}$$

2.2.2.2. Measure of the unitary response

The ED can be derived by a minimum distance principle, if studied in the framework of the Riemannian geometry of the projective Hilbert space. In fact, according to Eq. (2.9), the square of the distance between the rays associated with the unit vectors $|\phi\rangle$ and $\sigma_{\boldsymbol{v}}^\mu|\phi\rangle = |\sigma_{\boldsymbol{v}}^\mu\phi\rangle$, is

$$D_{FS}^2\left(|\phi\rangle, |\sigma_{\boldsymbol{v}}^\mu\phi\rangle\right) = 1 - |\langle\phi|\sigma_{\boldsymbol{v}}^\mu\phi\rangle|^2, \tag{2.30}$$

therefore

$$E_\mu\left(|\phi\rangle\right) = \inf_{\boldsymbol{v}^\mu} D_{FS}^2\left(|\phi\rangle, |\sigma_{\boldsymbol{v}}^\mu\phi\rangle\right). \tag{2.31}$$

In other words, the single qubit ED can be interpreted as the distance between a state and its image under the action of the least perturbing observable $\sigma_{\boldsymbol{v}}^{\mu}$.

This is consistent with Prop. 1.2.1: a pure state is separable in μ if and only if it is the eigenstate of eigenvalue ± 1 of some $\sigma_{\boldsymbol{v}}^{\mu}$ or, equivalently, if there exists a local projective measurement on μ that leaves such a state invariant.

The ED is also quite similar to the *stellar mirror entanglement* (SME) introduced in Ref. [61]. The latter turns out to be as a special case of *mirror entanglement*, and is given, for a bipartition $A - B$, by

$$E^*(|\psi\rangle) = \inf_{W_*} \left(1 - |\langle\psi| W_* |\psi\rangle|^2\right), \tag{2.32}$$

where W_* is a LU operator of the form $W_* = \sum_{j=1}^{d_A} e^{i(d_A - 2j + 1)\pi/d_A} |\phi_j\rangle \langle\phi_j|$, d_A is the dimension of the subsystem A and $\{|\phi_j\rangle\}_{j=1,\ldots,d_A}$ forms an orthonormal basis in $\mathcal{H}_A$.

Now consider a bipartition $\mu - \mu^c$. It can easily be checked that

$$\begin{aligned} E_\mu^*(|\psi\rangle) &= \inf_{W_*} \left(1 - |\langle\psi| W_* |\psi\rangle|^2\right) \\ &= \inf_U \left(1 - |\langle\psi| U e^{i\pi\sigma_z^\mu/2} U^\dagger |\psi\rangle|^2\right) \\ &= \inf_{\boldsymbol{v}^\mu} \left(1 - |\langle\psi| \sigma_{\boldsymbol{v}}^\mu |\psi\rangle|^2\right) = E_\mu(|\psi\rangle) \end{aligned} \tag{2.33}$$

2.2.2.3. Concurrence

Let us consider a general $M = 2$ qubits normalized pure state

$$|\psi\rangle = \sum_{j=x,y,z} w_j |j\rangle, \tag{2.34}$$

such that $\sum_{j=x,y,z} |w_j|^2 = 1$. The concurrence for pure state (2.34) is defined as [62]

$$C(|\psi\rangle) = |\langle\psi|\psi^\dagger\rangle|, \tag{2.35}$$

where $|\psi^\dagger\rangle = \sigma_2^0 \otimes \sigma_2^1 \sum_{j=x,y,z} w_j^* |j\rangle$. By direct computations we get [62]

$$C(|\psi\rangle) = 2|w_0 w_3 - w_1 w_2|. \tag{2.36}$$

and

$$E(|\phi\rangle) = 8[w_0^2 w_3^2 + w_1^2 w_2^2 - w_0^* w_3^* w_1 w_2 - w_0 w_3 w_1^* w_2^*]. \tag{2.37}$$

Therefore we get the following general result for $M = 2$ qubits states

$$\frac{1}{2} E(|\phi\rangle) = [C(|\phi\rangle)]^2. \tag{2.38}$$

This proves that the concurrence for pure states, is a special case of ED, valid for the case $M = 2$.

2.2.3. Examples

In this section, we apply our geometric method to investigate the entanglement properties of three one/multi-parameter families of states. In all the cases, the degree of entanglement of each state depends on these parameters and, in particular, they have known the values of the parameters corresponding to maximally entangled states for each one of the families.

The first is a one-parameter family of states which is related to the Greenberger-Horne-Zeilinger states [5] since for a suitable choice of the parameter one gets a Greenberger-Horne-Zeilinger state. We will name the elements of such family Greenberger-Horne-Zeilinger–like states (GHZLS). The second is a one-parameter family of states too. This class of states has been introduced by Briegel and Raussendorf in Ref. [25], for this reason, we name the elements in this family Briegel-Raussendorf states (BRS). The third is a $(M-1)$-parameters family of states, related to the W states. In particular, we consider a weighted combination of the M states that compose a W state of M qubits. In this case, the state with the higher degree of entanglement is known to correspond to the case with the same weights.

In the following, we consider the standard M-qubit basis $\{|0 \cdots 0\rangle,\ |0 \cdots 01\rangle, \ldots, |1 \cdots 1\rangle\}$ for $\mathcal{H}$, where $|0\rangle_\mu$ ($|1\rangle_\mu$) denotes the eigenstate of σ_3^μ with eigenvalue $+1$ (-1). Thus, each basis vector is identified by M integers $n_0, \ldots, n_{M-1} = 0, 1$ as $|\{n\}\rangle = |n_{M-1}\ n_{M-2}\quad n_0\rangle$. Therefore, we enumerate such basis vectors according to the binary integers representation $|k\rangle = |\{n^k\}\rangle$, with $k = \sum_{\mu=0}^{M-1} n_\mu^k 2^\mu$, where n_ν^k is the ν-th digit of the number k in binary representation and $k = 0, \ldots, 2^M - 1$.

2.2.3.1. Greenberger-Horne-Zeilinger–like states

In this section, we consider a one-parameter family of states, the GHZLS, defined according to

$$|GHZ, \theta\rangle_M = \cos(\theta)|0\rangle + \sin(\theta)|2^M - 1\rangle, \qquad (2.39)$$

where $0 \leq \theta \leq \pi/2$. For $\theta = 0, \pi/2$ the states are fully separable, whereas for $\theta = \pi/4$ the state has the maximum degree of entanglement. In this case, the trace for the metric tensor (2.16) results

$$\mathrm{Tr}(g) = M - \cos^2(2\theta) \sum_{\nu=0}^{M-1} (v_3^\nu)^2, \qquad (2.40)$$

and, consistently with (2.19), it is minimized by the values $\tilde{v}_1^\nu = \tilde{v}_2^\nu = 0$, $\tilde{v}_3^\nu = \pm 1$, for $\nu = 0 \ldots, M - 1$. Therefore, we have

$$\tilde{g} = \sin^2(2\theta) J_M \tag{2.41}$$

where J_M is the $M \times M$ matrix of ones. The ED per qubit for the GHZLS results

$$E(|GHZ, \theta\rangle_M)/M = \sin^2(2\theta) \,. \tag{2.42}$$

2.2.3.2. Briegel Raussendorf states

We denote with $\Pi_0^j = (\mathbb{I} + \sigma_3^j)/2$ and $\Pi_1^j = (\mathbb{I} - \sigma_3^j)/2$ the projector operators onto the eigenstates of σ_3^j, $|0\rangle_j$ (with eigenvalue $+1$) and $|1\rangle_j$ (with eigenvalue -1), respectively. Each M qubit state of the BRS class is derived by applying to the fully separable state

$$|r, 0\rangle = \bigotimes_{j=0}^{M-1} \frac{1}{\sqrt{2}}(|0\rangle_j + |1\rangle_j) \,, \tag{2.43}$$

the non-LU operator

$$U_0(\phi) = \exp(-i\phi H_0) = \prod_{j=1}^{M-1} \left(\mathbb{I} + \alpha \Pi_0^j \Pi_1^{j+1} \right) \,, \tag{2.44}$$

where $H_0 = \sum_{j=1}^{M-1} \Pi_0^j \Pi_1^{j+1}$ and $\alpha = (e^{-i\phi} - 1)$. The full operator (2.44) is diagonal on the states of the standard basis $\{|0\cdots 0\rangle, \, |0\cdots 01\rangle, \ldots, |1\cdots 1\rangle\}$.

In fact, the eigenvalue λ_k of the operator (2.44), corresponding to a given eigenstate $|k\rangle$ of this basis, results

$$\lambda_k = \sum_{j=0}^{n(k)} \binom{n(k)}{j} \alpha^j \,, \tag{2.45}$$

where $n(k)$ is the number ordered couples 01 inside the sequence of the base vector $|k\rangle$. For the initial state (2.43) we consistently get

$$|r, 0\rangle_M = 2^{-M/2} \sum_{k=0}^{2^M - 1} |k\rangle \,, \tag{2.46}$$

and, under the action of $U_0(\phi)$ we obtain

$$|r, \phi\rangle_M = 2^{-M/2} \sum_{k=0}^{2^M - 1} \sum_{j=0}^{n(k)} \binom{n(k)}{j} \alpha^j |k\rangle \,. \tag{2.47}$$

For $\phi = 2\pi k$, with $k \in \mathbb{Z}$, this state is separable, whereas, for all the other choices of the value ϕ, it is entangled. In particular, in [25] it is argued that the values

$\phi = (2k + 1)\pi$, where $k \in \mathbb{Z}$, give maximally entangled states.

Briegel Raussendorf states: case $M = 2$

In the case $M = 2$ the one-parameter family of BRS is

$$|r, \phi\rangle_2 = \sum_{k=0}^{3} c_k |k\rangle \,, \tag{2.48}$$

with $c_k = 1/2$ if $k \neq 1$, and $c_1 = e^{-i\phi}/2$, where $\phi \in [0, 2\pi]$. By direct calculation we obtain the trace of the Fubini-Study metric

$$\mathrm{Tr}(g) = \sum_{\nu=0}^{1} \left[1 - c^2 \left(c v_1^\nu + (-1)^{\nu+1} s v_2^\nu \right)^2 \right] \,, \tag{2.49}$$

where $c = \cos(\phi/2)$ and $s = \sin(\phi/2)$. Eq. (2.49) is minimized with the choice $\tilde{\boldsymbol{v}}^\nu = \pm(c, (-1)^{\nu+1}s, 0)$. Consistently, the EM and the ED per qubit result

$$\tilde{g} = s^2 J_2 \tag{2.50}$$

and

$$E(|r, \phi\rangle_2)/2 = s^2 \,. \tag{2.51}$$

Briegel Raussendorf states: case $M = 3$

In the case $M = 3$ we have

$$|r, \phi\rangle_3 = \sum_{k=0}^{7} c_k |k\rangle \,, \tag{2.52}$$

with $c_k = 1/2^{3/2}$ if $k \neq 1, 2, 3, 5$, and $c_k = e^{-i\phi}/2^{3/2}$ if $k = 1, 2, 3, 5$, where $\phi \in [0, 2\pi]$. The trace of g results

$$\mathrm{Tr}(g) = \left[3 - \left((c^2 v_1^0 + cs v_2^0)^2 + (c^2 v_1^1)^2 + (c^2 v_1^2 - cs v_2^2)^2 \right) \right] \,, \tag{2.53}$$

is minimized with the choices $\tilde{\boldsymbol{v}}^0 = (c, s, 0)$, $\tilde{\boldsymbol{v}}^1 = (1, 0, 0)$ and $\tilde{\boldsymbol{v}}^2 = (c, -s, 0)$. The EM and the ED per qubit, in this case result

$$\tilde{g} = s^2 \begin{pmatrix} 1 & c & 0 \\ c & 1 + c^2 & c \\ 0 & c & 1 \end{pmatrix} \,, \tag{2.54}$$

and

$$E(|r, \phi\rangle_3)/3 = s^2 \left(3 + c^2\right)/3 \,, \tag{2.55}$$

respectively.

Briegel Raussendorf states: case $M = 4$

For $M = 4$ we have

$$|r, \phi\rangle_4 = \sum_{k=0}^{15} c_k |k\rangle \,, \tag{2.56}$$

with $c_k = e^{-i\phi}/4$ if $k \neq 0, 5, 8, 12, 14, 15$, $c_5 = e^{-i2\phi}/4$, and $c_0 = c_8 = c_{12} = c_{14} = c_{15} = 1/4$, where $\phi \in [0, 2\pi]$. The trace of g results

$$\begin{aligned}
\mathrm{Tr}(g) = \Big[4 - \big((c^2 v_1^0 + cs v_2^0)^2 + (c^2 v_1^1)^2 + \\
(c^2 v_1^2)^2 + (c^2 v_1^3 - cs v_2^3)^2\big)\Big] \,,
\end{aligned} \tag{2.57}$$

is minimized with the choices $\tilde{\boldsymbol{v}}^0 = (c, s, 0)$, $\tilde{\boldsymbol{v}}^1 = (1, 0, 0)$, $\tilde{\boldsymbol{v}}^2 = (1, 0, 0)$ and $\tilde{\boldsymbol{v}}^3 = (c, -s, 0)$. The EM in this case results

$$\tilde{g} = s^2 \begin{pmatrix} 1 & c & 0 & 0 \\ c & 1+c^2 & c^2 & 0 \\ 0 & c^2 & 1+c^2 & c \\ 0 & 0 & c & 1 \end{pmatrix} \,, \tag{2.58}$$

thus the ED reads

$$E(|r, \phi\rangle_4)/4 = s^2 \left(4 + 2c^2\right)/4 \,. \tag{2.59}$$

2.2.3.3. W-states

In this section, we consider a $(M - 1)$-parameters family of states, the W states, defined according to

$$|W, \boldsymbol{\alpha}\rangle_M = \sum_{j=1}^{M} \alpha_j |2^{j-1}\rangle \,, \tag{2.60}$$

with

$$\alpha_1 = c_1$$

$$\alpha_2 = s_1 c_2$$

$$\vdots$$

$$\alpha_k = s_1 s_2 \cdots s_{k-1} c_k \qquad (2.61)$$

$$\vdots$$

$$\alpha_{M-1} = s_1 s_2 \cdots s_{M-2} c_{M-1}$$

$$\alpha_M = s_1 s_2 \cdots s_{M-2} s_{M-1} \,,$$

where we set $c_j = \cos(\theta_j)$, $s_j = \sin(\theta_j)$, and where $0 \le \theta_j \le \pi/2$, $j = 1, \ldots, M-1$. If the number of indices k such that $\alpha_k = 0$ is r, then the state (2.60) is r-partite. For $\alpha_k = 1/\sqrt{M}$, for each k, the state (2.60) is maximally entangled.

In the case of state (2.60), the trace of the metric tensor (2.16) results

$$\mathrm{Tr}(g) = \left[M - \sum_{\nu=0}^{M-1} [(1 - 2|\alpha_{j(\nu)}|^2) v_3^\nu]^2 \right] \,, \qquad (2.62)$$

where $j(\nu)$ is an invertible map $j : \{0, \ldots, M-1\} \to \{1, \ldots, M\}$. Consistently with (2.19), Eq. (2.62) is minimized by the values $\tilde{v}_1^\nu = \tilde{v}_2^\nu = 0$, $\tilde{v}_3^\nu = \pm 1$, for $\nu = 0 \ldots, M-1$. Therefore, the ED for these states results

$$E(|W, \boldsymbol{\alpha}\rangle_M)/M = 4(1 - \sum_j |\alpha_j|^4)/M \,. \qquad (2.63)$$

The state with the higher entanglement corresponds to the choice $\alpha_j = 1/\sqrt{M}$, for $j = 0, \ldots, M-1$. The corresponding value for the ED is

$$E(|W, \boldsymbol{\alpha}_M\rangle_M)/M = 4(1 - 1/M)/M \,. \qquad (2.64)$$

Therefore, except for the case $M = 2$, $E(|W, \boldsymbol{\alpha}\rangle_M)/M < 1$. This is due to the non-vanishing of the expectation values of the operators $\boldsymbol{\sigma}_v^\mu$ on the state with the higher entanglement. In this sense, such state could not be considered a maximally entangled state. Remarkably, the W state with maximal entanglement remains a maximal entanglement state under particle loss.

W-states: case $M = 2$

For $M = 2$ it is

$$|W, \boldsymbol{\alpha}\rangle_2 = \alpha_1 |1\rangle + \alpha_2 |2\rangle \,, \qquad (2.65)$$

where $\alpha_1 = \cos(\theta_1)$ and $\alpha_2 = \sin(\theta_1)$, and $\theta_1 \in [0, \pi/2]$. The choice $\tilde{v}_1^\nu = \tilde{v}_2^\nu = 0$,

$\tilde{v}_3^\nu = (-1)^\nu$, for $\nu = 0, 1$, by direct calculations we get the following expressions for the EM and ED

$$\tilde{g} = \sin^2(2\theta_1)J_2 \,, \tag{2.66}$$

$$E(|W, \boldsymbol{\alpha}\rangle_2)/2 = \sin^2(2\theta_1) \,, \tag{2.67}$$

respectively.

W-states: case $M = 3$

For $M = 3$ it is

$$|W, \boldsymbol{\alpha}\rangle_3 = \alpha_1|1\rangle + \alpha_2|2\rangle + \alpha_3|4\rangle \,, \tag{2.68}$$

where $\alpha_1 = \cos(\theta_1)$, $\alpha_2 = \sin(\theta_1)\cos(\theta_2)$ and $\alpha_3 = \sin(\theta_1)\sin(\theta_2)$. By direct calculations we get the ED

$$E(|W, \boldsymbol{\alpha}\rangle_3)/3 = \frac{4}{3}\Big[1 - \big(\cos^4(\theta_1) + \sin^4(\theta_1)\cos^4(\theta_2) + \\ \sin^4(\theta_1)\sin^4(\theta_2)\big)\Big] \,. \tag{2.69}$$

2.3. Correlations and projective measurements in maximally entangled states

We present in this section the results we recently published in [36].

The complete analysis of entanglement convokes numerous additional notions, as their *k-separability, k-producibility, entanglement depth* or *persistency of entanglement* [10, 25, 13].

Measurement processes and their understanding are of major importance in the field of quantum computing. Measurement-based quantum computation, which stands as a universal model of quantum computation, obviously heavily lie on the control of their effects on quantum states [63, 64, 65].

The ways of quantifying entanglement in multipartite states are manifold. In the present section, we solely employ the pure state ED defined in (2.21), section 2.2. In other words, we focus on the notion of *qubit-wise entanglement*, that is entanglement of bipartitions (μ, μ^C), and study how, in conjunction with the EM (2.16) and quantum correlators, it can be used to reveal the internal, network-like, entanglement structure in pure states, primarily focusing on maximally entangled ones.

We start, in Section 2.3.1, demonstrating a few simple theorems, which highlight the strong relationship between pre-measurement correlations and post-measurement average values, and show how the structure of the EM provides an upper bound to the persistency of entanglement. In section 2.3.2, we derive two

procedures in order to determine sets of measurement axis optimal with respect to pairwise correlators or with respect to the induced total entanglement breaking; the question of the equivalency of these two optimal sets arises as an interesting open problem, to our best knowledge, yet to be solved. We apply our methods to a few examples in Section 2.3.3. Finally, in Section 2.3.4, we synthesize our results, and make a few remarks on possible continuations of this work; in particular, we examine the effect of several successive projective measurements on expectation values, and argue that a more thorough study of entanglement breaking in quantum states should investigate the behaviour of higher order correlations.

2.3.1. First order projective measurements

Departing from a generic multipartite quantum state $|s\rangle \in \mathcal{H}$, the state $|s'\rangle$ obtained after a projective measurement of the qubit ν in the direction $\boldsymbol{m}^\nu$ write

$$|s\rangle \longrightarrow |s'\rangle = \frac{P_{\boldsymbol{m}}^\nu |s\rangle}{\sqrt{\langle s| P_{\boldsymbol{m}}^\nu |s\rangle}}, \tag{2.70}$$

with

$$P_{\boldsymbol{m}}^\nu := \frac{\mathbb{I} + \sigma_{\boldsymbol{m}}^\nu}{2} \tag{2.71}$$

the single qubit projector onto the eigenstate of $\sigma_{\boldsymbol{m}}^\nu$, of eigenvalue 1. For the sake of clarity, we hereafter denote with the letter $\boldsymbol{m}$ the vectors associated with actual projective measurements such as (2.70). In contrast, vectors denoted with the letter $\boldsymbol{v}$ denote the variables of the EM, i.e. *virtual* measurement axis.

In such a post-measurement state, the expectation value of an arbitrary qubit μ in the direction $\boldsymbol{v}^\mu$ can be expressed as a function of the expectation values and the correlator of $\sigma_{\boldsymbol{m}}^\nu$ and $\sigma_{\boldsymbol{v}}^\nu$ in the initial state.

Theorem 2.3.1. *If $|s\rangle$ is maximally entangled in ν and μ, and $|s'\rangle$ is the post-measurement state after a projective measure of $\sigma_{\boldsymbol{m}}^\nu$, then we have, for any measurement axis $\boldsymbol{v}^\mu$*

$$\langle s'| \sigma_{\boldsymbol{v}}^\mu |s'\rangle = \langle s| \sigma_{\boldsymbol{v}}^\mu \sigma_{\boldsymbol{m}}^\nu |s\rangle \tag{2.72}$$

Proof. From Eq.(2.70) we draw

$$\langle s'| \sigma_{\boldsymbol{v}}^\mu |s'\rangle = \frac{\langle s| P_{\boldsymbol{m}}^\nu \sigma_{\boldsymbol{v}}^\mu P_{\boldsymbol{m}}^\nu |s\rangle}{\langle s| P_{\boldsymbol{m}}^\nu |s\rangle} = \frac{\langle s| P_{\boldsymbol{m}}^\nu \sigma_{\boldsymbol{v}}^\mu |s\rangle}{\langle s| P_{\boldsymbol{m}}^\nu |s\rangle}$$
$$= \frac{\langle s| \sigma_{\boldsymbol{v}}^\mu |s\rangle + \langle s| \sigma_{\boldsymbol{v}}^\mu \sigma_{\boldsymbol{m}}^\nu |s\rangle}{1 + \langle s| \sigma_{\boldsymbol{m}}^\nu |s\rangle}, \tag{2.73}$$

where we used the fact that $P_{\boldsymbol{m}}^\nu$ and $\sigma_{\boldsymbol{v}}^\mu$ commute with each other, and that $P_{\boldsymbol{m}}^\nu$ is idempotent. By hypothesis, proposition 1.2.2 applies here, hence our Theorem. $\square$

Corollary. *If $|s\rangle$ is maximally entangled in ν and μ, and $\exists\, \boldsymbol{v}^\mu$ such that $|\langle s|\, \sigma_{\boldsymbol{v}}^\mu \sigma_{\boldsymbol{m}}^\nu\, |s\rangle\,| = 1$, then the measurement of ν along the axis $\boldsymbol{m}^\nu$ completely breaks the entanglement of μ, i.e. $E_\mu\big(\,|s'\rangle\,\big) = 0$.*

Proof. If Theorem 2.3.1 applies, we can rewrite the post-measurement ED of μ

$$E_\mu\big(\,|s'\rangle\,\big) = 1 - \max_{\boldsymbol{v}^\mu} |\langle s|\, \sigma_{\boldsymbol{v}}^\mu \sigma_{\boldsymbol{m}}^\nu\, |s\rangle\,|^2, \tag{2.74}$$

which equates 0 if the above condition is fulfilled. $\qquad\square$

Theorem 2.3.2. *For any state $|s\rangle$, $\forall \mu, \nu \in Q$ such that $\langle s|\, \sigma_{\boldsymbol{v}}^\mu \sigma_{\boldsymbol{v}}^\nu\, |s\rangle = 1$, the operators $\sigma_{\boldsymbol{v}}^\mu$ and $\sigma_{\boldsymbol{v}}^\nu$ are equivalent with respect to $|s\rangle$ (they act on it in the same fashion). In particular, this implies, $\forall \eta$,*

$$\langle s|\, \sigma_{\boldsymbol{v}}^\eta \sigma_{\boldsymbol{v}}^\nu\, |s\rangle = \langle s|\, \sigma_{\boldsymbol{v}}^\eta \sigma_{\boldsymbol{v}}^\mu\, |s\rangle\,, \tag{2.75}$$
$$\text{and}\ \ \langle s|\, \sigma_{\boldsymbol{v}}^\eta \sigma_{\boldsymbol{v}}^\mu \sigma_{\boldsymbol{v}}^\nu\, |s\rangle = \langle s|\, \sigma_{\boldsymbol{v}}^\eta\, |s\rangle\,. \tag{2.76}$$

It also results that the measure of $\sigma_{\boldsymbol{v}}^\nu$ yields the implicit measure of $\sigma_{\boldsymbol{v}}^\mu$.

Proof. By hypothesis, $|s\rangle$ is eigenvector of $\sigma_{\boldsymbol{v}}^\mu \sigma_{\boldsymbol{v}}^\nu$ of eigenvalue 1, and the following holds

$$\begin{aligned}
\sigma_{\boldsymbol{v}}^\mu \sigma_{\boldsymbol{v}}^\nu\, |s\rangle &= |s\rangle \\
\sigma_{\boldsymbol{v}}^\nu\, |s\rangle &= \sigma_{\boldsymbol{v}}^\mu\, |s\rangle \\
P_{\boldsymbol{v}}^\nu\, |s\rangle &= P_{\boldsymbol{v}}^\mu\, |s\rangle \\
P_{\boldsymbol{v}}^\nu\, |s\rangle &= P_{\boldsymbol{v}}^\nu P_{\boldsymbol{v}}^\mu\, |s\rangle\,.
\end{aligned} \tag{2.77}$$

$\qquad\square$

Let us now examine the consequences of these results on g. Its structure gives valuable insights on *persistency of entanglement P_e* in such maximally entangled states. First introduced in [25], it quantifies the minimal number of measurements needed to completely disentangle a quantum state. For the sake of clarity, we will hereafter drop dependence and adopt the shortened notation $g_{\nu\mu}\big(\,|s\rangle\,, \boldsymbol{v}^\mu, \boldsymbol{v}^\nu\big) = g_{\nu\mu}$.

Theorem 2.3.3. *Let $|s\rangle$ be a state maximally entangled $\forall \mu \in Q$ and $\{\boldsymbol{v}^\mu\}_\mu$ a choice of measurement directions such that $\forall \mu, \nu \in Q$, $g_{\mu\nu} = 0$ or ± 1. Then:*

- *Up to a reordering of its indices (equivalently, a relabelling of the qubits), g is diagonal by blocks filled with ± 1.*

- *The number n of such blocks provides an upper bound to the persistency of entanglement P_e of the state $|s\rangle$, i.e. $P_e \leq n$. In other words, the minimal number of local measurements necessary to fully break its entanglement is n or less.*

Proof. From proposition 1.2.2, it is clear that $\forall \mu, \nu \in Q$, Eq.(2.16) simplifies as

$$g_{\nu\mu} = \langle s | \sigma_{\boldsymbol{v}}^{\mu} \sigma_{\boldsymbol{v}}^{\nu} | s \rangle, \tag{2.78}$$

and, from Theorem 2.3.2, we see that $\forall \eta \in Q$, the following transitivity relation holds

$$|g_{\nu\mu}| = |g_{\nu\eta}| = 1 \implies |g_{\mu\eta}| = 1 \tag{2.79}$$

Added with the symmetry of g, this proves the first part of the Theorem.

Using Theorem 2.3.1 together with Eq.(2.78), we can rewrite the diagonal elements of g after a measure of $\sigma_{\boldsymbol{m}}^{\nu}$ as

$$g'_{\mu\mu} = 1 - |g_{\nu\mu}|^2 \tag{2.80}$$

where $g' = g(|s'\rangle)$. This straightforwardly implies that all diagonal elements of a block vanish after the measurement, along the appropriate direction, of any qubit belonging to the block, hence breaking entanglement of the whole block.

To complete our proof, we now need to show that the correlations in the other blocks cannot decrease after such a measurement. Consider two qubits μ and η that do not belong to the same block as ν, that is $g_{\mu\nu} = g_{\eta\nu} = 0$. Applying Theorem 2.3.1 to a correlator instead of a single qubit expectation value yields $\langle s' | \sigma_{\boldsymbol{v}}^{\mu} \sigma_{\boldsymbol{v}}^{\eta} | s' \rangle = \langle s | \sigma_{\boldsymbol{v}}^{\mu} \sigma_{\boldsymbol{v}}^{\eta} | s \rangle + \langle s | \sigma_{\boldsymbol{v}}^{\mu} \sigma_{\boldsymbol{v}}^{\eta} \sigma_{\boldsymbol{m}}^{\nu} | s \rangle$, and the post-measurement off-diagonal terms hence write

$$\begin{aligned} g'_{\mu\eta} &= \langle s' | \sigma_{\boldsymbol{v}}^{\mu} \sigma_{\boldsymbol{v}}^{\eta} | s' \rangle - \langle s' | \sigma_{\boldsymbol{v}}^{\mu} | s' \rangle \langle s' | \sigma_{\boldsymbol{v}}^{\eta} | s' \rangle \\ &= \langle s | \sigma_{\boldsymbol{v}}^{\mu} \sigma_{\boldsymbol{v}}^{\eta} | s \rangle + \langle s | \sigma_{\boldsymbol{v}}^{\mu} \sigma_{\boldsymbol{v}}^{\eta} \sigma_{\boldsymbol{m}}^{\nu} | s \rangle - \langle s | \sigma_{\boldsymbol{v}}^{\mu} \sigma_{\boldsymbol{m}}^{\nu} | s \rangle \langle s | \sigma_{\boldsymbol{v}}^{\eta} \sigma_{\boldsymbol{m}}^{\nu} | s \rangle \\ &= g_{\mu\eta} + \langle s | \sigma_{\boldsymbol{v}}^{\mu} \sigma_{\boldsymbol{v}}^{\eta} \sigma_{\boldsymbol{m}}^{\nu} | s \rangle \end{aligned} \tag{2.81}$$

If, furthermore, μ and η belonged to the same block, i.e. $g_{\mu\eta} = \pm 1$, Theorem 2.3.2 applies [1] and we have $\langle s | \sigma_{\boldsymbol{v}}^{\mu} \sigma_{\boldsymbol{v}}^{\eta} \sigma_{\boldsymbol{m}}^{\nu} | s \rangle = \pm \langle s | \sigma_{\boldsymbol{m}}^{\nu} | s \rangle = 0$, hence

$$g'_{\mu\eta} = \begin{cases} g_{\mu\eta} & \text{if } g_{\mu\eta} = \pm 1, \\ \langle s | \sigma_{\boldsymbol{v}}^{\mu} \sigma_{\boldsymbol{v}}^{\eta} \sigma_{\boldsymbol{m}}^{\nu} | s \rangle & \text{if } g_{\mu\eta} = 0. \end{cases} \tag{2.82}$$

It results that the measure of $\sigma_{\boldsymbol{m}}^{\nu}$ preserves or enlarges the size of remaining blocks, implying $n' \leq n - 1$, with n' the number of blocks in the post-measurement EM g'. At most one measurement by block is thus sufficient to fully break the entanglement of $|s\rangle$, and we have $P_e \leq n$, the second part of the theorem. $\qquad\square$

Remark that, in addition to the inequality $n' \leq n - 1$, a set $\{\boldsymbol{v}^{\mu}\}_{\mu}$ minimizing n for a given g, may not minimize n' for g', a post-measurement EM. It results that an optimally disentangling sequence of measurements cannot in general be found by an optimization procedure carried onto g.

---

[1] As $-\sigma_{\boldsymbol{v}}^{\mu} = \sigma_{-\boldsymbol{v}}^{\mu}$, Theorem 2.3.2 can easily be extended to negative correlators.

The notion of *persistency of entanglement* is distinct from that of *k-separability*[2]. They are however related, as the entanglement of a maximally entangled k-separable state can clearly be fully broken by k measurements. In other words, the persistency of entanglement provides an upper bound to the separability, and we have

$$k \leq P_e \leq n, \tag{2.83}$$

with $n, P_e, k \in \mathbb{N}^*$. As these three quantities are positive integers, both inequalities are saturated if $n = 1$, i.e. $k = P_e = n = 1$. Furthermore, since $n' \leq n - 1$, $n = 2 \implies n' = 1$, hence the second inequality is saturated for $n = 2$, i.e. $k \leq P_e = n = 2$.

Because g only encodes information on the effects of first order projective measurement (i.e. contains only two-point correlators), it may not capture the actual P_e, hence only provides an upper bound. This is due to the fact that new non-vanishing correlation patterns may arise after one or more projective measurements, entailing diminished P_e relative to our first guess. The Briegel Raussendorf state with $N > 4$, detailed in Section 2.3.3.1, constitutes an example of such a situation.

Let us stress the dependence of g on the set of unit vectors $\{\boldsymbol{v}^\mu\}$, representing directions of measurements. This point is of great importance because, as a different g will arise from a different set $\{\boldsymbol{v}^\mu\}$, such are also the correlation patterns and subsequent entanglement breaking highlighted in the above. In order to bound P_e as finely as possible, we thus need to find the appropriate set $\{\boldsymbol{v}^\mu\}$.

2.3.2. Optimization of the measure

We are now looking for the measurement directions $\boldsymbol{v}^\nu$ optimizing the spin correlators.

First, let us perform the pairwise optimization of the correlators

$$\langle s| \sigma_{\boldsymbol{v}}^\mu \sigma_{\boldsymbol{v}}^\nu |s\rangle = \sum_{i,j=1}^{3} v_i^\mu v_j^\nu \langle s| \sigma_i^\mu \sigma_j^\nu |s\rangle = (\boldsymbol{v}^\mu)^T \boldsymbol{C}_s^{\mu\nu} \boldsymbol{v}^\nu, \tag{2.84}$$

where $\boldsymbol{C}_s^{\mu\nu}$ is the non-symmetric real matrix of elements

$$\left(\boldsymbol{C}_s^{\mu\nu}\right)_{ij} = \langle s| \sigma_i^\mu \sigma_j^\nu |s\rangle \tag{2.85}$$

i.e. the spin correlation matrix. Optimization with respect to both measurement

---

[2]As a counter example, the state $\frac{1}{2}\big(|0000\rangle + |0011\rangle + |1100\rangle - |1111\rangle\big)$ has an EM with $n = 2$ blocks when $\forall \mu$, $\boldsymbol{v}^\mu = (0, 0, 1)$, hence has $P_e = 2$ and yet is not biseparable.

axis yields

$$\begin{aligned}
\boldsymbol{C}_s^{\mu\nu}\boldsymbol{v}^\nu &= \lambda\boldsymbol{v}^\mu \\
(\boldsymbol{v}^\mu)^T\boldsymbol{C}_s^{\mu\nu} &= \lambda(\boldsymbol{v}^\nu)^T,
\end{aligned} \tag{2.86}$$

where the superscript T stands for transpose. It can easily be checked by direct calculation that the eigenvalues indeed coincide. By the insertion of the transpose of these two equations, we infer the eigenvalue equations

$$\begin{aligned}
(\boldsymbol{C}_s^{\mu\nu})^T\boldsymbol{C}_s^{\mu\nu}\boldsymbol{v}^\nu &= \lambda^2\boldsymbol{v}^\nu \\
\boldsymbol{C}_s^{\mu\nu}(\boldsymbol{C}_s^{\mu\nu})^T\boldsymbol{v}^\mu &= \lambda^2\boldsymbol{v}^\mu,
\end{aligned} \tag{2.87}$$

of which the largest eigenvalue solutions evidently correspond to the measurement directions optimizing Eq.(2.84). Note that λ is not necessarily positive. However, this is of no importance, as it is always enough, in order to recover a positive correlator (2.84), to replace one of the two measurement vectors by its opposite. For our analysis, negative correlations are in fact equivalent to positive ones, as they possess the same significance relatively to entanglement and the effect of projective measurement.

We can instead be interested in finding the measurement axis $\boldsymbol{m}^\nu$ that optimally disentangle the entire state $|s\rangle$. Provided the latter is maximally entangled, we have, as a consequence of Theorem 2.3.1

$$\left|\langle s'|\,\boldsymbol{\sigma}^\mu\,|s'\rangle\,\right|^2 = \sum_{i=1}^3 \left|\,\langle s'|\,\sigma_i^\mu\,|s'\rangle\,\right|^2 = \sum_{i=1}^3 \left|\,\langle s|\,\sigma_i^\mu\sigma_{\boldsymbol{m}}^\nu\,|s\rangle\,\right|^2, \tag{2.88}$$

as each $\langle s'|\,\sigma_i^\mu\,|s'\rangle$ can simply be seen as a special case of Eq.(2.72), with $v_j^\mu = \delta_{ij}$. Hence the total entanglement after the measure

$$\begin{aligned}
E\big(|s'\rangle\big) &= \sum_\mu E_\mu(|s'\rangle) = N - 1 - \sum_{\mu\in\nu^C} |\,\langle s'|\,\boldsymbol{\sigma}^\mu\,|s'\rangle\,|^2 \\
&= N - 1 - \sum_{\mu\in\nu^C}\sum_{i=1}^3 \left|\,\langle s|\,\sigma_i^\mu\sigma_{\boldsymbol{m}}^\nu\,|s\rangle\,\right|^2 \\
&= N - 1 - \sum_{\mu\in\nu^C}\sum_{i=1}^3 \langle s|\,\sigma_{\boldsymbol{m}}^\nu\sigma_i^\mu\,|s\rangle\,\langle s|\,\sigma_i^\mu\sigma_{\boldsymbol{m}}^\nu\,|s\rangle \\
&= N - 1 - \langle s|\,\sigma_{\boldsymbol{m}}^\nu\bigg(\sum_{\mu\in\nu^C}\sum_{i=1}^3 \sigma_i^\mu\,|s\rangle\,\langle s|\,\sigma_i^\mu\bigg)\sigma_{\boldsymbol{m}}^\nu\,|s\rangle \\
&= N - 1 - \sum_{j,k=1}^3 m_j^\nu m_k^\nu\,\langle s|\,\sigma_j^\nu\bigg(\sum_{\mu\in\nu^C}\sum_{i=1}^3 \sigma_i^\mu\,|s\rangle\,\langle s|\,\sigma_i^\mu\bigg)\sigma_k^\nu\,|s\rangle\,,
\end{aligned} \tag{2.89}$$

with $\nu^C = Q \setminus \{\nu\}$. Let us define $\boldsymbol{B}_s^\nu$, the measurement-induced entanglement breaking matrices (MIEB) of the state $|s\rangle$, of elements

$$\left(\boldsymbol{B}_s^\nu\right)_{jk} = \langle s| \sigma_j^\nu \, \Sigma_s^{\nu^C} \, \sigma_k^\nu \, |s\rangle, \tag{2.90}$$

with $\Sigma_s^{\nu^C} = \sum_{\mu \in \nu^C} \sum_{i=1}^{3} \sigma_i^\mu \, |s\rangle \, \langle s| \, \sigma_i^\mu$. Its diagonalization straightforwardly yields the results of the optimization problem, as the eigenvectors $\widetilde{\boldsymbol{m}}^\nu$ associated with the largest (resp. smallest) eigenvalue of $\boldsymbol{B}^\nu\big(|s\rangle\big)$ corresponds to the minimum (resp. maximum) of Eq.(2.89). The eigenvalues themselves simply equate the total additional loss of entanglement after the corresponding measurement. It results that a comparison of the spectra of the N MIEB matrices allow to easily find the "weak spots" of $|s\rangle$, that is the qubits of which the measurement can break entanglement the most.

Interestingly, the largest eigenvalue of $\boldsymbol{B}_s^\nu$ might have multiplicity greater than one. In such cases, any of the corresponding eigenvectors or linear combination of them maximize Eq.(2.89).

This result can straightforwardly be adapted to find the measurement axis optimizing the entanglement breaking of a subset $Q' \subset Q$ with $\nu \notin Q'$, by simply replacing $\Sigma_s^{\nu^C}$ with $\Sigma_s^{Q'} = \sum_{\mu \in Q'} \sum_{i=1}^{3} \sigma_i^\mu \, |s\rangle \, \langle s| \, \sigma_i^\mu$.

The question naturally arises as to know whether the solutions of Eq.(2.84) correspond in general to those of Eq.(2.89).

Remark. *The existence, in the general case, of one (or several) set of measurement axes $\{\boldsymbol{v}^\nu\}_\nu^{opt}$ optimizing simultaneously every correlator in the EM remains unclear.* [3]

- *If $\{\boldsymbol{v}^\nu\}_\nu^{opt}$ indeed always exists, it would be enough, to completely probe the pairwise correlation patterns of a given state, to solve $\lceil N/2 \rceil$ equations of the form of Eq.(2.84) or, equivalently, to diagonalize N MIEB (2.90).*

- *If, on the contrary, it does not, such a complete probing requires to solve all of the $N(N-1)/2$ equations of the form of Eq.(2.84).*

Yet, in all of the examples we considered, the solutions of Eq.(2.84) equate those of Eq.(2.89), hence we were able to determine $\{\boldsymbol{v}^\nu\}_\nu^{opt}$. We were not able to find any counter-example. We will thus assume from now on that this set exists, in particular in Section 2.3.3, as this assumption allows us to remain much more concise, by only diagonalizing the N MIEB.

---

[3]To clarify the meaning of this problem, let us imagine a state $|s\rangle$ such that $\nexists \{\boldsymbol{v}^\nu\}_\nu^{opt}$. Then there exists some qubit μ of which the correlation with ν is maximal in a direction v_1^μ, and the correlation with $\eta \neq \nu$ is maximal in a direction $v_2^\mu \neq v_1^\mu$.

2.3.3. Examples

2.3.3.1. Briegel-Raussendorf states

The Briegel-Raussendorf states (BRS) form a family of quantum states, introduced in [25], They are, up to LU transformation, equivalent to cluster states (also coined as graph states in the literature), which were proposed as a model for the measurement-based quantum computer [64, 63, 66, 65].

BRS are defined, for an arbitrary number of qubits N on a d-dimensional lattice, as

$$|\phi(\varphi)\rangle = U(\varphi) |+\rangle^{\otimes N}, \tag{2.91}$$

where $|+\rangle^{\mu}$ is the eigenstate of the operator σ_1^{μ} of eigenvalue 1, and

$$U(\varphi) = \exp\left\{ - i\varphi \sum_{<\mu,\nu>} P_0^{\mu} P_1^{\nu} \right\}, \tag{2.92}$$

where the summation runs over all the pairs of nearest neighbours, and $P_{0(1)}^{\mu}$ is the projector onto the eigenstates of σ_3^{μ} of eigenvalue ± 1. We are solely interested in the case $\varphi = \pi$, as it results in a maximally entangled state. We will, furthermore, restrict ourselves to the study of the 1-dimensional case.

$$|\phi_N\rangle = \prod_{\mu=0}^{N-2} \frac{1}{2} \Big(\mathbb{I} - \sigma_3^{\mu} + \sigma_3^{\mu+1} + \sigma_3^{\mu} \sigma_3^{\mu+1} \Big) |+\rangle^{\otimes N}. \tag{2.93}$$

It has been shown in [56] that the $E_{\mu}(|\phi_N\rangle) = 0$, $\forall \mu$.

$N = 3$. It is known that the 3-qubit BR state is LU equivalent to the Greenberger-Horne-Zeilinger state [25], a prototypical example of maximally entangled and maximally correlated state. We hence expect that $\exists \{\boldsymbol{v}^{\mu}\}$ such that $\forall \mu, \nu$, $g_{\mu\nu} = 1$.

We only need to compute the three following MIEB matrices (2.90)

$$\begin{aligned}
\boldsymbol{B}_{\phi_3}^0 = \boldsymbol{B}_{\phi_3}^2 &= \begin{pmatrix} 2 & 0 & 0 \\ 0 & 0 & 0 \\ 0 & 0 & 0 \end{pmatrix}, \text{ hence } \boldsymbol{v}^0 = \boldsymbol{v}^2 = (1,0,0), \text{ and} \\
\boldsymbol{B}_{\phi_3}^1 &= \begin{pmatrix} 0 & 0 & 0 \\ 0 & 0 & 0 \\ 0 & 0 & 2 \end{pmatrix}, \text{ hence } \boldsymbol{v}^1 = (0,0,1).
\end{aligned} \tag{2.94}$$

The maximal eigenvalues of these matrices equate 2 because each qubit is maximally correlated with two others.

This yields the optimal EM

$$\tilde{g}\left(\,|\phi_3\rangle\,\right) = \begin{pmatrix} 1 & 1 & -1 \\ 1 & 1 & -1 \\ -1 & -1 & 1, \end{pmatrix} \tag{2.95}$$

thus, evidently, $n(|\phi_3\rangle) = 1$, hence saturating the inequality (2.83): $k(|\phi_3\rangle) = P_e(|\phi_3\rangle) = n(|\phi_3\rangle) = 1$. A single measurement is thus sufficient to completely disentangle $|\phi_3\rangle$, and this state is genuinely entangled.

$N = 4$. In this case, we have

$$\boldsymbol{B}_{\phi_4}^0 = \boldsymbol{B}_{\phi_4}^3 = \begin{pmatrix} 1 & 0 & 0 \\ 0 & 0 & 0 \\ 0 & 0 & 0 \end{pmatrix}, \text{ hence } \boldsymbol{v}^0 = \boldsymbol{v}^3 = (1, 0, 0), \text{ and}$$

$$\boldsymbol{B}_{\phi_4}^1 = \boldsymbol{B}_{\phi_4}^2 = \begin{pmatrix} 0 & 0 & 0 \\ 0 & 0 & 0 \\ 0 & 0 & 1 \end{pmatrix}, \text{ hence } \boldsymbol{v}^1 = \boldsymbol{v}^2 = (0, 0, 1), \tag{2.96}$$

thus the optimal EM writes

$$\tilde{g}\left(\,|\phi_4\rangle\,\right) = \begin{pmatrix} 1 & 1 & 0 & 0 \\ 1 & 1 & 0 & 0 \\ 0 & 0 & 1 & -1 \\ 0 & 0 & -1 & 1 \end{pmatrix}, \tag{2.97}$$

hence $n(|\phi_4\rangle) = 2$, so $k(|\phi_4\rangle) \leq P_e(|\phi_4\rangle) = n(|\phi_4\rangle) = 2$. Entanglement can be broken with at least two measurements, and it is genuinely entangled or biseparable.

$N > 4$. In general, for a chain of N qubits, we have

$$\boldsymbol{B}_{\phi_N}^0 = \boldsymbol{B}_{\phi_N}^N = \begin{pmatrix} 1 & 0 & 0 \\ 0 & 0 & 0 \\ 0 & 0 & 0 \end{pmatrix}, \text{ hence } \boldsymbol{v}^0 = \boldsymbol{v}^N = (1, 0, 0), \text{ and}$$

$$\boldsymbol{B}_{\phi_N}^1 = \boldsymbol{B}_{\phi_N}^{N-1} = \begin{pmatrix} 0 & 0 & 0 \\ 0 & 0 & 0 \\ 0 & 0 & 1 \end{pmatrix}, \text{ hence } \boldsymbol{v}^1 = \boldsymbol{v}^{N-1} = (0, 0, 1), \tag{2.98}$$

while $\boldsymbol{B}_{\phi_N}^\nu = \boldsymbol{0}$, $\forall \nu \notin \{0, 1, N-1, N\}$.

The EM hence contains two 2×2 blocks in its upper left and lower right corners, while the remaining part is just a diagonal filled with ones (which can be seen as trivial blocks of size 1×1), hence the number of its blocks is

$n(|\phi_N\rangle) = N - 2 \geq P_e(|\phi_N\rangle) \geq k(|\phi_N\rangle)$. Its persistency of entanglement is known to be $P_e(|\phi_N\rangle) = \lfloor \frac{N}{2} \rfloor$ [25].

Let us investigate further this discrepancy. From Eq. (2.93), it can be easily verified that the projective measure of qubit 1 along the axis $(0, 0, 1)$ yields

$$P_3^1 |\phi_N\rangle = |+\rangle \otimes |0\rangle \otimes \left(\sigma_3^2 |\phi_{N-2}\rangle \right), \tag{2.99}$$

where σ_3^2 applies to the third qubit of the N-long chain, hence to the first of the $(N - 2)$-long chain. Such a post-measurement state is hence LU equivalent to a product of two separated qubits with one BR chain of size $N - 2$. Considering for instance $N = 5$ we have, using the measurement axis' determined above, the optimal EM

$$\tilde{g}\left(|\phi_5\rangle \right) = \begin{pmatrix} 1 & 1 & 0 & 0 & 0 \\ 1 & 1 & 0 & 0 & 0 \\ 0 & 0 & 1 & 0 & 0 \\ 0 & 0 & 0 & 1 & -1 \\ 0 & 0 & 0 & -1 & 1 \end{pmatrix} \tag{2.100}$$

thus $n(|\phi_5\rangle) = 3$. Yet, after a projective measurement of σ_3^1, the optimal EM of the new state is, up to some irrelevant signs, the same as Eq.(2.95), added with the two extra qubits now disentangled from the rest of the chain.

$$\tilde{g}\left(P_3^1 |\phi_5\rangle \right) = \begin{pmatrix} 0 & 0 & 0 & 0 & 0 \\ 0 & 0 & 0 & 0 & 0 \\ 0 & 0 & 1 & -1 & 1 \\ 0 & 0 & -1 & 1 & -1 \\ 0 & 0 & 1 & -1 & 1, \end{pmatrix} \tag{2.101}$$

so $n(P_3^1 |\phi_5\rangle) = n(|\phi_3\rangle) = 1$. Thus we have $P_e(|\phi_5\rangle) = 2$.

This constitutes a paradigmatic example of the fact that Theorem 2.3.3 is in general insufficient to capture exactly P_e. Measurements can indeed be performed on $|\phi_N\rangle$, after which some elements of the EM will cease to be null. The post-measurement EM thus exhibits some new non-trivial blocks, accounting for this discrepancy.

2.3.3.2. Supersinglet States

The supersinglet states, first introduced in [67], form a class of maximally entangled pure states with the property of being invariant under any simultaneous LU operation acting on all qubits, i.e. $U^{\otimes N} |S_N\rangle = e^{i\phi} |S_N\rangle$, with U an arbitrary LU operator. [67, 68].

From this sole property, a number of facts can be drawn.

First, $\forall U$, $\forall \boldsymbol{v}^\nu$, we have

$$
\begin{aligned}
\langle S_N | \, \sigma_{\boldsymbol{v}}^\nu \, | S_N \rangle &= \langle S_N | \, U^{\dagger \otimes N} \sigma_{\boldsymbol{v}}^\nu U^{\otimes N} \, | S_N \rangle \\
&= \langle S_N | \, U^{\nu \dagger} \sigma_{\boldsymbol{v}}^\nu U^\nu \, | S_N \rangle = \langle S_N | \, \sigma_{\boldsymbol{v}'}^\nu \, | S_N \rangle \,,
\end{aligned}
\tag{2.102}
$$

yet Pauli expectation values cannot be isotropic unless null, hence $E_\nu(|S_N\rangle) = 1$, $\forall \nu$.

Theorem 2.3.1 hence applies here and, choosing U to be a rotation around the axis $\boldsymbol{m}^\nu$, hence leaving $\sigma_{\boldsymbol{m}}^\nu$ unchanged, we can write

$$
\begin{aligned}
\langle S_N' | \, \sigma_{\boldsymbol{v}}^\mu \, | S_N' \rangle &= \langle S_N | \, \sigma_{\boldsymbol{v}}^\mu \sigma_{\boldsymbol{m}}^\nu \, | S_N \rangle \\
&= \langle S_N | \, U^{\dagger \otimes N} \sigma_{\boldsymbol{v}}^\mu \sigma_{\boldsymbol{m}}^\nu U^{\otimes N} \, | S_N \rangle \\
&= \langle S_N | \left(U^{\mu \dagger} \sigma_{\boldsymbol{v}}^\mu U^\mu \right) \sigma_{\boldsymbol{m}}^\nu \, | S_N \rangle \\
&= \langle S_N | \, \sigma_{\boldsymbol{v}'}^\mu \sigma_{\boldsymbol{m}}^\nu \, | S_N \rangle = \langle S_N' | \, \sigma_{\boldsymbol{v}'}^\mu \, | S_N' \rangle \,,
\end{aligned}
\tag{2.103}
$$

where $|S_N'\rangle$ is the state post-measurement of $\sigma_{\boldsymbol{m}}^\nu$. The same argument as above leads to $\langle S_N | \, \sigma_{\boldsymbol{v}}^\mu \sigma_{\boldsymbol{m}}^\nu \, | S_N \rangle \neq 0$ if and only if $\boldsymbol{v}^\mu = \boldsymbol{v}^{\mu\prime}$, that is if $\boldsymbol{v}^\mu = \pm \boldsymbol{m}^\nu$.

It results $\boldsymbol{B}_{S_N}^\mu \propto \mathbb{I}$, $\forall \mu \in Q$. This means that, provided that the qubits are measured along the same axis, the correlators are always maximal. The optimal set of measurement axis is thus any uniform set $\{\boldsymbol{v}^\mu\}^{uni}$.

The whole class of supersinglet states of four qubits is spanned by the following two states

$$
\begin{aligned}
|S_4^1\rangle &= \frac{1}{\sqrt{3}} \Big(|0011\rangle + |1100\rangle - \frac{1}{2} \big(|0101\rangle + |0110\rangle + |1001\rangle + |1010\rangle \big) \Big) \\
|S_4^2\rangle &= \frac{1}{2} \Big(|0101\rangle + |1010\rangle - |0110\rangle - |1001\rangle \big) \Big).
\end{aligned}
\tag{2.104}
$$

We can hence write a general 4-qubit supersinglet state as $|S_4(a,b)\rangle = a\,|S_4^1\rangle + b\,|S_4^2\rangle$, with $|a|^2 + |b|^2 = 1$.

We can choose arbitrarily a single measurement axis, for instance $\boldsymbol{x} = (1,0,0)$, and straightforwardly compute the optimal EM

$$
\tilde{g}\big(|S_4(a,b)\rangle\big) = \begin{pmatrix} 1 & \alpha & \gamma & \beta \\ \alpha & 1 & \beta & \gamma \\ \gamma & \beta & 1 & \alpha \\ \beta & \gamma & \alpha & 1 \end{pmatrix},
\tag{2.105}
$$

with

$$\alpha = \frac{|a|^2}{3} - |b|^2,$$

$$\beta = \frac{2}{3}\big(\sqrt{3}\,\mathrm{Re}(\bar{a}b) - |a|^2\big), \text{ and} \qquad (2.106)$$

$$\gamma = -\frac{2}{3}\big(\sqrt{3}\,\mathrm{Re}(\bar{a}b) + |a|^2\big),$$

where the bar over a letter denotes complex conjugation and $\mathrm{Re}(\bar{a}b)$ is the real part of the complex number $\bar{a}b$.

This simple expression for the EM allows us to remark some interesting cases arising for specific values of the parameters a and b.

Trivially, if $a = 0$ and $|b| = 1$, we immediately get a block diagonal matrix containing two blocks, as is to be expected, since $|S_4^{(2)}\rangle$ is a tensor product of two Bell states $|\phi_-\rangle = \frac{1}{\sqrt{2}}(|01\rangle - |10\rangle)$. In this case, we thus have $n(|S_4(0,1)\rangle) = P_e(|S_4(0,1)\rangle) = 2$ and the state is, of course, biseparable.

Setting $a = \frac{\sqrt{3}e^{i\phi_a}}{2}$ and $b = \frac{e^{i\phi_b}}{2}$, a few calculations lead to

$$\tilde{g}\Big(|S_4(\phi_a, \phi_b)\rangle\Big) = \begin{pmatrix} 1 & 0 & -c^2 & -s^2 \\ 0 & 1 & -s^2 & -c^2 \\ -c^2 & -s^2 & 1 & 0 \\ -s^2 & -c^2 & 0 & 1 \end{pmatrix}, \qquad (2.107)$$

with $c = \cos\left(\frac{\phi_a - \phi_b}{2}\right)$ and $s = \sin\left(\frac{\phi_a - \phi_b}{2}\right)$. Thus, for $\phi_a = \phi_b$ and for $\phi_b = \phi_a + \pi$, the optimal EM of this state, up to qubits permutations, contains two blocks, thus $n(|S_4(\phi_a, \phi_a)\rangle) = P_e(|S_4(\phi_a, \phi_a)\rangle) = 2$ and $n(|S_4(\phi_a, \phi_a + \pi)\rangle) = P_e(|S_4((\phi_a, \phi_a + \pi)\rangle) = 2$.

2.3.4. Discussion

In this section, we showed how, in pure quantum states, entanglement entails a strong link between correlations and post-measurement expectation values.

The EMs, i.e. covariance matrices, contain valuable information on the statistics of post-measurement states, and on the patterns that can emerge from projective measurements of entangled states. In particular, its block structure is directly linked to the persistency of entanglement.

We further provided two straightforward procedures of optimization of the Pauli correlators, and observe that they might not, in principle, yield equivalent results. By doing so, we unravel an opened problem, which hasn't, to our best knowledge, been tackled with yet, namely the existence of a set of measurement axes simultaneously optimizing all of these correlators.

These procedures further allow us to recover, if it exists, the optimal EM, along

with an upper bound for the persistency of entanglement.

Unfortunately, as previously emphasized, the information retrieved by the use of the EM is incomplete: since the effect of more than one measurement are not accounted for in this framework, our approach fails to recover a number of important features of some complex entangled states (as BR states or cluster states), amongst which the exact persistency of entanglement.

Multipartite maximally entangled states might indeed possess qubits with only vanishing two-point correlations, regardless of the choice of measurement axes. Somehow counter-intuitively, the measurement of such qubits, though disentangling the concerned qubit from the rest of the system, do not break any entanglement on the latter. Yet it modifies the state, and in particular might bring along some new non-vanishing correlators (i.e. off-diagonal terms in the EM).

This observation motivates the study of higher order measurement schemes.

Let us consider an ordered subset $\mathcal{M} \subset Q$ of M qubits on which successive projective measurements are performed.

The generalization of (2.70) then yields

$$|s\rangle \longrightarrow |s^{\mathcal{M}}\rangle = \frac{\prod\limits_{\nu \in \mathcal{M}} P_{\boldsymbol{m}}^{\nu} |s\rangle}{\sqrt{\langle s| \prod\limits_{\nu \in \mathcal{M}} P_{\boldsymbol{m}}^{\nu} |s\rangle}}, \tag{2.108}$$

and, accordingly, the expectation value of an arbitrary unmeasured qubit μ after such a series of measurement

$$\langle s^{\mathcal{M}}| \sigma_{\boldsymbol{v}}^{\mu} |s^{\mathcal{M}}\rangle = \frac{\sum\limits_{k=0}^{M-1} \sum\limits_{X \in [\mathcal{M}]^k} \langle s| \sigma_{\boldsymbol{v}}^{\mu} \prod\limits_{\nu \in X} \sigma_{\boldsymbol{m}}^{\nu} |s\rangle}{\sum\limits_{k=0}^{M-1} \sum\limits_{X \in [\mathcal{M}]^k} \langle s| \prod\limits_{\nu \in X} \sigma_{\boldsymbol{m}}^{\nu} |s\rangle}, \tag{2.109}$$

where $[\mathcal{M}]^k$ is the set of all the unordered k-subsets (i.e. subsets of cardinal k) of $\mathcal{M}$.

It results that, if all the two-point correlators vanish, we can examine higher order correlators to investigate the breaking of entanglement after a series of measurement rather a single one.

It would be of great interest to pursue the work introduced in the present section by a thorough study of higher order covariance tensors, or to devise new procedures and methods, in order to grasp the effects of series of measurements on entangled states, in a more exhaustive fashion.

3. Quantum Correlation and Entanglement in Mixed States

The following chapter addresses the problem of measuring entanglement and quantum correlation in mixed states, mainly reproducing the original work we published in [34].

We start in Section 3.1, by adapting the construction developed in Chapter 2 to the framework of mixed states, thus obtaining a measure of quantum correlation, the *Quantum Correlation Distance* (QCD), and show that it fulfils most requirements for a *bona fide* measure. Section 3.2 proposes an original method to build, from the QCD, a measure of entanglement for mixed states, the *Regularized Entanglement Distance*, and shows that it is bounded from above by the quadratic-weights convex roof extension of the pure state Entanglement Distance. We apply in Section 3.3 these two measures to a series of simple examples. In Section 3.4, we present the so-called *local ancilla problem* that affects these two measures, and propose a simple modification to address it. Finally, we summarize and discuss our results in Section 3.5,

3.1. The Quantum Correlation Distance

We consider the Hilbert space $\mathcal{H} = \mathcal{H}^0 \otimes \mathcal{H}^1 \cdots \mathcal{H}^{M-1}$ tensor product of M two qubits Hilbert spaces. The Hilbert-Schmidt distance D between two general square matrices, A and B, is given by

$$D(A, B) = \sqrt{\frac{1}{2} \operatorname{Tr}[(A - B)^\dagger (A - B)]}. \tag{3.1}$$

We derive from the latter, the distance between two close density matrices of a quantum state in $\mathcal{H}$, by

$$d_{dm}^2(\rho, \rho + d\rho) = \frac{1}{2} \operatorname{Tr}\left[(d\rho)^\dagger (d\rho)\right]. \tag{3.2}$$

The Hilbert-Schmidt distance is not the only possible choice, e.g. the Bures' distance represents an appropriate alternative option. The infinitesimal variation

$d\rho$ of state ρ is

$$
\begin{aligned}
d\rho &= \sum_{j=0}^{M-1} d\tilde{U}^\mu \rho + \rho \sum_{\mu=0}^{M-1} d\tilde{U}^{\mu\dagger} \\
&= -i \sum_{\mu=0}^{M-1} \sum_{j=1}^{3} \left[\sigma_j^\mu, \rho \right] n_j^\mu d\xi^\mu \,,
\end{aligned}
\tag{3.3}
$$

where $[,]$ is the commutator, and $d\tilde{U}^\mu$ is as defined previously in Eq. (2.14). Here and in the following we use the notation $(\boldsymbol{\sigma_n})^\mu = (\boldsymbol{n}^\mu \cdot \boldsymbol{\sigma}^\mu)$, and for $\mu = 0, \dots, M-1$, we denote by σ_1^μ, σ_2^μ and σ_3^μ the three Pauli matrices operating on the μ-th qubit, where the index μ labels the spins. We have

$$
d_{dm}^2(\rho, \rho + d\rho) = \sum_{\mu,\nu=0}^{M-1} g_{\mu\nu}(\rho, \boldsymbol{n}) d\xi^\mu d\xi^\nu \,,
\tag{3.4}
$$

where

$$
g_{\mu\nu}(\rho, \boldsymbol{n}) = \frac{1}{2} \sum_{i,j=1}^{3} \mathrm{Tr}\left[\rho \left\{ \sigma_i^\mu, \sigma_j^\nu \right\} \rho - 2\rho\sigma_i^\mu \rho\sigma_j^\nu \right] n_i^\mu n_j^\nu \,,
\tag{3.5}
$$

with $\{,\}$ we mean the anticommutator. In particular, we have

$$
g_{\mu\mu}(\rho, \boldsymbol{n}^\mu) = \mathrm{Tr}\left(\rho^2 \right) - \sum_{i,j=1}^{3} \mathrm{Tr}\left[\rho\sigma_i^\mu \rho\sigma_j^\mu \right] n_i^\mu n_j^\mu \,.
\tag{3.6}
$$

We can now define $C_\mu(\rho)$, a measure of QCs deriving from a distance, that we thus name QC distance (QCD). The QCD of the subsystem μ for the state ρ is

$$
\begin{aligned}
C_\mu(\rho) &= \inf_{\{\boldsymbol{n}^\nu\}_\nu} g_{\mu\mu}(\rho, \boldsymbol{n}^\mu)) \\
&= \inf_{\{\boldsymbol{n}^\nu\}_\nu} \mathrm{Tr}\left(\rho^2 \right) - \mathrm{Tr}[\rho\sigma_{\boldsymbol{n}}^\mu \rho\sigma_{\boldsymbol{n}}^\mu] \,.
\end{aligned}
\tag{3.7}
$$

Finally, by defining the symmetric matrices $A^\mu(\rho)$, for $\mu = 0, \dots, M-1$, whose entries are

$$
A_{ij}^\mu(\rho) = \mathrm{Tr}\left[\rho\sigma_i^\mu \rho\sigma_j^\mu \right] \,,
\tag{3.8}
$$

we obtain the closed-form expression for the QCD of ρ,

$$
C_\mu(\rho) = \mathrm{Tr}\left(\rho^2 \right) - \lambda_{max}^\mu(\rho)
\tag{3.9}
$$

where $\lambda_{max}^\mu(\rho)$ is the maximum of the eigenvalues of $A^\mu(\rho)$. The QC is the minimum value of the trace of g under the variation of the unit vectors, and its value is therefore invariant under LU transformations.

3. Quantum Correlation and Entanglement in Mixed States

We further define the total QCD

$$C(\rho) = \sum_{\mu=0}^{M-1} C_\mu(\rho). \tag{3.10}$$

The QCD is a directly computable measure of the degree of QCs of ρ. Remarkably, Eq. (3.9) contains two competing terms. The first term is named Purity, which takes account of the degree of statistical mixing of ρ, its upper bound 1 corresponds to a pure state. The second term ranges between 0 and 1, and derives from the degree of correlation of ρ, with the lower value, 0, corresponding to the higher correlation.

The time complexity of the closed-form formula for the QCD is that of $D \times D$ matrix multiplications, that is $o(D^3)$, where D is the dimension of the full Hilbert space. In particular, the QCD possesses a closed formula and does not require any optimization (other than finding the largest eigenvalue of 3×3 matrices). This is in contrast with other measures of QC which, to our best knowledge, all require time-costly optimization procedures, except for some specific classes of states [23].

The QCD (3.9) fulfils requirements **C1**, **C2** and **C3** for a *bona fide* measure of QC [23]:

1. $C_\mu(\rho) = 0$ if $\rho \in \mathcal{C}_\mu$, i.e. if ρ is classical in the subsystem μ. Indeed, $\forall \rho \in \mathcal{C}_\mu$ we can write $\rho = \sum_k p_k \rho_k^{\mu_C} \otimes |k\rangle\langle k|^\mu$, where the $\{|k\rangle^\mu\}$ form an orthonormal basis in $\mathcal{H}^\mu$, μ_C is the complement of the subsystem μ and $\sum_k p_k = 1$. Then $\exists \boldsymbol{n}^\mu$ such that $\forall k$, $\boldsymbol{n}^\mu \cdot \boldsymbol{\sigma}^\mu |k\rangle^\mu = \pm 1$, hence $\lambda_{max}^\mu(\rho) = 1$ and $C_\mu(\rho) = 0$. It results that $C(\rho) = 0$ if $\rho \in \mathcal{C}$, i.e. if ρ is fully classical.

2. $C(U\rho U^\dagger) = C(\rho)$, i.e. it is invariant under LU transformations.

3. In the case of a pure state $\rho = |\psi\rangle\langle\psi|$, $C(|\psi\rangle\langle\psi|)$ reduces to the ED for pure states defined in section 2.2.

Requirement **C4** is not *per se* satisfied by the QCD, because of the *local ancilla problem* arising from the use of the Hilbert-Schmidt distance. We address this particular issue in Section 3.4, by defining the modified QCD $\tilde{C}(\rho) = C(\sqrt{\rho})$ and showing that it fulfils requirement **C4**.

Yet, in the remainder of this chapter, we kept employing the original QC, as our results are not, in all the cases considered, impacted by the local ancilla problem.

Additionally, the following proposition holds.

Proposition 3.1.1. *If $C_\mu(\rho) = \mathrm{Tr}(\rho^2)$ then all of its realizations $\{p_k, |k\rangle\}$ contain only pure states maximally entangled in μ. Formally,*

$$C_\mu(\rho) = \mathrm{Tr}\left(\rho^2\right) \implies \forall k \text{ such that } p_k \neq 0, \ E_\mu(|k\rangle) = 1 \tag{3.11}$$

Proof. For any mixed state $\rho = \sum_k p_k \left| k \right\rangle \left\langle k \right|$,

$$A_{ii}^{\mu}(\rho) = \sum_{k,l} p_k p_l \left| \left\langle k \right| \sigma_i^{\mu} \left| l \right\rangle \right|^2 \tag{3.12}$$

It follows that, if $\forall i = 1, 2, 3$, $A_{ii}^{\mu}(\rho) = 0$, then $\forall k, l$ such that $p_k, p_l \neq 0$, $\forall i = 1, 2, 3$, $\left\langle k \right| \sigma_i^{\mu} \left| l \right\rangle = 0$, which in turn implies that $\boldsymbol{A}^{\mu}(\rho) = \boldsymbol{0}$, where $\boldsymbol{0}$ is the null matrix. In particular, $\left\langle k \right| \sigma_i^{\mu} \left| k \right\rangle = 0$, and from Eq.(2.21), we can write

$$\boldsymbol{A}^{\mu}(\rho) = \boldsymbol{0} \implies \forall k \text{ such that } p_k \neq 0, \ E_{\mu}(\left| k \right\rangle) = 1, \tag{3.13}$$

Hence the proposition. $\qquad\qquad\qquad\qquad\qquad\qquad\qquad\qquad\qquad\qquad\qquad\Box$

3.2. Generalized Entanglement Distance

As stated above, for a mixed state, the existence of QC is not a sufficient condition to guarantee the presence of entanglement, even less to precisely measure it. To extract this information from a given state ρ, we propose a procedure of regularization for density operators ρ, with the aim of repurposing the QCD to obtain a novel entanglement monotone. We have hope that this somewhat unconventional method would allow for a much simpler optimization process, at least in some cases and under some conditions that are yet to be determined precisely.

Given a state ρ, we consider all of its possible decomposition $\{p_k, \rho_k\}$, such that

$$\rho = \sum_k p_k \rho_k \,, \tag{3.14}$$

where $\sum_k p_k = 1$ and $\text{Tr}[\rho_k] = 1$. Also, we consider all the possible local partial transformation on qubit μ:

$$\rho_U\left(\{p_k, \rho_k, U_k\}\right) = \sum_k p_k U_k \rho_k U_k^{\dagger} \,, \tag{3.15}$$

where, $\forall k$, U_k is an $SU(2)$ LU operator. To avoid this transformation to trivially send any state to a classical state, we impose the restriction $\forall \rho_k = \rho_l$, $U_k = U_l$. We define the entanglement measure

$$E\left(\rho\right) = \inf_{\{p_k, \rho_k\}} \left\{ \sum_{\mu=1}^{M-1} \inf_{\{U_k\}} C_{\mu}\left(\rho_U\left(\{p_k, \rho_k, U_k\}\right)\right) \right\} . \tag{3.16}$$

Since this measure is issued by a regularization procedure, applied to the QCD, we call it, in the remaining of this work, the regularized entanglement distance (RED), to distinguish it from the convex roof extension of the ED to mixed states. Remark that the RED applied to a pure state reduces to the ED (2.20); both can hence be

denoted E. Since the convex roof extension of the ED to mixed states (2.22) is in general intractable, we will not employ it in the remaining of this work, thus avoiding risk of confusion.

Note that, similarly to the QCD, we can define $E_\mu(\rho)$ as the RED of the subsystem μ, simply discarding the complement in the sum on μ in (3.16).

The RED (3.16) fulfils the strong version of requirement 2, namely

Proposition 3.2.1. $E(\rho) = 0$ *if and only if* $\rho \in \mathcal{S}$.

Proof. Let $\rho \in \mathcal{S}_\mu$. It then admits a decomposition $\{p_k, \rho_k\}$, where, $\forall k$, $\rho_k = \rho_k^\mu \otimes \rho_k^{\mu^C}$, where the ρ_k^μ do not necessarily form an orthonormal basis. It is always possible to determine local partial operators U_k, such that, after transformation (3.15) it results $\rho_U^\mu = \sum_k p_k |k\rangle\langle k|^\mu \otimes \rho_k^{\mu^C}$, where the $|k\rangle$ are orthonormal and, since the QCD fulfils property **C1**, it follows $E_\mu(\rho) = 0$. This property straightforwardly extends to the full measure, that is if $\rho \in \mathcal{S}$, then $E(\rho) = 0$.

Now, let ρ be such that $E(\rho) = 0$. First of all, we note that, for each $\mu = 0, \ldots, M-1$, $\lambda_{max}^\mu(\rho) \le \mathrm{Tr}(\rho^2)$. In fact, for each μ and for each unit vector $\boldsymbol{n}^\mu$ it is possible to determine a unitary local operator U, so that

$$\mathrm{Tr}[(\rho \sigma_{\boldsymbol{n}}^\mu \rho \sigma_{\boldsymbol{n}}^\mu)] = \mathrm{Tr}[\tilde{\rho}\sigma_3^\mu \tilde{\rho}\sigma_3^\mu],$$

where $\tilde{\rho} = U\rho U^\dagger$. Furthermore

$$\mathrm{Tr}[\tilde{\rho}\sigma_3^\mu \tilde{\rho}\sigma_3^\mu] = \sum_j \tilde{\rho}_{jj}^2 + 2\sum_{i \ne j} \pm|\tilde{\rho}_{ij}|^2 \le \sum_j \tilde{\rho}_{jj}^2 + 2\sum_{i \ne j} |\tilde{\rho}_{ij}|^2 = \mathrm{Tr}\left[\tilde{\rho}^2\right] = \mathrm{Tr}\left[\rho^2\right].$$

Moreover, for each pair $i \ne j$, $\exists \mu$ such that the term $|\tilde{\rho}_{ij}|^2$ appears in $\mathrm{Tr}[(\tilde{\rho}\sigma_3^\mu)^2]$ with a negative sign. Yet, $E(\rho) = 0$ implies that there exist a decomposition of ρ, let's say $\overline{\rho}$, for which

$$\sup_{\boldsymbol{n}^\mu} \mathrm{Tr}[\overline{\rho}\sigma_{\boldsymbol{n}}^\mu \overline{\rho}\sigma_{\boldsymbol{n}}^\mu] = \mathrm{Tr}\left[\overline{\rho}^2\right]$$

for each μ. We hence have $|\overline{\rho}_{ij}|^2 = 0$ for each $i \ne j$. But this implies that $\overline{\rho}$ is diagonal, hence $\rho \in \mathcal{S}$, which concludes our proof. $\qquad\square$

Furthermore, the following holds

Proposition 3.2.2. *The RED is convex, i.e.* $\forall\{p_k, \rho_k\}$ *such that* $\rho = \sum_k p_k \rho_k$,

$$E_\mu(\rho) \le \sum_k p_k E_\mu(\rho_k) \tag{3.17}$$

Proof. Let us choose a decomposition $\{p_k, \rho_k\}$, where the ρ_k are pure states, and let $\tilde{\rho}_k = U_k \rho_k U_k^\dagger$. Eq. (3.16) can be rewritten, discarding all of the minimization

procedures and considering a single qubit μ

$$\sum_{kl} p_k p_l \left(\text{Tr}\left[\tilde{\rho}_k \tilde{\rho}_l\right] - \text{Tr}\left[\tilde{\rho}_k \sigma_{\boldsymbol{n}}^{\mu} \tilde{\rho}_l \sigma_{\boldsymbol{n}}^{\mu}\right] \right)$$
$$= \sum_k p_k^2 \left(1 - \text{Tr}\left[(\tilde{\rho}_k \sigma_{\boldsymbol{n}}^{\mu})^2\right] \right) + \sum_{k \neq l} p_k p_l \left(\text{Tr}\left[\tilde{\rho}_k \tilde{\rho}_l\right] - \text{Tr}\left[\tilde{\rho}_k \sigma_{\boldsymbol{n}}^{\mu} \tilde{\rho}_l \sigma_{\boldsymbol{n}}^{\mu}\right] \right). \tag{3.18}$$

We now consider, as in Eq. (1.7), the formulation of the ρ_k in terms of summations of Pauli matrices combinations, and define $\forall k$, $\boldsymbol{n}_k^{\mu} = \text{Tr}\left[\tilde{\rho}_k \boldsymbol{\sigma}^{\mu}\right]$. The transformations U_k can be chosen so that $\forall k, l$, $\text{Tr}\left[\rho_k \rho_l\right] = \delta_{kl}$, and that $\forall k$, $\boldsymbol{n}_k^{\mu} \propto \boldsymbol{u}^{\mu}$, where $\boldsymbol{u}^{\mu}$ is a unit vector defining the axis with which all substates are now aligned. $\boldsymbol{n}^{\mu} = \boldsymbol{u}^{\mu}$ appears quite a natural candidate to minimize Eq.(3.18), and yields $\text{Tr}\left[(\tilde{\rho}_k \sigma_{\boldsymbol{n}}^{\mu})^2\right] = |\boldsymbol{n}_k^{\mu}|^2$, $\forall k$. With these choices, Eq.(3.18) rewrites

$$\sum_k p_k^2 \left(1 - |\boldsymbol{n}_k^{\mu}|^2 \right) - \sum_{k \neq l} p_k p_l \, \text{Tr}\left[\tilde{\rho}_k \sigma_{\boldsymbol{n}}^{\mu} \tilde{\rho}_l \sigma_{\boldsymbol{n}}^{\mu}\right]. \tag{3.19}$$

Evidently, the left-hand term is the sum of the ED (2.21) of the pure states ρ_k, weighted by the p_k^2, while the right-hand term remains strictly negative, hence

$$E_{\mu}(\rho) \leq \sum_k p_k^2 E_{\mu}(\rho_k) - \sum_{k \neq l} p_k p_l \, \text{Tr}\left[\tilde{\rho}_k \sigma_{\boldsymbol{n}}^{\mu} \tilde{\rho}_l \sigma_{\boldsymbol{n}}^{\mu}\right] \leq \sum_k p_k^2 E_{\mu}(\rho_k) \leq \sum_k p_k E_{\mu}(\rho_k) \tag{3.20}$$

$\square$

For a given density matrix decomposition $\{p_k, \rho_k\}$, the minimization on the LU partial transformations, entailed by Eq. (3.16), can be addressed by studying the local minima of $C\left(\rho\left(\{p_k, \rho_k, U_k\}\right)\right)$ under variation of $\{U_k\}$. Nevertheless, it can be shown that such fixed points do correspond only to cases where $E\left(\rho\right) = 0$, hence to separable states. Therefore, the minima of (3.16) in the case of non-separable states, do not correspond to fixed points, but rather to nonlocal (boundary) minima.

Remarkably, the minima of the minimization procedure (3.16) can, at least in some cases, be realized by a decomposition $\{p_k, \rho_k\}$ including entangled pure states ρ_k. In particular, for two-qubit states diagonal in the Bell basis (the Bell-diagonal (BD) states, see [52, 45]) the minima can always be realized on the eigendecomposition (hence, where the ρ_k are Bell states).

This, of course, greatly simplifies the problem, as the full exploration of the $\{p_k, \rho_k\}$-space is avoided. It is worth emphasizing that BD states are representative of the larger class of two-qubits states of maximally mixed marginals (that is, for which $\forall \mu$ and $\forall j = x, y, z$, $\text{Tr}\left[\rho \sigma_j^{\mu}\right] = 0$, see [52]), hence (3.16) is tractable in the same manner for this class of states.

Leaning on numerical evidences, we further conjecture that, for a given state $\rho(\boldsymbol{\gamma})$ depending on parameters $\boldsymbol{\gamma} = (\gamma_1, \gamma_2, ...)$, the decomposition realizing the minimum (3.16) is the same in the whole parametric domain of $\boldsymbol{\gamma}$, and can hence be inferred from the fixed points found in the domains where this state is separable, if such a

domain exists. This suggests that the minimization over all possible decompositions $\{p_k, \rho_k\}$ might in fact possess *non-trivial* general solutions, depending on the class of states under consideration. Here, by "non-trivial solutions" of the minimization procedure, we mean solutions which do not require to find the decomposition of ρ in terms of pure product states $\rho_k = \bigotimes_\mu |k\rangle \langle k|^\mu$.

A subsequent more thorough work on such a classification of the solutions of this procedure could thus lead to an entanglement measure of relatively low computational cost, in particular for systems symmetric under qudit permutations, and with low $\text{rank}(\rho)$.

3.3. Examples

3.3.1. Bell-Diagonal States

As a first and seminal example of application of this procedure, we consider general BD states. They can be expressed as:

$$\rho_{BD}(\{p_\alpha\}) = \sum_{\alpha=1}^{4} p_\alpha |\psi_\alpha\rangle\langle\psi_\alpha|$$

$$= \frac{1}{4}\left(\mathbb{I} + \sum_{i=x,y,z} c_i \sigma_i^0 \sigma_i^1\right), \tag{3.21}$$

where the $|\psi_\alpha\rangle$ are the four Bell states: $|\psi_\pm\rangle = \frac{1}{\sqrt{2}}(|00\rangle \pm |11\rangle)$ and $|\phi_\pm\rangle = \frac{1}{\sqrt{2}}(|01\rangle \pm |10\rangle)$. Furthermore, we have $\forall i, |c_i| \leq 1$, and the c_i are such that the vector (c_1, c_2, c_3), fully characterizing the state, belongs to the tetrahedron $\mathcal{T}$ of vertices $(-1, 1, 1), (1, -1, 1), (1, 1, -1), (-1, -1, -1)$. The separable BD states belong to the octahedron $\mathcal{O}$ of vertices $(\pm 1, 0, 0), (0, \pm 1, 0), (0, 0, \pm 1)$, corresponding to the condition $\forall \alpha, p_\alpha \leq 2$, and the classical BD states are located on the Cartesian axis $(c_1, 0, 0), (0, c_2, 0), (0, 0, c_3)$ [52, 45, 69, 70]. Direct calculation yields the following result for the QCD of general BD states

$$C(\rho_{BD}(\{p_\alpha\})) = 2\sum_{\alpha=1}^{4} p_\alpha^2 - 4 \max_{P\{i,j,k,l\}} \{p_i p_j + p_k p_l\}, \tag{3.22}$$

where the maximum is taken on all permutations $P\{i, j, k, l\}$ of the indices $\{1, 2, 3, 4\}$. Figure 3.1 shows the QCD of BD states on a face of $\mathcal{T}$.
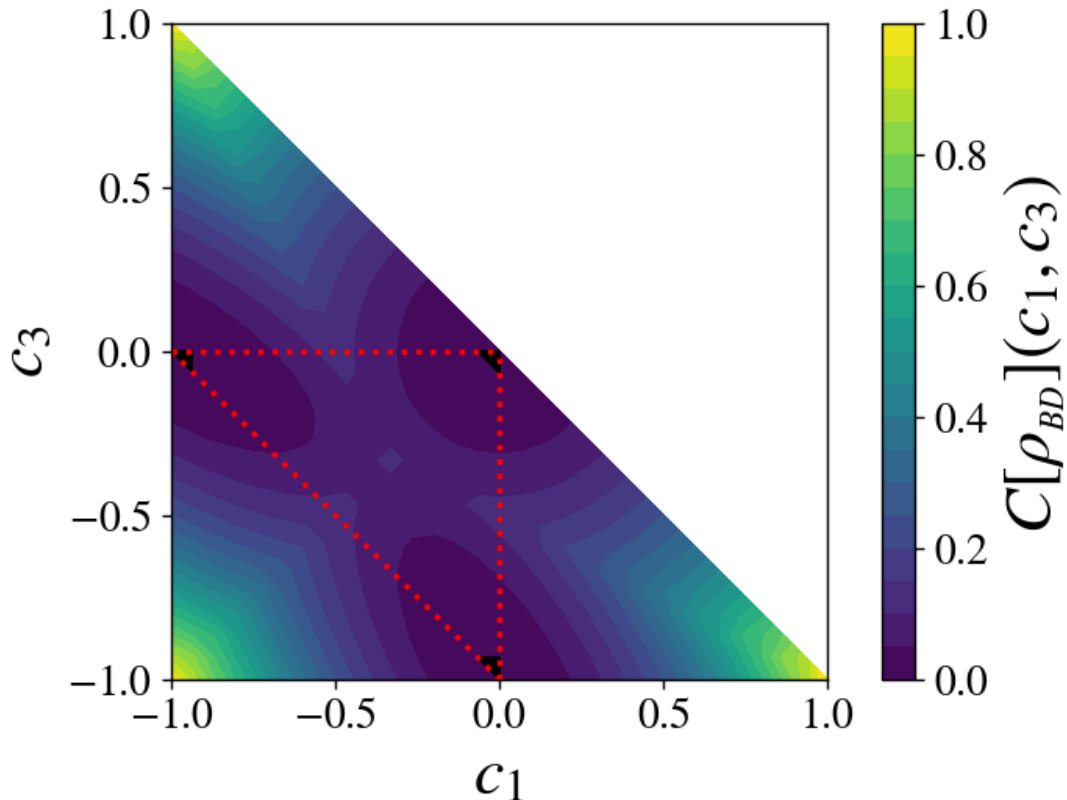
Figure 3.1.: QCs $C[\rho_{BD}](c_1, c_2 = c_1, c_3)/2$ for a face of the BD state tetrahedron $\mathcal{T}$, corresponding to a mixture of three Bell states. The red dotted line defines the smaller triangle where the state is separable, according to the PPT criterion [71, 60]. The vertices of the larger triangle correspond to pure Bell states. Those of the red dotted triangle, of vanishing QCD, correspond to equal-weight mixtures of two Bell states, which are evidently the three only *classical* states in the domain represented here.

We were not able to find a simple analytic solution of the minimization procedure for the most general case of BD states. However, numerical minimization (for these calculations, we have applied a gradient steepest-descent method) provided us with empirical evidence that the procedure (3.16), applied on the eigendecomposition (i.e. the decomposition into a mixture of BD states) also leads for these states to the squared concurrence, as shown in Figure 3.2, which represents a face of the tetrahedral domain of BD states. It is interesting to note that the ED, as the concurrence and unlike the QCD, is constant on planes parallel to the boundary faces of the separability region: the ED of any given state indeed equates the QCD of the closest point located on a hinge of $\mathcal{T}$, hence the closest mixture of only two Bell states.
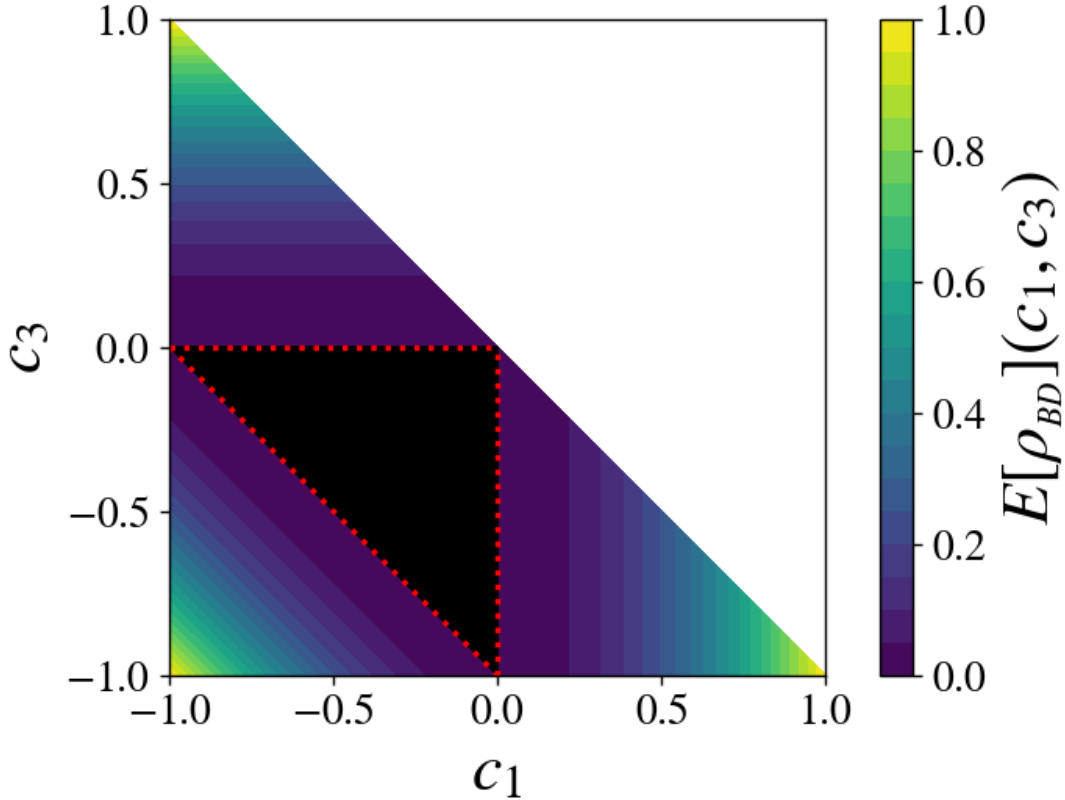
Figure 3.2.: Entanglement distance $E[\rho_{BD}](c_1, c_2 = c_1, c_3)/2$ for a face of the BD
state tetrahedron $\mathcal{T}$, corresponding to a mixture of three Bell states.
The red dotted line defines the smaller triangle where the state is
separable, according to the PPT criterion [71, 60] and a number of
alternative derivations available in the literature (see e.g. [52]). Values
below the threshold of 10^{-3} have been represented in black to emphasize
that they correspond to a numerical zero, given the level of precision
allowed by such time-costly minimization. The vertices of the large
triangle correspond to pure Bell states, and those of the smaller black
triangle to equal-weight mixtures of two Bell states.

3.3.2. Werner states

Let us now consider the two-qubit Werner states (WS) [72], which stems as a
special case of BD state, for which a simple analytical solution for the proposed
procedure is available. WS are used as a test bed since they illustrate many features
of mixed-state entanglement [19]. It is well-established that Werner states are
separable in the parametric region $p \geq 1/2$ [72]; yet, in Appendix A, we propose a
new demonstration of this fact, highlighting how the internal statistical structure
of a state can be analysed to evidentiate its alternative realizations.

Using Eq. (3.21), WS can simply be expressed as

$$\rho_W(p) = \rho_{BD}\left(\frac{p}{3}, \frac{p}{3}, \frac{p}{3}, (1-p)\right).$$ (3.23)

Via direct calculations, we get for the QCD of the WS

$$C(\rho_W(p)) = 2(1 - \frac{4}{3}p)^2.$$ (3.24)

WS yields a relatively simple solution to the minimization procedure (3.16). In fact, leaning on our previous knowledge of the separability region of WS, we were able to analytically retrieve the optimal local partial transformations (3.15), as depicted with more details in Appendix A. It can be easily verified that, setting

$$U_{|\psi_+\rangle}(\theta) = U_z^\mu(\theta)U_x^\mu(\pi),$$
$$U_{|\psi_-\rangle}(\theta) = U_z^\mu(\pi - \theta)U_x^\mu(\pi),\ \text{and}$$
$$U_{|\phi_+\rangle} = U_{|\phi_-\rangle} = \mathbb{I},$$ (3.25)

with $\mu = 0, 1$ arbitrarily chosen, the fixed points are found for $\theta = \arccos\left(\frac{3}{2p} - 2\right)$. This last expression has a solution if and only if $p \geq 1/2$, which is the parametric region of separability for $\rho_W(p)$ (as can be verified by the application of the positive partial trace criterion (PPT), see [60]). Hence, $E(\rho_W) = 0$ for $p \geq 1/2$. For $p < 1/2$ numerical minimization yields $E(\rho_W) = 4p^2 - 4p + 1$. This corresponds to $\theta = 0$ uniformly on this whole domain, which is also the value previously determined at $p = 1/2$: hence, the minimum after this point cease to be a fixed point, but keeps the last position in terms of the parameters governing the rotations. We can understand this as the fixed point reaching the boundary of the parametric domain as the geometry of the state is changing continuously, becoming a simple point on a slope, located at this boundary. Altogether, for Werner states, the result of our entanglement measure exactly equates twice the square of the concurrence [18], that is

$$E(\rho_W(p)) = 2\Theta(1/2 - p)(1 - 2p)^2,$$ (3.26)

Fig. 3.3 shows $C(\rho_W(p))/2$ versus p, there it is clear that the only state with no QC, i.e. *classical state* according to the conventional terminology [23], is the one corresponding to the value $p = 3/4$, whereas the maximally quantum-correlated state is that of $p = 0$. On the other hand, the state is entangled only in the region $p < 1/2$, and separable otherwise, a well-known fact that can be easily checked by the application of the PPT criterion [71, 60]. Alternatively, we can find, in the separable region, the expression of ρ_W convex combination of (non-orthogonal) product states, using a more involved calculation resorting to the so-called Bloch representation.
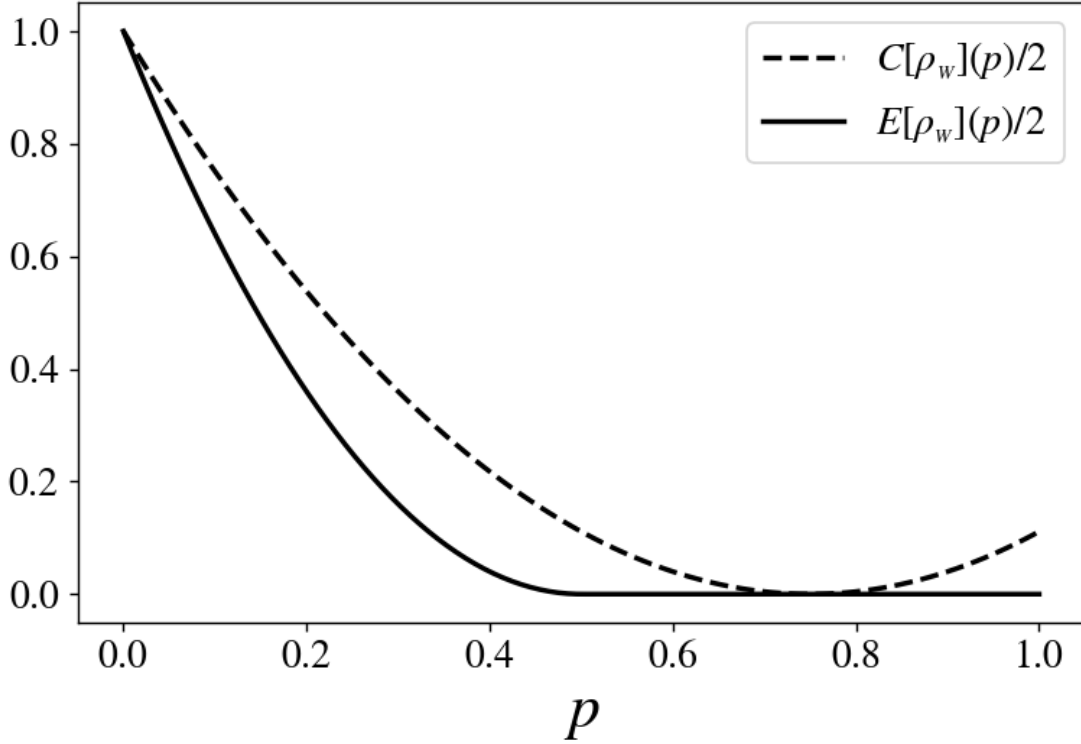
Figure 3.3.: $C[\rho_W](p)/2$ and $E[\rho_W](p)/2$ versus p for state (3.23). It is clear that the state $\rho_W(p = 0)$ is, as expected, the maximally-entangled, and that the states $\rho_W(p > 1/2)$ are fully-separable, as can be verified using the PPT criterion [71, 60]. This plot emphasizes that separable states can contain QC (i.e. not be classical). Note that, here $E[\rho_W](p)/2 = C_2^2[\rho_W](p)$, that is, the ED equates twice the squared concurrence for 2-qubits Werner states.

3.3.3. Generalized Werner states

Let us now consider as a multipartite example the following one-parameter density matrix

$$\rho_{W_3}(p) = p|GHZ_+\rangle\langle GHZ_+| + \frac{(1-p)}{8}\mathbb{I}_8 \,, \tag{3.27}$$

where $|GHZ_+\rangle = (|000\rangle + |111\rangle)/\sqrt{2}$, $\mathbb{I}_8$ is the identity operator of the three-qubit Hilbert space and $0 \leq p \leq 1$. This is a generalization of the Werner states to three qubits, termed generalized Werner states [73, 74, 75]. The states $\rho_{W_3}(p)$ are known to be fully separable for $0 \leq p \leq 1/5$ [73, 76, 74] and genuinely multipartite entangled states in the region $3/7 < p \leq 1$. In the region $1/5 < p \leq 3/7$ the states $\rho_{W_3}(p)$ are bi-separable yet inseparable under any fixed bipartition [77]. Via direct calculations, we get

$$C(\rho_{W_3}(p)) = 3p^2 \,. \tag{3.28}$$

63

Numerical minimization provided the values for the ED shown in Fig. 3.4. There, we report in dotted line the QCD per qubit and continuous line the ED per qubit for the states $\rho_{W_3}(p)$. Fig. 3.4 clearly shows that $ED(\rho_{W_3}(p)) > 0$ only for $p > 3/7$, that is when the states are generally entangled. As for the region $1/5 < p \leq 3/7$ where ED should not be zero according to $ii)$, we got numerical zero which we assume corresponds to very weak, but finite values. We interpreted this as a consequence of the fact that, in this region, the states $\rho_{W_3}(p)$ are not separable under any fixed bipartition, thus assuming the decomposition of the form $\sum_j \rho_j^1 \otimes \rho_j^{23} + \rho_j^2 \otimes \rho_j^{13} + \rho_j^3 \otimes \rho_j^{12}$. Hence the regularization procedure reaches easily small values for the ED.
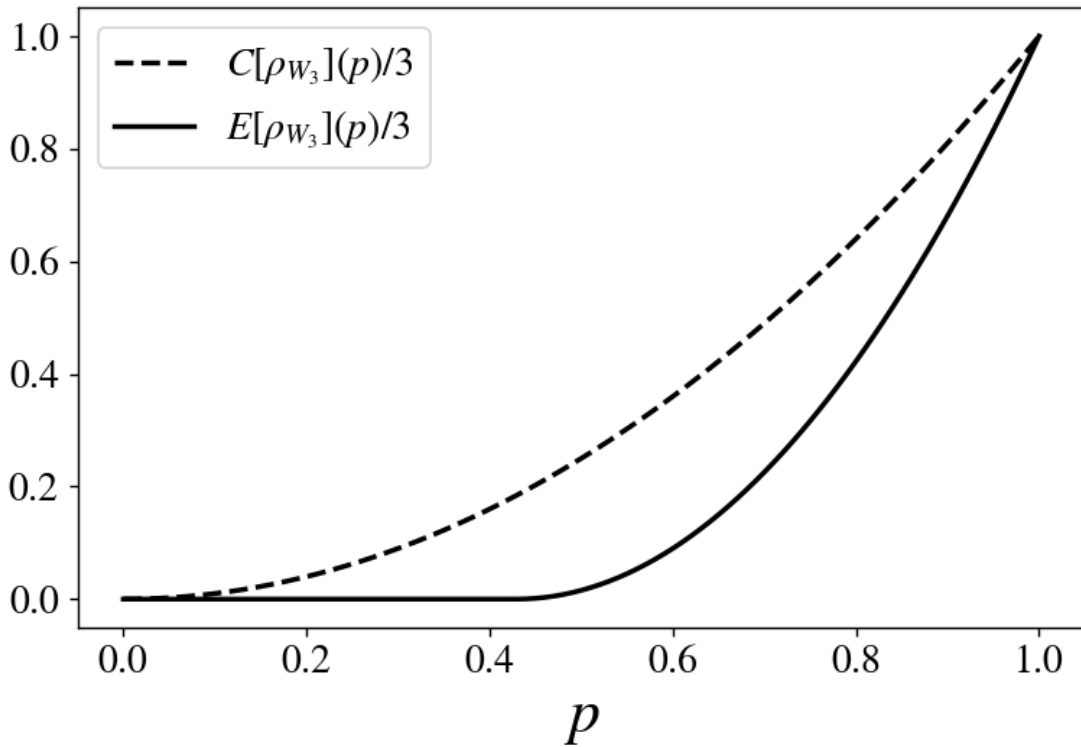
Figure 3.4.: $C[\rho_{W_3}](p)/3$ (dotted line) and $E[\rho_{W_3}](p)/3$ (continuous line) versus p for state (3.27). It is clear that the state $\rho_{W_3}(p = 1)$ is, as expected, the maximally entangled, and that the states $\rho_{W_3}(p > 3/7)$ are not separable. The latter are genuine three-partite entangled states.

3.3.4. Three-qubit States Interpolating Between Bi-separable and Genuine Entangled States

Let consider a further multipartite example, that is the one-parameter density matrix

$$\rho_3(p) = w_+|GHZ_+\rangle\langle GHZ_+| + w_2|\psi_2\rangle\langle\psi_2| + w\frac{(1-p)}{8}\mathbb{I}_8 , \qquad (3.29)$$

where

$$\begin{aligned}
w_+ &= p[1 - 4p(1 - p)]\,, \\
w_2 &= (1 - p)[1 - 4p(1 - p)]\,, \\
w &= 4p(1 - p)\,,
\end{aligned} \tag{3.30}$$

$|\psi_2\rangle = |0\rangle(|00\rangle + |11\rangle)/\sqrt{2}$ and $0 \leq p \leq 1$. For $p = 0$, $\rho_3(p = 0)$ is a pure bi-separable state, for $p = 1/2$, $\rho_3(p = 1/2)$ is a maximally mixed state of three qubits and for $p = 1$, $\rho_3(p = 1)$ is a pure maximally entangled state. Via direct calculations, we get

$$C(\rho_3(p)) = \frac{(1 - 2p)^4}{2}\left[5 - 10p + 11p^2 - (1 - p)\sqrt{1 - 2p(1 - p)}\right]\,. \tag{3.31}$$

Using numerical minimization, we have obtained the results for the ED shown in Fig. 3.5. In this figure, we report as a dotted line the QCD per qubit and as a continuous line the ED per qubit, for the states $\rho_3(p)$. Fig. 3.5 shows that $E(\rho_3(p)) > 0$ for $0 \leq p \lesssim 0.18$ and for $0.81 \lesssim p \leq 1$. Furthermore, the maximum value for ED per qubit in the region $0 \leq p \lesssim 0.18$ is located at $p = 0$ and has the value $2/3$. $2/3$ is the maximum value for ED per qubit, in the case of bi-separable three-qubit states. This confirms that the states of this region are stably bi-separable and that the state $|\psi_2\rangle\langle\psi_2|$ has the maximum local degree of entanglement. The maximum value for ED per qubit in the region $0.81 \lesssim p \leq 1$ is located at $p = 1$ and has value 1. Therefore, the states of this region are not separable and, at least close to $p = 1$, are certainly genuinely entangled. For $0.18 < p < 0.81$ the entanglement is numerically null, thus suggesting the states of this region are separable or bi-separable yet inseparable under any fixed bipartition, hence not genuinely three-partite entangled states. Remarkably, the QCD is null only for the state corresponding to $p = 1/2$, which is the maximally mixed one.
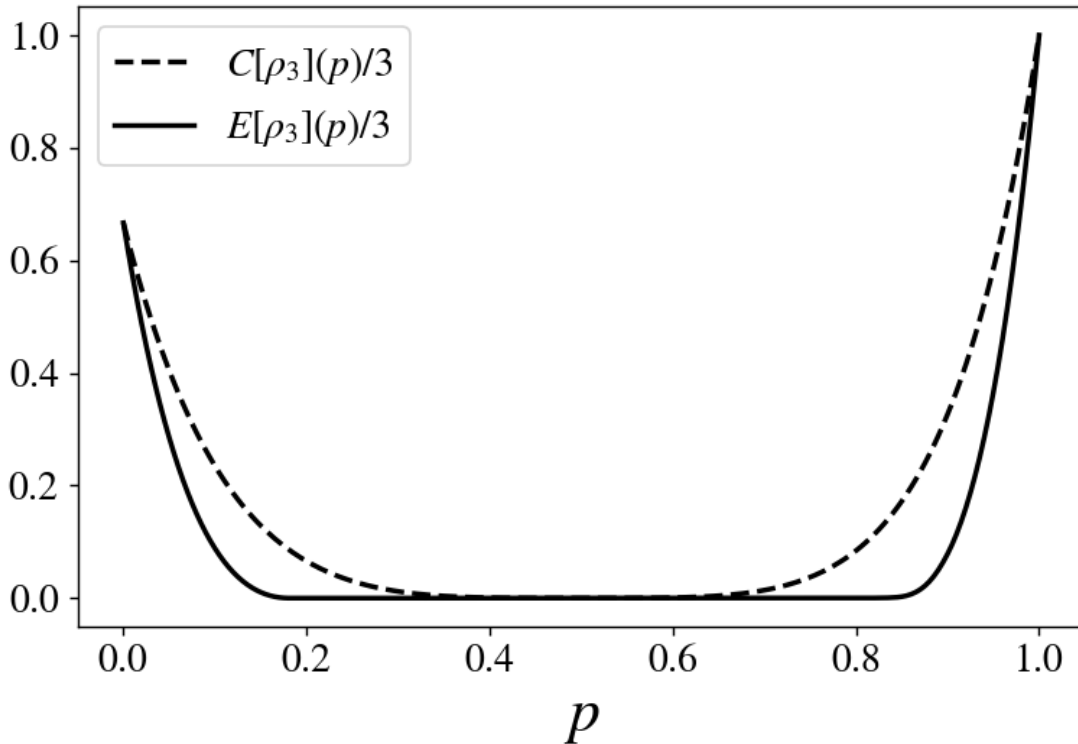
Figure 3.5.: $C[\rho_3](p)/3$ (dotted line) and $E[\rho_3](p)/3$ (continuous line) versus p for state (3.29). It is clear that the state $\rho_3(p = 1)$ is, as expected, the maximally entangled one, and that the states $\rho_3(p > 0.81)$ or $\rho_3(p < 0.18)$ are not separable.

3.4. The Local Ancilla Problem

We were able to express the QCD, our measure of QCs, in the simple closed form (3.9), owing to the simplicity of the Hilbert-Schmidt distance (3.1). As we saw in the above, this simplicity allows ease of computation, but also direct analysis and interpretation of its behaviours relative to the considered states and their decompositions.

However, it has been argued that the Hilbert-Schmidt norm is unfit to define distance-induced entanglement or QC measures [23, 78, 79, 80].

This is due to the fact that, in contrast with the Bures distance or the trace distance, it is not contractive under the addition or removal of an uncorrelated *ancilla*.

In fact, consider the product $\rho \otimes \rho^a$, where ρ^a is a possibly mixed arbitrary local *ancilla*. Then, reminding that $\text{Tr}[O_1 \otimes O_2] = \text{Tr}[O_1]\,\text{Tr}[O_2]$, it is straightforward to see that, $\forall \mu \notin a$

$$C_\mu \left(\rho \otimes \rho^a \right) = C_\mu \left(\rho \right) \text{Tr}\left[\left(\rho^a \right)^2 \right]. \tag{3.32}$$

In turn, this implies that, in general, discarding the uncorrelated ancilla ρ^a using the partial trace operation can increase the value of C_μ, namely

$$C_\mu(\rho \otimes \rho^a) \leq C_\mu(\rho) \tag{3.33}$$

Yet, as pointed out in references [23, 78, 79, 80], this property violates requirement **C4**. Clearly, the ED inherits this undesirable property from the QCD it is built from.

One may claim that Eq. (3.33) remains a somewhat benign pathology, as it amounts to a scaling problem, which can be easily overcome, or even discarded as an irrelevant detail. On the contrary, this problem is in fact quite serious. First, it was shown in [81] that a mere rescaling by the purity $C(\rho)/\operatorname{Tr}[\rho^2]$ does not fully solve the issue. Second, Eq. (3.33) implies in fact a more systematic issue.

As an example, let (A, B) be a bipartition of Q such that $\mu \notin B$, and ρ be a biseparable state $\rho = \sum_k p_k \rho^A \otimes \rho^B$. For such a state, Eq. (3.7) may be rewritten

$$C_\mu(\rho) = \inf_{\boldsymbol{n}^\mu} \sum_{kl} p_k p_l \operatorname{Tr}\left[\rho_k^B \rho_l^B\right] \left(\operatorname{Tr}\left[\rho_k^A \rho_l^A\right] - \operatorname{Tr}\left[\rho_k^A \sigma_{\boldsymbol{n}}^\mu \rho_l^A \sigma_{\boldsymbol{n}}^\mu\right]\right). \tag{3.34}$$

It can be verified that the following is a CPTP map acting on B

$$\mathbb{I}^A \otimes \boldsymbol{\mathcal{M}}^B[\rho] = \operatorname{Tr}_B[\rho] \otimes |0\rangle\langle 0|^B = \sum_k p_k \rho_k^A \otimes |0\rangle\langle 0|^B = \rho^A \otimes |0\rangle\langle 0|^B. \tag{3.35}$$

Evidently, $C\left(\rho^A \otimes |0\rangle\langle 0|^B\right) = C\left(\rho^A\right) \geq C(\rho)$.

Nevertheless, this drawback can be overcome by defining the modified measure

$$\widetilde{C}(\rho) = C(\sqrt{\rho}), \tag{3.36}$$

as was already proposed for the geometric discord (Ref. [79]).

As noted in [79], the insertion of $\sqrt{\rho}$ in the QCD appears in fact quite natural. Square root of density matrices are evocative of probability amplitudes, and are widely employed in the field of quantum information, for instance in the celebrated Wigner-Yanase skew information [82].

Recall that, for any pure state $|k\rangle$, $\sqrt{|k\rangle\langle k|} = |k\rangle\langle k|$, implying that $\sqrt{\rho}$ retains the spectral properties of ρ, namely, for any $\rho = \sum_k p_k |k\rangle\langle k|$, where $\{p_k, |k\rangle\}$ is the spectrum of ρ, we have

$$\sqrt{\rho} = \sum_k \sqrt{p_k} |k\rangle\langle k|. \tag{3.37}$$

It immediately results that $\widetilde{C}(\rho)$ inherits properties **C3** and **C2**. Requirement **C1** is also fulfilled, because the square root of a classical-quantum state can always be written as $\sqrt{\rho^{AB}} = \sum_k \Pi_k^A \otimes \sqrt{p_k \rho_k^B}$ with $\{\Pi_k^A\}$ an orthonormal basis for A,

hence the argument drawn in Section 3.1 still holds. While $\widetilde{C}(\rho)$ clearly does not suffer the local ancilla problem, it remains unclear if there exists some other CPTP channels $\Lambda_{\nu\neq\mu}^{CPTP}$ such that $\widetilde{C}_\mu\left(\Lambda_{\nu\neq\mu}^{CPTP}[\rho]\right) > \widetilde{C}_\mu(\rho)$; yet Refs. [79, 23] claims that unitary response measures, such as ours, are indeed fully fixed by the square root trick; hence the modified QCD satisfies **C4**.

It is not clear whether inserting the modified QCD in place of the QCD, into the regularized ED (3.16), yields the same results. Unfortunately, while $\sqrt{\rho}$ and ρ share the same eigenvectors, $\sqrt{\rho}$ cannot in general be written as a linear combination of arbitrary realizations of ρ. Formally, $\rho = \sum_k p_k \rho_k$ does not necessarily imply $\sqrt{\rho} = \sum_k \tilde{p}_k \rho_k$, except in the special case where the ρ_k form an eigenbasis. In particular, nothing guarantees that the optimal realization $\{p_k, \rho_k\}$ that minimizes (3.16) can be used to minimize $E(\sqrt{\rho})$. As a result, we cannot straightforwardly extend our results showing the monotonicity of $E(\rho)$, to $E(\sqrt{\rho})$.

However, given the large dimensionality of the space which is explored by the minimization procedure (3.16), added with the deep informational meaning of the concept of matrix square root, it is not improbable that $E(\sqrt{\rho})$ is an entanglement monotone, and that further research could isolate subspaces of minimization in which the procedure is tractable in practice.

3.5. Discussion

Our goal in this work has been to derive a directly computable and genuine QC measure and a numerically affordable entanglement measure, from the geometric properties of the projective Hilbert space describing a quantum multipartite system.

In our derivation, to extract from a given state ρ its entanglement essence, we have defined a regularization procedure for the density matrix that turns our measure of QC into a measure of entanglement. This regularization is applied to a given realization of ρ in terms of pure states; in the absence of further clues, it hence involves, as the overwhelming majority of mixed state entanglement monotones do, an additional minimization over all the possible decompositions of ρ, that in the general case requires a practically intractable numerical optimization. However, relying on the results we obtained on a few examples, we have hope that further research in this direction will, at least for some classes of states, identify the optimal realization, thereby significantly relieving the total computational cost.

We have proved that the entanglement and quantum-correlation measures derived do satisfy the most important requirements for suitable measures of these quantities; we further shown that the remaining local ancilla problem should not be considered a significant drawback, as it can be solved resorting to the square root of the density matrix, though the latter technique makes it difficult to analytically prove LOCC monotonicity.

To test our QC and entanglement measures, we have applied them to two classes

of mixed two-qubit states of which the entanglement properties are well-known, and we have verified the accordance between our measures and the expected results. Furthermore, we have applied the QC and entanglement measures to Werner state generalization to three qubits, and to a one-parameter family of three-qubit mixed states. The latter interpolate between a bi-separable state and a genuine multipartite state, passing through a fully separable state. Also in these cases of multipartite states, then we have verified a satisfactory agreement between the behaviours of our measures and the ones expected or already known from the literature.

4. Entanglement, quantum correlators and connectivity in graph states

In this chapter, we depict the work we issued in [37], presenting a novel analysis of the structure of Graph States, that employs an original perspective.

We start in Section 4.1 by introducing the framework of *Graph States* and *Pseudo Graph Gtates*, presenting how the former stem as the key resource in measurement-based quantum computation. Then, in Section 4.2, we quantify the entanglement of Pseudo Graph States, using the entanglement distance (2.21). In Section 4.3, we present a novel approach to probe the underlying graph connectivity of genuine Graph States, using correlators of Pauli matrices; we first do so by studying correlations of pairs of qubits (i.e. *two-point correlators*), revealing how these quantities solely depend on the relation between their respective neighbourhoods (namely, in the language of graph theory, if they are *twins*, *adjacent twins*, leaf vertices, etc...); we then notice the possibility of more general probing of graph properties, through the use of higher order correlators (i.e. involving more than two qubits). In Section 4.4, we further remark interesting implications in terms of measurement processes, namely how our approach can highlight the equivalence of some projective measurements. We conclude in Section 4.5, by underlining the simplicity of data analysis in this context, coming from the fact that all of the correlators derived take values -1, 0 or 1, and by summing up the advantages of our method, with respect to the stabilizer formalism, and highlighting how both complete each other in the aim of characterizing GS and use them as building blocks for quantum algorithms.

4.1. Definition of graph states

Graph States (GSs) constitute a class of maximally entangled pure quantum states that have emerged as a powerful resource for quantum information processing [25, 83, 84, 85]. Indeed, they are valuable for realizing quantum gates and enabling fault-tolerant quantum computation. Additionally, GSs serve as the foundation for various quantum computing protocols, especially for the one-way quantum computer, also known as the measurement-based quantum computer [83, 84, 85, 63].

4. Entanglement, quantum correlators and connectivity in graph states

It can be shown [63] that any quantum circuit can be efficiently simulated using a GS, on which appropriate measurements are performed; as such, GSs represent a *universal resource for quantum computing.* Therefore, any result obtained for the GS model can, in principle, be extrapolated to other models of quantum computation. GS are complex high-dimensional superpositions of states of N qubits, prepared as follows.

Let V be the set of indices that identify a set of N qubits and let E be a set of pairs of indices (a, b), with $a, b \in V$. Let's start with the initial product state $|\Psi\rangle = |+\rangle^V := \bigotimes_{\mu \in V} |+\rangle^\mu$, where every $|+\rangle^\mu = \frac{1}{\sqrt{2}}(|0\rangle^\mu + |1\rangle^\mu)$ is the eigenstate of σ_x^μ with eigenvalue $+1$, for $\mu \in V$. For each pair $(a, b) \in E$, we consider the fine-tuned unitary operator

$$U_{ab}(\varphi_{ab}) = e^{-i\frac{\varphi_{ab}}{4}} e^{i\frac{\varphi_{ab}}{4}\sigma_z^a} e^{i\frac{\varphi_{ab}}{4}\sigma_z^b} e^{-i\frac{\varphi_{ab}}{4}\sigma_z^a\sigma_z^b} , \qquad (4.1)$$

where $\varphi_{ab} \in \mathbb{R}$. For sake of simplicity we will assume here $\forall (a, b)$, $\varphi_{ab} = \varphi$. The pseudo-graph state (PGS) is defined as

$$|G(\varphi)\rangle = \prod_{(a,b)\in E} U_{ab}(\varphi)|\Psi\rangle , \qquad (4.2)$$

while the genuine GS correspond to the case $\varphi = \pi$

$$|G\rangle = \prod_{(a,b)\in E} U_{ab}(\pi)|\Psi\rangle . \qquad (4.3)$$

Note that all the operators (4.1) commute with each other.
Each of the operators (4.1) entangles a pair of qubits[1].

It has been shown that a general GS does not correspond to the ground state of a physical system. However, a GS can be obtained artificially in a physical system that allows the activation of Ising-like interactions $\sigma_z^a\sigma_z^b$. In this case, the time duration of the interaction determines the value of φ (hereinafter referred to as *interaction strength*). Physical implementations of such systems were performed on some of the quantum computer prototypes developed by IBM [86, 87]. In practice, any physical device for universal quantum computing, can be used to realize GS in the way described above [84].

Since a GS is uniquely defined by a couple of sets (V, E), it is uniquely defined by a undirected graph $G(V, E)$, where each qubit (associated with an element of

---

[1]As an example to clarify this point, consider the simplest case $V = \{a, b\}$, $E = \{(a, b)\}$ and $\varphi_{ab} = \pi$. We have:

$$|G\rangle = U_{ab}(\varphi = \pi)|++\rangle = \frac{1}{2}(|++\rangle + |-+\rangle + |+-\rangle - |--\rangle) = \frac{1}{\sqrt{2}}(|+0\rangle + |-1\rangle) ,$$

a maximally entangled state of two qubits.

V) is a vertex, and each pair in E is an edge (or a link) of the graph. In most of the literature, the preferred terminology is to refer to GSs defined on lattices as *cluster states*. However, in the present work, we address the study of GS in the general case and therefore associated with generic graphs.

The genuine GS $|G(\pi)\rangle = |G\rangle$ of a given graph $G(V, E)$ is the unique common eigenvector with eigenvalue $+1$ of the operators

$$K_\mu = \sigma_x^\mu \sigma_z^{N(\mu)}, \tag{4.4}$$

where $\mu \in V$ and $N(\mu)$ denotes the set of neighbours of μ. The group $\mathcal{S}$ generated by the set $\left\{K_\mu\right\}_{\mu \in V}$ is called the "stabilizer" of the GS. Clearly, $\forall g \in \mathcal{S}$, $g|G\rangle = |G\rangle$, and the projector onto a GS can be expressed as $|G\rangle\langle G| = \frac{1}{2^N} \sum g \in \mathcal{S}g$.

GS vectors are thus in one-to-one correspondence with their stabilizer $\mathcal{S}$, and any operation applied to $|G\rangle$ can be mapped to an operation applied to $\mathcal{S}$. For example, for any unitary operation U (i.e., any quantum gate), if $\mathcal{S}$ stabilizes $|G\rangle$, then $U\mathcal{S}U^\dagger$ stabilizes $U|G\rangle$ [88].

The group $\mathcal{S}$ is completely determined by its N generators $\left\{K_\mu\right\}_{\mu \in V}$ (which belong to the Pauli group and thus have a simple algebra). On the other hand, to explicitly write the corresponding state vector, it is necessary to determine the 2^N amplitudes. For this reason, the stabilizer formalism usually provides a significant computational advantage.

Furthermore, the stabilizer formalism is often used as a preferred framework to compare different models of quantum computation, for example, for implementing error-correcting codes or examining the effects of quantum gates and measurement processes [88, 63].

However, we believe that, while the stabilizer representation is more useful for studying known initial states and how they transform under the action of such operations, it proves to be an unnecessary complication in other contexts, such as the probing and tomography of unknown states. This is because the calculation of correlations and expectation values requires taking into account all elements of $\mathcal{S}$ rather than its mere generators.

Thus, in this work, we do not resort to the stabilizer formalism but rather employ more intuitive notion of correlation and expectation values.

We start by quantifying the entanglement in the general case of PGS using the ED, previously defined in Section 2.2. Subsequently, we explore a novel approach to investigate the underlying graph connectivity of genuine GS using correlators of Pauli matrices. In particular, we compute correlations between pairs of qubits (i.e., two-qubit correlators) and demonstrate that these quantities depend exclusively on the relation between their neighbourhoods (i.e., in graph theory language, whether they are *twins*, *adjacent twins*, *leaf vertices*, etc.). We discuss the possibility of a

more comprehensive exploration of graph properties through the use of higher-order correlators (involving more than two qubits). Furthermore, we show that our approach can highlight when two projective measurements are equivalent. Also, we emphasize the simplicity of data analysis offered by our approach in this context, as all correlators can only assume the values of -1, 0, or 1. We conclude this work by summarizing the advantages of our method with respect to the stabilizer formalism, by showing that these two approaches offer a complementary characterization of GS.

4.2. Entanglement in Pseudo Graph States

The ways of quantifying entanglement in multipartite states are manifold [10, 13]. In this work, we will solely refer to *qubit-wise entanglement*, that is entanglement of bipartitions (μ, μ^C), where μ is a qubit, and μ^C is its complement relative to the set of all qubits in the system.

The Entanglement Distance (ED), first defined in Ref. [56], is an entanglement measure for general multipartite pure states; it has been adapted in Ref. [34] to the more general framework of multipartite mixed states. It has already found since then some interesting applications [12, 11, 34]. It finds its theoretical grounds on the Fubini-Study metric associated to the local-unitary invariant projective Hilbert space, called in this context the Entanglement Metric, of which deep geometric meaning has been further explored in Ref. [35].

The single-qubit ED is defined as

$$E_\mu(|s\rangle) := 1 - \sum_{j=x,y,z} |\langle s| \sigma_j^\mu |s\rangle|^2, \tag{4.5}$$

which equates 1 if μ is maximally entangled with the rest of the system, and 0 if it is fully factorizable. Eq. (4.5) thus stems as a measure of bipartite entanglement on the bipartition (μ, μ^C).

We choose here to use the latter definition of entanglement, which possesses the advantage of being very easy to compute, relative to the von Neumann entropy. We further define the total entanglement of a state as $\sum_{\mu \in Q} E_\mu(|s\rangle)$.

From the anticommutation relations of the Pauli matrices

$$\{\sigma_i^\mu, \sigma_j^\nu\} = 2\mathbb{I}\delta_{ij}\delta_{\mu\nu} + 2\sigma_i^\mu \sigma_j^\nu (1 - \delta_{\mu\nu}), \tag{4.6}$$

we straightforwardly derive

$$\sigma_x^a U_{ab}(\varphi) = e^{-i\frac{\varphi}{2}\sigma_z^a} e^{i\frac{\varphi}{2}\sigma_z^a\sigma_z^b} U_{ab}(\varphi)\sigma_x^a$$
$$\sigma_y^a U_{ab}(\varphi) = e^{-i\frac{\varphi}{2}\sigma_z^a} e^{i\frac{\varphi}{2}\sigma_z^a\sigma_z^b} U_{ab}(\varphi)\sigma_y^a$$
$$\sigma_z^a U_{ab}(\varphi) = U_{ab}(\varphi)\sigma_z^a$$
$$\sigma_j^\nu U_{ab}(\varphi) = U_{ab}(\varphi)\sigma_j^\nu \ , \ \forall j = x,y,z, \ \forall \nu \neq a,b$$

$$(4.7)$$

Defining $U_G(\varphi) = \prod_{(a,b)\in E} U_{ab}(\varphi)$, we obtain

$$\sigma_x^a U_G(\varphi) = U_G(\varphi)\left(\prod_{b\in N(a)} e^{-i\frac{\varphi}{2}\sigma_z^a} e^{i\frac{\varphi}{2}\sigma_z^a\sigma_z^b}\right)\sigma_x^a$$
$$\sigma_y^a U_G(\varphi) = U_G(\varphi)\left(\prod_{b\in N(a)} e^{-i\frac{\varphi}{2}\sigma_z^a} e^{i\frac{\varphi}{2}\sigma_z^a\sigma_z^b}\right)\sigma_y^a$$
$$\sigma_z^a U_G(\varphi) = U_G(\varphi)\sigma_z^a$$

$$(4.8)$$

The expectation values of the first Pauli matrix hence write

$$\begin{aligned} \langle G(\varphi)|\sigma_x^\nu|G(\varphi)\rangle &= \langle\Psi|U_G^\dagger(\varphi)\sigma_x^\nu U_G(\varphi)|\Psi\rangle \\ &= \langle\Psi|U_G^\dagger(\varphi)U_G(\varphi)\left(\prod_{\mu\in N(\nu)} e^{-i\frac{\varphi}{2}\sigma_z^\nu} e^{i\frac{\varphi}{2}\sigma_z^\nu\sigma_z^\mu}\right)\sigma_x^\nu|\Psi\rangle \\ &= \langle\Psi|e^{-i\frac{n_\nu\varphi}{2}\sigma_z^\nu}\left(\prod_{\mu\in N(\nu)} e^{i\frac{\varphi}{2}\sigma_z^\nu\sigma_z^\mu}\right)|\Psi\rangle \\ &= \cos(n_\nu\varphi/2)\cos^{n_\nu}(\varphi/2) \ , \end{aligned}$$

$$(4.9)$$

where $N(\nu)$ is the set of the first neighbours of ν, and $n_\nu = |N(\nu)|$ is its cardinality. We used the fact that all the terms including a Pauli matrix σ_z^μ acting on some $\mu \in N(\nu)$ vanish, since they appear only once and $\forall\mu$, $\langle\Psi|\sigma_z^\mu|\Psi\rangle = 0$.

The expectation value of the second Pauli matrix write

$$\begin{aligned} \langle G(\varphi)|\sigma_y^\nu|G(\varphi)\rangle &= \langle\Psi|U_G^\dagger(\varphi)\sigma_y^\nu U_G(\varphi)|\Psi\rangle \\ &= -i\langle\Psi|\left(\prod_{\mu\in N(\nu)} e^{-i\frac{\varphi}{2}\sigma_z^\nu} e^{i\frac{\varphi}{2}\sigma_z^\nu\sigma_z^\mu}\right)\sigma_y^\nu|\Psi\rangle \\ &= -i\langle\Psi|e^{-i\frac{n_\nu\varphi}{2}\sigma_z^\nu}\left(\prod_{\mu\in N(\nu)} e^{i\frac{\varphi}{2}\sigma_z^\nu\sigma_z^\mu}\right)|\Psi_\nu^-\rangle \\ &= -\sin(n_\nu\varphi/2)\cos^{n_\nu}(\varphi/2), \end{aligned}$$

$$(4.10)$$

where $|\Psi_\nu^-\rangle = |+\rangle^{V\setminus\{\nu\}} \otimes |-\rangle^\nu$, that is, the pure product state with every qubit in the state $|+\rangle$ except for qubit ν which is in the state $|-\rangle$. The final result stems from the fact that the only non-vanishing terms are the ones including one and only one Pauli matrix σ_z^ν acting on ν, since $\forall\mu$, $\langle\Psi|\sigma_z^\mu|\Psi_\nu^-\rangle = \delta_{\mu\nu}$.

Finally, the commutation relations (4.8) trivially imply

$$\langle G(\varphi)|\sigma_z^\nu|G(\varphi)\rangle = \langle \Psi|U_G^\dagger(\varphi)\sigma_z^\nu U_G(\varphi)|\Psi\rangle$$
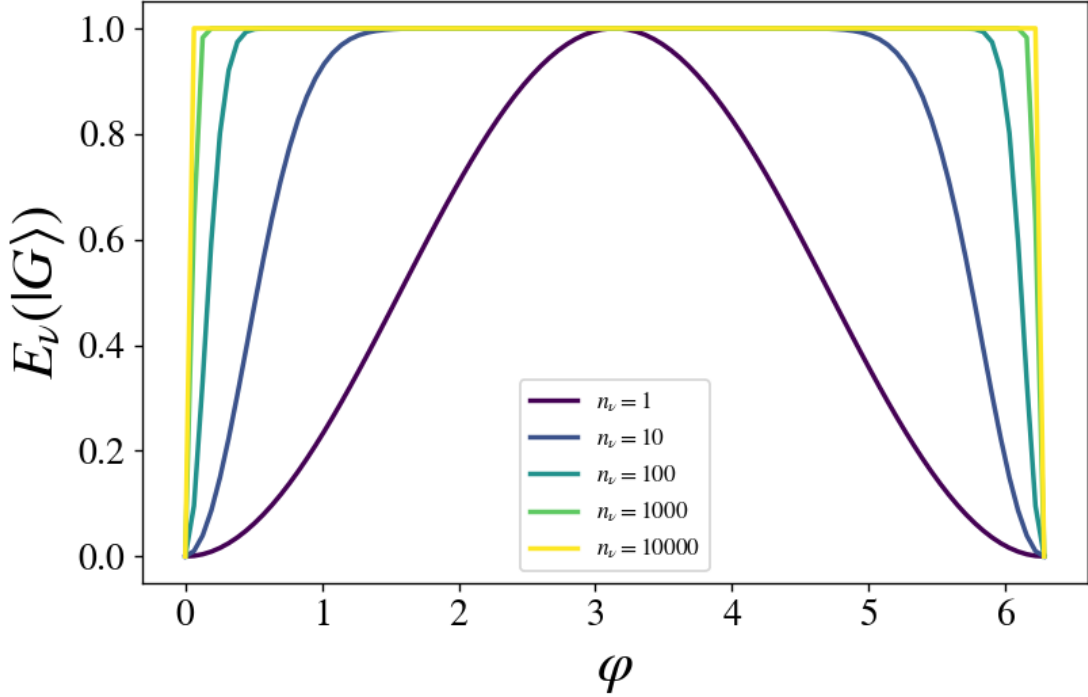$$= \langle \Psi|\sigma_z^\nu|\Psi\rangle = 0 \tag{4.11}$$
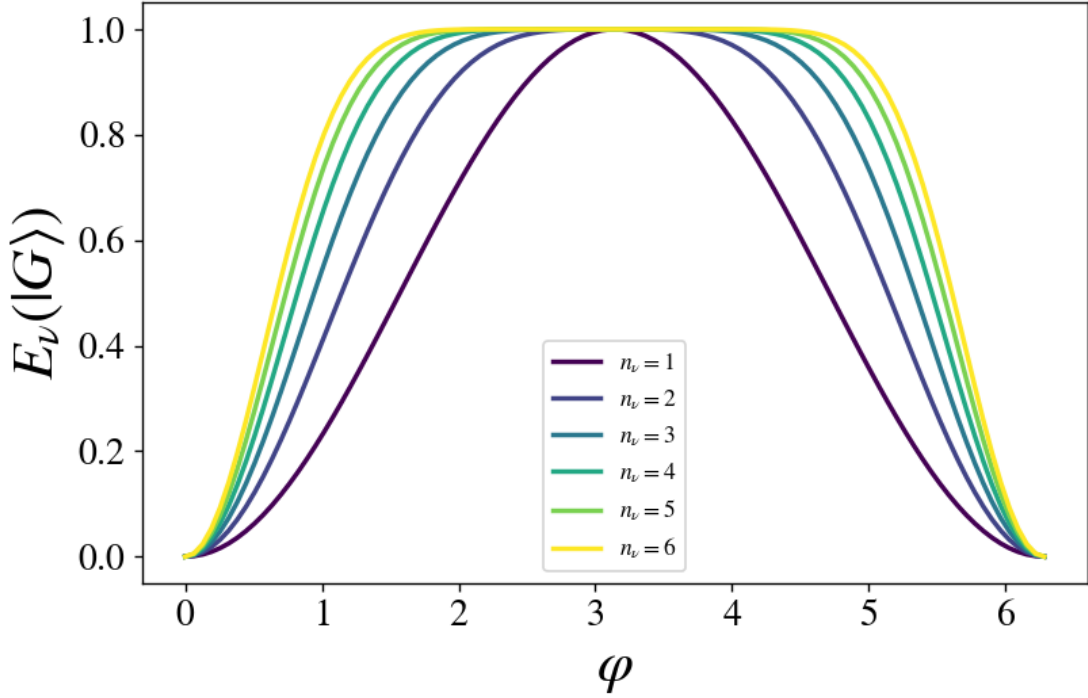
Figure 4.1.: The ED of a single qubit, as a function of the interaction strength (or duration), for different numbers n_ν of nearest neighbours. The numerical results agree perfectly with the analytical one of Equation (4.12).

It results that the single-qubit ED of a given qubit ν in a PGS depends on both the interaction strength φ and on the number n_ν of its nearest neighbours

$$E_\nu(|G(\varphi)\rangle) = 1 - \cos(\varphi/2)^{2n_\nu} \tag{4.12}$$

The numerical confirmation of this result is displayed in **Figure 4.1**.

As stated before, the value $\varphi = \pi$ corresponds to the genuine GS, in which every non-isolated qubit is maximally entangled, regardless of the number of its neighbours. Consider a PGS close to the genuine GS, i.e. where this typical interaction strength is added with a small error $\delta\varphi$, we retrieve

$$E_\nu(|G(\pi + \delta\varphi)\rangle) \approx 1 - \left(\frac{\delta\varphi}{2}\right)^{2n_\nu}, \tag{4.13}$$
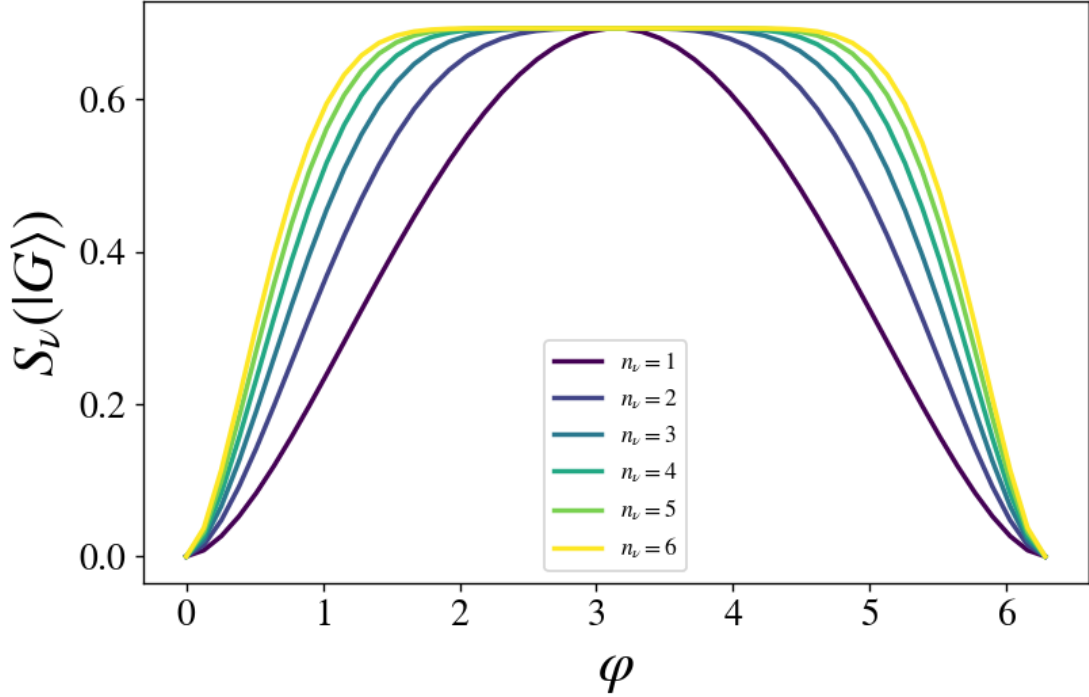
Figure 4.2.: The entropy of entanglement for a bipartition (ν, ν^C), as a function of the interaction strength (or duration), for different numbers n_ν of nearest neighbours, numerically computed. The scaling and behaviour of this well-known measure of bipartite entanglement is evidently very similar to that of the ED.

hence the qubits in a quasi GS get exponentially closer to the maximal value of entanglement as the number of their nearest neighbours increases; this is in agreement with previous results presented in the literature, where it has been found that the entanglement of single qubits in GS depends on the degree of the corresponding vertex (i.e. on n_ν) [86, 87]. The only non-trivial case where the small error could be relevant is the one of a qubit with only one link, where the correction is of $o(\delta\varphi^2)$.

It results, as **Figure 4.3** emphasizes, that the limit for a large number of bounds writes

$$E_\nu(|G(\varphi)\rangle) \xrightarrow[n_\nu \to \infty]{} \begin{cases} 0 & \text{if } \varphi = 2n\pi, \ \forall n \in \mathbb{N} \\ 1 & \text{else.} \end{cases} \tag{4.14}$$

i.e., up to a null measure set of values of φ, the ED of a single qubit approaches 1 when the number of its neighbours becomes very large. In other words, even if the pairwise interaction is very weak, the qubit-wise entanglement, in the sense of (4.5), can be very close to its maximal value.

Note that, as can be seen in **Figure 4.2** the entropy of entanglement shows

Figure 4.3.: The ED of a single qubit, as a function of the interaction strength (or duration), for different numbers n_ν of nearest neighbours.

the same behaviour and scaling as the ED, suggesting that the later stems as a valid alternative to the former as a measure of bipartite entanglement. It also has the benefit of being easier to compute, both numerically and analytically, as it only requires the calculation of expectation values, in contrast with the entropy of entanglement, which requires to compute partial trace and matrix logarithms.

4.3. Correlators and the Effects of Measurement in Graph States

We now focus on the case of *genuine* GS, i.e. when $\varphi = \pi$. In particular, we want to compute the various two-point correlators. We denote

$$U_G := \prod_{(a,b)\in E} U_{ab}(\varphi = \pi) = \prod_{(a,b)\in E} \frac{\mathbb{I} + \sigma_z^a + \sigma_z^b - \sigma_z^a \sigma_z^b}{2}. \tag{4.15}$$

From (4.8), we derive the commutation relations

$$
\begin{aligned}
\sigma_x^a U_G &= U_G \sigma_z^{N(a)} \sigma_x^a \\
\sigma_y^a U_G &= U_G \sigma_z^{N(a)} \sigma_y^a \\
\sigma_z^a U_G &= U_G \sigma_z^a,
\end{aligned}
\tag{4.16}
$$

Note that, for two ensembles A and B, we have

$$
\sigma_z^A \sigma_z^B = \sigma_z^{A \cup B} = \sigma_z^{A \triangle B},
$$

where $A \triangle B = (A \cup B) \setminus (A \cap B)$ is the symmetric difference between sets A and B.

This operation is commutative and associative. Remark that $A \triangle B = \emptyset$ if and only if $A = B$. Furthermore, $\underset{i}{\triangle} A_i := A_0 \triangle A_1 \triangle \cdots \triangle A_k \triangle \cdots = \emptyset$ if and only if $\forall \nu$, there is an even number k of sets A_i containing ν.

We can now calculate the correlators, taking advantage of the fact that $\forall A \neq \emptyset$, $\langle \Psi | \sigma_z^A | \Psi \rangle = 0$.

4.3.1. Two-point correlators

We start here by computing pairwise correlations.

$$
\begin{aligned}
\langle G | \sigma_x^\nu \sigma_x^\mu | G \rangle &= \langle \Psi | U_G \sigma_x^\nu \sigma_x^\mu U_G | \Psi \rangle \\
&= \langle \Psi | \sigma_z^{N(\nu)} \sigma_z^{N(\mu)} | \Psi \rangle \\
&= \langle \Psi | \sigma_z^{N(\nu) \triangle N(\mu)} | \Psi \rangle \\
&= \begin{cases} 1 & \text{if } N(\nu) = N(\mu), \\ 0 & \text{else.} \end{cases}
\end{aligned}
\tag{4.17}
$$

since $(N(\nu) \cup N(\mu)) \setminus (N(\nu) \cap N(\mu)) = \emptyset$ if and only if $N(\nu) = N(\mu)$. In terms of graph theory, $\langle G | \sigma_x^\nu \sigma_x^\mu | G \rangle = 1$ if and only if μ and ν are *twins* (see **Figure 4.4** for a visual example.).

$$
\begin{aligned}
\langle G | \sigma_x^\nu \sigma_y^\mu | G \rangle &= \langle \Psi | U_G \sigma_x^\nu (-i \sigma_z^\mu \sigma_x^\mu) U_G | \Psi \rangle \\
&= -i \langle \Psi | \sigma_z^{N(\nu)} \sigma_z^{N(\mu)} \sigma_z^\mu | \Psi \rangle \\
&= -i \langle \Psi | \sigma_z^{N(\nu) \triangle N(\mu) \triangle \{\mu\}} | \Psi \rangle \\
&= 0,
\end{aligned}
\tag{4.18}
$$

because, the graph being undirected, if $\nu \in N(\mu)$ then also $\mu \in N(\nu)$, hence $N(\nu) \triangle N(\mu) \neq \{\mu\}$, where $\{\mu\}$ is the singleton set containing the qubit μ only.

4. Entanglement, quantum correlators and connectivity in graph states

$$\begin{aligned}
\langle G|\sigma_x^\nu \sigma_z^\mu|G\rangle &= \langle\Psi|U_G \sigma_x^\nu \sigma_z^\mu U_G|\Psi\rangle \\
&= \langle\Psi|\sigma_z^{N(\nu)} \sigma_z^\mu|\Psi\rangle \\
&= \langle\Psi|\sigma_z^{N(\nu)\triangle\{\mu\}}|\Psi\rangle \\
&= \begin{cases} 1 & \text{if } N(\nu) = \{\mu\}, \\ 0 & \text{else.} \end{cases}
\end{aligned} \tag{4.19}$$

In terms of graph theory, $\langle G|\sigma_x^\nu \sigma_z^\mu|G\rangle = 1$ if and only if ν is a *leaf vertex* (or *pendant vertex*) attached to G through μ (see **Figure 4.4** for a visual example.).

$$\begin{aligned}
\langle G|\sigma_y^\nu \sigma_y^\mu|G\rangle &= \langle\Psi|U_G(i\sigma_x^\nu \sigma_z^\nu)(-i\sigma_z^\mu \sigma_x^\mu)U_G|\Psi\rangle \\
&= \langle\Psi|\sigma_z^{N(\nu)} \sigma_z^\nu \sigma_z^\mu \sigma_z^{N(\mu)}|\Psi\rangle \\
&= \langle\Psi|\sigma_z^{N(\nu)\triangle\{\nu\}\triangle N(\mu)\triangle\{\mu\}}|\Psi\rangle \\
&= \langle\Psi|\sigma_z^{\left(N(\nu)\cup\{\nu\}\right)\triangle\left(N(\mu)\cup\{\mu\}\right)}|\Psi\rangle \\
&= \begin{cases} 1 & \text{if } N(\nu)\cup\{\nu\} = N(\mu)\cup\{\mu\}, \\ 0 & \text{else.} \end{cases}
\end{aligned} \tag{4.20}$$

In terms of graph theory, $\langle G|\sigma_y^\nu \sigma_y^\mu|G\rangle = 1$ if and only if μ and ν are *adjacent twins* (see **Figure 4.4** for a visual example.).

$$\begin{aligned}
\langle G|\sigma_y^\nu \sigma_z^\mu|G\rangle &= \langle\Psi|U_G(i\sigma_x^\nu \sigma_z^\nu)\sigma_z^\mu U_G|\Psi\rangle \\
&= i\langle\Psi|\sigma_z^{N(\nu)} \sigma_z^\nu \sigma_z^\mu|\Psi\rangle \\
&= i\langle\Psi|\sigma_z^{\left(N(\nu)\cup\{\nu\}\right)\triangle\{\mu\}}|\Psi\rangle \\
&= 0,
\end{aligned} \tag{4.21}$$

$$\langle G|\sigma_z^\nu \sigma_z^\mu|G\rangle = \langle\Psi|\sigma_z^\nu \sigma_z^\mu|\Psi\rangle = 0, \tag{4.22}$$

For two arbitrary measurements, performed in the directions determined by the unitary vectors $\boldsymbol{v}^\nu$ and $\boldsymbol{v}^\mu$, the correlation then writes

$$\begin{aligned}
\langle G|\sigma_{\boldsymbol{v}}^\nu \sigma_{\boldsymbol{v}}^\mu|G\rangle &= \sum_{i,j=x,y,z} v_i^\nu v_j^\mu \langle G|\sigma_i^\nu \sigma_j^\mu|G\rangle \\
&= v_x^\nu v_x^\mu \quad \text{if } N(\nu) = N(\mu) \\
&\quad + v_x^\nu v_z^\mu \quad \text{if } N(\nu) = \{\mu\} \\
&\quad + v_z^\nu v_x^\mu \quad \text{if } N(\mu) = \{\nu\} \\
&\quad + v_y^\nu v_y^\mu \quad \text{if } N(\nu)\cup\{\nu\} = N(\mu)\cup\{\mu\},
\end{aligned} \tag{4.23}$$

where we denoted $\sigma_{\boldsymbol{v}}^{\mu} = \sum_{j=x,y,z} v_j^{\mu} \sigma_j^{\mu}$. It is fairly obvious that any such correlator can henceforth be fully determined by a quick inspection of the adjacency matrix A_G associated to G. For instance, the condition $N(\nu) = N(\mu)$ is equivalent to $A_\nu = A_\mu$.
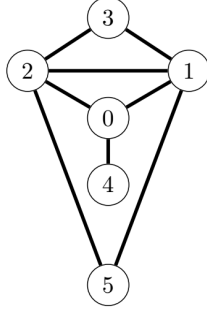
Figure 4.4.: Example of a graph. Here, vertices 3 and 5 are *twins*, 1 and 2 are *adjacent twins* and 4 is a *leaf*.

This result makes it clear that non-vanishing pairwise correlations arise only for very specific connectivity properties of the sites being considered. More precisely, graphs which contain neither twins, nor adjacent twins, nor leaf vertex, have only vanishing pairwise correlations. This is for instance the case for regular lattices.

Quite interestingly, this also implies that, in GS, most measurements that can be performed on one qubit yield no information on other qubits, and leaves the rest of the system entangled. Such entangled states hence contain *persistent entanglement*: a relatively large number of measurements are necessary to completely break their entanglement.

One can also exploit the properties of these correlators to probe the connectivity properties of a graph. Such a procedure could be for instance useful to check that, in a physical apparatus realizing the GS, the implementation of the link operators U_{ab} was successful and free of errors (that would be, the unwanted presence or absence of some of them).

From the above results, checking for twins, adjacent twins and leaf vertices will follow a fairly obvious measurement procedure. Yet it is possible to go further and check for instance for the mere pairwise neighbourhood, by removing irrelevant vertices from the graph. To do this, we can use the well-known fact that projective measurement of a single qubit in the direction z effectively removes it from the graph, i.e. isolates it [84]. Formally,

$$
\begin{aligned}
P_{z\pm}^a |G\rangle = P_{z\pm}^a U_G |\Psi\rangle &= U_G P_{z\pm}^a |+\rangle^a \otimes |+\rangle^{V\backslash\{a\}} \\
&= \begin{cases} \frac{1}{\sqrt{2}} U_G |0\rangle^a \otimes |+\rangle^{V\backslash\{a\}} = \frac{1}{\sqrt{2}} |0\rangle^a \otimes |G\backslash\{a\}\rangle \\ \frac{1}{\sqrt{2}} U_G |1\rangle^a \otimes |+\rangle^{V\backslash\{a\}} = \frac{1}{\sqrt{2}} |1\rangle^a \otimes \sigma_z^{N(a)} |G\backslash\{a\}\rangle. \end{cases}
\end{aligned} \tag{4.24}
$$

Since $\sigma_z^{N(a)}|G \setminus \{a\}\rangle$ is local-unitary equivalent to $|G \setminus \{a\}\rangle$, such projective measurement results in an equivalent statistics as the desired GS with graph $G \setminus \{a\}$, up to some rotations of the measurement axis.

With a few computations, it can easily be checked that

$$
\langle G| \left(\prod_{\mu \neq a,b} P_{z\pm}^\mu \right) \sigma_y^a \sigma_y^b \left(\prod_{\mu \neq a,b} P_{z\pm}^\mu \right) |G\rangle
$$
$$
= \begin{cases} \pm 1 & \text{if } b \in N(a) \, (\leftrightarrow a \in N(b)) \\ 0 & \text{else.} \end{cases} \tag{4.25}
$$

It is hence enough, in order to examine the existence of a given link (a, b), to perform a projective measurement on the rest of the graph, or at least on the sites that may be linked to a or b, prior to measuring the correlator $\langle \sigma_y^a \sigma_y^b \rangle$.

4.3.2. Higher order correlators

The inspection of higher order correlators can be used to retrieve information on more general properties of the graph.

4.3.2.1. Neighbourhood probing

Given an educated guess $\widetilde{N}(\nu)$ for the neighbourhood of ν, one can check its validity by computing the correlator

$$
\langle G|\sigma_x^\nu \sigma_z^{\widetilde{N}(\nu)}|G\rangle \begin{cases} 1 & \text{if } \widetilde{N}(\nu) = N(\nu) \\ 0 & \text{else,} \end{cases} \tag{4.26}
$$

4.3.2.2. Topological probing

The correlator

$$
\langle G|\sigma_x^V|G\rangle = \begin{cases} 1 & \text{if } \triangle_{\mu \in V} \, N(\mu) = \emptyset \\ 0 & \text{else,} \end{cases} \tag{4.27}
$$

results in 1 if and only if every site has an even number of neighbours.

Furthermore,

$$
\langle G|\sigma_y^V|G\rangle = \begin{cases} i^{|V|} & \text{if } \triangle_{\mu \in V} \, (N(\mu) \cup \{\mu\}) = \emptyset \\ 0 & \text{else,} \end{cases} \tag{4.28}
$$

results in ± 1 if and only if every site has an odd number of neighbours. It is 1 if $|V| \bmod 4 = 0$, -1 if $|V| \bmod 4 = 2$.

Euler's handshaking lemma states that, in any undirected graph, there is always an even number of vertices ν such that n_ν is odd. This guarantees that, as expected, this correlator never takes imaginary values.

In particular, if both (4.27) and (4.28) are null, G is not a regular graph (i.e. for which $\exists k \in \mathbb{N}$ such that $\forall \nu,\ n_\nu = k$). For instance, it can't be a lattice with periodic boundary conditions.

4.4. Relation to measurement processes

As already mentioned in the introduction, GS were proposed as a support for measurement-based quantum computation. To this aim, the system is first prepared in a GS of which the associated graph $G(V, E)$ is a regular lattice (usually, a finite square lattice). Then, a quantum circuit is built from this state by performing series of local projective measurements.

Hereafter, we thus investigate the effects of such measurements on the overall state, in the light shed by the above results.

As noticed in Ref. [34], if the expectation value of a product of Pauli observables (i.e. any product of Pauli matrices) on a given pure state $|s\rangle$, i.e. a generalized correlator, equates 1, then these observables are equivalent with respect to this state. Namely, they act on the state in the same fashion, and the associated projective measurements are themselves equivalent.

Formally, for any couple of observables $A,\ B$ such that $A^2 = B^2 = \mathbb{I}$, $\langle s|\, AB\, |s\rangle = 1$ implies

$$
\begin{aligned}
AB\, |s\rangle &= |s\rangle \\
B\, |s\rangle &= A\, |s\rangle \\
P_B\, |s\rangle &= P_A\, |s\rangle \\
P_B\, |s\rangle &= P_B P_A\, |s\rangle ,
\end{aligned}
\tag{4.29}
$$

where $P_O = \frac{1}{2}(\mathbb{I} + O)$ are projectors onto the eigenstates of O of eigenvalue $+1$.

The projective measurement of A is thus equivalent to that of B.

For instance, Equation (4.17) implies that, if μ and ν are twin vertices, the projective measure of σ_x^ν is equivalent to that of σ_x^μ.

The case of higher order correlators leads to somewhat less trivial observations. Consider a measurement of σ_x^ν with an outcome of $+1$. Formally, this corresponds to applying the projector $P_x^\nu = \frac{1}{2}(\mathbb{I} + \sigma_x^\nu)$ to the GS $|G\rangle$, up to renormalization. Yet Equation (4.26) together with Equation (4.29) tells us that this is in fact equivalent to applying $P_z^{N(\nu)} = \frac{1}{2}\left(\mathbb{I} + \sigma_z^{N(\nu)}\right)$. Notice that the latter projector is a non-local

one, as it can't be written as the product of local single-qubit projectors; its effect is to project $|G\rangle$ onto the subspace $\left\{ |\varphi\rangle \,\middle|\, \sigma_z^{N(\nu)} |\varphi\rangle = |\varphi\rangle \right\}$.

Non-locality implies that it does not correspond in itself to any physical measurement process, and rather stems as an entangling operation. It may indeed map a product state to an entangled state.

Let us examine further the effect of this projector on a GS. Omitting the renormalization factor, we obtain

$$
\begin{aligned}
P_x^\nu |G\rangle = P_z^{N(\nu)} |G\rangle &= P_z^{N(\nu)} U_G |\Psi\rangle = U_G P_z^{N(\nu)} |\Psi\rangle \\
&= \frac{1}{2} U_G |+\rangle^{V \setminus N(\nu)} \otimes \left(|+\rangle^{N(\nu)} + |-\rangle^{N(\nu)} \right).
\end{aligned}
\tag{4.30}
$$

It results that, as can also be seen by considering the commutation relations (4.8), the operation $U_G P_x^\nu U_G$ effectively entangles every qubit $\mu \in N(\nu)$ in a state local-unitary equivalent to the Greenberger–Horne–Zeilinger state of n_ν qubits, a prototypical case of maximally entangled state.

4.5. Conclusion

In an ideal setting, relatively few measurements should, in principle, be enough to compute all of these correlators.

This is due to the fact that, for perfect GS, their outcomes can only be 1, -1 or 0. Yet the measurement of a Pauli observable can only result in outcomes of ± 1, whether it is a single-qubit or a multi-qubit (i.e. correlator) observable.

Hence if the statistics yields, for a given Pauli observable P, an expectation value of $\langle G|P|G\rangle = 1$, we expect to measure only ones. It is thus enough to have measured a single -1 to conclude that $\langle G|P|G\rangle = 0$. The same reasoning obviously applies to the case of opposite value $\langle G|P|G\rangle = -1$.

Conversely, if the statistics yields an expectation value of 0, the probability of a measurement outcome ± 1 is $\frac{1}{2}$, hence a uniform series of measurement outcomes becomes exponentially less likely as the number of measurements M grows. Precisely, if the value 1 has been measured M times in a row (and the value -1 has never been measured) the statistics yields $\langle G|P|G\rangle = 1$ with a probability of $1 - 2^{-M}$. Hence one would need at most $M = -\log_2(\epsilon)$ measurement samples to retrieve the true statistics with a confidence of $1 - \epsilon$.

In a *quasi* GS (i.e. $\varphi = \pi + \delta\varphi$), the link operators write $U_{ab}(\pi + \delta\varphi) = U_{ab}\, \delta U_{ab}$, with

$$
\delta U_{ab} = \mathbb{I} - i\frac{\delta\varphi}{4} \left(\mathbb{I} - \sigma_z^a - \sigma_z^b + \sigma_z^a \sigma_z^b \right),
\tag{4.31}
$$

up to $o(\delta\varphi^2)$. The resulting commutation relations write

$$\sigma_k^a U_{ab}\,\delta U_{ab} = U_{ab}\,\delta U_{ab}\left(\sigma_z^b + i\frac{\delta\varphi}{2}\sigma_z^a - i\frac{\delta\varphi}{2}\sigma_z^a\sigma_z^b\right)\sigma_k^a, \qquad (4.32)$$

for $k = x, y$, while $[\sigma_z^a, U_{ab}\,\delta U_{ab}] = 0$.

Yet expectation values are always real, thus only even powers of $i\delta\varphi$ can appear in their final expression.

It results that the error on the correlators computed above is at most of order $o(\delta\varphi^2)$.

Throughout this work, we have developed a new approach to characterize GS. This approach is complementary to the stabilizer formalism widely used in the quantum computing community. While the stabilizer approach is a powerful tool for the analysis and construction of quantum algorithms with GS, the approach we propose relies on quantities, such as correlators, with a more straightforward interpretation.

Formally, a pure quantum state constitutes a statistical distribution for all possible measurement outcomes. As such, it is entirely determined by its statistical moments. In other words, knowing all possible expectation values and correlators of a state is equivalent to knowing the whole state. Although characterizing a pure state solely through expectation values may seem unreasonable from a computational point of view, a number of relevant partial information can be obtained this way.

Correlators possess the desirable property of being both easily calculable and physically meaningful. In fact, they allow encoding the complexity of a graph state in terms of experimentally accessible quantities, revealing the structure of interactions between the composing qubits. Using this framework, we have been able to highlight simple relations between correlators and the connectivity properties of the graph defining a given graph state. The presented results offer a toolbox to investigate the topological structure of GS that can be used to verify the presence of local errors in their physical implementation. Moreover, since GS represents a universal resource for quantum computations, these results can be exported to any other universal resource, provided the appropriate mapping is carried out.

Furthermore, we have shown that correlators have the additional advantage of highlighting when pairs of projective measurements are equivalent with respect to a given state. This provides a new approach to understanding the effects of projective measurements on GS, revealing how multipartite entanglement emerges from simple binary interactions. Additionally, it could potentially enable determining simpler ways to implement quantum gates.

A follow-up to this work would be to thoroughly examine the formal connections between stabilizer-based and correlator-based approaches to improve the characterization of GSs and their structure.

5. Quantum Phase Transition in the Tavis-Cummings Model

The past few years, quantum correlation (QC) and, more specifically, entanglement has been proposed as fundamental resources for the realization of high-efficiency quantum batteries [89, 90, 91]; more specifically, it has been shown that a quantum speedup, resulting in super-extensive power of quantum batteries, could theoretically be achieved by *entangling operation*[92]s. Some of the models adopted as promising candidates to realize quantum batteries are inspired by the Tavis-Cummings (TC) and Dicke models[93, 94, 95, 96]. It was shown in [89] that the extensive advantage could not be achieved without global operations, that is, formally, non-local operators acting on the whole system at once; it is, however, not clear if systems such as the TC model fall into this category, as the interaction between the atomic degrees of freedom is somewhat indirect, *mediated* by an electromagnetic cavity. It is therefore of great interest to assert if, the superradiance is accompanied by entanglement between the atoms, thus producing an *effective* global entangling operation.

In this study, we limit ourselves to the zero-temperature regime, thus only investigating the ground state of the model and its dependence to the control parameters; thus, thermal decoherence effects are not taken into account.

We start by fully introducing the TC model in Section 5.1. In Section 5.2, we show that, despite its finite number of degrees of freedom, the model undergoes a Quantum Phase Transition (QPT), the superradiant phase transition, that has the shape of a spontaneous symmetry breaking (SSB) and corresponds to successive crossings, in a narrow region, of the subspaces of minimal energy. Resorting to the QCD (3.10), we further show in Section 5.3 that this QPT is accompanied by a crossover in the QCs between the atoms (i.e. qubits); this behaviour of the QCD, persistent when the system size is increased, can henceforth be considered a suitable order parameter for this transition. In Section 5.4, we discuss how the concurrence computed in the two-atom system, added with the application of an entanglement criterion to several finite-sized systems, and with the QCD previously calculated, all strongly suggest that the superradiant phase transition in this model is accompanied by a transition in the entanglement between the atoms. We finally discuss our results in Section 5.5.

An article presenting the following results is in preparation [38].

5.1. The Tavis-Cummings Model

The Rabi model, describing the dynamics of a two-level atom coupled with a single-mode quantized field [97, 98], raised a lot of attention since it was formulated. While not exactly solvable, its dynamics was extensively studied, for instance through perturbative analysis [99, 100]. Previous work on the Rabi model [101], it has been shown that also the Rabi model undergoes a QPT for finite systems.

On the contrary, the Dicke model [102, 98], the multi-atom generalization of the Rabi model, is known to display a QPT only in the limit of an infinite number of atoms.

The Jaynes–Cummings (JC) model was initially proposed in 1963 [103] to describe the interaction of a two-level atom with an electromagnetic field. It is a fully solvable quantum model of a qubit in interaction with a quantized single-mode field. The technical progress nowadays achieved, has made this system experimentally realizable [104, 105], and, this has given new interest to this model. Besides the applicative interest, the JC model is still considered an intriguing model by virtue of the many physical effects it exhibits, like, for instance, Rabi oscillations, collapses and revivals of Rabi oscillations and the superradiant QPT [106, 107, 108, 109].

Recently, in Ref. [110] , it has been shown that the JC model exhibits a QPT at a finite number of components. In particular, it has been shown that this model undergoes a superradiant second-order QPT. In the broken-symmetry phase, the ground state forms a photon condensate characterized by a macroscopic photon occupation number.

The TC model is a generalization of the JC model, where M two-level atoms (qubits) interacting with a single mode of a quantized electromagnetic field are considered [111]. The TC model, indeed, gives the opportunity to observe further non-classical effects, such as state squeezing and quantum state entanglement. These latter phenomena, in particular, are considered of primary importance, for instance, in pushing the performance of optical atomic clocks toward the Heisenberg limit [112]. The TC model Hamiltonian reads

$$H = \omega_c a^\dagger a + \omega_z S_3 - \frac{\lambda}{\sqrt{M}}(a^\dagger S_- + a S_+) \,, \tag{5.1}$$

where $a^\dagger$ and a are the creation and annihilation operators of photons in the cavity and satisfying $[a, a^\dagger] = 1$. The total spin operator components S_j, $j = x, y, z$, satisfy the usual commutations $[S_i, S_j] = i\epsilon_{ijk}S_k$ and $S_\pm = S_x \pm iS_y$. Here and in the following we consider units in which $\hbar = 1$. In terms of the Pauli matrices σ_j^α ($j = x, y, z$), where $\alpha = 0, \ldots, M-1$ runs on the index of the -distinguishable- atoms, we have $S_j = \sum_{\alpha=0}^{M-1} \sigma_j^\alpha / 2$. The model has three tuning parameters, the photon frequency ω_c, the atomic energy splitting ω_z, and the photon–atom coupling λ.

The calculation of the eigenstates can be made easier by writing down the Hamiltonian of the full system as a sum of two commuting terms. It results $H = H_I + H_{II}$, where $H_I = \omega_c(a^\dagger a + S_z)$, $H_{II} = \Delta S_z - \lambda/\sqrt{M}(a^\dagger S_- + a S_+)$ and $\Delta = \omega_z - \omega_c$ is the detuning.

5.2. Quantum Phase Transition

The TC model has an infinite-dimensional Hilbert space, due to the unbounded number of photons. However, $[H_I, H] = 0$, thus one can choose a (finite dimension) basis of states which are -simultaneous- eigenstates for H and H_I.

The eigenvalues of the conserved quantity H_I are $E_k^I = \omega_c(k - M/2)$, their corresponding multiplicities $d_k^I = \min(k+1, M+1)$, with $k \in \mathbb{N}$ the total excitation number. Therefore, to determine the energy spectrum of the full Hamiltonian, one has to diagonalize H_{II} in each of the eigenspaces $\mathcal{H}_k^I$ (of dimension d_k^I) associated with the eigenvalues of H_I, for $k \in \mathbb{N}$. Let us denote with $|n, M_z\rangle$ the tensor product of a n-photon Fock state and a normalized eigenstate of S_z with eigenvalue M_z, $-M/2 \leq M_z \leq M/2$. Note that the states $|n, M_z\rangle$ are obviously also eigenstate of $\mathbf{S}^2$ with eigenvalues $M/2(M/2+1)$. The k-th eigenspace $\mathcal{H}_k^I$ is spanned by the vectors $|k, -M/2\rangle, \ldots, |0, k - M/2\rangle$, for $k \leq M$ and $|k, -M/2\rangle, \ldots, |k - M, M/2\rangle$, for $k > M$. Let us denote with E_k the lowest eigenvalue of H in each $\mathcal{H}_k^I$. The full-Hamiltonian spectrum can be determined via numerical methods. Nevertheless, we can catch some hints about the mechanism at the base of the quantum phase transition that the system undergoes, by investigating the properties of the lowest levels of $\mathcal{H}_k^I$, for $k = 0, 1$.

The vacuum state $|E_0(g)\rangle = |0, -M/2\rangle$ is the eigenstate in $\mathcal{H}_0^I$ with eigenvalue $E_0(g) = -\omega_z M/2$. The minimum energy level of H in $\mathcal{H}_x^I$ reads

$$E_1(g) = \frac{\omega_c}{2} + \frac{\omega_z}{2}[1 - M] - \frac{\omega_z}{2}\sqrt{\left(1 - \frac{1}{\eta}\right)^2 + \frac{4g^2}{\eta}}, \tag{5.2}$$

where we have introduced the dimensionless parameters $\eta = \omega_z/\omega_c$ and $g = \lambda/\sqrt{\omega_c \omega_z}$. The corresponding eigenstate is

$$|E_1(g)\rangle = \sin(\beta/2)|0, 1 - M/2\rangle - \cos(\beta/2)|1, -M/2\rangle, \tag{5.3}$$

where

$$\beta = \arccos[(1 - \eta^{-1})/\sqrt{(1 - \eta^{-1})^2 + 4g^2\eta^{-1}}]. \tag{5.4}$$

For $g < 1$, the ground state for the full Hamiltonian (5.1) is $|E_0(g)\rangle$. Yet, at $g = g_1 := 1$ level $E_0(g)$ crosses level $E_1(g)$. This first level crossing is followed by further crossing between minimum energy levels of successive multiplets: by increasing the magnitude of g, the minimum energy level $E_k(g)$ of $\mathcal{H}_k^I$ crosses the minimum energy level $E_{k+1}(g)$ of $\mathcal{H}_{k+1}^I$ in $g = g_k$, $\forall k$. Figure 5.1 shows the crossing

of the minimum energy eigenvalues of the multiplets of $\mathcal{H}_k$, for $k = 0, \ldots, 50$. Figure 5.2 shows a zoom of the crossing of the levels E_0, E_1, E_2, E_3, E_4.
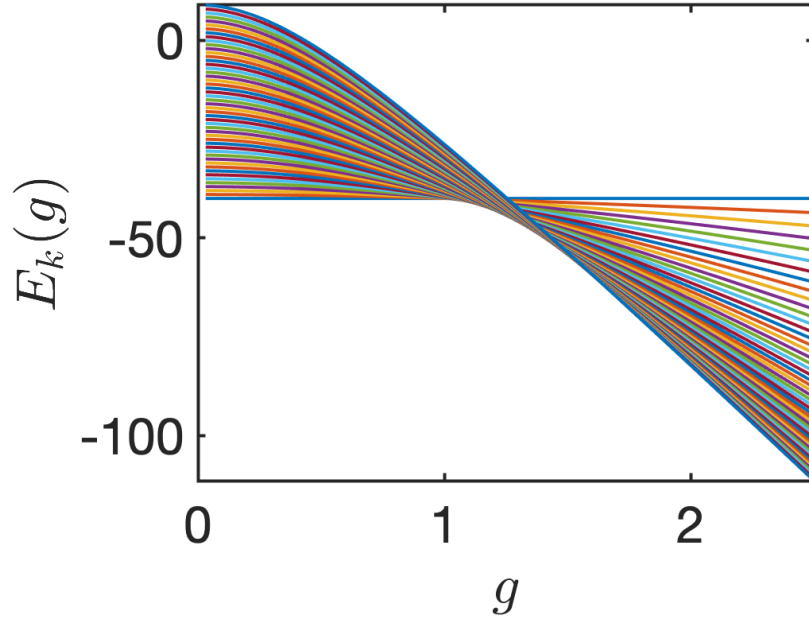
Figure 5.1.: Minimum energy eigenvalues versus g, for the first fifty multiplets. The figure refers to a system of $M = 8$ qubits and with $\eta = 10$.
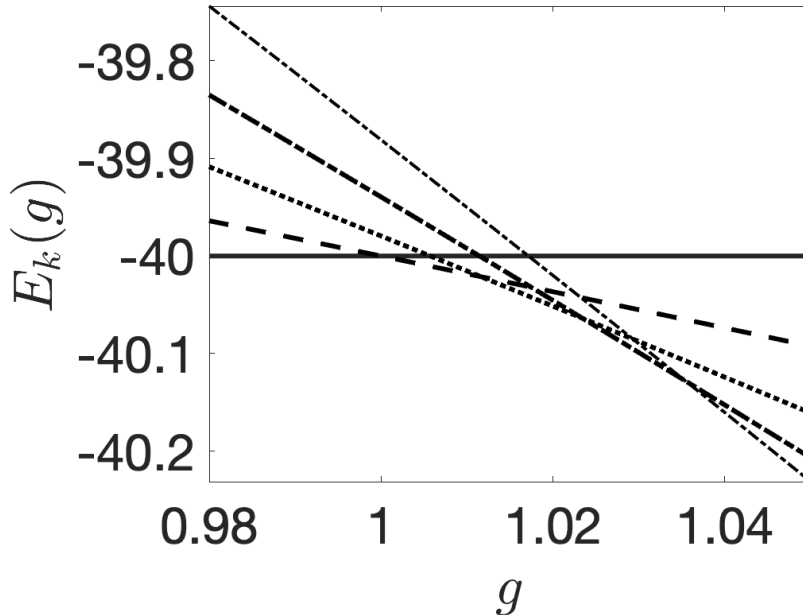
Figure 5.2.: The figure shows a zoom the energy levels E_0 (continuous line), E_1 (dashed line), E_2 (dotted line), E_3 (dot-dash line), E_4 (gray dot-dash line) versus g. The parameters are the same as for Figure 5.1.

At $g = 1$, the system undergoes a QPT under the form of a spontaneous symmetry breaking. In fact, Hamiltonian (5.1) is invariant under the continuous $U(1)$ symmetry group associated to the unitary operators $e^{iT\phi}$, where $T = H_{II} + \mathbb{I}\Delta M/2$ and $\phi \in \mathbb{R}$, since $[H, T] = 0$. Now, for $g < 1$ the ground state is invariant under the action of such operators, since $T|E_0\rangle = 0$, on the contrary, for $g > 1$ the ground state is no longer invariant under the same symmetry, bringing the system to a spontaneous symmetry breaking.

In the asymptotic limit $k \gg M$, the following approximation for the full Hamiltonian holds

$$H \approx \omega_c \left(k - \frac{M}{2}\right) \mathbb{I} + \omega_z \left(1 - \frac{1}{\eta}\right) J_z - 2\omega_z g\sqrt{\frac{k}{\eta M}} J_x, \qquad (5.5)$$

where the operators J_j, for $j = x, y, z$, are the usual angular momentum operators. We introduce the usual basis of eigenstates for $\boldsymbol{J}^2$ and J_z derived from the basis vectors of $\mathcal{H}_k^I$, according to the following mapping

$$|J = M/2; J_z = M_z\rangle := |k - M/2 - M_z, M_z\rangle, \qquad (5.6)$$

for $M_z = -M/2, \ldots, M/2$. The minimum energy level of the approximated Hamil-

tonian (5.5) in each eigenspace $\mathcal{H}_k^I$ is

$$\tilde{E}_k(g) = \omega_c\left(k - \frac{M}{2}\right) - \omega_z\frac{M}{2}\sqrt{\left(1 - \frac{1}{\eta}\right)^2 + \frac{4g^2k}{\eta M}}, \qquad (5.7)$$

and the corresponding eigenvector is

$$|\tilde{E}_k(g)\rangle = \sum_{n=-M/2}^{M/2}\binom{M}{M/2+n}^{1/2}c_k^{M/2-n}s_k^{M/2+n}|k - M/2 - n, n\rangle, \qquad (5.8)$$

where $c_k = \cos(\beta_k/2)$, $s_k = \sin(\beta_k/2)$ and

$$\beta_k = \arccos\left[(1 - \eta^{-1})/\sqrt{(1 - \eta^{-1})^2 + 4g^2\eta^{-1}k/M}\right]. \qquad (5.9)$$
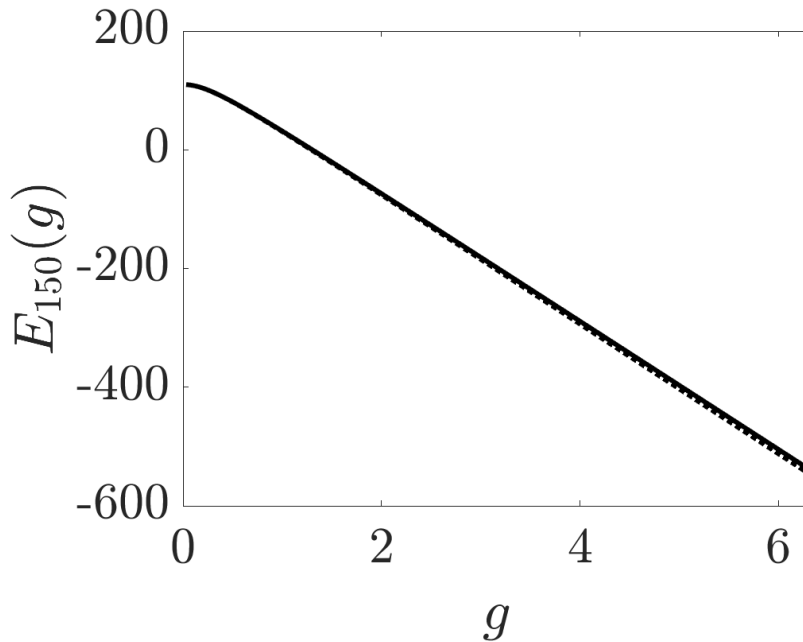
Figure 5.3.: The figure compares the plots of the energy level E_{150} versus g, corresponding to the minimum energy eigenvalue of the eigenspace $\mathcal{H}_k^I$, $k = 150$. Here we have considered a system with $M = 8$ qubits and with $\eta = 10$. In a continuous line, we report $E_{150}(g)$ derived by numeric diagonalization of the full Hamiltonian (5.1) and in dashed line the approximated level given in Eq. (5.7). The agreement between the two curves is very good.

In Fig. 5.3 we compare the plots of the minimum energy eigenvalue of the eigenspace $\mathcal{H}_{150}$, $E_{150}(g)$ as a function of g, derived by direct numeric diagonalization

of the full Hamiltonian (5.1) and the approximated level $\tilde{E}_{150}(g)$ of Eq. (5.7). The agreement between the two plots is very good on a wide range of values for g. Furthermore, after Eq. (5.7) it is easy to prove that the crossing between the approximated minimum level in $\mathcal{H}_k^I$, $\tilde{E}_k(g)$, and the one in $\mathcal{H}_{k+1}^I$, that is $\tilde{E}_{k+1}(g)$, corresponds to the following value for g

$$g_k \approx \left\{ \frac{2k}{\eta M} \left[1 + \sqrt{1 + (M(\eta - 1)k^{-1}/2)^2} \right] \right\}^{1/2} . \tag{5.10}$$

Thus, for each $k \gg M$, for $g \lesssim g_k$, $\tilde{E}_k(g) < \tilde{E}_{k+1}(g)$ is the energy of the ground state $|\tilde{E}_k(g)\rangle$ and, beyond the level crossing, for $g \gtrsim g_k$, $\tilde{E}_{k+1}(g)$ is the subsequent energy for the new ground state $|\tilde{E}_{k+1}(g)\rangle$. Remarkably, in the limit of strong spin energy separation, that is $\eta \to \infty$, all the crossing-level points merge at the QPT point $g = 1$.

5.3. Quantum Correlations

The QCD between the atoms is computed by applying definition (3.10) to the atomic density matrix $\rho_s(g)$. The latter is a function of the coupling parameter g and is derived from the density matrix $\rho(g) = |GS(g)\rangle\langle GS(g)|$ of the ground state of the full system, by tracing out the photons' degrees of freedom, therefore we have $\rho_s(g) = \mathrm{tr}_{ph}[\rho(g)]$. The g-dependent ground state of the full system is

$$|GS(g)\rangle = |E_k(g)\rangle \text{ such that } E_k(g) = \min_n\{E_n(g)\} . \tag{5.11}$$

In the general case, we compute the QCD by numeric calculations. Nevertheless, to better explain our method we consider the explicit calculation in three cases: when $g < 1$, in the vicinity of the first level crossing $g \gtrsim 1$, and in the $k \gg M$ limit. In our calculation we will resort to the Dicke states $|D_n^M\rangle$ of M-qubits. A state $|J = \frac{M}{2}, M_z = n - \frac{M}{2}\rangle$ is in fact one (degenerate) state of n excited qubits, in one-to-one correspondence with the Dicke state $|D_n^M\rangle$. These latter are defined as

$$|D_n^M\rangle = \binom{M}{n}^{-1/2} \sum_j P_j\{|1\rangle^{\otimes n} \otimes |0\rangle^{\otimes M-n}\}, \tag{5.12}$$

here we denote with $\sum_j P_j$ the sum over all the possible permutations and, for $\mu = 0, \ldots, M - 1$, $|0\rangle^\mu$ and $|1\rangle^\mu$ are the eigenstates of σ_z^μ with eigenvalues $+1$ and -1, respectively.

Case $g < 1$ In this case, the full system ground state is $|E_0(g)\rangle$ and $\rho_s(g) = \mathrm{tr}_{ph}[|E_0(g)\rangle\langle E_0(g)|] = |D_M^M\rangle\langle D_M^M|$, thus $\rho_s^2 = \rho_s$. Furthermore, by placing

$$\langle D_M^M|\sigma_j^\mu|D_M^M\rangle = -\delta_{j,3} \tag{5.13}$$

in Eq. (3.8) we get $A_{ij}^{\mu} = \delta_{i3}\delta_{j3}$. Thus, finally we have $C(\rho_s(g))/M = 0$ for $g < 1$.

Case $g \gtrsim 1$ $|GS(g)\rangle = |E_1(g)\rangle$ reported in Eq. (5.3) and we have

$$\rho_s = s^2 |D_{M-1}^M\rangle\langle D_{M-1}^M| + c^2 |D_M^M\rangle\langle D_M^M| \,, \tag{5.14}$$

where $s = \sin(\beta/2)$, $c = \cos(\beta/2)$ and β is given in Eq. (5.4). Remarkably, the fact that the partial trace operation results in a mixed state, highlights that the photonic and atomic parts of the system are entangled in this case. By direct calculation one derives $\text{tr}(\rho_s^2) = s^4 + c^4$. Furthermore, by plugging in Eq. (3.8) the following identities

$$\begin{aligned}
\langle D_{M-1}^M | \sigma_i^{\mu} | D_M^M \rangle &= (\delta_{i,1} - i\delta_{i,2})/\sqrt{M} \,, \\
\langle D_{M-1}^M | \sigma_i^{\mu} | D_{M-1}^M \rangle &= \delta_{i,3}(2 - M)/M \,,
\end{aligned} \tag{5.15}$$

one can derive $\lambda_{max}^{\mu}(\rho_s)$, the maximum eigenvalues of the matrices $A^{\mu}(\rho)$. It results

$$\lambda_{max}^{\mu}(\rho_s) = s^4 + c^4 - 4s^4(1 - 1/M)/M \,. \tag{5.16}$$

Thus, we have

$$C(\rho_s(g))/M = \frac{4s^4}{M}\left(1 - \frac{1}{M}\right) \,. \tag{5.17}$$

Case $k \gg M$ We now consider the approximated ground states of Eq. (5.8), $|GS\rangle = |E_k\rangle$. In this case, one can perform some analytical computation. From Eq. (5.8), we draw the spin density matrix

$$\rho_s = \sum_{n=0}^{M} \binom{M}{n} c_k^{2M-2n} s_k^{2n} |D_{M-n}^M\rangle\langle D_{M-n}^M| \,. \tag{5.18}$$

Once again, the mixedness of this state indicates a strong entanglement between the photonic and atomic parts of the system. By direct calculation one gets

$$\text{tr}\left(\rho_s^2\right) = \sum_{n=0}^{M} \left[\binom{M}{n} c_k^{2M-2n} s_k^{2n}\right]^2 \,, \tag{5.19}$$

and

$$\langle D_n^M | \sigma_x^\mu | D_{n'}^M \rangle = \sqrt{\left(1 - \frac{(n-1)}{M} \right) \frac{n}{M}} \delta_{n,n'+1} +$$

$$+ \sqrt{\left(1 - \frac{n}{M} \right) \left(\frac{n+1}{M} \right)} \delta_{n,n'-1},$$

$$\langle D_n^M | \sigma_y^\mu | D_{n'}^M \rangle = i \sqrt{\left(1 - \frac{(n-1)}{M} \right) \frac{n}{M}} \delta_{n,n'+1} +$$

$$- i \sqrt{\left(1 - \frac{n}{M} \right) \left(\frac{n+1}{M} \right)} \delta_{n,n'-1},$$

$$\langle D_n^M | \sigma_z^\mu | D_{n'}^M \rangle = \left(1 - 2\frac{n}{M} \right) \delta_{n,n'}.$$

(5.20)

From the latter identities it is possible to derive the eigenvalues of the matrices $A^\mu(\rho)$. After some calculation we get

$$\lambda_{zz}^\mu(\rho_s) = \sum_{n=0}^{M} \binom{M}{n}^2 c_k^{4(M-n)} s_k^{4n} \left(1 - 2\frac{n}{M} \right)^2,$$

$$\lambda_{xy}^\mu(\rho_s) = 2 \sum_{n=0}^{M} \binom{M}{n}^2 c_k^{4(M-n)-2} s_k^{4n+2} \left(1 - \frac{n}{M} \right)^2.$$

(5.21)

Note that there is a crossover between the λ_{zz}^μ and λ_{xy+}^μ, in the region $g \gtrsim 1$, at which the QCD displays a peak. Finally, we get

$$C(\rho_s(g))/M = \min \left\{ \sum_{n=0}^{M} \binom{M}{n}^2 c_k^{4M-4n} s_k^{4n} \times 4\frac{n}{M} \left(1 - \frac{n}{M} \right), \right.$$

$$\left. \sum_{n=0}^{M} \binom{M}{n}^2 c_k^{4M-4n} s_k^{4n} \times \left(1 - 2\left(\frac{s}{c}\right)^2 \left(1 - \frac{n}{M} \right)^2 \right) \right\}.$$

(5.22)
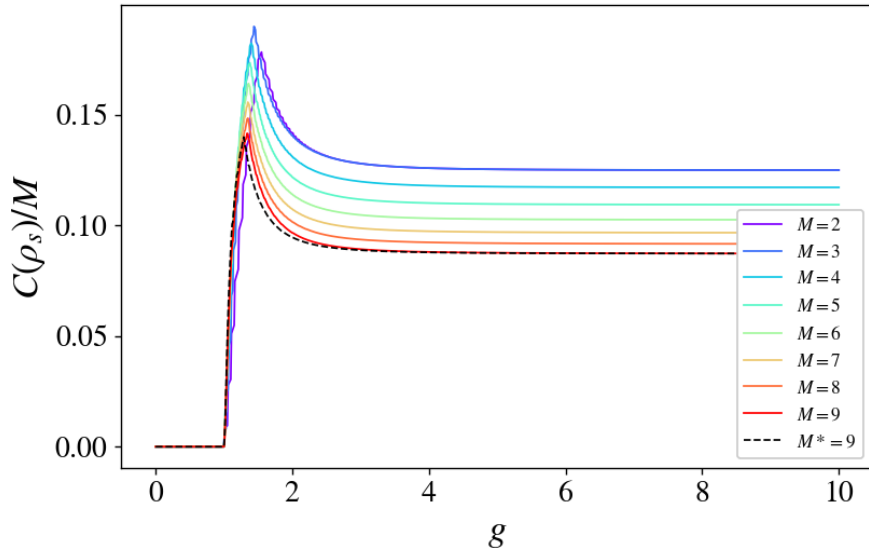
Figure 5.4.: The figure plots the QCD per qubits $C(\rho_s)/M$ versus g, derived by numerical calculations. The lines refer to the cases of a system with $M = 2, 3, 4, 5, 6, 7, 8, 9$ qubits. Line $M^* = 9$ shows the asymptotic prediction (5.22), valid in the limit $k \gg M$. All the cases consider $\eta = 10$.
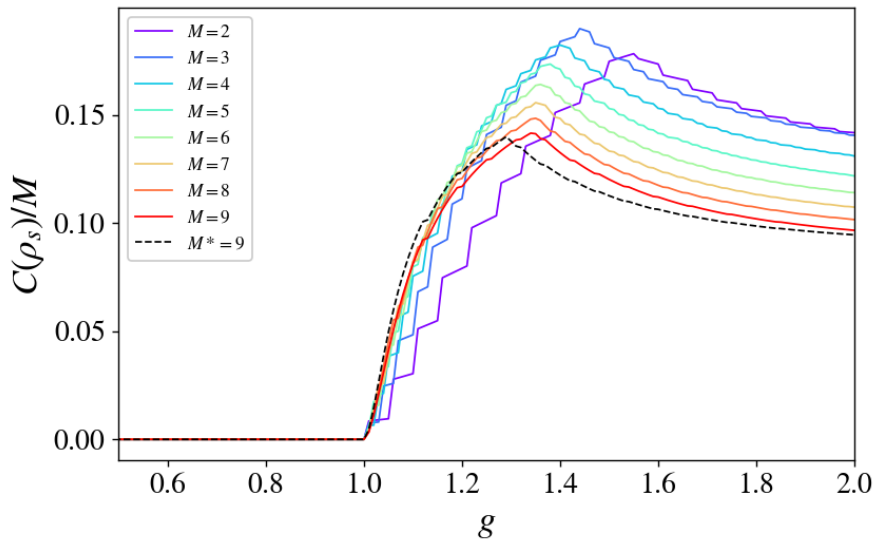
Figure 5.5.: The figure reports a magnification of Fig. 5.4.

Figures 5.4 and 5.5 report the QCD per qubit $C(\rho_s)/M$ as a function of g, achieved by numerical calculations. The lines refer to the cases $M = 2, 3, 4, 5, 6, 7, 8, 9$ and the asymptotic predictions, valid in the limit $k \gg M$, for the case $M^* = 9$ (see the

legend). The agreement between the numerical results and the analytical prediction valid in the limit $k \gg M$ is very good in the strong coupling regime.

Here, it is evident that the QCD is decreasing in average, as a function of M, even around the transition, at $g \gtrsim 1$. We however claim that this is primarily due to the high degree of mixing of $\rho_s(g > 1)$: as explained in Section 3.4, the QCD being built using the Hilbert-Schmidt norm, it scales as the purity. We indeed verified, as shown in Figure 5.6, that the purity $\mathrm{tr}(\rho_s^2)$ is a decreasing function of g and a decreasing function of M.
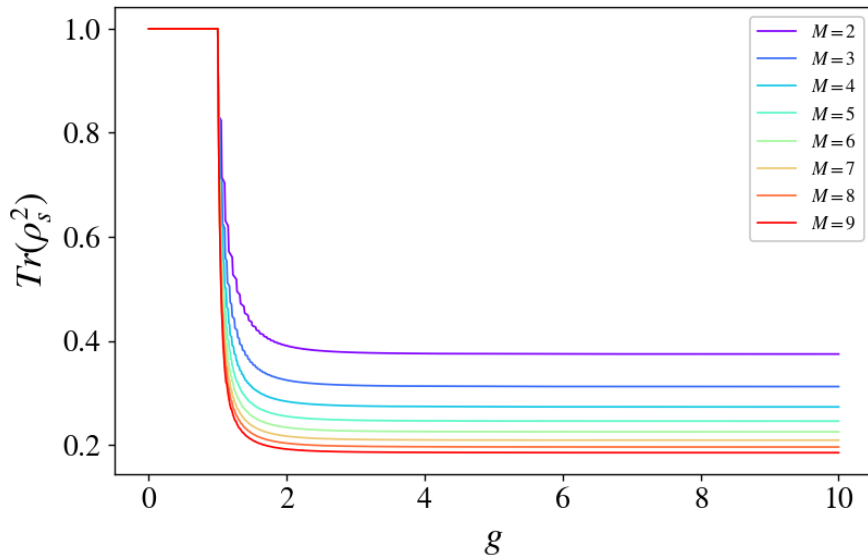
Figure 5.6.: The figure reports the purity $\mathrm{tr}(\rho_s^2)$ as a function of the coupling g, derived by numerical calculations, in the cases $M = 2, 3, 4, 5, 6, 7, 8, 9$. Also in all these cases $\eta = 10$.

Motivated by the observations we made in Section 3.4, we thus deem especially useful in this case to also consider the rescaled measure (3.36).

The Dicke states form an orthonormal basis, so $\sqrt{\rho_s}$ is straightforwardly obtained by substituting, in Eqs. (5.14) and (5.18), the probability weights (i.e. the eigenvalues of ρ_s) by their square root, owing to (3.37). It results, in the case $g \gtrsim 1$,

$$\widetilde{C}(\rho_s(g))/M = \frac{4s^2}{M}\left(\frac{1}{2} - \frac{1}{M}\right), \tag{5.23}$$

and in the case $k \gg M$,

$$\widetilde{C}(\rho_s(g))/M = \min\left\{ \sum_{n=0}^{M} \binom{M}{n} c_k^{2M-2n} s_k^{2n} \times 4\frac{n}{M}\left(1 - \frac{n}{M}\right),\right.$$
$$\left.\sum_{n=0}^{M} \binom{M}{n} c_k^{2M-2n} s_k^{2n} \times \left(1 - 2\frac{s}{c}\sqrt{\frac{M-n}{n+1}}\left(1 - \frac{n}{M}\right)\right)\right\}.$$
$$(5.24)$$

Figure 5.7 and 5.8 report the rescaled QCD per qubit $\widetilde{C}(\rho_s(g))/M$ as a function of g, achieved by numerical calculations. Once again, the agreement between the numerical results and the analytical prediction valid in the limit $k \gg M$ is very good in the strong coupling regime. The rescaled QCD clearly converges, with increasing M, toward a finite value both at $g \gtrsim 1$ (where it approaches a value greater than 0.6) and for $g \gg 1$ (where it approaches 0.5).
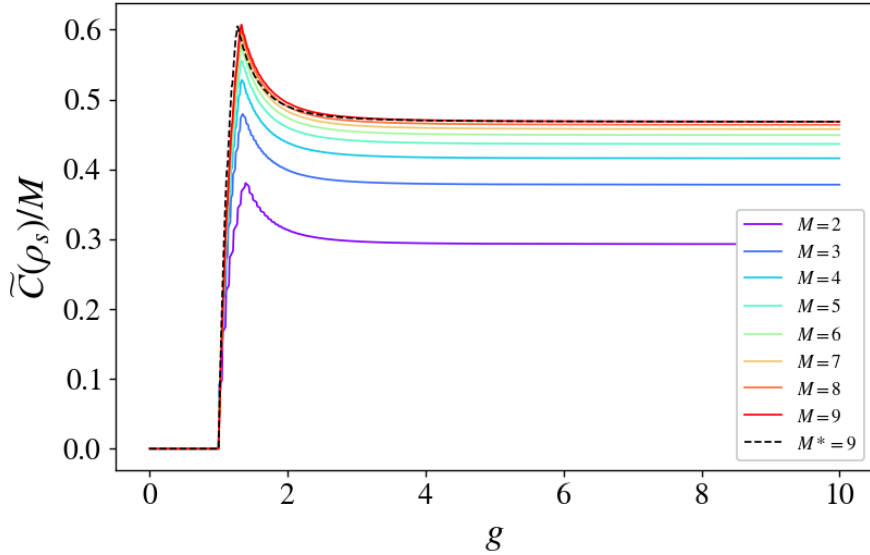
Figure 5.7.: The figure reports the rescaled QCD per qubit $\widetilde{C}(\rho_s)/M$ as a function of the coupling g, derived by numerical calculations, in the cases $M = 2, 3, 4, 5, 6, 7, 8, 9$ and with the approximated relation for the QCD of Eq. (5.22) in the case $M^* = 9$. Also in all these cases $\eta = 10$.
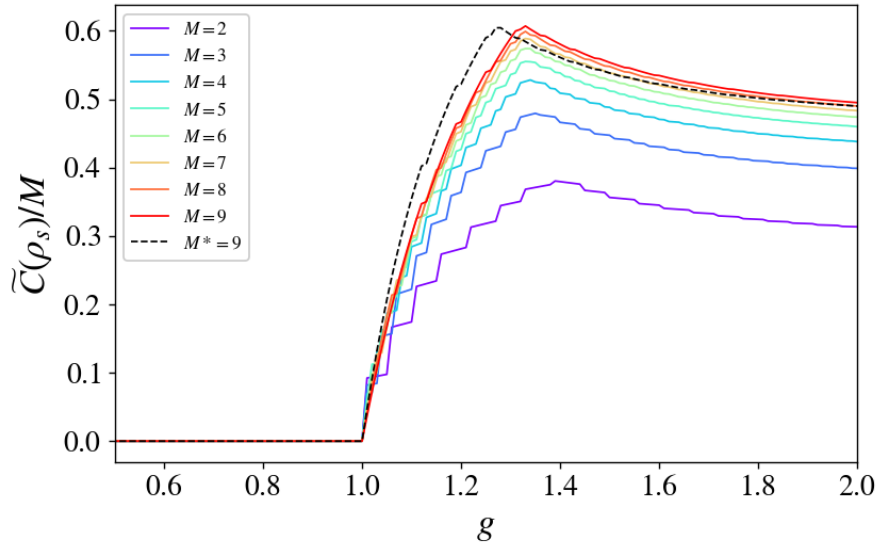
Figure 5.8.: The figure reports a magnification of Fig. 5.7.

In Figure 5.9, we show the behaviour of the excitation number k^* of the ground state as a function of g. We clearly see that the slope gets steeper with larger M. We furthermore observed in Figure 5.10 that, in the region $g \lesssim 2.5$, the curves k^*/M all collapse onto the same straight line, showing that, in this region, k^* is roughly linear in M. This suggests that, in the thermodynamic limit, all the level crossings collapse at $g \approx 1$, and that k^* diverges in this region, accounting for the phenomenon of superradiance.
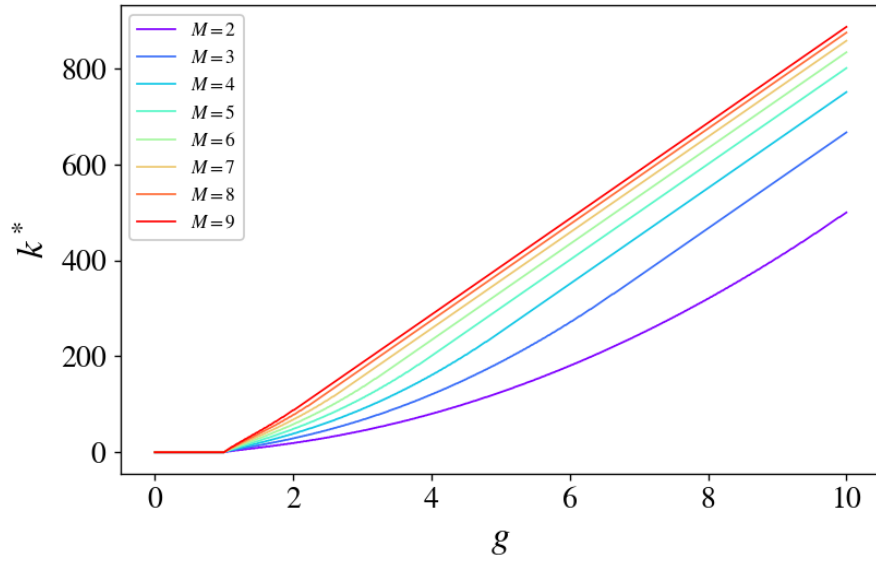
Figure 5.9.: The figure reports the excitation number k^* of the ground state, as a function of the coupling g, derived by numerical calculations, in the cases $M = 2, 3, 4, 5, 6, 7, 8, 9$. Also in all these cases $\eta = 10$.
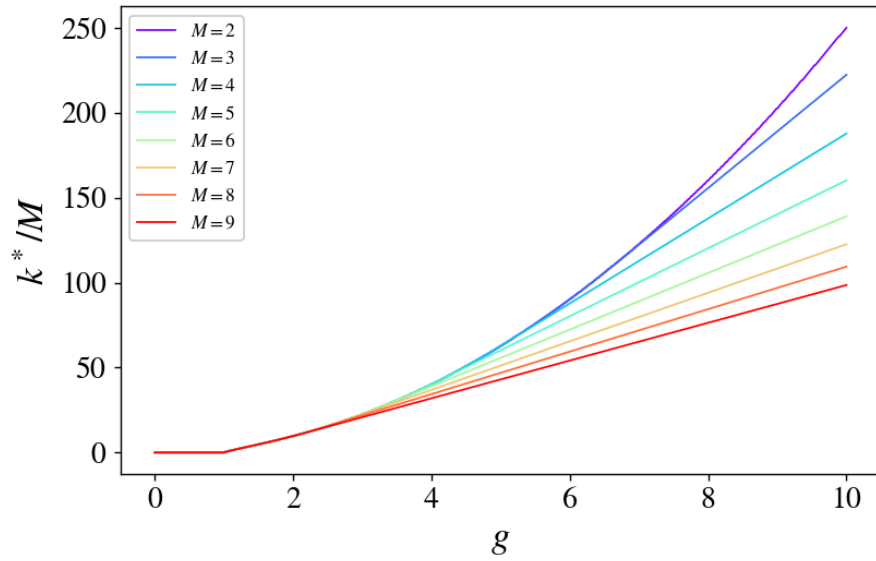
Figure 5.10.: The figure reports the excitation number per qubit k^*/M of the ground state, as a function of the coupling g, derived by numerical calculations, in the cases $M = 2, 3, 4, 5, 6, 7, 8, 9$. Also in all these cases $\eta = 10$.

5.4. Quantum entanglement

In the case $M = 2$ we can compare with the concurrence $\mathcal{C}$. (5.18),
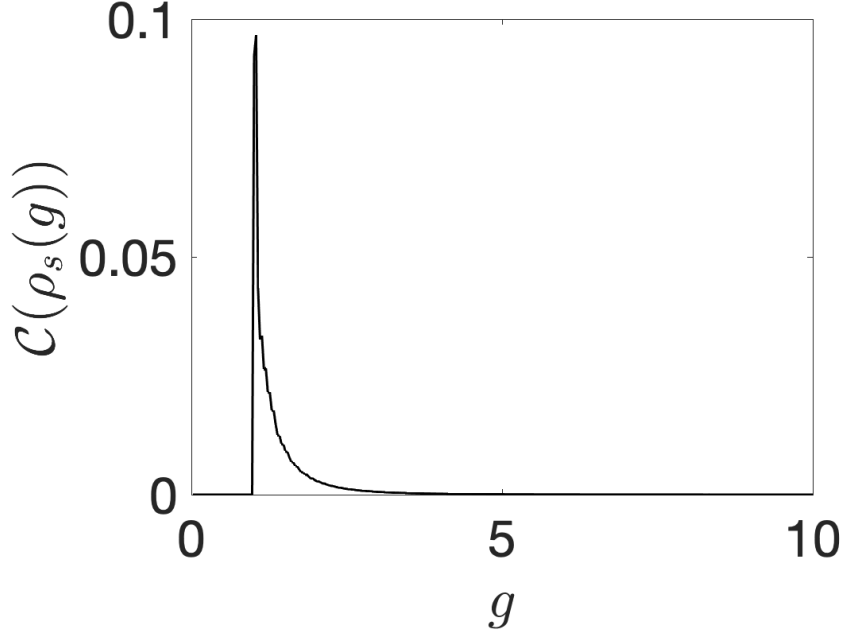
Figure 5.11.: The figure plots the concurrence $\mathcal{C}(\rho_s)$ versus g, derived by numerical calculations. In this case $M = 2$ qubits and $\eta = 10$.

It is clear on Figure 5.11 that $\mathcal{C}\left(\rho_s(g)\right) \xrightarrow[g \to +\infty]{} 0$. This result can also easily be retrieved analytically. Notice that $k \xrightarrow[g \to +\infty]{} \infty$, so the large $k \gg M$ approximation is valid for large g, thus Eqs. (5.9) and (5.18) hold. Yet $\beta_k \xrightarrow[g \to +\infty]{} \pi/2$, which yields

$$\rho_s \xrightarrow[g \to +\infty]{} \frac{1}{2^M} \sum_{n=0}^{M} \binom{M}{n} |D_{M-n}^M\rangle\langle D_{M-n}^M| , \tag{5.25}$$

and in the case $M = 2$:

$$\begin{aligned} \rho_{s2} &\xrightarrow[g \to +\infty]{} \frac{1}{4} \left(|D_2^2\rangle\langle D_2^2| + 2|D_1^2\rangle\langle D_1^2| + |D_0^2\rangle\langle D_0^2| \right) \\ &= \frac{1}{4} \left(|00\rangle\langle 00| + 2 |\phi_+\rangle\langle\phi_+| + |11\rangle\langle 11| \right) , \end{aligned} \tag{5.26}$$

where $|\phi_+\rangle = \frac{1}{\sqrt{2}} \left(|01\rangle + |10\rangle \right)$ is a Bell state. Direct calculation straightforwardly then leads to $\mathcal{C}(\rho_{s2}) \xrightarrow[g \to +\infty]{} 0$.

The fact that, in the 2-atom system, entanglement vanishes for large g, suggests that it also vanishes for larger systems. We are naturally led to think that the

parametric region that yields true entanglement is near the transition $g \gtrsim 1$.

In Ref. [59], a separability criterion for mixtures of Dicke states was proposed. Given a state of the form $\rho = \sum_j w_j |D_j^M\rangle\langle D_j^M|$, it relies on the positive semi-definiteness of Hankel matrices formed with the weights w_j; an equivalent formulation of the same criterion involves the positive semi-definiteness of ρ^Γ, where Γ stands for the partial transpose of $\left\lfloor \frac{N}{2} \right\rfloor$ subsystems.

We applied both of these methods on the atomic reduced ground states ρ_s of Eq. (5.18), and found that, for each considered M, it is entangled for $g > 1$, and separable otherwise.

Unfortunately, this criterion, as effective as it may be, lacks a quantitative aspect. Hence, though $\rho_s(g > 1)$ is entangled for all of the values of M we considered, the degree of entanglement could be tending to zero as we approach the thermodynamic limit. However, for lack of a computationally affordable measure of entanglement, considering the QCD and rescaled QCD provides valuable information. In fact, entanglement is a type of QC; precisely, if a state is entangled, it has non-vanishing QC, while the reciprocal isn't always true. The behaviour of the QCD, and in particular of the rescaled QCD, shown in Fig. 3.9, added with the exact result obtained for the concurrence in the two-atom system, stem as strong clues suggesting that entanglement isn't asymptotically vanishing in large systems, and rather attain a finite value, at least in the region $g \gtrsim 1$ where we found a prominent peak.

5.5. Discussion

The Tavis-Cummings model undergoes a superradiant QPT that we have shown to be embodied in a spontaneous symmetry-breaking mechanism. Here, we have tried answered the question if this phenomenon also generates entanglement between the atoms.

We have shown that the mentioned QPT is associated with a crossover of the QC of the M-qubit density matrix of the system ground state. By resorting to the QCD we developed in Section 3.1, we have been able to quantify the degree of QCs among the atoms, as a function of the atom-cavity coupling strength g. Our study shows that there exists a critical value of g beyond which the T-symmetry introduced above is broken, the cavity field is macroscopically occupied (hence the superradiance) and the QCD acquires a finite value, which visibly does not vanish in the thermodynamic limit. Therefore, in this view, the QCD (or any other valid measure of QC) represents an order parameter for the superradiant phase transition.

We further showed that, crossing the critical value of g, the system becomes entangled, although we were not able to quantify it, and thus cannot verify if the entanglement is an extensive quantity, thus if it is a meaningful feature in the large N limit; the clues we obtained with our studies seem to indicate that it is the case only around, or precisely at the critical value of the parameter g, hence requiring

fine tuning.

We expect our results are valid in general in the superradiant phase transition, thus further investigations i.e. on Dicke models are required.

A further interesting subject is to investigate the deep relation between quantum-phase transitions and entanglement in general, we think that the general method we have proposed here is suitable for this purpose. We believe that our method can be profitably applied also in the study of superradiance at finite temperature, where thermal decoherence effects take place.

Conclusion of part I

The growing interest in quantum information experimental applications has created a need for the development of effective measures of correlation and entanglement in mixed multipartite states. These measures should be easily computable and applicable to a wide range of scenarios. While several measures have been proposed for pure states and mixed states, there are still challenges when applying them to general multipartite mixed states; many of them are only applicable to bipartite systems, while others lack a closed form.

In the present work, we have introduced a new entanglement measure, the Entanglement Distance, applicable to general multipartite pure states. This measure is based on an adapted application of the Fubini-Study metric, defined in projective Hilbert spaces. We showed that the Entanglement Distance, along with its convex roof extension to mixed states, is a valid entanglement monotone, according to the criteria provided by the literature. We further validated the entanglement distance measure, applying it to various examples.

We then showed how, in maximally entangled pure states, the structure of the correlation matrix yields information on the *persistency of entanglement*, and thus on the *k-separability* of the state. We drew simple relations showing the link between pre-measurement correlators and post-measurement expectation values, as well as projection equivalences, and devise a method to find the measurement directions optimally breaking entanglement.

We investigated from a new point of view the graph states, a class of pure quantum states often involved in measurement-based quantum computing schemes, associated to a graph structure. We showed that the quantum correlators computed on these states provide information on the connectivity properties of the associated graphs.

We then extended our study to mixed quantum states. Using the same method as for the entanglement distance, and resorting to the definition of distance implied by the Hilbert-Schmidt norm, we built a measure of quantum correlation in mixed multipartite states.

We further developed a regularization procedure, using the quantum correlation measure to construct an entanglement measure applicable to mixed multipartite states. This regularization procedure relies on an involved optimization procedure that amounts to the usual convex roof optimization over all the realizations of a mixed state; however, we found encouraging clues that, at least for classes of states, optimal choices of mixed state decomposition can be identified, effectively

reducing greatly the space to explore. We have tested these two measures on specific examples, confirming their validity.

Finally, we studied the superradiant phase transition in the Tavis-Cummings model, using our measure to show that it is accompanied by a transition of the degree of quantum correlations between the atoms; we also discuss why, most likely, entanglement between the atoms become extensive at the critical value of the coupling constant g.

Overall, our work contributes to the development of measures for the correlation and entanglement in mixed multipartite states. The entanglement distance measure, along with the extension to quantum correlation and the regularization procedure, offers valuable tools for characterizing and studying entanglement in various quantum systems.

Part II.

Metastability, dynamical freezing and phase transitions in classical systems

Introduction of part II

"Real-life" many-body systems are often characterized by their complexity, that is the difficulty to understand and predict their behaviour, due to very large numbers of objects, often interacting in a nonlinear fashion. In fact, the physics of *complex systems* stems as one of the great challenges of contemporaneous science, and many associated issues are still out of the reach of our best computational abilities.

Though a wide variety of techniques have been developed to address complex systems, they still, as of today, often require to be solved and studied on a case-by-case basis, for the lack of general theories.

The foundational work of Ludwig Boltzmann in statistical physics provided a wonderful toolbox allowing the study of many well-behaved many-body systems (that is, in particular, systems described by a quadratic Hamiltonian), at *thermodynamic equilibrium*.

This conventional framework, despite its paradigmatic importance, fails to describe a plethora of situations. Indeed, standard thermodynamics relies on a number of hypotheses that are in practice violated by most physical systems.

First, while many fundamental results are valid only in the thermodynamic limits, it is often the case that a system exhibits non-trivial emergent phenomena, despite containing a number of *degrees of freedom* (DOF) much smaller than the Avogadro number; in fact, there exists a range of system sizes, too small to be well approximated by the thermodynamic limit, yet too large to be studied analytically, considering the microscopic dynamics of each DOF.

Another important drawback of the conventional approach to statistical mechanics is its appeal to the ergodic hypothesis, namely, the requirement that ensemble average should equate the time average. Ergodicity-breaking, ubiquitous in nature, originates from a high degree of constraint, the presence of time-dependent potential, periodic behaviours or, to some extent, freezing of the dynamics. It is to be understood as the trapping of the system in a subregion of *state space*. The structure of the accessible state space, that is its geometric and topological characteristics, in fact encodes all the information on a given system, and their study allows for a better understanding of the profound mechanisms behind ergodicity-breaking phenomena.

For instance, it can be separated into subregions, either connected by a bottleneck (that can reduce to a tunnel of null measure in the thermodynamic limit), or not connected at all, as it is the case in the presence of symmetry breaking. Its geometrical characteristics, i.e. the shape of its landscape (in terms of cur-

vatures), may also lead to dynamical freezing or periodic (or *effectively periodic*) behaviours. Remark that periodicity may arise, in nonlinear systems, as a result of the interactions between the DOFs, that can entail an emergent collective motion.

The search of a general theory of phase transitions constitutes a prototypical example of a challenge of modern statistical physics. Indeed, PTs are generally associated with the loss of analyticity of the derivative of thermodynamic potentials, which can be explained by Yang-Lee theory only in the context of the thermodynamic limit; it results that finite-sized systems exhibiting phase transitions are as of yet not well understood either.

Furthermore, the elegant heuristic theory of Lev Landau, linking PT with spontaneous symmetry breaking (characterized by an *order parameter*), despite its great success, fails to explain all of them. Namely, a variety of PT is not accompanied by symmetry breaking and are not associated with any order parameter; this is for instance the case of the Kosterlitz–Thouless PT and topological PTs. It is also true of the *glass transition* which, characterized by a diverging viscosity below the transition temperature (hence in the glassy phase), doesn't present any symmetry breaking, as these materials are amorphous in both the liquid and glassy phase.

Interestingly, the latter can be understood as a result of ergodicity-breaking, in the sense that vitrification is entailed by the freezing of the dynamics that *effectively* breaks ergodicity. In turn, the dynamical freezing is most probably due to the presence of a large number of local minima of the potential energy, namely, a landscape of deep wells in which the system stays stuck.

A promising attempt to account for many of these limiting cases is the topological theory of phase transitions. The latter is a relatively new theory, more general and encompassing the previous ones, relying on the idea that phase transitions can be seen as a mere consequence of changes of the topology of the iso-potential hypersurfaces that foliate state space. It has been successfully tested on a variety of models, from the Kosterlitz–Thouless PT to protein folding.

Arguably, the microcanonical ensemble is the most fundamental of Gibbs ensembles, as it describes isolated physical systems, thus approaching them with a purely mechanical perspective. Furthermore, it is somewhat more natural to place ourselves in the microcanonical ensemble, in order to study the structural properties of the accessible state space. Indeed, the latter is, in this case, an hypersurface of constant energy, of which the properties, as a Riemannian manifold, appear more evident than in the canonical ensemble.

This part of the thesis is henceforth devoted to the study of two instances of isolated systems, exhibiting ergodicity breaking, equilibrium or dynamical PT, and characterized by a high degree of non-linearity.

First, in Chapter 6, we address the Hamiltonian Mean Field model, a mean-field

instance of the celebrated XY-model, exhibiting a long-lived metastable state at low energy; we manage to rewrite, using time-scale separation and averaging techniques, the interactions of the system as single effective time-dependent potential, providing an explanation for the observed frequencies and for occurrence of bimodal metastable states (coined as a *biclusters*). In Chapter 7, we present the results of the numerical simulation of a glass-forming binary Lennard-Jones mixture; resorting to parallel tempering Monte Carlo scheme, we manage to sample the constant energy state spaces, and evidentiate that, as suspected, the glass transition is accompanied by changes of its topology.

Chapter 6 reports the work published in Ref. [113], while Chapter 7 presents the preliminary results of an ongoing investigation on the topological origins of the glass transition.

6. Fast collective oscillations and clustering phenomena in an antiferromagnetic mean-field model

In this chapter, we reproduce the results we published in [114], pertaining to the occurrence of long-lived metastable states in the Hamiltonian Mean Field model at low energy.

6.1. Introduction

The Hamiltonian Mean Field (HMF) model has raised much attention in the last two decades [115, 116, 117, 118, 119, 120, 121, 122, 123, 124]. This simple toy model indeed exhibits a plethora of phenomena going beyond the scope of equilibrium statistical mechanics, as it is typically the case in long-range interacting systems. As an interesting physical interpretation, the HMF model can be seen as the first Fourier mode approximation of sheet models in one dimension; the antiferromagnetic HMF model corresponds to a charged sheets model, while the ferromagnetic HMF model corresponds to a massive sheets model [116, 125, 126].

The ferromagnetic HMF undergoes a second order phase transition in both the canonical and microcanonical ensembles [115, 113], while, to the best of our knowledge, there exists no equilibrium phase transition in the antiferromagnetic HMF. However, both the ferromagnetic and the antiferromagnetic HMF are known to present a variety of long-lived metastable states, with relaxation times diverging with the size of the system, thus entailing ergodicity breaking [115, 119, 116, 118, 120, 127].

More recently, promising generalizations of the HMF model have been proposed, in which some of these interesting features can be preserved. Notably, some of the aforementioned long-lived metastable states have been shown to be robust with respect to the addition of a (small enough) nearest-neighbour coupling to the model. Phase transition phenomena are still observed in this extended framework [119, 113]. Finite-range versions of the HMF model have also been considered [128, 129], as well as extensions with higher dimensional spins [120, 127], and quantum versions [130], still presenting a rich phenomenology, namely the emergence of

non-trivial collective behaviours.

Let us introduce the Hamiltonian of the model. We consider an assembly of N planar classical rotators, endowed with a kinetic energy, subjected to an infinite-range "antiferromagnetic" coupling. This system can also be seen as a collisionless plasma in a one-dimensional ring, with an all-to-all repulsive interaction [117]. The Hamiltonian coordinates of the rotators are $\{\theta_j, p_j\}$. The model can be defined through the Hamiltonian

$$
H = \sum_{i=1}^{N} \frac{p_i^2}{2} + V(\{\theta_i\}) \,,
$$
$$
\text{with } V(\{\theta_i\}) = \frac{1}{2N} \sum_{i,j=1}^{N} \cos\left(\theta_i - \theta_j\right) = \frac{N\boldsymbol{M}^2}{2} \,,
$$

(6.1)

where $\boldsymbol{M}$ is the magnetization vector per rotator, defined as

$$
\boldsymbol{M} = \frac{1}{N} \sum_{j=1}^{N} \begin{pmatrix} \cos\left(\theta_j\right) \\ \sin\left(\theta_j\right) \end{pmatrix} .
$$

(6.2)

The equations of motions are

$$
\dot{p}_j(t) = M_x \sin\left(\theta_j\right) - M_y \cos\left(\theta_j\right) .
$$

(6.3)

The potential of this Hamiltonian is self-consistent, a feature characteristic of mean-field models: the magnetization depends on the single rotator dynamics, which in turn depends on the former.

A homogeneous distribution of the angles of the rotators, implying a vanishing magnetization, is expected at equilibrium in both the canonical and the micro-canonical ensemble. However, numerical studies have shown that a long-living coherent structure, namely a bicluster, can spontaneously form in the Hamiltonian dynamics at low energy [116, 117, 118, 121, 122]. This long-lived metastable state consists in the gathering of an extensive quantity of rotators on two opposite angles, and is quantified by the norm M_2 of the vector

$$
\boldsymbol{M_2} = \frac{1}{N} \sum_{j=1}^{N} \begin{pmatrix} \cos\left(2\theta_j\right) \\ \sin\left(2\theta_j\right) \end{pmatrix} .
$$

(6.4)

The parameter M_2 varies from 0 in the homogeneous state, to 1 in a bicluster state with no dispersion of the rotators [121, 116, 117].

Notably, bicluster states are also characterized by a non-zero magnetization, with $M \sim \sqrt{e}$, where $e = E/N$ is the total energy density, with $E = H(\{\theta_i(0), p_i(0)\})$. Using the kinetic definition of the temperature $T = \langle p^2 \rangle$, this entails an anomalous energy-temperature relation, with respect to the expected equilibrium linear rela-

tion $T = 2e$ [121, 116].

Remark that this phenomenon is not compatible with linear stability analysis of the Vlasov equation [115, 117][1], which predicts the homogeneous states to be stable for all energies, for a wide class of initial distributions of momenta.

The class of initial conditions leading to a bicluster is yet not precisely known. Let $\gamma_0 = V_0/E$, with $V_0 = V(\{\theta_i(0)\})$. Previous studies [122] have shown that, at a given energy, for initially uniformly random distributions of angles and momenta (i.e. waterbag distributions, defined later in Sec. 6.4), the closer we are to $\gamma_0 = 1$, the more likely is the formation of the bicluster, and the larger is the stationary value of M_2. We chose to use this ratio as a control parameter for our simulations in section 6.4.
Nevertheless, it is worth noting that biclusters can also arise from initial sinusoidal distributions of momenta (i.e. $p_i(0) \propto \sin(\theta_i(0))$), in which case the parameter γ_0 becomes irrelevant [122]. In the present work, we will solely focus on waterbag initial distributions.

Previously, a theory has been devised to explain the formation and stabilization of a bicluster, as the equilibrium state of an averaged Hamiltonian [117], derived by using a variational method inspired by Ref. [131]. The authors of Ref. [117], separating fast and slow variables in the Lagrangian, notably predicted the occurrence of two collective high frequencies $\omega_\pm$, and gave accurate quantitative results.

In the following, we propose a new approach, to get a better understanding of the dynamical mechanism at the base of the bicluster formation and stabilization. We derive the same high frequencies $\omega_\pm$ in Section 6.2, by directly studying the dynamics of the magnetization vector, which is the driving force of the system (see Eq. (6.3)). This allows us, in Section 6.3, to rewrite the equations of motions in a non-autonomous form, and thereby perform an averaging over the fast variables in a very simple fashion. An expression for the effective force is found, with associated low frequency ω_0, and its dependence to initial conditions is discussed.
Section 6.4 exposes our numerical results, showing excellent agreement with the theory.
In Section 6.5, we discuss our results and develop a heuristic argument to explain the birth and stabilization of the bicluster states. We conclude by mentioning possible analogies with other models, and proposing further developments.

---

[1]In Ref. [115], linear stability analysis was performed for the ferromagnetic model. Stability in the antiferromagnetic case can be retrieved by a simple change of sign.

6.2. Dynamics of the Total Magnetization

We are interested in deriving a dynamical equation for the macroscopic quantity $\boldsymbol{M}$. We are considering here the low energy regime, for which biclusters are known to occur. From Eq. (6.2), we get

$$\frac{d^2}{dt^2}\boldsymbol{M}(t) = \frac{1}{N}\sum_{j=1}^{N}\begin{pmatrix} -\dot{p}_j\sin\left(\theta_j\right) - p_j^2\cos\left(\theta_j\right) \\ \dot{p}_j\cos\left(\theta_j\right) - p_j^2\sin\left(\theta_j\right) \end{pmatrix}. \tag{6.5}$$

We identify in this expression the correlator $\langle p^2\cos\left(\theta\right)\rangle \sim o(MT) \sim o(e^{3/2})$, that we can neglect in the low energy regime, since the other term turns out to be of order $o(M) \sim o(e^{1/2})$. We are left with

$$\frac{d^2}{dt^2}\boldsymbol{M}(t) \approx \frac{1}{N}\sum_{j=1}^{N}\begin{pmatrix} -\dot{p}_j\sin\left(\theta_j\right) \\ \dot{p}_j\cos\left(\theta_j\right) \end{pmatrix}. \tag{6.6}$$

Then, inserting the equations of motion (6.3), we obtain the eigenproblem

$$\frac{d^2}{dt^2}\begin{pmatrix} M_x(t) \\ M_y(t) \end{pmatrix} \approx \begin{pmatrix} -\frac{1-M_x^{(2)}}{2} & \frac{M_y^{(2)}}{2} \\ \frac{M_y^{(2)}}{2} & -\frac{1+M_x^{(2)}}{2} \end{pmatrix}\begin{pmatrix} M_x(t) \\ M_y(t) \end{pmatrix}. \tag{6.7}$$

The eigenvalues are $-\omega_{\pm}^2 = -\frac{1\pm M_2}{2}$, of corresponding eigenvectors

$$\boldsymbol{M}_+ = \begin{pmatrix} \cos\left(\phi_2/2\right) \\ \sin\left(\phi_2/2\right) \end{pmatrix}, \quad \boldsymbol{M}_- = \begin{pmatrix} -\sin\left(\phi_2/2\right) \\ \cos\left(\phi_2/2\right) \end{pmatrix}, \tag{6.8}$$

where ϕ_2 is defined as the phase of $\boldsymbol{M_2}$. We hence expect the system to globally rotate with $\phi_2/2$, which already stresses the importance of $\boldsymbol{M_2}$ in the characterization of the dynamics.

Let us emphasize the consistency of this result with that one of Ref. [117], in which the modes $\omega_{\pm}$ were found to be the eigenvalues of the fast Lagrangian, and where $\phi_2/2$ was already recognized as the system's center of mass. These frequencies, arising from nonlinear mode interaction, can be seen as a splitting of the single normal mode $\omega = 1/\sqrt{2}$, present in the homogeneous state [122]. This normal mode can also be found by linear analysis of the Vlasov equation [117].

Assuming $\boldsymbol{M_2}$ constant, after a global rotation of $-\phi_2/2$, we get

$$\boldsymbol{M} = \begin{pmatrix} M_-\cos\left(\omega_- t + \phi_-\right) \\ M_+\cos\left(\omega_+ t + \phi_+\right) \end{pmatrix}, \tag{6.9}$$

where $\phi_{\pm}$ are arbitrary constant phases. It is worth remarking that, in the ferromagnetic case, the eigenvalues read $\lambda_{\pm} \approx \frac{1\pm M_2}{2}$, and under the same low energy

hypothesis, $\boldsymbol{M}$ will rather converge to a constant, following a slow drift motion [116].

(a)

(b)

(c)

(d)
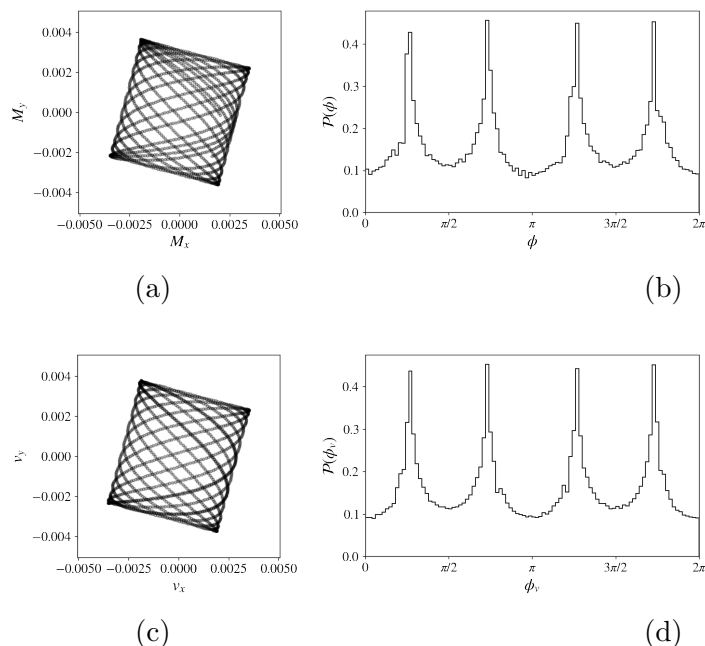
Figure 6.1.: The dynamics and histogram of ϕ, the phase of $\boldsymbol{M}$, measured in a simulation with $\gamma_0 = 1$, $M_2 = 0.52$ (see Sec. 6.4, Fig. 6.3a). A few other examples are provided in Appendix B. We define a vector $\boldsymbol{v}$ according to Eq. (6.9). The frequencies $\omega_\pm$ are drawn from measurements of M_2, the amplitudes $v_{-,+}$ respectively defined through $\max(M_{x,y})$ (after $\boldsymbol{M}$ was rotated of $-\phi_2/2$), and we finally rotate $\boldsymbol{v}$ of $\phi_2/2$, as suggested by Eq. (6.8). We show in Cartesian coordinates the dynamic, measured over the time interval $t \in [10000, 10100]$, of $\boldsymbol{M}$ (resp. $\boldsymbol{v}$) in Fig. 6.1a (resp. c). The corresponding distributions $\mathcal{P}(\phi)$ (resp. $\mathcal{P}(\phi_v)$) are reported in Fig. 6.1b (resp. d). The histograms are derived from a sample of values retrieved in the time interval $t \in [10000, 11000]$. We used the time step $\Delta t = 0.05$.

Fig. 6.1 shows the behaviour of $\boldsymbol{M}$ measured by numerical integration of the full equations of motion (6.3), and the one of a vector $\boldsymbol{v}$ defined according to Eq. (6.9). Namely, $\boldsymbol{v} = \left(v_- \cos\left(\omega_- t\right), v_+ \cos\left(\omega_+ t\right) \right)$, where $\omega_\pm$ are computed from the average value of M_2 and $v_\pm$ are measured by taking the maximum value of $M_{x,y}$, after a rotation of $-\phi_2/2$. Also, we present later, in Fig. 6.2a the frequency spectrum of the components M_x, M_y, derived by a fast Fourier transform, also performed after a rotation of $-\phi_2/2$. Better agreement is found for well-formed biclusters ($M_2 \gtrsim 0.1$), as we will discuss in Section 6.4. A few other examples are displayed in B.

The parametric curves defined by Eq. (6.9) are named Lissajous curves. Such

curves are bounded in the (M_x, M_y)-plane by a rectangle of sides M_- and M_+, and are known to densely fill its area, provided that the ratio ω_-/ω_+ is irrational, condition that is almost always fulfilled. The norm M evidently possesses four maxima, each located at a fixed angular position. One can see from Eq. (6.9) that $\dot{M}$ approaches 0 as M approaches $(\pm M_-, \pm M_+)$ (when M is maximal), making these regions favoured in terms of the amount of time spent there by the system, as illustrated in Fig. 6.1b.

Note that, when $M_2 \approx 0$, the curve is an ellipse, hence M exhibits two maxima. This is also the case when $M_- \ll M_+$ (or $M_- \gg M_+$). The probability density function for M is hence bimodal (at least during a first transient phase) or quadrimodal, in the considered low energy regime.

This simple derivation already provides us with a heuristic explanation for the occurrence of a bimodal distribution of the rotators in the antiferromagnetic HMF model. Indeed, as we will show below, if the rotators are slow enough with respect to $\omega_\pm$, they effectively experience a bimodal potential.

It is fairly obvious from Fig. 6.1 that, as this regime persists for very long times, it brings on a breaking of ergodicity. Indeed, the accessible state space is bounded by the Lissajous curve, entailing a probability density $\mathcal{P}(\phi, M)$ anomalous with respect to the expected one from equilibrium statistics. In particular, while the time average of M is null, the one of M is not. These coherent oscillations hence allow for a non-vanishing (extensive) average potential energy.

6.3. Time Scale Separation

We found above an explicit time dependence for the bare potential. By doing this, we also decoupled it from the generalized coordinates $\{\theta_j\}$. This allows us to fully take advantage of the mean-field nature of the model, hence to actually consider single rotators as uncoupled pendula, evolving under the action of an external potential driven by the oscillating "magnetic field" M.

We first insert Eq. (6.9) in Eq.(6.3), thus

$$\dot{p}_j(t) = \epsilon a_- \cos(\omega_- t + \phi_-) \sin(\theta_j) - \epsilon a_+ \cos(\omega_+ t + \phi_+) \cos(\theta_j), \qquad (6.10)$$

with $\epsilon a_\pm = M_\pm$, so that we have $a_+^2 + a_-^2 = 1$, and $\epsilon = \sqrt{M_+^2 + M_-^2} \sim \sqrt{e}$.

We are now able to perform a simple approximation, related to the *ponderomotive effect*, well-known in the area of plasma physics [132]. As the one employed in Ref. [117], it relies on the clear separation of time scales between fast and slow variables, and is somehow analogous to the method first proposed by Landau and Lifshitz to solve systems exhibiting two distinct time scales [133]. The prototypical example of such systems is the Kapitza pendulum [134].

Our use of this approximation method is justified by the consideration that,

already in Eq. (6.10), one can clearly identify the two time scales of the motion. The first is a fast one, related to the motion of the phase, which is set by the frequencies $\omega_\pm \sim 1$. The second is a slow one, and is proportional to the square root of the amplitude of the acceleration, giving a time scale of the order $\sqrt{\epsilon}$, which in fact characterizes the motion of a pendulum at the bottom of the potential.

Let us decompose the variables in a fast and a slow component. We set the magnitude of the fast component to be $o(\epsilon)$, and introduce a "slow time" $\tau = \epsilon t$, associated with the slow oscillations, insuring $\langle \dot{p}_j^2 \rangle \sim \epsilon^2$,

$$\theta_j(t) = \theta_j^0(\tau, t) + \epsilon f_j(t) . \tag{6.11}$$

The single rotator dynamics thus presents a fast motion of small amplitude, superimposed with a slow motion of large amplitude.

Expanding Eq. (6.10) up to first order in ϵf_j, we obtain

$$\epsilon^2 \frac{d^2}{d\tau^2} \theta_j^0(\tau, t) + \epsilon \frac{d^2}{dt^2} f_j(t)$$
$$= \epsilon \Big(a_- \cos(\omega_- t + \phi_-) \sin(\theta_j^0(\tau)) - a_+ \cos(\omega_+ t + \phi_+) \cos(\theta_j^0(\tau)) \Big) \tag{6.12}$$
$$+ \epsilon^2 f_j(t) \Big(a_- \cos(\omega_- t + \phi_-) \cos(\theta_j^0(\tau)) + a_+ \cos(\omega_+ t + \phi_+) \sin(\theta_j^0(\tau)) \Big) .$$

By identifying terms order by order, we get the following expression for the fast variables

$$\frac{d^2}{dt^2} f_j(t) = a_- \cos(\omega_- t + \phi_-) \sin(\theta_j^0(\tau)) - a_+ \cos(\omega_+ t + \phi_+) \cos(\theta_j^0(\tau)) , \tag{6.13}$$

which we can straightforwardly integrate, since $\theta_j^0(\tau)$ is considered constant on the time scale of $f_j(t)$. It results

$$f_j(t) = -\frac{a_-}{\omega_-^2} \cos(\omega_- t + \phi_-) \sin(\theta_j^0(\tau)) + \frac{a_+}{\omega_+^2} \cos(\omega_+ t + \phi_+) \cos(\theta_j^0(\tau)) . \tag{6.14}$$

Then, by substituting this expression for $f_j(t)$ in Eq. (6.12), we obtain after some manipulations (for convenience, we dropped the time dependence and the constant phases $\phi_\pm$)

$$\frac{d^2}{dt^2} \theta_j^0 = \frac{1}{4} \left[\frac{M_+^2}{\omega_+^2} \Big(1 + \cos(2\omega_+ t)\Big) - \frac{M_-^2}{\omega_-^2} \Big(1 + \cos(2\omega_- t)\Big) \right] \sin(2\theta_j^0)$$
$$+ \frac{1}{4} \left[\frac{M_+ M_-}{\omega_+^2} \Big(1 + \cos(2\theta_j^0)\Big) - \frac{M_+ M_-}{\omega_-^2} \Big(1 - \cos(2\theta_j^0)\Big) \right] \tag{6.15}$$
$$\times \Big(\cos((\omega_- + \omega_+)t) + \cos((\omega_- - \omega_+)t) \Big) .$$

If M_2 is of the order of ϵ then $(\omega_+ - \omega_-)$ is of the order of ϵ, a low frequency that cannot be neglected by averaging over the fast oscillations. Then, our computation holds when $M_2 \gg \epsilon$, and a priori does not account for the beginning of the transient. By averaging over the fast oscillations, we get the expression for the slow variables

$$\frac{d^2}{dt^2}\theta_j^0 \approx \frac{1}{4}\left(\frac{M_+^2}{\omega_+^2} - \frac{M_-^2}{\omega_-^2}\right)\sin\left(2\theta_j^0\right). \tag{6.16}$$

Assuming that the prefactor is negative, we can consider a rotator in the bottom of one potential well, located at $\theta_j^0 \approx k\pi$, with $k \in \mathbb{Z}$, so $\sin\left(2\theta_j^0\right) \approx 2\theta_j^0 - 2k\pi$. We then have

$$\theta_j^0(t) \approx k\pi + A_j \cos\left(\omega_0 t + \phi_j\right), \text{ with} \tag{6.17}$$

$$\omega_0 = \frac{1}{\sqrt{2}}\sqrt{\frac{M_-^2}{\omega_-^2} - \frac{M_+^2}{\omega_+^2}}. \tag{6.18}$$

ω_0 is of the order of M, namely the square of the natural frequency. This emphasizes that the effective force emerges from the non-linearity, linked to the self-consistency of the magnetization.

The attractive or repulsive nature of this bimodal effective interaction is related to the sign of the prefactor in Eq. (6.16), namely

$$\Delta - M_2 < 0 , \tag{6.19}$$

with $\Delta = \frac{M_+^2 - M_-^2}{M_+^2 + M_-^2}$. The effective force is self-consistent, in the sense that its strength is proportional to M_2, which is governed by the force itself. Thus, we are brought to assume that M_+, M_- and M_2 are evolving during a transient phase in an interdependent fashion, following a dynamics which is determined by the initial conditions. In particular, we will comment in next section, based on numerical observations that the bicluster forms and stabilizes when the initial condition is a waterbag such that $\gamma_0 \sim 1$.

This result provides a dynamical explanation for the stabilization of biclusters over very long times.

6.4. Numerical results

Our simulations were performed at energies ranging from 10^{-5} to 10^{-4}, with $N = 1000$. The equations of motions have been integrated using a fourth-order sympleptic scheme [135]. For most of the figures, we used a time step $\Delta t = 0.05$, which gives a conservation of the energy up to $\Delta e \sim 10^{-12}$. On the contrary, to produce Fig. 6.5, we used a more efficient time step $\Delta t = 0.5$, yielding $\Delta e \sim 10^{-6}$. For the purpose of measuring a low frequency, with an efficient integrating scheme

and at these ranges of energy, such a time step remains of an acceptable precision. We initially set a water-bag distribution, picking the positions and momenta uniformly at random in a domain $[-\pi, \pi] \times [-p_0, p_0]$. We used the prescription of Ref. [122] to use γ_0 as a control parameter. To do this, we first find, by iterating multiple times, a distribution of positions giving a potential energy in the desired range. Then we choose p_0 to set $T = \langle \dot{\theta}_j^2 \rangle$ accordingly, and globally shift the momenta to set the constant of motion $\langle p_j \rangle = 0$.

The averages are taken after a transient, typically of the order of 10000 proper times. We have checked that the averages do not change by increasing the duration of the transient. By looking directly at the time series, we have also checked that the system has reached a steady state after the transient.
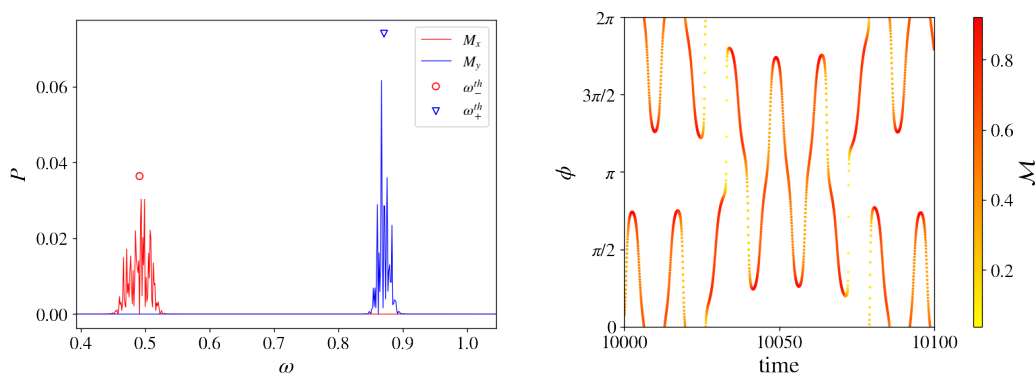
(a) Frequency spectrum of M_x and M_y.   (b) Short time phase trajectory of $\boldsymbol{M}$.

Figure 6.2.: Power spectrum and detail of the trajectory of $\boldsymbol{M}$, with $\gamma_0 = 1$, $M2 = 0.52$, $\Delta = -0.09$ (see Fig. 6.3a).

In the literature [117, 121, 116], as well as in our own simulations, the parameter M_2 has never been reported to exceed 0.8.

In Fig. 6.2 is shown an example of the short-term dynamics of $\boldsymbol{M}$, along with the corresponding Fourier spectra of its components, performed after a global rotation of $-\phi_2/2$. Here, the agreement of experimental data with Eq. (6.9) is excellent.

For small M_2, the agreement of $\boldsymbol{M}$ with Eq. (6.9) is not as good. Though collective oscillations still occur, the envelopes $M_\pm$ fluctuate, and the trajectories of the magnetization lose their regularity.

However, we observed the fast collective oscillations to be present from the beginning, regardless of the later formation of a bicluster (hence of the value of γ_0), and before the system has reached a steady state.

The average value of $\mathcal{M} = M/\sqrt{2e}$ is related to γ_0: a high initial value leads to an accordingly high average of $\langle \mathcal{M} \rangle$.

Fig. 6.3 shows the general dynamics of the system, at different values of the

(a) $\gamma_0 = 1$, $M2 = 0.52$, $\Delta = -0.09$

(b) $\gamma_0 = 1$, $M_2 = 0.51$, $\Delta = -0.98$

(c) $\gamma_0 = 0.46$, $M_2 = 0.06$, $\Delta = -0.94$

(d) $\gamma_0 = 0.05$, $M_2 = 0.03$, $\Delta = -0.11$
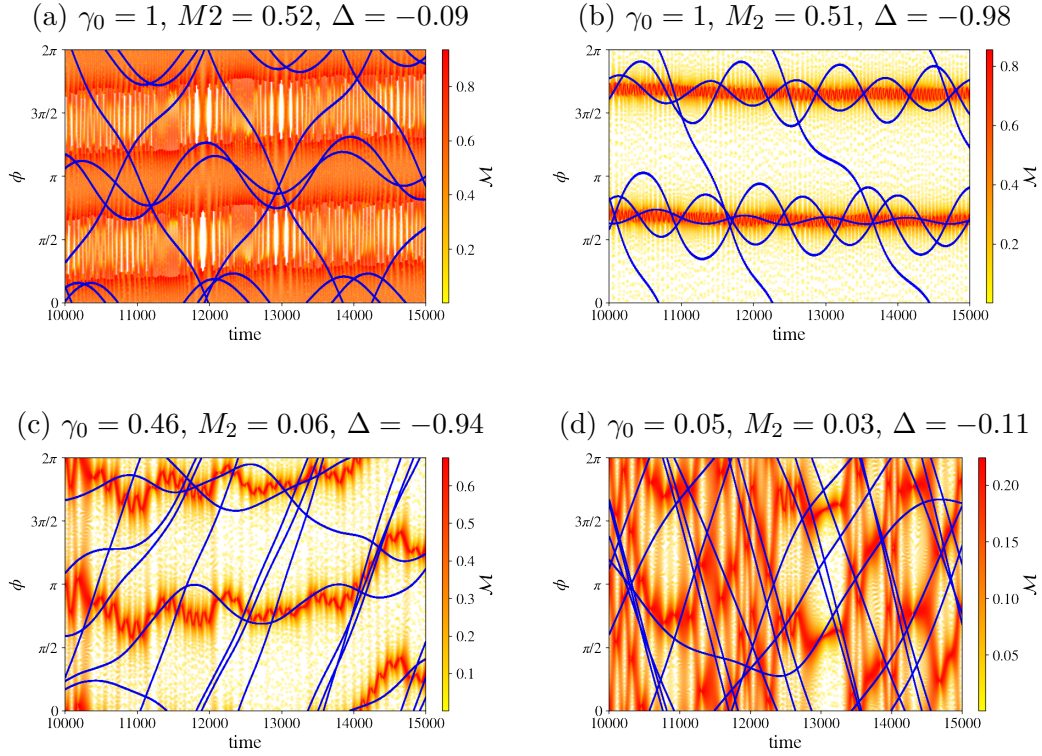
Figure 6.3.: Some rotators trajectories are shown in blue, along with the magnetization in a red gradient; the color gradient indicates the rescaled norm $\mathcal{M} = M/\sqrt{2e}$. Energy was set to $e \sim 10^{-5}$.

parameters. Here, the existence of two distinct time scales is manifest: the one associated to the fast oscillation of $\boldsymbol{M}$, is visibly much smaller than the one associated to the long-term behaviour of the single rotator dynamics. In this view, it is evident that the dynamics associated to the slow variables is similar to one of a rotator in a bimodal potential.

Indeed, we can clearly see two angular regions "favoured" by $\boldsymbol{M}$ in terms of the time spent as well as in magnitude. These are the locations of the two clusters, following as expected the same slow linear drift as $\phi_2/2$. Around these regions some trapped rotators (below the separatrix) slowly oscillate, while some untrapped ones (above the separatrix) are evolving in an almost ballistic fashion.

Note that well-formed biclusters seem to occur regardless of the value of Δ. Indeed, we were not able to find a clear relation of the stationary value of Δ neither with γ_0 nor with the stationary value of M_2.

Although we have found that the effective force Eq. (6.16) can become very slightly repulsive when $\gamma_0 \approx 0$, it ends up attractive in the vast majority of cases. Also, Δ and M_2 evolve, at a slow time scale with respect with $\omega_\pm$, towards values satisfying Eq. (6.19).
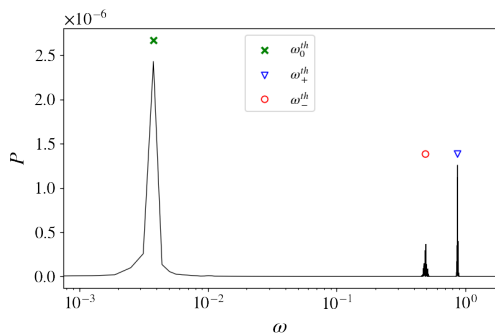
Figure 6.4.: Power spectrum of a single trapped rotator from figure 6.3a.
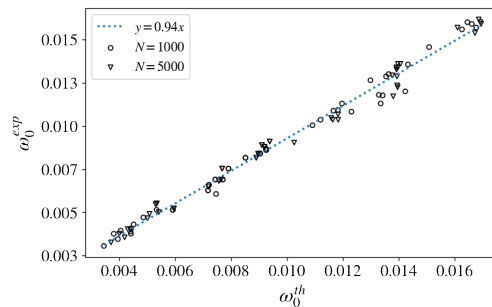
Figure 6.5.: Comparison of ω_0 theoretical and experimental. We performed Fourier transforms on small random subsets of trapped rotators, at energies ranging from 10^{-5} to 10^{-4}.

To investigate the spectral properties of the rotator trajectories, we focused on initial conditions leading to sufficiently well-formed biclusters, i.e. $M_2 \gtrsim 0.2$ ($\gamma_0 > 0.7$), and performed the global rotation of $-\phi_2/2$ to follow the center of mass.

Fig. 6.4 shows an example of a single rotator Fourier spectrum, trapped in a potential well and oscillating with a small amplitude. The slow mode ω_0 is not present in the spectra of the untrapped rotators, or is very weak and with a higher discrepancy with Eq. (6.18).

In the considered regime, the low frequency observed in simulations agrees with our theoretical value, up to a multiplicative factor of order 1, namely $\omega_0^{exp} \approx 0.94 \omega_0^{th}$, as shown in Fig. 6.5.

6.5. Conclusions and Perspectives

In the light shed by these results, let us synthesize and propose a scenario accounting for the formation of biclusters in the antiferromagnetic HMF model, from a waterbag initial distribution.

At low energy, an initial state of small but non-vanishing magnetization generates a collective oscillatory regime. This is due to the self-consistency of $\boldsymbol{M}$, which repels all of the rotators, entailing its own motion towards the opposite angle, in a periodic fashion. The time scale associated to this collective motion is much smaller than the typical time scale of the individual rotators. We observe a cyclic high frequency transfer of energy between kinetic and potential, and the system periodically returns close to its initial high value of the $\gamma = M^2/2E$ ratio. This

entails the non-vanishing $\langle M \rangle$. If, initially, the temperature is small with respect to the potential energy, the magnetization vector $\boldsymbol{M}$ follows a Lissajous-type regular curve parametrized by $\omega_\pm = \sqrt{\frac{1-M_2}{2}}$ and $M_\pm$, as described in Eq. (6.9). The phase of $\boldsymbol{M}$ is rapidly oscillating between two or four symmetric angles, and we thus have $\langle \boldsymbol{M} \rangle = \boldsymbol{0}$ and, near one of the maxima, rotators are subjected to repulsive and attractive forces, alternatively.

In the very beginning, as $M_2 \approx 0$, $\omega_- \approx \omega_+ \approx 1/\sqrt{2}$, and $\boldsymbol{M}$ follows an almost elliptic trajectory, and thus exhibits two maxima in magnitude at two opposite angular positions. The variables $\omega_\pm$, $M_\pm$, are evolving concomitantly with M_2, at a slow rate. As M_2 increases, the unique frequency of $\boldsymbol{M}$ split into two, and the two maxima (generally) split into four.

When the difference between the two frequencies becomes large enough, a bimodal effective force can be derived, accounting for the stabilization of the bicluster.

The nature of this effective force is determined by Eq. (6.19). A full understanding of the conditions leading to a stable bicluster would thus involve a thorough study of the transient dynamics of the slow macroscopic variables $\boldsymbol{M_2}$, M_+ and M_-.

It would also require to explain how other types of initial distributions (in particular, initial sinusoidal distributions of momenta, with vanishing initial magnetization) relate to the processes described above.

The study of the dynamics of this simple mean-field model provides valuable insights into the mechanisms leading to ergodicity breaking in long-range interacting systems.

We have stressed the importance of the self-consistency of the potential, giving rise to nonlinear effects, solvable through multiscale analysis. This self-consistency is characteristic of mean-field models; an interesting development would hence be to look for the presence of biclusters and collective oscillations in modified versions of the antiferromagnetic HMF, weakening this self-consistency. This emergent behaviour has been shown to be preserved in presence of a nearest-neighbour ferromagnetic or antiferromagnetic perturbative interaction [113]; the phenomenon is hence not specific of pure mean-field models.

In recent studies, it has been noticed that the HMF model presents strong similarities with systems of cold atoms in optical cavities [136, 137]. Such systems can be considered as almost isolated, thus opening the possibility of performing a "real-life experiment" showing the non-trivial ordered phases discussed in this paper.

7. Glass Transition

This chapter presents the preliminary results of our ongoing investigation of the topological origins of the glass transition. Though incomplete, the data we managed to acquire in the present day is very promising and already allows us to draw some interesting conclusions.

7.1. Introduction

As of today, the glass transition still stems as an opened problem of contemporaneous physics. Indeed, as glasses are amorphous solids, no symmetry breaking is associated with this transition, which is hence not described by the theory of Landau [1]. It has further been argued that *glass forming material*s (at least *strong* glass formers in Angell's classification [138]) do not even exhibit a transition in the conventional sense, as it yields no dynamical singularity; the transition temperature T_g is in fact purely conventional, usually defined by the passing of a threshold value of the viscosity or of the relaxation time.

In a number of references [139, 140, 141], it has been shown that glass transitions most likely correspond to *geometric transition*. Namely, the *critical* points of the potential energy were studied, and in particular their instability index (i.e. the number of negative eigenvalues of the Hessian matrix). It was found that the average index density vanishes at the so-called mode-coupling temperature (MCT).

Yet it is known, from Morse theory [142, 1], that any change of stability indices of a surface is accompanied by a change of its topology.

Furthermore, the relatively recent topological theory of phase transitions [1, 143, 144, 145], unravelled a deep link between classical phase transitions and changes in the topology of the potential level sets (PLS) Σ_Φ, i.e. the iso-energy hypersurfaces. One advantage of this topological theory of phase transitions is that it applies to small systems (mesoscopic and nanoscopic scales), thus escaping the *thermodynamic limit dogma* upon which is built the Yang–Lee theory of phase transitions. Furthermore, it applies to phase transitions in the absence of symmetry-breaking (hence in the absence of a well-defined order parameter). That second point is of great interest to us, as the glass transition notoriously falls in the latter category.

These observations compel us to investigate glass-forming systems, resorting to a few elegant theorems linking the topological invariants and geometric quantities such as the mean curvature.

In Section 7.2, we present the model of glass-former under investigation, expressing its potential energy. Section 7.3 is devoted to the presentation of geometric quantities that are linked to topology by a handful of useful theorems; we show how these quantities can be measured in our simulations. In Section 7.4, we present our numerical results. We found a two-step transition marked by peaks of the specific heat, that we classify as a second order transition, using analytic tools developed specifically for the microcanonical ensemble; furthermore, we show that to this transition correspond to jumps of the bond-orientational order parameters, and is hence accompanied by modifications of the short-range structural properties of the system. Finally, we observe singular behaviours of various geometric quantities, in correspondence with the observed transition, conclusively implying an underlying change in the topology of the potential energy level sets.

7.2. Model

The system we chose here to consider consists in a binary Lennard-Jones mixture, first introduced in [146], of Hamiltonian $H(\{\boldsymbol{q}_i\}_{i=1,...,N}) = K + \Phi(\{\boldsymbol{q}_i\}_{i=1,...,N})$, where K is the total kinetic energy, the $\boldsymbol{q}_i$ are the N 3-dimensional position variables, and

$$
\begin{aligned}
\Phi(\boldsymbol{\Gamma}) = &\quad \Phi_{11}(\boldsymbol{\Gamma}) \quad + \quad \Phi_{22}(\boldsymbol{\Gamma}) \quad + \quad\quad\quad \Phi_{12}(\boldsymbol{\Gamma}) \\
= &\quad \sum_{i,j\in\Lambda_1} 4\epsilon_{11}\left(\frac{\sigma_{11}}{r_{ij}}\right)^{12} + \sum_{i,j\in\Lambda_2} 4\epsilon_{22}\left(\frac{\sigma_{22}}{r_{ij}}\right)^{12} + \sum_{\substack{i\in\Lambda_1,\\j\in\Lambda_2}} 4\epsilon_{12}\left[\left(\frac{\sigma_{12}}{r_{ij}}\right)^{12} - \left(\frac{\sigma_{12}}{r_{ij}}\right)^{6}\right],
\end{aligned}
$$
(7.1)

where we introduced the shorthand notation $\boldsymbol{\Gamma} = \{\boldsymbol{q}_i\}_{i=1,...,N}$ for the instantaneous configuration of the system, Λ_1, Λ_2 are the set of particles belonging to species 1 and 2 respectively, and $r_{ij} = |\boldsymbol{q}_i - \boldsymbol{q}_j|$. The interaction parameters are set as

$$
\begin{aligned}
\sigma_{22}/\sigma_{11} &= 0.85 & \sigma_{12}/\sigma_{11} &= 0.49 \\
\epsilon_{12}/\epsilon_{11} &= 6 & \epsilon_{22}/\epsilon_{11} &= 1,
\end{aligned}
$$

and $\epsilon_{11} = 1$, $\sigma_{11} = 1$. The density $\rho = 1.6$ and the respective concentrations of the two species are $c_1 \approx 0.33$ and $c_2 \approx 0.67$ (the latter are not exact because $N \times c_{1(2)}$ might not be an integer). As is it customary, we set the Boltzmann constant $k_B = 1$.

In this numerical study, we do not take into account the microscopic details of the kinetic energy K; in the Monte Carlo scheme we employed, described in Appendix C, K is in fact employed as a "*demon*", allowing us to keep the total energy E constant.

7.3. Geometric Signatures of Topological Changes

Entropy stems as a fundamental building block of thermodynamics. In particular, in the microcanonical ensemble, most macroscopic observables can be retrieved from its derivatives. Furthermore, it has recently been proposed [147] a microcanonical ensemble classification of phase transitions, analogous to the notorious classification of Ehrenfest, heuristically associating first and second order phase transitions to discontinuity of the second and third derivatives, respectively, of the entropy.

In standard Hamiltonian systems as ours, that is where H is a quadratic function of the momenta, the kinetic part of the canonical partition is known to be trivial, as it reduces to a constant factor. In the microcanonical ensemble, the dissociation of the kinetic and configurational parts of the partition function is somewhat less evident, but can nevertheless be performed through Laplace transform techniques [148]; in particular, this separation allows for the practical expression of the microcanonial probability density (C.2). It results that the relevant information is entirely contained in the configurational entropy

$$S(\varphi) = \frac{1}{3N} \log \int d\mathbf{\Gamma} \, \Theta \left(\varphi - \Phi(\mathbf{\Gamma}) \right), \tag{7.2}$$

where $\Theta(x)$ is the Heaviside step function, which vanishes for $x < 0$ and equates one for $x \geq 0$. Yet the latter expression can be rewritten in terms of the PLS volumes [149, 1]

$$S(\varphi) = \frac{1}{3N} \log \int_0^\varphi d\phi \, \int_{\Sigma_\phi} \frac{d\sigma}{|\boldsymbol{\nabla}\Phi|}, \tag{7.3}$$

$\boldsymbol{\nabla}$ being here the gradient operator, $d\sigma$ is the elementary volume induced by the immersion in $\mathbb{R}^{3N}$ of the PLS Σ_ϕ, hypersurface of dimension $3N - 1$ defined as

$$\Sigma_\phi = \left\{ \mathbf{\Gamma} \in \Omega \middle| \Phi(\mathbf{\Gamma}) = \phi \right\}, \tag{7.4}$$

where Ω is the full state space, and ϕ is the fixed value defining the PLS. Finally, it has been shown that Eq. (7.3) can be expressed in terms of topological invariants, namely [1]

$$S(\varphi) = \frac{1}{3N} \log \left[Vol(\mathbb{S}_1^{3N-1}) \sum_{i=0}^{3N} b_i(\Sigma_\varphi) + \mathcal{R}_1(\varphi) \right] + \frac{1}{N} \log \mathcal{R}_2(\varphi), \tag{7.5}$$

where $\mathcal{R}_1, \mathcal{R}_2$ are smooth functions of the potential, $Vol(\mathbb{S}_1^{3N-1})$ is the volume of the unit ball of dimension $3N - 1$, and $b_i(\Sigma_\varphi)$ is the ith Betti number of the manifold Σ_φ.

Eq. (7.3) highlights the dependence of the configurational entropy on topological aspects of the PLS, encoded in the Betti numbers b_i. This observation was at the root of the *topological hypothesis*, stating that the deep mathematical origin of a

phase transition was to be found in a topological change of the PLS. It is worth noting that, whereas any phase transition is rooted in a topological change, not all topological changes entail a phase transition.

In the present work, we thus aim at establishing a correspondence of the glass transition with topological changes of the PLS.

Probing the topology of the high-dimensional manifolds that are the PLS is by no means a simple task. To our best knowledge, there exists no way of fully characterizing it by means of measurable average observables, namely the tools accessible to us. For lack of a complete reconstruction of the topology of the submanifolds of interest, it is however possible to probe *topological changes*, which are, in the end, our true object of study. There fortunately exist a few theorems of differential topology drawing sufficiently strong links between geometrical and topological quantities, allowing us to observe, when they are present, sharp topological *changes.*

We now introduce very roughly a few notions of differential extrinsic geometry, that will be useful to the development of our topological probing. For a more extensive development of this framework, we refer the reader to Ref. [150, 1, 149].

In order to alleviate our notations, we now drop the dependence in $\mathbf{\Gamma}$.

We first present Pinkall's theorem, relating the average dispersion of principal curvatures with the weighted sum of the Betti numbers

$$\frac{\int_{\Sigma_\phi} \sigma_\kappa^2(\mathbf{\Gamma})d\mathbf{\Gamma}}{\int_{\Sigma_\phi} d\mathbf{\Gamma}} = \left[Vol(\mathbb{S}_1^D) \sum_{i=1}^{D} \left(\frac{i}{D-1} \right)^{D/2-i} b_i(\Sigma_\phi) \right]^{2/D} - r(\Sigma_\phi), \qquad (7.6)$$

where D is the dimension of the manifold, $\sigma_\kappa^2 = \langle \kappa_i^2 \rangle - \langle \kappa_i \rangle^2$ is the dispersion of the principal curvatures, and $r(\Sigma_\phi)$ is a remainder, which stays small provided that σ_κ^2 doesn't exhibit too large variations on the submanifold Σ_ϕ.

Another geometric quantity that connects to topological invariants is the range of variability of the sectional curvatures Δ_{sec}. Overholt's theorem indeed states that it provides an upper bound to the sum of Betti numbers

$$\Delta_{sec} \geq \left[\frac{Vol(\mathbb{S}^D) \sum_{i=0}^{D} b_i(\Sigma_\phi)}{2Vol(\Sigma_\phi)} \right]^{2/D}. \qquad (7.7)$$

In turn, Δ_{sec} is related to the variance of the scalar curvature R_Σ, as the latter is simply defined as the sum of all the sectional curvatures at a given point $\mathbf{\Gamma}$

$$R_\Sigma = \sum_{i \neq j} K_{ij} = \sum_{i \neq j} \kappa_i \kappa_j, \qquad (7.8)$$

where K_{ij} is the sectional curvatureof sectional plane (u_i, u_j), and $\{u_j\}_{j=1,...,D}$ forms

an orthonormal basis in the tangent space at this point.

It results

$$\frac{\langle R_\Sigma^2 \rangle - \langle R_\Sigma \rangle^2}{N(N-1)} \approx \Delta_{sec},\tag{7.9}$$

Up to our best knowledge, the simplest way to compute these quantities in the context of numerical simulations, is by considering the *Weingarten operator*, also called *shape operator*. A most useful tool characterizing the extrinsic geometry of hypersurfaces, it is the operator such that, for $\boldsymbol{X} \in T\Sigma$ a vector field in the tangent bundle of Σ, we have

$$\mathcal{W}_{\boldsymbol{n}}(\boldsymbol{X}) = -\nabla_{\boldsymbol{X}}\boldsymbol{n},\tag{7.10}$$

where $\nabla_{\boldsymbol{X}}$ is the Levi-Civita connexion on Σ, and

$$\boldsymbol{n} = \frac{\boldsymbol{\nabla}\phi}{|\boldsymbol{\nabla}\phi|}\,(\boldsymbol{\Gamma})$$

is the normal to Σ at a given point $\boldsymbol{\Gamma}$.

The trace of the shape operator and of its square can be expressed in terms of mere derivatives of Φ, namely

$$\mathrm{Tr}\,[\mathcal{W}_{\boldsymbol{n}}] = \frac{\Delta\Phi}{|\boldsymbol{\nabla}\Phi|} - \frac{\boldsymbol{\nabla}\Phi^* \cdot \mathrm{Hess}\,(\Phi) \cdot \boldsymbol{\nabla}\Phi}{|\boldsymbol{\nabla}\Phi|^3}$$

$$\mathrm{Tr}\,\left[\mathcal{W}_{\boldsymbol{n}}^2\right] = \frac{\mathrm{Tr}\,\left[\mathrm{Hess}\,(\Phi)^2\right]}{|\boldsymbol{\nabla}\Phi|^2} + \frac{|\boldsymbol{\nabla}\Phi^* \cdot \mathrm{Hess}\,(\Phi) \cdot \boldsymbol{\nabla}\Phi|^2}{|\boldsymbol{\nabla}\Phi|^6} - 2\frac{|\mathrm{Hess}\,(\Phi) \cdot \boldsymbol{\nabla}\Phi|^2}{|\boldsymbol{\nabla}\Phi|^4},\tag{7.11}$$

where $\Delta\Phi$ and $\mathrm{Hess}\,(\Phi)$ denotes respectively the Laplacian and the Hessian of ϕ, and "$\cdot$" the scalar product.

The eigenvalues of $\mathcal{W}_{\boldsymbol{n}}$ are the D principal curvatures κ_i. It results that the above-mentioned geometric quantities can all be expressed with combinations of $\mathrm{Tr}\,[\mathcal{W}_{\boldsymbol{n}}]$ and $\mathrm{Tr}\,[\mathcal{W}_{\boldsymbol{n}}^2]$, namely

$$M_\Sigma = \frac{\mathrm{Tr}\,[\mathcal{W}_{\boldsymbol{n}}]}{D}$$

$$\sigma_\kappa^2 = \frac{\mathrm{Tr}\,[\mathcal{W}_{\boldsymbol{n}}^2]}{D} - \frac{\mathrm{Tr}\,[\mathcal{W}_{\boldsymbol{n}}]^2}{D^2}\tag{7.12}$$

$$R_\Sigma = \mathrm{Tr}\,[\mathcal{W}_{\boldsymbol{n}}]^2 - \mathrm{Tr}\,\left[\mathcal{W}_{\boldsymbol{n}}^2\right].$$

The combination of formulae (7.11) and (7.12) clearly provide a straightforward way of obtaining the quantities of interest in the context of numerical simulations, simply by computing and combining the gradient and Hessian of the potential function Φ at each measurement step.

The latter geometric quantities pertain to the geometrical characteristics of the PLS, while our simulations are performed at constant total energy E. However, at large N, the fluctuations of Φ and K tend to vanish, and surfaces of constant $K(\{\boldsymbol{p}_i\}_{i=1,...,N}) = \sum_i p_i^2/2$ are diffeomorphic to $3N$-hyperspheres; the energy level sets can then be seen as product manifolds $\Sigma_E \sim \mathbb{S}_K^{3N} \times \Sigma_\phi$. We thus consider $\phi(E)$ stable enough for the corresponding PLSs to be diffeomorphic to one another, and for the general behaviour of the above-defined geometric quantities to be trusted.

7.4. **Numerical results**

Using an involved microcanonical ensemble Monte Carlo scheme described in the appendix C, we explored the behaviour of the model defined by (7.1).

We simulated a system of size $N = 216$ particles and another of size $N = 512$ particles, hereafter denoted the smaller and larger system, respectively.

It is worth noting that these simulations were, as is often the case in so-called glassy systems, very time consuming and hard to equilibrate.

An exact estimation of the total computation time is in practice difficult to assert, partly due to the fact that the set of energies we considered was changed multiple times during this extensive work. To provide an idea of the involved time scales, the simulation of the larger system for performed for a duration exceeding 600 hours in CPU time per replica, with 120 replicas; the workstation at our disposal being endowed with only 64 processors, we only simulated 60 replicas in parallel at any given time, so the real duration of the simulation was more than 1200 hours, that is 50 days. In this estimation, we only took into account the *efficient* simulation time, disregarding earlier simulations employed to test the program for coding errors, and to search for the set of energies optimizing the replica swapping rate.

In comparison, the smaller system evolved much faster, and only required 50 replicas, due to the larger dispersion of the distribution of potential energies (see Section C.4. In this case, we estimate the efficient simulation time to be around 250 hours.

It appears that the larger system did not equilibrate well, in comparison with the smaller one, as can be inferred from the large error bars in the specific heat computed from kinetic energy fluctuations, as displayed in figure 7.1b, and the overall less regular behaviour of the quantities displayed in the present section.

It is worth emphasizing that none of the two systems reached a perfect equilibrium. The results of various equilibration tests we performed were not completely satisfactory.

Our parallel tempering algorithm (i.e. replica exchange) was quite efficient in a

first phase of equilibration, with some replicas crossing the whole range of energies, from the highest to the lowest; yet, in the second, current phase of equilibration, it became restricted to the exchange of replicas of neighbouring energies, thus do not achieve the desired retrieval of ergodicity we aim for. The continuation of our quest for equilibrium would require new optimized choices of a set of energies to simulate, perhaps accompanied by a increased number of parallel replicas.

We however claim that, at least in the case of the smaller system, we find ourselves close enough to draw some interesting conclusions from what we could observe.

7.4.1. Characterization of the phase transition

Preliminary to our analysis of the geometry and topology of the PLS, we show here the that a phase transition is indeed occurring, and try to determine its precise nature.

To this end, we examined quantities that are usually expected to exhibit singular behaviour at the transition.

7.4.1.1. Specific heat, caloric curve and entropy derivatives

The specific heat c_v typically displays these critical behaviours in most phase transitions; this can be due to the presence of latent heat, in the case of first order phase transition, or to critical fluctuations, in the case of continuous phase transitions.

In the microcanonical ensemble, the specific heat can be computed according to

$$c_v = \left(\frac{dT}{dE}\right)^{-1}, \tag{7.13}$$

where $T = \frac{2\langle K \rangle}{3N}$ is the kinetic temperature. Alternatively, we can also use the results of [148], which used the Laplace-transform techniques to propose a variety of alternative definitions for usual thermodynamical observables. Amongst three different formulas for c_v, we only display one here, as we obtained with the others the same results, up to the accessible precision.

$$c_v = \frac{3}{2}\left[1 - \frac{3N}{2}\left(\frac{\langle K^2 \rangle}{\langle K \rangle^2} - 1\right)\right]^{-1}. \tag{7.14}$$

The comparison of the curves obtained with both Eq. (7.13) and (7.14) is commonly employed as an equilibration test (see for instance [151]).
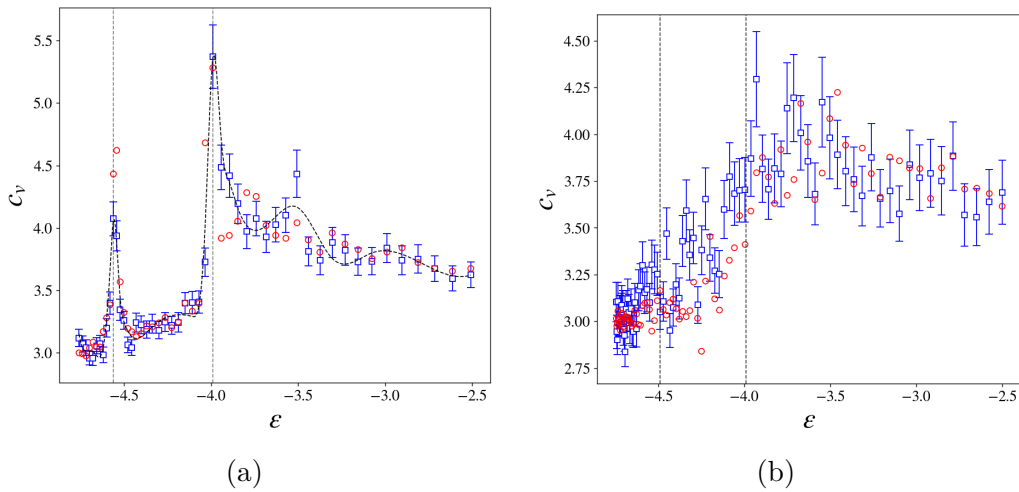
Figure 7.1.: Specific heat c_v as a function of the energy density $\epsilon = E/N$, in the systems with $N = 216$ (a)) and $N = 512$ (b). The blue squares were obtained using Eq. (7.14), while the red circles were obtained using Eq. (7.13). Because of its great sensitivity to the (arbitrarily chosen) set of energies, we were not able to compute reasonable standard errors for the latter.

Inspection of figure 7.1a shows two clear peaks of the specific heat, indicators of a two-step transition occurring in the smaller system. Figure 7.1b shows that the large system seems to roughly exhibit the same behaviour, though much less pronounced, presumably due to the imperfect equilibration. Such a behaviour is, according Ehrenfest classification of phase transitions, the marker of a second order phase transition.

In the following graphs, for both system sizes, we flag the positions of the two peaks of figure 7.1a with two vertical dotted lines. We denote ϵ_1 and ϵ_2 the critical energy density of the first and the second peak, respectively.

Figure 7.2 makes it clear that, for the smaller system of best equilibration, to E_1 and E_2 correspond jumps of the potential energy density, indicating a sensible change of the internal arrangement of the Lennard-Jones mixture. These jumps are accompanied by an inflexion of the slope; interestingly, an inflexion point is found also in the larger system, positioned at E_2.
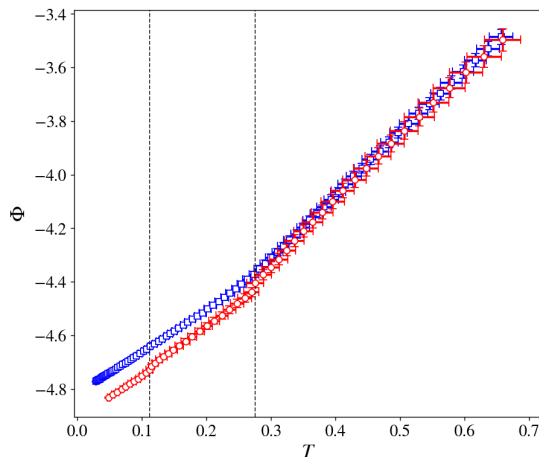
Figure 7.2.: Average potential energy $\langle\Phi\rangle$ as a function of the average temperature T, in the system with $N = 216$ (red circles) and the system with $N = 512$ (blue squares).

Ehrenfest classification of order transitions relies on the loss of analyticity of Helmoltz free energy. However, the relevant thermodynamic potential in the microcanonical ensemble is the entropy, which is perhaps a quantity of deeper physical and mathematical meaning. Yet, after (7.13), the microcanonical specific heat can be rewritten as

$$c_v(\epsilon) = - \left(\frac{\partial S}{\partial E}\right)^2 \left(\frac{\partial^2 S}{\partial E^2}\right)^{-1}, \qquad (7.15)$$

emphasizing that the observed singular behaviour of c_v can, in principle, find its origin in a divergence of the first order derivative of the entropy, or in the vanishing of its second order derivative. To better understand the underlying phenomenon, it is hence desirable to inspect more closely these quantities. Furthermore, while, in the canonical ensemble, the average specific energy $\langle\epsilon\rangle(T)$ usually displays clear critical behaviours at the transition temperature, the microcanonical ensemble inverse temperature $\beta(\epsilon) = \frac{1}{T(\epsilon)}$ is often much less sensitive.

Motivated by these observations, in Refs. [152, 147, 153, 154], novel methods of classification of phase transitions in the microcanonical ensemble were proposed, relying on the analysis of inflexion points of the derivatives of the entropy. In fact, in the absence of a phase transition, all derivatives of S of even order are strictly concave, and those of odd order strictly convex.

In figure 7.3, we show the four lowest order derivatives of S with respect to ϵ,

that is

$$\beta(\epsilon) = \frac{\partial S}{\partial E} \tag{7.16}$$

$$\gamma(\epsilon) = \frac{\partial^2 S}{\partial E^2} = \frac{\partial \beta}{\partial E} \tag{7.17}$$

$$\delta(\epsilon) = \frac{\partial^3 S}{\partial E^3} = \frac{\partial^2 \beta}{\partial E^2} \tag{7.18}$$

$$\omega(\epsilon) = \frac{\partial^4 S}{\partial E^4} = \frac{\partial^3 \beta}{\partial E^3} \tag{7.19}$$

To retrieve these quantities, we departed from the kinetic temperature T straightforwardly obtained from simulation, and differentiated β with respect to the energy.
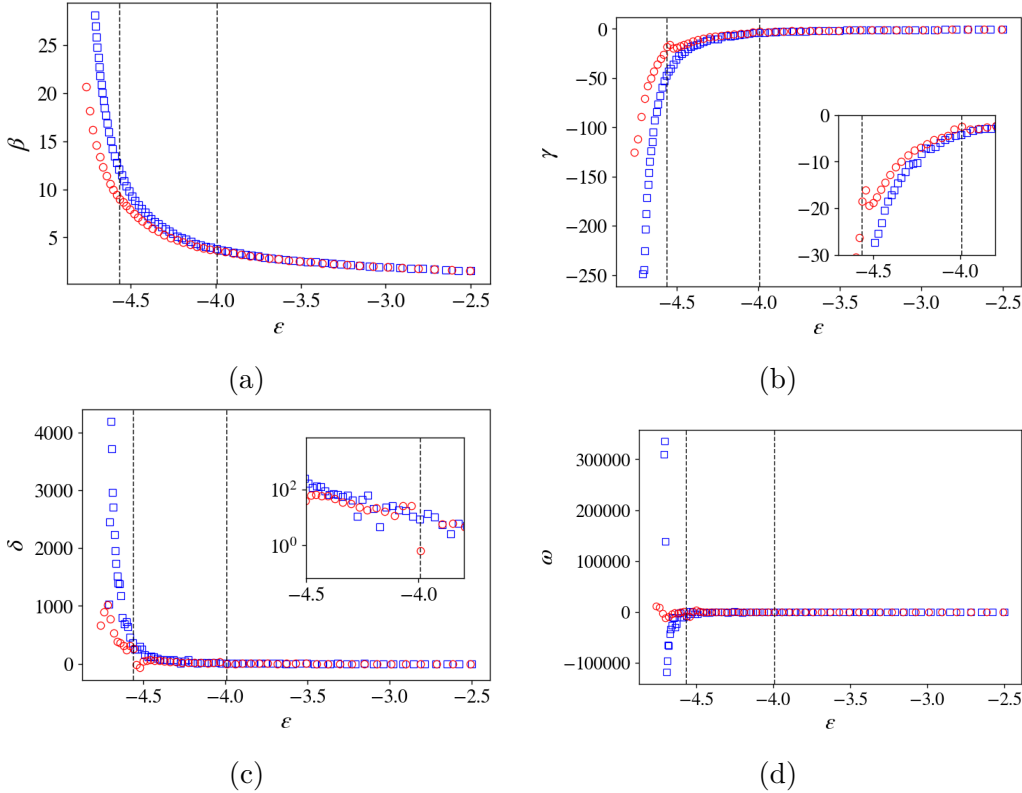
Figure 7.3.: β (a), γ(b), δ(c) and ω(d) as functions of the energy density $\epsilon = E/N$.

No sensible inflection point can be found on the inverse temperature, which stays convex on the whole range of energies considered. In the smaller system, $\gamma(\epsilon)$ shows a local (negative) maximum at the low energy transition point, and another "bump", albeit less visible, at the high-energy transition point. This suggests, once again, the occurrence of a second order phase transition, according to the classification of [154]: $\gamma(\epsilon_1)$, $\gamma(\epsilon_2)$ approach 0, hence $\beta(\epsilon_1)$, $\beta(\epsilon_1)$ must display corresponding sharply localized region of lesser sensitivity to energy changes.

Furthermore, $\delta(\epsilon)$ displays a local maximum and a local minimum, closely before and after ϵ_1, respectively, and a minimum at ϵ_2. These critical points stem as signatures of the local maxima of $\gamma(\epsilon)$ present at these points.

These results are remarkably similar to those displayed in [154] for the ferromagnetic phase transition of the 2-dimensional Ising model.

Remarkably, $\delta(\epsilon)$ and $\omega(\epsilon)$ exhibit pronounced divergent behaviours at very low energy, below E_1, especially in the larger system. It is however likely to be an artefact, confirming a serious lack of equilibration in this region: the system, due to the frozen dynamics, remained stuck in the pseudo-crystalline configuration that we implemented as an initial condition (for detail, see appendix C).

7.4.1.2. Orientational and Translational Order

Another set of quantities that we employed to study this transition are the bond-orientational order parameters Q_l, first defined in [155] to characterize crystalline order in Lennard-Jones liquids. For a given $l \in \mathbb{N}$, it writes

$$Q_l = \sqrt{\frac{4\pi}{2l+1} \sum_{m=-l}^{l} |Q_{lm}|^2}, \qquad (7.20)$$

with

$$Q_{lm} = \frac{1}{n_B} \sum_{(i,j) \in B} Y_{lm}\left(\theta(\boldsymbol{r}_{ij}), \varphi(\boldsymbol{r}_{ij})\right) \qquad (7.21)$$

, where B is the considered set of bonds, n_B its cardinality, $\theta(\boldsymbol{r}_{ij})$ and $\varphi(\boldsymbol{r}_{ij})$ are respectively the azymutal and polar angles of the bond vector $\boldsymbol{r}_{ij}$ in a fixed reference frame, and the Y_{lm} are spherical harmonics.

Two particles i, j are considered *bonded* if $r_{ij} < c_b$, where c_b is an arbitrary cutoff. As is often prescribed [156, 157, 158], we set c_b to be the approximate position of the second minimum of the radial distribution functions right after the first peak.

The authors of Ref. [146] showed that this model exhibits a short to medium-range order, namely a local tetrahedral ordering, coined as a *tetrahedral network*. The results displayed in figures 7.4 and 7.5 seem to corroborate this observation, as the order parameters defined in Eq. (7.20) exhibit clear steps at the transitions energies ϵ_1, ϵ_2, for certain values of l.

Interestingly, in the smaller system, at energy density ϵ_1, most of the Q_l exhibit singular behaviours, whether it be a positive of a negative peak, suggesting a temporary rearrangement of the particles upon cooling.
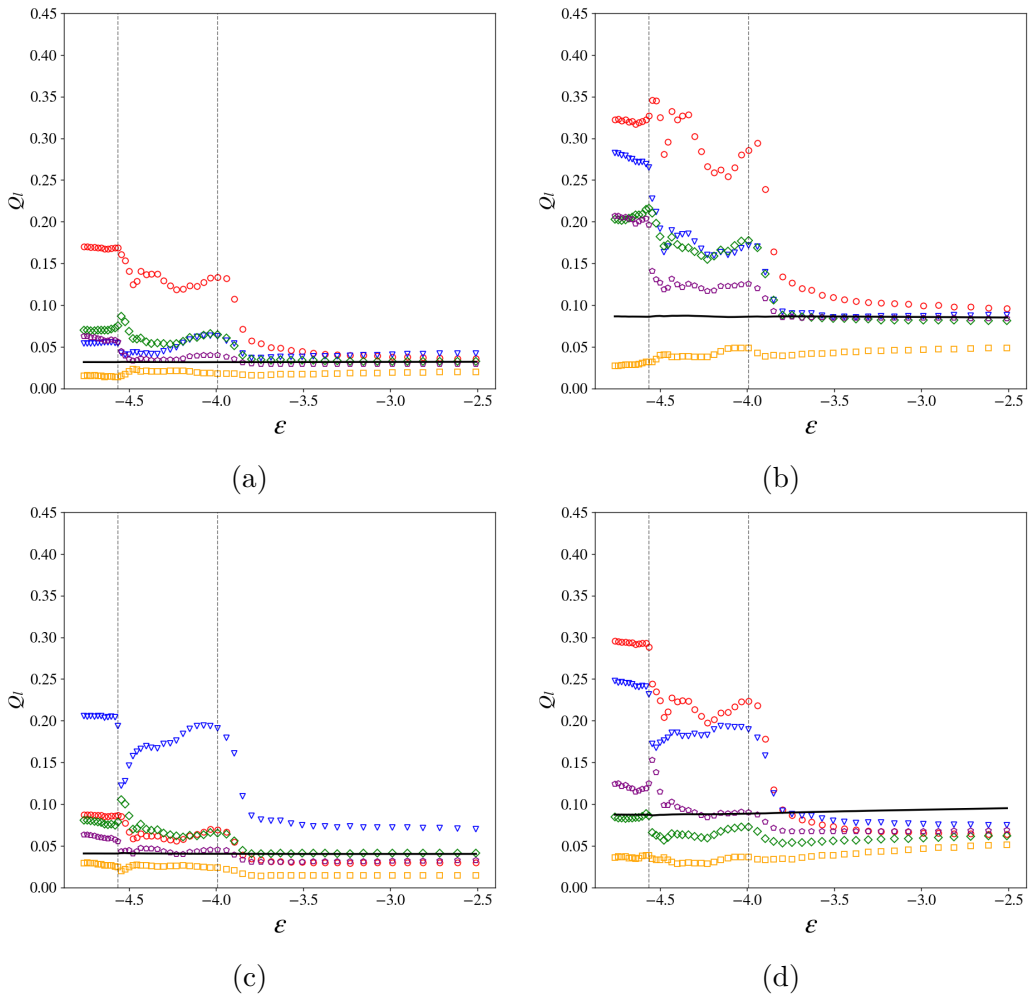
Figure 7.4.: Bond-oriential order parameters Q_l as a function of the energy density $\epsilon = E/N$, for all bonds (7.4a), $1 - 1$ bonds (b), $2 - 2$ bonds (c) and $1 - 2$ bonds (d), in the $N = 216$ system. Represented are the parameters Q_2 (yellow squares), Q_4 (red circles), Q_6 (blue triangles), Q_8 (green diamonds) and Q_{10} (purple pentagons). The value $\frac{1}{\sqrt{n_B}}$, expected in a fully disordered system, is shown as a black line.
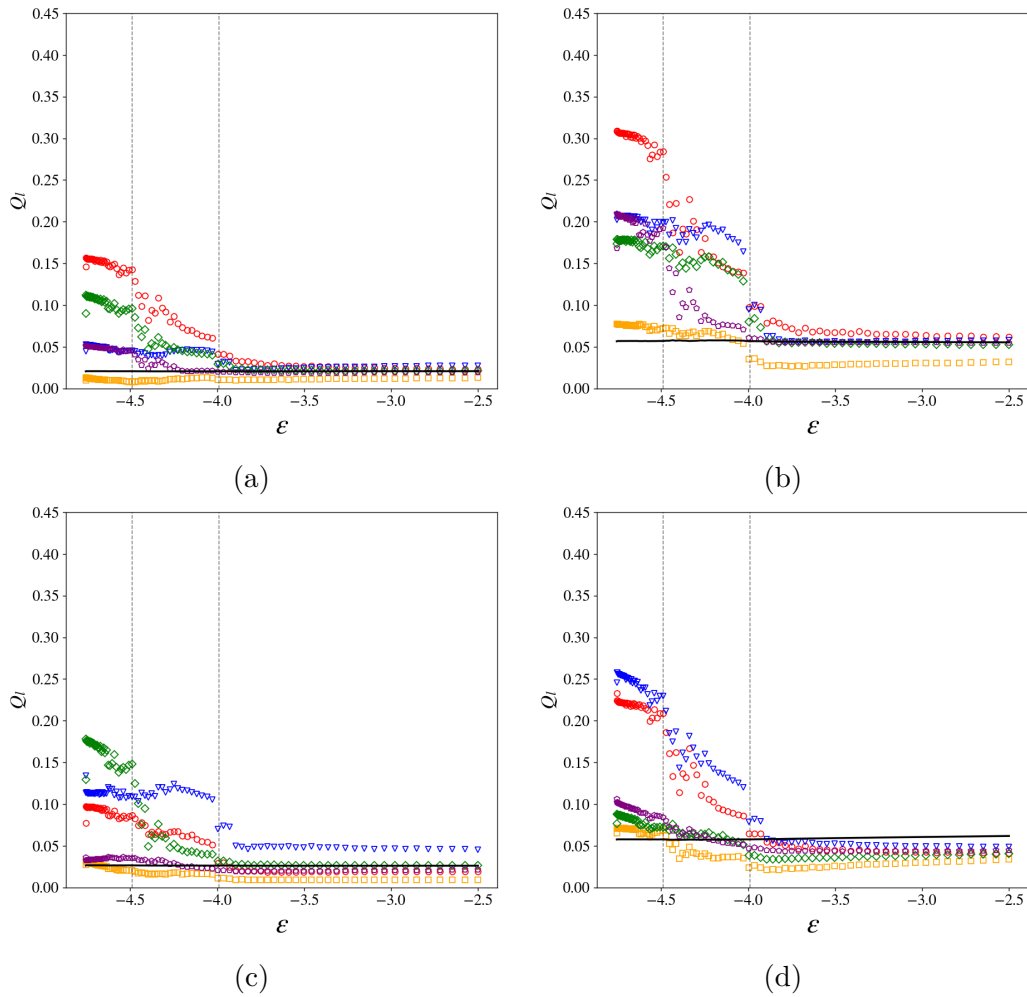
Figure 7.5.: Bond-oriential order parameters Q_l as a function of the energy density $\epsilon = E/N$, for all bonds (a), $1-1$ bonds (b), $2-2$ bonds (c) and $1-2$ bonds (d), in the $N = 512$ system. Represented are the parameters Q_2 (yellow squares), Q_4 (red circles), Q_6 (blue triangles), Q_8 (green diamonds) and Q_{10} (purple pentagons). The value $\dfrac{1}{\sqrt{n_B}}$, expected in a fully disordered system, is shown as a black line.

A more exhaustive analysis has yet to be performed, in order to assert precisely the kinds of local structures that emerge in our simulations. Yet, as expected, a local ordering seems to have emerged in the smaller system, as exemplifies the projective view of figure 7.6a, where we clearly see an aperiodic repetition of pentagonal arrangements. On the other hand, figure 7.6b confirms, by its pronounced regularity and the obvious periodicity it exhibits, that the larger system stayed stuck, at low energies, in the initial lattice-like configuration; note that this too regular pattern disappears at energies higher than $\epsilon \approx 4.2$.
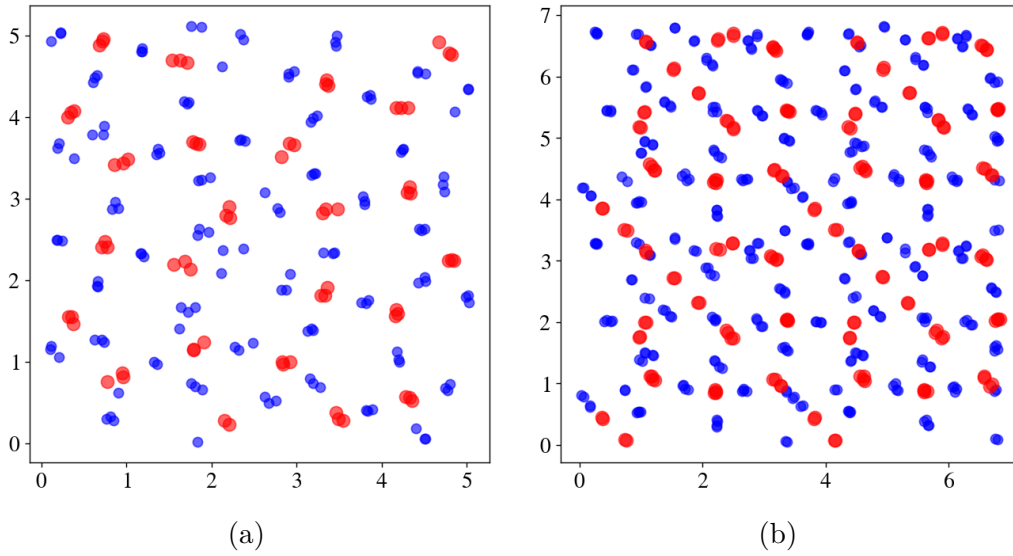
Figure 7.6.: Instantaneous configuration in the systems with $N = 216$ (a) and $N = 512$ (b), projected onto an arbitrary plane, at energy density $\epsilon \approx -4.75$. Particles of species 1(2) are represented in red(blue) respectively.

7.4.2. Topological Changes
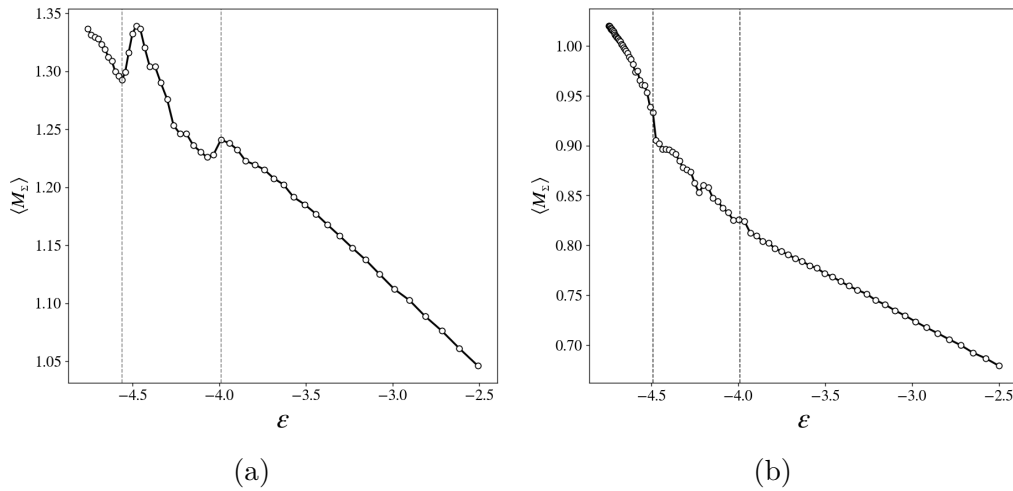
Figure 7.7.: Total mean curvature as a function of the energy.

Figure 7.7 shows, in correspondence with the two c_v-peaks, inflexion points of the total mean curvature of the submanifold Σ_ϕ, indication of a change of the landscape of this hypersurface. In the smaller system, these inflexion points correspond to a local minimum and a local maximum, for the first and the second peak, respectively.

133

In the larger system, though abrupt changes are still visible at the transitions, the behaviour between the two critical points is sensibly different, and roughly monotonous.

(a)

(b)
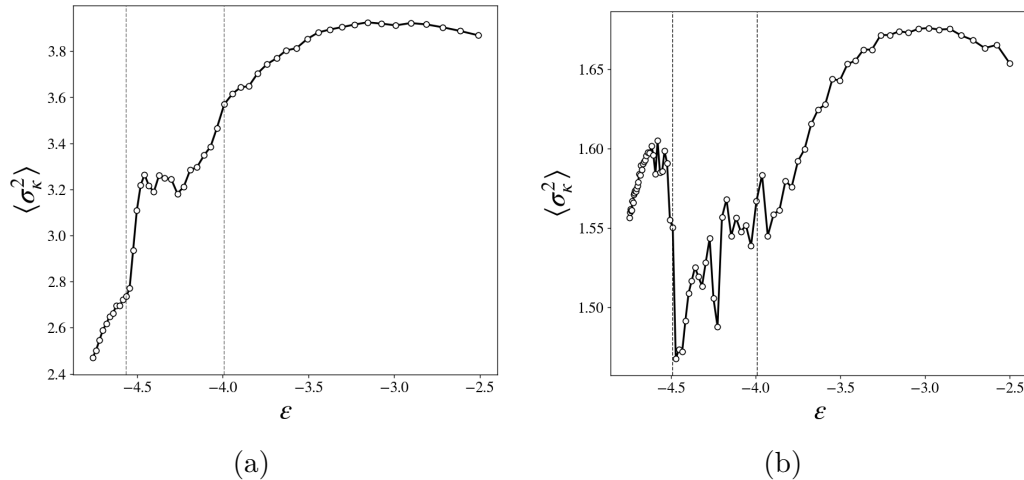
Figure 7.8.: Dispersion of the principal curvatures as a function of the energy.

The average variance of the principal curvatures, shown in figure 7.8, also seems to exhibit singular behaviours at these transition points, providing a strong indication of a change of the topology of Σ_ϕ, in virtue of Pinkall's theorem (7.6). Namely, such a change is necessarily due to a change in the values of the Betti numbers, hence of the topological properties of Σ_ϕ; though the precise nature of these changes is not accessible to our analysis, we can expect that, from the high temperature chaotic phase to the low temperature crystalline phase, Σ_ϕ loses connectivity and the system is more easily confined to restricted regions of state-space.

It is again worth noticing that the behaviour of $\langle \sigma_\kappa \rangle$ is quite different for the larger, less well-equilibrated system, as it displays a sharp fall in the intermediary region, not present in the smaller system. For the latter, $\langle \sigma_\kappa \rangle$ is almost everywhere increasing with increasing ϵ, with a small plateau in the intermediary region.

Finally, the variance of the scalar curvature, shown in figure 7.9, jumps at the low energy transition point, for both system sizes, exhibiting a wide peak in the intermediary region, in the case of the smaller system.
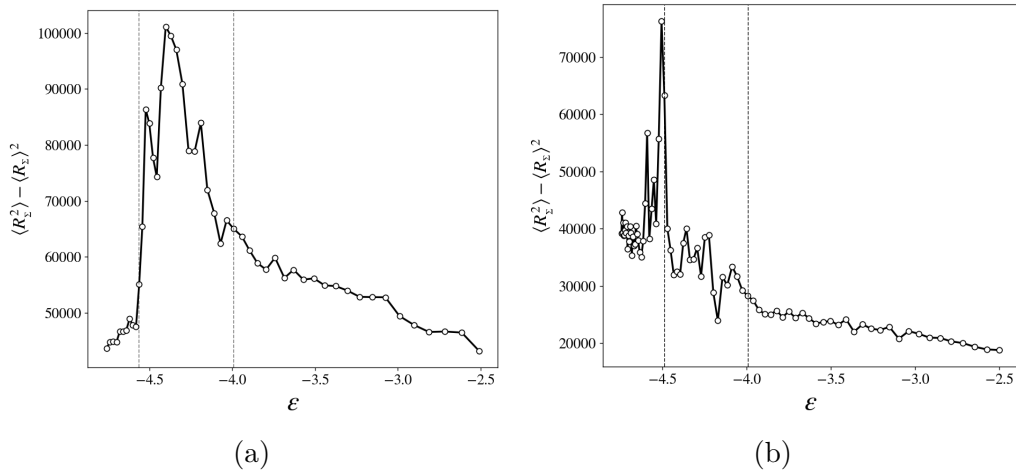
Figure 7.9.: Variance of the scalar curvature as a function of the energy.

All of these observations suggest that there are indeed important changes in the topology of Σ_ϕ at play during this phase transition, particularly pronounced between the two c_v-peaks, hence in a finite range of energy density. In this intermediary region, the overall shape of the manifold Σ_ϕ most probably dramatically changes, possibly in many steps of topological discontinuities. These changes correspond to the rearrangement of particle configurations in a crystalline order, of which the scale gradually increases up to the point of exhibiting a genuine long-range order, with a high degree of global symmetry.

Conclusion of part II

In this part of our thesis, we investigated ergodicity-breaking, phase transitional phenomena, resorting to the analysis of the behaviour of the potential functions defining the models.

We proposed a scenario explaining the formation of biclusters in the low energy HMF model, showing how the non-linearity of its potential generates a collective motion of the particles that amounts to a time-dependent effective force. Exploiting time scale separation, and applying time-averaging techniques similar to these employed in plasma physics, we were able to retrieve the characteristic frequencies observed in this Hamiltonian system. We further proposed a scenario thoroughly explaining the formation and stability of the biclusters by the stroboscopic and bimodal nature of the effective force.

It would be of great interest to try and study the antiferromagnetic HMF under the point of view of the topological theory of phase transitions. In fact, while the apparition of biclusters does not stem as a phase transition in the conventional sense, as it is a metastable, out-of-equilibrium state highly depending on the initial conditions, its state-space topology might, however, exhibit non-trivial behaviours that could improve our comprehension of metastability. Furthermore, it has been shown in former work [118] that it can in fact be seen as the equilibrium of an effective dynamics; this yields the possibility of applying phase transition theories to such out-of-equilibrium features, with a wide range of potential applications.

We then studied a binary Lennard-Jones mixture, known to be a glass-forming model, through an elaborate microcanonical Monte Carlo scheme. We found that the model indeed exhibits a second order phase transition that occurs in two steps, marked by two peaks of the specific heat; though no long-range order was found, we identified short-range structures, corroborating the finding of previous studies. We finally showed that, as was expected, it is accompanied by dramatic changes of the topological properties of the potential level sets.

Though we were able to draw some conclusive results, it is worth noting that we did not fully reach, in this work, the statistical equilibrium of this glass-forming model at all considered energies. Achieving equilibrium in the systems we considered will lead us to finer results, in particular concerning the behaviour of geometrical quantities below the high energy transition. Another important follow-up would be to duplicate our results for diverse system sizes, in order to decisively discard finite size effects. Finally, it would be of great interest to perform similar analysis onto other glass-forming models, and in particular inspect, under this geometrical prism,

glass transitions that are provoked by supercooling procedures (at variance with the model we studied, which is frustrated and does not possess a crystalline phase).

Discussion and future developments

The work presented in this thesis focused, for the first part, on the characterization of correlations and entanglement properties in quantum states and for the second part on a study of classical phase transitions leaning on the geometric and topological properties of the potential energy surfaces. Thus, as a follow up of this work, we now aim at utilizing this dual approach, to develop tools and methodologies that enable a comprehensive analysis of quantum phase transitions.

As demonstrated in the Tavis-Cummings model, we have observed that quantum phase transitions can be accompanied by a sudden change in entanglement, which can be regarded as an order parameter in this particular context. By further exploring the topological properties of the accessible state space in the corresponding quantum dynamics, we anticipate a deeper understanding of these phenomena and the emergence of new avenues for research.

Evidently, it is not as straightforward to compute quantities as the gradient or Hessian of a quantum Hamiltonian, as it is for a classical one. This is because quantum Hamiltonians are operators acting on Hilbert spaces (i.e. matrices), rather than functions of real variables. A possible workaround to this drawback is to apply the time-dependent variational principle to such quantum models; thus doing, we can approximate the state of the system as a time-dependent vector, from which an effective, classical-like potential function can be derived.

Approaching in this fashion the quantum dynamics with a classical formulation could allow us to perform the desired geometric analysis, and might provide more fundamental explanation for the occurrence of quantum phase transitions and their links to entanglement and quantum correlations.

Bibliography

[1] M. Pettini, *Geometry and Topology in Hamiltonian Dynamics and Statistical Mechanics* (Interdisciplinary Applied Mathematics), en, S. S. Antman, J. E. Marsden, and L. Sirovich, Eds. New York, NY: Springer New York, 2007, vol. 33, ISBN: 978-0-387-30892-0 978-0-387-49957-4. DOI: 10.1007/978-0-387-49957-4 (cit. on pp. 10, 120, 122, 123).

[2] A. Einstein, B. Podolsky, and N. Rosen, "Can Quantum-Mechanical Description of Physical Reality Be Considered Complete?", *Phys. Rev.*, vol. 47, no. 10, pp. 777–780, May 1935. DOI: 10.1103/PhysRev.47.777 (cit. on pp. 14, 16).

[3] E. Schrödinger, "Discussion of Probability Relations between Separated Systems", en, *Mathematical Proceedings of the Cambridge Philosophical Society*, vol. 31, no. 4, pp. 555–563, Oct. 1935, ISSN: 1469-8064, 0305-0041. DOI: 10.1017/S0305004100013554 (cit. on p. 14).

[4] E. Schrödinger, "Probability relations between separated systems", en, *Mathematical Proceedings of the Cambridge Philosophical Society*, vol. 32, no. 3, pp. 446–452, Oct. 1936, ISSN: 1469-8064, 0305-0041. DOI: 10.1017/S0305004100019137 (cit. on p. 14).

[5] D. M. Greenberger, M. A. Horne, and A. Zeilinger, "Going beyond bell's theorem", *Bell's theorem, quantum theory and conceptions of the universe*, M. Kafatos, Ed., Dordrecht: Springer Netherlands, 1989, pp. 69–72, ISBN: 978-94-017-0849-4. DOI: 10.1007/978-94-017-0849-4_10 (cit. on pp. 14, 35).

[6] J. S. Bell, "On the Einstein Podolsky Rosen paradox", *Physics Physique Fizika*, vol. 1, no. 3, pp. 195–200, Nov. 1964. DOI: 10.1103/PhysicsPhysiqueFizika.1.195 (cit. on p. 14).

[7] A. Aspect, "Proposed experiment to test the nonseparability of quantum mechanics", *Physical Review D*, vol. 14, pp. 1944–1951, Oct. 1976, ISSN: 1550-79980556-2821. DOI: 10.1103/PhysRevD.14.1944 (cit. on p. 14).

[8] A. Aspect, P. Grangier, and G. Roger, "Experimental Tests of Realistic Local Theories via Bell's Theorem", *Physical Review Letters*, vol. 47, pp. 460–463, Aug. 1981, ISSN: 0031-9007. DOI: 10.1103/PhysRevLett.47.460 (cit. on p. 14).

[9]   G. C. Ghirardi, A. Rimini, and T. Weber, "A general argument against superluminal transmission through the quantum mechanical measurement process", en, *Lett. Nuovo Cimento*, vol. 27, no. 10, pp. 293–298, Mar. 1980, ISSN: 1827-613X. DOI: 10.1007/BF02817189 (cit. on p. 14).

[10] O. Gühne and G. Toth, "Entanglement detection", *Physics Reports*, vol. 474, no. 1, pp. 1–75, 2009, ISSN: 0370-1573. DOI: https://doi.org/10.1016/j.physrep.2009.02.004 (cit. on pp. 14, 40, 73).

[11] A. Nourmandipour, A. Vafafard, A. Mortezapour, and R. Franzosi, "Entanglement protection of classically driven qubits in a lossy cavity", *Scientific Reports*, vol. 11, no. 1, p. 16 259, Aug. 2021. DOI: 10.1038/s41598-021-95623-1 (cit. on pp. 14, 73).

[12] A. Vafafard, A. Nourmandipour, and R. Franzosi, "Multipartite stationary entanglement generation in the presence of dipole-dipole interaction in an optical cavity", *Phys. Rev. A*, vol. 105, no. 5, p. 052 439, May 2022. DOI: 10.1103/PhysRevA.105.052439 (cit. on pp. 14, 73).

[13] R. Horodecki, P. Horodecki, M. Horodecki, and K. Horodecki, "Quantum entanglement", *Rev. Mod. Phys.*, vol. 81, no. 2, pp. 865–942, Jun. 2009. DOI: 10.1103/RevModPhys.81.865 (cit. on pp. 14, 40, 73).

[14] J. Sperling and I. A. Walmsley, "Entanglement in macroscopic systems", *Phys. Rev. A*, vol. 95, no. 6, p. 062 116, Jun. 2017. DOI: 10.1103/PhysRevA.95.062116 (cit. on p. 14).

[15] V. Giovannetti, S. Mancini, D. Vitali, and P. Tombesi, "Characterizing the entanglement of bipartite quantum systems", *Phys. Rev. A*, vol. 67, no. 2, p. 022 320, Feb. 2003. DOI: 10.1103/PhysRevA.67.022320 (cit. on p. 14).

[16] S. Popescu and D. Rohrlich, "Thermodynamics and the measure of entanglement", *Phys. Rev. A*, vol. 56, no. 5, R3319–R3321, Nov. 1997. DOI: 10.1103/PhysRevA.56.R3319 (cit. on p. 15).

[17] M. B. Plenio and S. S. Virmani, "An Introduction to Entanglement Theory", en, *Quantum Information and Coherence*, E. Andersson and P. Öhberg, Eds., Cham: Springer International Publishing, 2014, pp. 173–209, ISBN: 978-3-319-04062-2 978-3-319-04063-9. DOI: 10.1007/978-3-319-04063-9_8 (cit. on pp. 15, 25, 26).

[18] W. K. Wootters, "Entanglement of formation of an arbitrary state of two qubits", *Phys. Rev. Lett.*, vol. 80, no. 10, pp. 2245–2248, Mar. 1998. DOI: 10.1103/PhysRevLett.80.2245 (cit. on pp. 15, 62).

[19] C. H. Bennett, D. P. DiVincenzo, J. A. Smolin, and W. K. Wootters, "Mixed-state entanglement and quantum error correction", *Phys. Rev. A*, vol. 54, no. 5, pp. 3824–3851, Nov. 1996. DOI: 10.1103/PhysRevA.54.3824 (cit. on pp. 15, 61).

[20] C. H. Bennett, G. Brassard, S. Popescu, B. Schumacher, J. A. Smolin, and W. K. Wootters, "Purification of noisy entanglement and faithful teleportation via noisy channels", *Phys. Rev. Lett.*, vol. 76, no. 5, pp. 722–725, Jan. 1996. DOI: 10.1103/PhysRevLett.76.722 (cit. on p. 15).

[21] M. Horodecki, P. Horodecki, and R. Horodecki, "Mixed-state entanglement and distillation: Is there a "Bound" entanglement in nature?", *Phys. Rev. Lett.*, vol. 80, no. 24, pp. 5239–5242, Jun. 1998. DOI: 10.1103/PhysRevLett.80.5239 (cit. on p. 15).

[22] V. Vedral, M. B. Plenio, M. A. Rippin, and P. L. Knight, "Quantifying entanglement", *Phys. Rev. Lett.*, vol. 78, no. 12, pp. 2275–2279, Mar. 1997. DOI: 10.1103/PhysRevLett.78.2275 (cit. on pp. 15, 26, 31).

[23] G. Adesso, T. R. Bromley, and M. Cianciaruso, "Measures and applications of quantum correlations", *Journal of Physics A: Mathematical and Theoretical*, vol. 49, no. 47, p. 473 001, Nov. 2016. DOI: 10.1088/1751-8113/49/47/473001 (cit. on pp. 15, 22, 26, 27, 55, 62, 66–68).

[24] W. Dür, G. Vidal, and J. I. Cirac, "Three qubits can be entangled in two inequivalent ways", *Phys. Rev. A*, vol. 62, no. 6, p. 062 314, Nov. 2000. DOI: 10.1103/PhysRevA.62.062314 (cit. on p. 15).

[25] H. J. Briegel and R. Raussendorf, "Persistent entanglement in arrays of interacting particles", *Phys. Rev. Lett.*, vol. 86, no. 5, pp. 910–913, Jan. 2001. DOI: 10.1103/PhysRevLett.86.910 (cit. on pp. 15, 35, 36, 40, 42, 47, 49, 70).

[26] J. Eisert and H. J. Briegel, "Schmidt measure as a tool for quantifying multiparticle entanglement", *Phys. Rev. A*, vol. 64, no. 2, p. 022 306, Jul. 2001. DOI: 10.1103/PhysRevA.64.022306 (cit. on p. 15).

[27] V. Coffman, J. Kundu, and W. K. Wootters, "Distributed entanglement", *Phys. Rev. A*, vol. 61, no. 5, p. 052 306, Apr. 2000. DOI: 10.1103/PhysRevA.61.052306 (cit. on p. 15).

[28] A. R. R. Carvalho, F. Mintert, and A. Buchleitner, "Decoherence and multipartite entanglement", *Phys. Rev. Lett.*, vol. 93, no. 23, p. 230 501, Dec. 2004. DOI: 10.1103/PhysRevLett.93.230501 (cit. on p. 15).

[29] S. L. Braunstein and C. M. Caves, "Statistical distance and the geometry of quantum states", *Phys. Rev. Lett.*, vol. 72, no. 22, pp. 3439–3443, May 1994. DOI: 10.1103/PhysRevLett.72.3439 (cit. on p. 15).

[30] L. Pezzé and A. Smerzi, "Entanglement, nonlinear dynamics, and the heisenberg limit", *Phys. Rev. Lett.*, vol. 102, no. 10, p. 100 401, Mar. 2009. DOI: 10.1103/PhysRevLett.102.100401 (cit. on p. 15).

[31] P. Hyllus, W. Laskowski, R. Krischek, *et al.*, "Fisher information and multiparticle entanglement", *Phys. Rev. A*, vol. 85, no. 2, p. 022 321, Feb. 2012. DOI: 10.1103/PhysRevA.85.022321 (cit. on p. 15).

[32]   G. Tóth, "Multipartite entanglement and high-precision metrology", *Phys. Rev. A*, vol. 85, no. 2, p. 022 322, Feb. 2012. DOI: `10.1103/PhysRevA.85.022322` (cit. on p. 15).

[33]   S. Scali and R. Franzosi, "Entanglement estimation in non-optimal qubit states", *Annals of Physics*, vol. 411, p. 167 995, 2019, ISSN: 0003-4916. DOI: `https://doi.org/10.1016/j.aop.2019.167995` (cit. on p. 15).

[34]   A. Vesperini, G. Bel-Hadj-Aissa, and R. Franzosi, "Entanglement and quantum correlation measures for quantum multipartite mixed states", *Scientific Reports*, vol. 13, no. 1, p. 2852, Feb. 2023. DOI: `10.1038/s41598-023-29438-7` (cit. on pp. 15, 53, 73, 82).

[35]   A. Vesperini, G. Bel-Hadj-Aissa, L. Capra, and R. Franzosi, *Unveiling the geometric meaning of quantum entanglement*, Jul. 2023. DOI: `10.48550/arXiv.2307.16835` (cit. on pp. 15, 28, 32, 73).

[36]   A. Vesperini, "Correlations and projective measurements in maximally entangled multipartite states", *Annals of Physics*, p. 169 406, 2023, ISSN: 0003-4916. DOI: `https://doi.org/10.1016/j.aop.2023.169406` (cit. on pp. 15, 28, 40).

[37]   A. Vesperini and R. Franzosi, *Entanglement, quantum correlators and connectivity in graph states*, Aug. 2023. DOI: `10.48550/arXiv.2308.07690` (cit. on pp. 15, 70).

[38]   A. Vesperini, M. Cini, and R. Franzosi, "Entanglement signature of the Superradiant Quantum Phase Transition", Manuscript in preparation (cit. on pp. 15, 85).

[39]   P. S. LaPlace, *Essai philosophique sur les probabilités*, fre. Paris: Courcier, 1814 (cit. on p. 16).

[40]   D. Hanneke, J. P. Home, J. D. Jost, J. M. Amini, D. Leibfried, and D. J. Wineland, "Realization of a programmable two-qubit quantum processor", en, *Nature Phys*, vol. 6, no. 1, pp. 13–16, Jan. 2010, ISSN: 1745-2473, 1745-2481. DOI: `10.1038/nphys1453` (cit. on p. 17).

[41]   J. Koch, T. M. Yu, J. Gambetta, *et al.*, "Charge-insensitive qubit design derived from the Cooper pair box", en, *Phys. Rev. A*, vol. 76, no. 4, p. 042 319, Oct. 2007, ISSN: 1050-2947, 1094-1622. DOI: `10.1103/PhysRevA.76.042319` (cit. on p. 17).

[42]   Y. Nakamura, Y. A. Pashkin, and J. S. Tsai, "Coherent control of macroscopic quantum states in a single-Cooper-pair box", en, *Nature*, vol. 398, no. 6730, pp. 786–788, Apr. 1999, ISSN: 0028-0836, 1476-4687. DOI: `10.1038/19718` (cit. on p. 17).

[43]   T. E. Roth, R. Ma, and W. C. Chew, *An Introduction to the Transmon Qubit for Electromagnetic Engineers*, en, Jun. 2021 (cit. on p. 17).

[44] D. E. Bernal, S. Tayur, and D. Venturelli, *Quantum Integer Programming (QuIP) 47-779: Lecture Notes*, en, Jan. 2021 (cit. on p. 17).

[45] B. Aaronson, R. Lo Franco, and G. Adesso, "Comparative investigation of the freezing phenomena for quantum correlations under nondissipative decoherence", *Phys. Rev. A*, vol. 88, no. 1, p. 012 120, Jul. 2013. DOI: 10.1103/PhysRevA.88.012120 (cit. on pp. 17, 20, 58, 59, 157, 159).

[46] D. A. Meyer and N. R. Wallach, "Global entanglement in multiparticle systems", *Journal of Mathematical Physics*, vol. 43, no. 9, pp. 4273–4278, Aug. 2002, ISSN: 0022-2488. DOI: 10.1063/1.1497700 (cit. on p. 18).

[47] G. K. Brennen, "An observable measure of entanglement for pure states of multi-qubit systems", *Quantum Info. Comput.*, vol. 3, no. 6, pp. 619–626, Nov. 2003, ISSN: 1533-7146 (cit. on p. 18).

[48] J. Řeháček, Z. Hradil, and M. Ježek, "Iterative algorithm for reconstruction of entangled states", en, *Phys. Rev. A*, vol. 63, no. 4, p. 040 303, Mar. 2001, ISSN: 1050-2947, 1094-1622. DOI: 10.1103/PhysRevA.63.040303 (cit. on p. 20).

[49] Z. Hradil, J. Řeháček, J. Fiurášek, and M. Ježek, "3 Maximum-Likelihood Methodsin Quantum Mechanics", *Quantum State Estimation*, M. Paris and J. Řeháček, Eds., vol. 649, Berlin, Heidelberg: Springer Berlin Heidelberg, Aug. 2004, pp. 59–112, ISBN: 978-3-540-22329-0 978-3-540-44481-7. DOI: 10.1007/978-3-540-44481-7_3 (cit. on p. 20).

[50] R. Blume-Kohout, "Optimal, reliable estimation of quantum states", en, p. 26, (cit. on p. 20).

[51] K. Banaszek, G. M. D'Ariano, M. G. A. Paris, and M. F. Sacchi, "Maximum-likelihood estimation of the density matrix", en, *PHYSICAL REVIEW A*, p. 4, (cit. on p. 20).

[52] R. Horodecki and M. Horodecki, "Information-theoretic aspects of inseparability of mixed states", *Phys. Rev. A*, vol. 54, no. 3, pp. 1838–1843, Sep. 1996. DOI: 10.1103/PhysRevA.54.1838 (cit. on pp. 20, 33, 58, 59, 61).

[53] H. Ollivier and W. H. Zurek, "Quantum Discord: A Measure of the Quantumness of Correlations", *Phys. Rev. Lett.*, vol. 88, no. 1, p. 017 901, Dec. 2001. DOI: 10.1103/PhysRevLett.88.017901 (cit. on p. 22).

[54] G. Vidal, "Entanglement monotones", *Journal of Modern Optics*, vol. 47, no. 2-3, pp. 355–376, Feb. 2000, ISSN: 1362-3044. DOI: 10.1080/09500340008244048 (cit. on pp. 25, 26).

[55] L. Gurvits, "Classical deterministic complexity of Edmonds' Problem and quantum entanglement", en, *Proceedings of the thirty-fifth annual ACM symposium on Theory of computing*, San Diego CA USA: ACM, Jun. 2003, pp. 10–19, ISBN: 978-1-58113-674-6. DOI: 10.1145/780542.780545 (cit. on p. 25).

[56] D. Cocchiarella, S. Scali, S. Ribisi, B. Nardi, G. Bel-Hadj-Aissa, and R. Franzosi, "Entanglement distance for arbitrary M-qudit hybrid systems", *Phys. Rev. A*, vol. 101, no. 4, p. 042 129, Apr. 2020. DOI: `10.1103/PhysRevA.101.042129` (cit. on pp. 28, 30, 47, 73).

[57] G. Gibbons, "Typical states and density matrices", *Journal of Geometry and Physics*, vol. 8, no. 1, pp. 147–162, 1992, ISSN: 0393-0440. DOI: `10.1016/0393-0440(92)90046-4` (cit. on p. 29).

[58] J. P. Provost and G. Vallee, "Riemannian structure on manifolds of quantum states", *Communications in Mathematical Physics*, vol. 76, no. 3, pp. 289–301, Sep. 1980. DOI: `10.1007/BF02193559` (cit. on p. 29).

[59] N. Yu, "Separability of a mixture of Dicke states", en, *Phys. Rev. A*, vol. 94, no. 6, p. 060 101, Dec. 2016, ISSN: 2469-9926, 2469-9934. DOI: `10.1103/PhysRevA.94.060101` (cit. on pp. 33, 100).

[60] M. Horodecki, P. Horodecki, and R. Horodecki, "Separability of mixed states: Necessary and sufficient conditions", *Physics Letters A*, vol. 223, no. 1, pp. 1–8, 1996, ISSN: 0375-9601. DOI: `https://doi.org/10.1016/S0375-9601(96)00706-2` (cit. on pp. 33, 60–63).

[61] A. Monras, G. Adesso, S. M. Giampaolo, G. Gualdi, G. B. Davies, and F. Illuminati, "Entanglement quantification by local unitary operations", *Phys. Rev. A*, vol. 84, no. 1, p. 012 301, Jul. 2011. DOI: `10.1103/PhysRevA.84.012301` (cit. on p. 34).

[62] W. K. Wootters, "Entanglement of formation and concurrence", *Quantum Info. Comput.*, vol. 1, no. 1, pp. 27–44, Jan. 2001, ISSN: 1533-7146 (cit. on p. 34).

[63] M. A. Nielsen, "Cluster-state quantum computation", en, *Reports on Mathematical Physics*, vol. 57, no. 1, pp. 147–161, Feb. 2006, ISSN: 00344877. DOI: `10.1016/S0034-4877(06)80014-5` (cit. on pp. 40, 47, 70–72).

[64] R. Raussendorf and H. J. Briegel, "A one-way quantum computer", *Phys. Rev. Lett.*, vol. 86, no. 22, pp. 5188–5191, May 2001. DOI: `10.1103/PhysRevLett.86.5188` (cit. on pp. 40, 47).

[65] R. Raussendorf, D. E. Browne, and H. J. Briegel, "Measurement-based quantum computation on cluster states", *Phys. Rev. A*, vol. 68, no. 2, p. 022 312, Aug. 2003. DOI: `10.1103/PhysRevA.68.022312` (cit. on pp. 40, 47).

[66] M. A. Nielsen, "Quantum computation by measurement and quantum memory", *Physics Letters A*, vol. 308, no. 2-3, pp. 96–100, Feb. 2003. DOI: `10.1016/s0375-9601(02)01803-0` (cit. on p. 47).

[67] Adán Cabello, "Supersinglets", *Journal of Modern Optics*, vol. 50, no. 6-7, pp. 1049–1061, 2003. DOI: `10.1080/09500340308234551` (cit. on p. 49).

[68]   A. Cabello, "Six-qubit permutation-based decoherence-free orthogonal basis", *Phys. Rev. A*, vol. 75, no. 2, p. 020 301, Feb. 2007. DOI: `10.1103/PhysRevA.75.020301` (cit. on p. 49).

[69]   M. D. Lang and C. M. Caves, "Quantum Discord and the Geometry of Bell-Diagonal States", en, *Phys. Rev. Lett.*, vol. 105, no. 15, p. 150 501, Oct. 2010, ISSN: 0031-9007, 1079-7114. DOI: `10.1103/PhysRevLett.105.150501` (cit. on pp. 59, 159).

[70]   B. Dakić, V. Vedral, and Č. Brukner, "Necessary and Sufficient Condition for Nonzero Quantum Discord", en, *Phys. Rev. Lett.*, vol. 105, no. 19, p. 190 502, Nov. 2010, ISSN: 0031-9007, 1079-7114. DOI: `10.1103/PhysRevLett.105.190502` (cit. on pp. 59, 159).

[71]   A. Peres, "Separability criterion for density matrices", *Phys. Rev. Lett.*, vol. 77, no. 8, pp. 1413–1415, Aug. 1996. DOI: `10.1103/PhysRevLett.77.1413` (cit. on pp. 60–63).

[72]   R. F. Werner, "Quantum states with Einstein-Podolsky-Rosen correlations admitting a hidden-variable model", *Phys. Rev. A*, vol. 40, no. 8, pp. 4277–4281, Oct. 1989. DOI: `10.1103/PhysRevA.40.4277` (cit. on p. 61).

[73]   A. O. Pittenger and M. H. Rubin, "Note on separability of the Werner states in arbitrary dimensions1This work was supported in part by the National Security Agency.1", *Optics Communications*, vol. 179, no. 1, pp. 447–449, May 2000, ISSN: 0030-4018. DOI: `10.1016/S0030-4018(00)00612-X` (cit. on p. 63).

[74]   W. Dür and J. I. Cirac, "Classification of multiqubit mixed states: Separability and distillability properties", *Phys. Rev. A*, vol. 61, no. 4, p. 042 314, Mar. 2000. DOI: `10.1103/PhysRevA.61.042314` (cit. on p. 63).

[75]   C. Eltschka and J. Siewert, "Entanglement of Three-Qubit Greenberger-Horne-Zeilinger–Symmetric States", *Phys. Rev. Lett.*, vol. 108, no. 2, p. 020 502, Jan. 2012. DOI: `10.1103/PhysRevLett.108.020502` (cit. on p. 63).

[76]   R. Schack and C. M. Caves, "Explicit product ensembles for separable quantum states", en, *Journal of Modern Optics*, vol. 47, no. 2-3, pp. 387–399, Feb. 2000, ISSN: 0950-0340, 1362-3044. DOI: `10.1080/09500340008244050` (cit. on p. 63).

[77]   O. Gühne and M. Seevinck, "Separability criteria for genuine multiparticle entanglement", en, *New J. Phys.*, vol. 12, no. 5, p. 053 002, May 2010, ISSN: 1367-2630. DOI: `10.1088/1367-2630/12/5/053002` (cit. on p. 63).

[78]   M. Ozawa, "Entanglement measures and the Hilbert-Schmidt distance", en, *Physics Letters A*, vol. 268, no. 3, pp. 158–160, Apr. 2000, ISSN: 03759601. DOI: `10.1016/S0375-9601(00)00171-7` (cit. on pp. 66, 67).

[79] L. Chang and S. Luo, "Remedying the local ancilla problem with geometric discord", en, *Phys. Rev. A*, vol. 87, no. 6, p. 062 303, Jun. 2013, ISSN: 1050-2947, 1094-1622. DOI: 10.1103/PhysRevA.87.062303 (cit. on pp. 66–68).

[80] M. Piani, "Problem with geometric discord", en, *Phys. Rev. A*, vol. 86, no. 3, p. 034 101, Sep. 2012, ISSN: 1050-2947, 1094-1622. DOI: 10.1103/PhysRevA.86.034101 (cit. on pp. 66, 67).

[81] X. Hu, H. Fan, D. L. Zhou, and W.-M. Liu, "Quantum correlating power of local quantum channels", en, *Phys. Rev. A*, vol. 87, no. 3, p. 032 340, Mar. 2013, ISSN: 1050-2947, 1094-1622. DOI: 10.1103/PhysRevA.87.032340 (cit. on p. 67).

[82] E. P. Wigner and M. M. Yanase, "INFORMATION CONTENTS OF DISTRIBUTIONS", en, *Proc. Natl. Acad. Sci. U.S.A.*, vol. 49, no. 6, pp. 910–918, Jun. 1963, ISSN: 0027-8424, 1091-6490. DOI: 10.1073/pnas.49.6.910 (cit. on p. 67).

[83] M. Hein, J. Eisert, and H. J. Briegel, "Multi-party entanglement in graph states", en, *Phys. Rev. A*, vol. 69, no. 6, p. 062 311, Jun. 2004, ISSN: 1050-2947, 1094-1622. DOI: 10.1103/PhysRevA.69.062311 (cit. on p. 70).

[84] M. Hein, W. Dür, J. Eisert, R. Raussendorf, M. V. d. Nest, and H.-J. Briegel, "Entanglement in Graph States and its Applications", en, *arXiv:quant-ph/0602096*, Feb. 2006 (cit. on pp. 70, 71, 80).

[85] R. Raussendorf and T.-C. Wei, "Quantum computation by local measurement", en, *Annu. Rev. Condens. Matter Phys.*, vol. 3, no. 1, pp. 239–261, Mar. 2012, ISSN: 1947-5454, 1947-5462. DOI: 10.1146/annurev-conmatphys-020911-125041 (cit. on p. 70).

[86] K. P. Gnatenko and N. A. Susulovska, "Geometric measure of entanglement of multi-qubit graph states and its detection on a quantum computer", en, *EPL*, vol. 136, no. 4, p. 40 003, Mar. 2022, ISSN: 0295-5075. DOI: 10.1209/0295-5075/ac419b (cit. on pp. 71, 76).

[87] K. P. Gnatenko and V. M. Tkachuk, "Entanglement of graph states of spin system with Ising interaction and its quantifying on IBM's quantum computer", *Physics Letters A*, vol. 396, p. 127 248, Apr. 2021, ISSN: 0375-9601. DOI: 10.1016/j.physleta.2021.127248 (cit. on pp. 71, 76).

[88] M. A. Nielsen and I. L. Chuang, *Quantum computation and quantum information: 10th anniversary edition*. Cambridge: Cambridge University Press, 2010. DOI: 10.1017/CBO9780511976667 (cit. on p. 72).

[89] J.-Y. Gyhm, D. Šafránek, and D. Rosa, "Quantum Charging Advantage Cannot Be Extensive Without Global Operations", en, *Phys. Rev. Lett.*, vol. 128, no. 14, p. 140 501, Apr. 2022, ISSN: 0031-9007, 1079-7114. DOI: 10.1103/PhysRevLett.128.140501 (cit. on p. 85).

[90] R. Alicki and M. Fannes, "Entanglement boost for extractable work from ensembles of quantum batteries", en, *Phys. Rev. E*, vol. 87, no. 4, p. 042 123, Apr. 2013, ISSN: 1539-3755, 1550-2376. DOI: 10.1103/PhysRevE.87.042123 (cit. on p. 85).

[91] F. C. Binder, S. Vinjanampathy, K. Modi, and J. Goold, "Quantacell: Powerful charging of quantum batteries", en, *New J. Phys.*, vol. 17, no. 7, p. 075 015, Jul. 2015, ISSN: 1367-2630. DOI: 10.1088/1367-2630/17/7/075015 (cit. on p. 85).

[92] F. Campaioli, F. A. Pollock, F. C. Binder, *et al.*, "Enhancing the Charging Power of Quantum Batteries", en, *Phys. Rev. Lett.*, vol. 118, no. 15, p. 150 601, Apr. 2017, ISSN: 0031-9007, 1079-7114. DOI: 10.1103/PhysRevLett.118.150601 (cit. on p. 85).

[93] S. Seah, M. Perarnau-Llobet, G. Haack, N. Brunner, and S. Nimmrichter, "Quantum speed-up in collisional battery charging", en, *Phys. Rev. Lett.*, vol. 127, no. 10, p. 100 601, Aug. 2021, ISSN: 0031-9007, 1079-7114. DOI: 10.1103/PhysRevLett.127.100601 (cit. on p. 85).

[94] V. Shaghaghi, V. Singh, G. Benenti, and D. Rosa, "Micromasers as Quantum Batteries", en, *Quantum Sci. Technol.*, vol. 7, no. 4, 04LT01, Oct. 2022, ISSN: 2058-9565. DOI: 10.1088/2058-9565/ac8829 (cit. on p. 85).

[95] V. Shaghaghi, V. Singh, M. Carrega, D. Rosa, and G. Benenti, "Lossy Micromaser Battery: Almost Pure States in the Jaynes–Cummings Regime", en, *Entropy*, vol. 25, no. 3, p. 430, Feb. 2023, ISSN: 1099-4300. DOI: 10.3390/e25030430 (cit. on p. 85).

[96] D. Ferraro, M. Campisi, G. M. Andolina, V. Pellegrini, and M. Polini, "High-Power Collective Charging of a Solid-State Quantum Battery", en, *Phys. Rev. Lett.*, vol. 120, no. 11, p. 117 702, Mar. 2018, ISSN: 0031-9007, 1079-7114. DOI: 10.1103/PhysRevLett.120.117702 (cit. on p. 85).

[97] I. I. Rabi, "On the process of space quantization", *Phys. Rev.*, vol. 49, no. 4, pp. 324–328, Feb. 1936. DOI: 10.1103/PhysRev.49.324 (cit. on p. 86).

[98] D. Braak, "Integrability of the rabi model", *Phys. Rev. Lett.*, vol. 107, no. 10, p. 100 401, Aug. 2011. DOI: 10.1103/PhysRevLett.107.100401 (cit. on p. 86).

[99] V. Penna, F. A. Raffa, and R. Franzosi, "Algebraic properties and spectral collapse in nonlinear quantum Rabi models", *J. Phys. A: Math. Theor.*, vol. 51, no. 4, p. 045 301, Jan. 2018, ISSN: 1751-8113, 1751-8121. DOI: 10.1088/1751-8121/aa9da6 (cit. on p. 86).

[100] V. Penna and F. A. Raffa, "Off-resonance regimes in nonlinear quantum Rabi models", en, *Phys. Rev. A*, vol. 93, no. 4, p. 043 814, Apr. 2016, ISSN: 2469-9926, 2469-9934. DOI: 10.1103/PhysRevA.93.043814 (cit. on p. 86).

[101] M.-J. Hwang, R. Puebla, and M. B. Plenio, "Quantum phase transition and universal dynamics in the rabi model", *Phys. Rev. Lett.*, vol. 115, no. 18, p. 180 404, Oct. 2015. DOI: `10.1103/PhysRevLett.115.180404` (cit. on p. 86).

[102] K. Hepp and E. H. Lieb, "On the superradiant phase transition for molecules in a quantized radiation field: The dicke maser model", *Annals of Physics*, vol. 76, no. 2, pp. 360–404, 1973, ISSN: 0003-4916. DOI: `https://doi.org/10.1016/0003-4916(73)90039-0` (cit. on p. 86).

[103] E. Jaynes and F. Cummings, "Comparison of quantum and semiclassical radiation theories with application to the beam maser", *Proceedings of the IEEE*, vol. 51, no. 1, pp. 89–109, 1963. DOI: `10.1109/PROC.1963.1664` (cit. on p. 86).

[104] A. Retzker, E. Solano, and B. Reznik, "Tavis-Cummings model and collective multiqubit entanglement in trapped ions", *Phys. Rev. A*, vol. 75, no. 2, p. 022 312, Feb. 2007. DOI: `10.1103/PhysRevA.75.022312` (cit. on p. 86).

[105] M. Feng, Y. P. Zhong, T. Liu, *et al.*, "Exploring the quantum critical behaviour in a driven Tavis–Cummings circuit", *Nature Communications*, vol. 6, no. 1, p. 7111, May 2015, ISSN: 2041-1723. DOI: `10.1038/ncomms8111` (cit. on p. 86).

[106] J. Larson, "Dynamics of the Jaynes–Cummings and Rabi models: Old wine in new bottles", *Physica Scripta*, vol. 76, no. 2, pp. 146–160, Jul. 2007. DOI: `10.1088/0031-8949/76/2/007` (cit. on p. 86).

[107] A. Ghoshal, S. Das, A. Sen(De), and U. Sen, "Population inversion and entanglement in single and double glassy Jaynes-Cummings models", *Phys. Rev. A*, vol. 101, no. 5, p. 053 805, May 2020. DOI: `10.1103/PhysRevA.101.053805` (cit. on p. 86).

[108] J.-F. Huang, J.-Q. Liao, and L.-M. Kuang, "Ultrastrong jaynes-cummings model", *Phys. Rev. A*, vol. 101, no. 4, p. 043 835, Apr. 2020. DOI: `10.1103/PhysRevA.101.043835` (cit. on p. 86).

[109] K. Fischer, S. Sun, D. Lukin, Y. Kelaita, R. Trivedi, and J. Vŭcčković, "Pulsed coherent drive in the Jaynes-Cummings model", *Phys. Rev. A*, vol. 98, no. 2, p. 021 802, Aug. 2018. DOI: `10.1103/PhysRevA.98.021802` (cit. on p. 86).

[110] M.-J. Hwang and M. B. Plenio, "Quantum phase transition in the finite jaynes-cummings lattice systems", *Phys. Rev. Lett.*, vol. 117, no. 12, p. 123 602, Sep. 2016. DOI: `10.1103/PhysRevLett.117.123602` (cit. on p. 86).

[111] M. Tavis and F. W. Cummings, "Exact solution for an N-Molecule—Radiation-Field hamiltonian", *Phys. Rev.*, vol. 170, no. 2, pp. 379–384, Jun. 1968. DOI: `10.1103/PhysRev.170.379` (cit. on p. 86).

[112]   I. D. Leroux, M. H. Schleier-Smith, and V. Vuletić, "Implementation of cavity squeezing of a collective atomic spin", *Phys. Rev. Lett.*, vol. 104, no. 7, p. 073 602, Feb. 2010. DOI: 10.1103/PhysRevLett.104.073602 (cit. on p. 86).

[113]   A. Vesperini, "Dynamics and thermodynamics of the HMF model with additional short-range interactions", SISSA, Trieste, Master thesis, Jun. 2020 (cit. on pp. 107, 108, 119).

[114]   A. Vesperini, R. Franzosi, S. Ruffo, A. Trombettoni, and X. Leoncini, "Fast collective oscillations and clustering phenomena in an antiferromagnetic mean-field model", *Chaos, Solitons & Fractals*, vol. 153, p. 111 487, Dec. 2021, ISSN: 0960-0779. DOI: 10.1016/j.chaos.2021.111487 (cit. on p. 108).

[115]   A. Campa, T. Dauxois, and S. Ruffo, "Statistical mechanics and dynamics of solvable models with long-range interactions", en, *Physics Reports*, vol. 480, no. 3-6, pp. 57–159, Sep. 2009, ISSN: 03701573. DOI: 10.1016/j.physrep.2009.07.001 (cit. on pp. 108, 110).

[116]   M. Antoni and S. Ruffo, "Clustering and relaxation in Hamiltonian long-range dynamics", en, *Phys. Rev. E*, vol. 52, no. 3, pp. 2361–2374, Sep. 1995, ISSN: 1063-651X, 1095-3787. DOI: 10.1103/PhysRevE.52.2361 (cit. on pp. 108–110, 112, 116).

[117]   J. Barre, F. Bouchet, T. Dauxois, and S. Ruffo, "Birth and long-time stabilization of out-of-equilibrium coherent structures", en, *The European Physical Journal B - Condensed Matter*, vol. 29, no. 4, pp. 577–591, Oct. 2002, ISSN: 1434-6028, 1434-6036. DOI: 10.1140/epjb/e2002-00342-3 (cit. on pp. 108–111, 113, 116).

[118]   J. Barré, F. Bouchet, T. Dauxois, and S. Ruffo, "Out-of-Equilibrium States as Statistical Equilibria of an Effective Dynamics in a System with Long-Range Interactions", en, *Phys. Rev. Lett.*, vol. 89, no. 11, p. 110 601, Aug. 2002, ISSN: 0031-9007, 1079-7114. DOI: 10.1103/PhysRevLett.89.110601 (cit. on pp. 108, 109, 136).

[119]   A. Campa, A. Giansanti, D. Mukamel, and S. Ruffo, "Dynamics and thermodynamics of rotators interacting with both long- and short-range couplings", en, *Physica A: Statistical Mechanics and its Applications*, vol. 365, no. 1, pp. 120–127, Jun. 2006, ISSN: 03784371. DOI: 10.1016/j.physa.2006.01.003 (cit. on p. 108).

[120]   T. Dauxois, V. Latora, A. Rapisarda, S. Ruffo, and A. Torcini, "The Hamiltonian Mean Field Model: From Dynamics to Statistical Mechanics and back", en, *arXiv:cond-mat/0208456*, Aug. 2002 (cit. on p. 108).

[121] T. Dauxois, P. Holdsworth, and S. Ruffo, "Violation of ensemble equivalence in the antiferromagnetic mean-field XY model", en, *Eur. Phys. J. B*, vol. 16, no. 4, pp. 659–667, Aug. 2000, ISSN: 1434-6028. DOI: 10.1007/s100510070183 (cit. on pp. 108–110, 116).

[122] D. Jeong, J. Choi, and M. Y. Choi, "Collective oscillations, bicluster motion, and dynamical order in a system of globally coupled rotors with repulsive interactions", eng, *Phys Rev E Stat Nonlin Soft Matter Phys*, vol. 74, no. 5 Pt 2, p. 056 106, Nov. 2006, ISSN: 1539-3755. DOI: 10.1103/PhysRevE.74.056106 (cit. on pp. 108–111, 116).

[123] X. Leoncini, T. L. V. D. Berg, and D. Fanelli, "Out of Equilibrium Solutions in the XY-Hamiltonian Mean Field model", en, *Europhys. Lett.*, vol. 86, no. 2, p. 20 002, Apr. 2009, ISSN: 0295-5075, 1286-4854. DOI: 10.1209/0295-5075/86/20002 (cit. on p. 108).

[124] Y. Y. Yamaguchi, J. Barr'e, F. Bouchet, T. Dauxois, and S. Ruffo, "Stability criteria of the Vlasov equation and quasi-stationary states of the HMF model", en, *Physica A: Statistical Mechanics and its Applications*, vol. 337, no. 1-2, pp. 36–66, Jun. 2004, ISSN: 03784371. DOI: 10.1016/j.physa.2004.01.041 (cit. on p. 108).

[125] J. Dawson, "One-Dimensional Plasma Model", *The Physics of Fluids*, vol. 5, no. 4, pp. 445–459, 1962. DOI: 10.1063/1.1706638 (cit. on p. 108).

[126] O. C. Eldridge and M. Feix, "One-Dimensional Plasma Model at Thermodynamic Equilibrium", *The Physics of Fluids*, vol. 5, no. 9, pp. 1076–1080, 1962. DOI: 10.1063/1.1724476 (cit. on p. 108).

[127] X. Leoncini, "Self-organized regularity in long-range systems", *Nonlinear Dynamics New Directions*, ser. Nonlinear Systems and Complexity, E. Ugalde and H. Gonzales-Aguilar, Eds., vol. 12, Springer, 2015, pp. 79–109. DOI: 10.1007/978-3-319-09864-7 (cit. on p. 108).

[128] A. Turchi, D. Fanelli, and X. Leoncini, "Emergence of a collective crystal in a classical system with long-range interactions", en, *EPL*, vol. 111, no. 3, p. 30 011, Aug. 2015, ISSN: 0295-5075, 1286-4854. DOI: 10.1209/0295-5075/111/30011 (cit. on p. 108).

[129] S. De Nigris and X. Leoncini, "Emergence of a non trivial fluctuating phase in the XY model on regular networks", en, *EPL*, vol. 101, no. 1, p. 10 002, Jan. 2013, ISSN: 0295-5075, 1286-4854. DOI: 10.1209/0295-5075/101/10002 (cit. on p. 108).

[130] R. Plestid, P. Mahon, and D. H. J. O'Dell, "Violent relaxation in quantum fluids with long-range interactions", *Phys. Rev. E*, vol. 98, no. 1, p. 012 112, Jul. 2018. DOI: 10.1103/PhysRevE.98.012112 (cit. on p. 108).

[131] G. B. Whitham, *Linear and Nonlinear Waves*, en. John Wiley & Sons, Oct. 2011, ISBN: 978-1-118-03120-9 (cit. on p. 110).

[132] G. Schmidt, "II - Motion of Charged Particles in Electromagnetic Fields", *Physics of High Temperature Plasmas (Second Edition)*, G. Schmidt, Ed., Second Edition, Academic Press, 1979, pp. 5–54, ISBN: 978-0-12-626660-3. DOI: 10.1016/B978-0-12-626660-3.50006-7 (cit. on p. 113).

[133] L. D. Landau and E. M. Lifshitz, "Chapter V - Small oscillations", *Mechanics (Third Edition)*, L. D. Landau and E. M. Lifshitz, Eds., Third Edition, Oxford: Butterworth-Heinemann, 1976, pp. 58–95, ISBN: 978-0-7506-2896-9. DOI: 10.1016/B978-0-08-050347-9.50010-1 (cit. on p. 113).

[134] P. Kapitza, "Collected Papers of PL Kapitza, edited by D. ter Haar Pergamon", *Oxford*, vol. 1941, pp. 714, 726, 1965 (cit. on p. 113).

[135] R. I. McLachlan and P. Atela, "The accuracy of symplectic integrators", en, *Nonlinearity*, vol. 5, no. 2, pp. 541–562, Mar. 1992, ISSN: 0951-7715. DOI: 10.1088/0951-7715/5/2/011 (cit. on p. 115).

[136] S. Schütz, S. B. Jäger, and G. Morigi, "Dissipation-assisted prethermalization in long-range interacting atomic ensembles", en, *Phys. Rev. Lett.*, vol. 117, no. 8, p. 083 001, Aug. 2016, ISSN: 0031-9007, 1079-7114. DOI: 10.1103/PhysRevLett.117.083001 (cit. on p. 119).

[137] S. Schütz and G. Morigi, "Prethermalization of Atoms Due to Photon-Mediated Long-Range Interactions", en, *Phys. Rev. Lett.*, vol. 113, no. 20, p. 203 002, Nov. 2014, ISSN: 0031-9007, 1079-7114. DOI: 10.1103/PhysRevLett.113.203002 (cit. on p. 119).

[138] C. Angell, "Perspective on the glass transition", en, *Journal of Physics and Chemistry of Solids*, vol. 49, no. 8, pp. 863–871, Jan. 1988, ISSN: 00223697. DOI: 10.1016/0022-3697(88)90002-9 (cit. on p. 120).

[139] G. Parisi, "The physics of the glass transition", en, *Physica A: Statistical Mechanics and its Applications*, vol. 280, no. 1-2, pp. 115–124, May 2000, ISSN: 03784371. DOI: 10.1016/S0378-4371(99)00626-3 (cit. on p. 120).

[140] L. Angelani, R. Di Leonardo, G. Ruocco, A. Scala, and F. Sciortino, "Saddles in the Energy Landscape Probed by Supercooled Liquids", en, *Phys. Rev. Lett.*, vol. 85, no. 25, pp. 5356–5359, Dec. 2000, ISSN: 0031-9007, 1079-7114. DOI: 10.1103/PhysRevLett.85.5356 (cit. on p. 120).

[141] K. Broderix, K. K. Bhattacharya, A. Cavagna, A. Zippelius, and I. Giardina, "Energy Landscape of a Lennard-Jones Liquid: Statistics of Stationary Points", en, *Phys. Rev. Lett.*, vol. 85, no. 25, pp. 5360–5363, Dec. 2000, ISSN: 0031-9007, 1079-7114. DOI: 10.1103/PhysRevLett.85.5360 (cit. on p. 120).

[142] M. Morse, *The calculus of variations in the large* (Colloquium publications / American Mathematical Society 18), eng, Repr. Providence, R.I: American Mathematical Society, 2014, ISBN: 978-0-8218-1018-7 (cit. on p. 120).

[143] M. Gori, R. Franzosi, and M. Pettini, "Topological origin of phase transitions in the absence of critical points of the energy landscape", *J. Stat. Mech.*, vol. 2018, no. 9, p. 093 204, Sep. 2018, ISSN: 1742-5468. DOI: 10.1088/1742-5468/aad6b6 (cit. on p. 120).

[144] L. Di Cairano, M. Gori, and M. Pettini, "Topology and Phase Transitions: A First Analytical Step towards the Definition of Sufficient Conditions", en, *Entropy*, vol. 23, no. 11, p. 1414, Nov. 2021, ISSN: 1099-4300. DOI: 10.3390/e23111414 (cit. on p. 120).

[145] L. Di Cairano, M. Gori, G. Pettini, and M. Pettini, "Hamiltonian chaos and differential geometry of configuration space–time", en, *Physica D: Nonlinear Phenomena*, vol. 422, p. 132 909, Aug. 2021, ISSN: 01672789. DOI: 10.1016/j.physd.2021.132909 (cit. on p. 120).

[146] D. Coslovich and G. Pastore, "Dynamics and energy landscape in a tetrahedral network glass-former: Direct comparison with models of fragile liquids", en, *J. Phys.: Condens. Matter*, vol. 21, no. 28, p. 285 107, Jul. 2009, ISSN: 0953-8984, 1361-648X. DOI: 10.1088/0953-8984/21/28/285107 (cit. on pp. 121, 130).

[147] G. Bel-Hadj-Aissa, M. Gori, V. Penna, G. Pettini, and R. Franzosi, "Geometrical Aspects in the Analysis of Microcanonical Phase-Transitions", en, *Entropy*, vol. 22, no. 4, p. 380, Apr. 2020, ISSN: 1099-4300. DOI: 10.3390/e22040380 (cit. on pp. 122, 128).

[148] E. M. Pearson, T. Halicioglu, and W. A. Tiller, "Laplace-transform technique for deriving thermodynamic equations from the classical microcanonical ensemble", en, *Phys. Rev. A*, vol. 32, no. 5, pp. 3030–3039, Nov. 1985, ISSN: 0556-2791. DOI: 10.1103/PhysRevA.32.3030 (cit. on pp. 122, 126, 165).

[149] L. Di Cairano, R. Capelli, G. Bel-Hadj-Aissa, and M. Pettini, "Topological origin of the protein folding transition", *Phys. Rev. E*, vol. 106, no. 5, p. 054 134, Nov. 2022. DOI: 10.1103/PhysRevE.106.054134 (cit. on pp. 122, 123).

[150] G. Bel-Hadj-Aissa, M. Gori, R. Franzosi, and M. Pettini, "Geometrical and topological study of the Kosterlitz–Thouless phase transition in the XY model in two dimensions", *J. Stat. Mech.*, vol. 2021, no. 2, p. 023 206, Feb. 2021, ISSN: 1742-5468. DOI: 10.1088/1742-5468/abda27 (cit. on p. 123).

[151] T. S. Grigera and G. Parisi, "Fast Monte Carlo algorithm for supercooled soft spheres", en, *Phys. Rev. E*, vol. 63, no. 4, p. 045 102, Mar. 2001, ISSN: 1063-651X, 1095-3787. DOI: 10.1103/PhysRevE.63.045102 (cit. on pp. 126, 166).

[152] G. Pettini, M. Gori, R. Franzosi, C. Clementi, and M. Pettini, "On the origin of phase transitions in the absence of symmetry-breaking", en, *Physica A: Statistical Mechanics and its Applications*, vol. 516, pp. 376–392, Feb. 2019, ISSN: 03784371. DOI: 10.1016/j.physa.2018.10.001 (cit. on p. 128).

[153] S. Schnabel, D. T. Seaton, D. P. Landau, and M. Bachmann, "Microcanonical entropy inflection points: Key to systematic understanding of transitions in finite systems", en, *Phys. Rev. E*, vol. 84, no. 1, p. 011 127, Jul. 2011, ISSN: 1539-3755, 1550-2376. DOI: 10.1103/PhysRevE.84.011127 (cit. on p. 128).

[154] K. Qi and M. Bachmann, "Classification of Phase Transitions by Microcanonical Inflection-Point Analysis", en, *Phys. Rev. Lett.*, vol. 120, no. 18, p. 180 601, Apr. 2018, ISSN: 0031-9007, 1079-7114. DOI: 10.1103/PhysRevLett.120.180601 (cit. on pp. 128–130).

[155] P. J. Steinhardt, D. R. Nelson, and M. Ronchetti, "Bond-orientational order in liquids and glasses", en, *Phys. Rev. B*, vol. 28, no. 2, pp. 784–805, Jul. 1983, ISSN: 0163-1829. DOI: 10.1103/PhysRevB.28.784 (cit. on p. 130).

[156] J. R. Errington, P. G. Debenedetti, and S. Torquato, "Quantification of order in the Lennard-Jones system", en, *The Journal of Chemical Physics*, vol. 118, no. 5, pp. 2256–2263, Feb. 2003, ISSN: 0021-9606, 1089-7690. DOI: 10.1063/1.1532344 (cit. on p. 130).

[157] L.-C. Valdes, F. Affouard, M. Descamps, and J. Habasaki, "Mixing effects in glass-forming Lennard-Jones mixtures", en, *The Journal of Chemical Physics*, vol. 130, no. 15, p. 154 505, Apr. 2009, ISSN: 0021-9606, 1089-7690. DOI: 10.1063/1.3106759 (cit. on p. 130).

[158] T. M. Truskett, S. Torquato, and P. G. Debenedetti, "Towards a quantification of disorder in materials: Distinguishing equilibrium and glassy sphere packings", en, *Phys. Rev. E*, vol. 62, no. 1, pp. 993–1001, Jul. 2000, ISSN: 1063-651X, 1095-3787. DOI: 10.1103/PhysRevE.62.993 (cit. on p. 130).

[159] M. E. J. Newman and G. T. Barkema, *Monte Carlo methods in statistical physics*. Oxford : New York: Clarendon Press ; Oxford University Press, 1999, ISBN: 978-0-19-851796-2 978-0-19-851797-9 (cit. on p. 163).

[160] J. R. Ray, "Microcanonical ensemble Monte Carlo method", en, *Phys. Rev. A*, vol. 44, no. 6, pp. 4061–4064, Sep. 1991, ISSN: 1050-2947, 1094-1622. DOI: 10.1103/PhysRevA.44.4061 (cit. on p. 165).

[161] R. Lustig, "Microcanonical Monte Carlo simulation of thermodynamic properties", en, *The Journal of Chemical Physics*, vol. 109, no. 20, pp. 8816–8828, Nov. 1998, ISSN: 0021-9606, 1089-7690. DOI: 10.1063/1.477552 (cit. on p. 165).

[162] K. Hukushima, "Domain-wall free energy of spin-glass models: Numerical method and boundary conditions", en, *Phys. Rev. E*, vol. 60, no. 4, pp. 3606–3613, Oct. 1999, ISSN: 1063-651X, 1095-3787. DOI: 10.1103/PhysRevE.60.3606 (cit. on p. 168).

[163] I. Rozada, M. Aramon, J. Machta, and H. G. Katzgraber, "Effects of setting the temperatures in the parallel tempering Monte Carlo algorithm", en, *Phys. Rev. E*, vol. 100, no. 4, p. 043 311, Oct. 2019, ISSN: 2470-0045, 2470-0053. DOI: 10.1103/PhysRevE.100.043311 (cit. on p. 168).

[164] B. L. Holian and D. J. Evans, "Shear viscosities away from the melting line: A comparison of equilibrium and nonequilibrium molecular dynamics", en, *The Journal of Chemical Physics*, vol. 78, no. 8, pp. 5147–5150, Apr. 1983, ISSN: 0021-9606, 1089-7690. DOI: 10.1063/1.445384 (cit. on p. 170).

APPENDICES

A. Separable Form of Werner States

Hereafter, we show how Werner states (WS) can be expressed in the form (1.7), to reveal some of its alternative realizations as a mixture of pure states. Doing so, we retrieve the values of the probability weight at which it is separable, and further find the local partial transformations (3.15) optimizing (3.16).

A.1. Pauli Matrix Formulation

To develop our proof, we will need to express a number a pure state density matrices in terms of the Pauli matrices $\sigma_x, \sigma_y, \sigma_z$; in particular, we will use the products:

$$
\begin{aligned}
\sigma_x\sigma_x &= \begin{pmatrix} 0 & 1 \\ 1 & 0 \end{pmatrix} \otimes \begin{pmatrix} 0 & 1 \\ 1 & 0 \end{pmatrix} = \begin{pmatrix} 0 & 0 & 0 & 1 \\ 0 & 0 & 1 & 0 \\ 0 & 1 & 0 & 0 \\ 1 & 0 & 0 & 0 \end{pmatrix} \\
\sigma_y\sigma_y &= \begin{pmatrix} 0 & -i \\ i & 0 \end{pmatrix} \otimes \begin{pmatrix} 0 & -i \\ i & 0 \end{pmatrix} = \begin{pmatrix} 0 & 0 & 0 & -1 \\ 0 & 0 & 1 & 0 \\ 0 & 1 & 0 & 0 \\ -1 & 0 & 0 & 0 \end{pmatrix} \\
\sigma_z\sigma_z &= \begin{pmatrix} 1 & 0 \\ 0 & -1 \end{pmatrix} \otimes \begin{pmatrix} 1 & 0 \\ 0 & -1 \end{pmatrix} = \begin{pmatrix} 1 & 0 & 0 & 0 \\ 0 & -1 & 0 & 0 \\ 0 & 0 & -1 & 0 \\ 0 & 0 & 0 & 1 \end{pmatrix}
\end{aligned}
\tag{A.1}
$$

Consider the Bell states

$$
\begin{aligned}
|\psi_\pm\rangle &= \frac{1}{\sqrt{2}}(|00\rangle \pm |11\rangle) \\
|\phi_\pm\rangle &= \frac{1}{\sqrt{2}}(|01\rangle \pm |10\rangle)
\end{aligned}
\tag{A.2}
$$

A. Separable Form of Werner States

The corresponding density operators can be written [45]:

$$|\psi_\pm\rangle\langle\psi_\pm| = \frac{1}{2}\begin{pmatrix} 1 & 0 & 0 & \pm1 \\ 0 & 0 & 0 & 0 \\ 0 & 0 & 0 & 0 \\ \pm1 & 0 & 0 & 1 \end{pmatrix} = \frac{1}{4}(\mathbb{I}_4 \pm \sigma_x\sigma_x \mp \sigma_y\sigma_y + \sigma_z\sigma_z)$$

$$|\phi_\pm\rangle\langle\phi_\pm| = \frac{1}{2}\begin{pmatrix} 0 & 0 & 0 & 0 \\ 0 & 1 & \pm1 & 0 \\ 0 & \pm1 & 1 & 0 \\ 0 & 0 & 0 & 0 \end{pmatrix} = \frac{1}{4}(\mathbb{I}_4 \pm \sigma_x\sigma_x \pm \sigma_y\sigma_y - \sigma_z\sigma_z)$$

(A.3)

Finally, notice that

$$(|\boldsymbol{n}\rangle\langle\boldsymbol{n}|) \otimes (|-\boldsymbol{n}\rangle\langle-\boldsymbol{n}|) + (|-\boldsymbol{n}\rangle\langle-\boldsymbol{n}|) \otimes (|\boldsymbol{n}\rangle\langle\boldsymbol{n}|) = \frac{\mathbb{I}+\sigma_n}{2} \otimes \frac{\mathbb{I}-\sigma_n}{2} + \frac{\mathbb{I}-\sigma_n}{2} \otimes \frac{\mathbb{I}+\sigma_n}{2}$$

$$= \frac{\mathbb{I}\otimes\mathbb{I}-}{2}$$

$$(|\boldsymbol{n}\rangle\langle\boldsymbol{n}|) \otimes (|\boldsymbol{n}\rangle\langle\boldsymbol{n}|) + (|-\boldsymbol{n}\rangle\langle-\boldsymbol{n}|) \otimes (|-\boldsymbol{n}\rangle\langle-\boldsymbol{n}|) = \frac{\mathbb{I}+\sigma_n}{2} \otimes \frac{\mathbb{I}+\sigma_n}{2} + \frac{\mathbb{I}-\sigma_n}{2} \otimes \frac{\mathbb{I}-\sigma_n}{2}$$

$$= \frac{\mathbb{I}\otimes\mathbb{I}+}{2}$$

(A.4)

where $\sigma_n := \boldsymbol{n}\cdot\boldsymbol{\sigma}$ and the kets $|\pm\boldsymbol{n}\rangle$ represent opposite single qubits along the axis $\boldsymbol{n}$ of the Bloch sphere; in particular:

$$|+-\rangle\langle+-| + |-+\rangle\langle-+| = \frac{\mathbb{I}\otimes\mathbb{I} - \sigma_x\sigma_x}{2}$$

$$|y_+y_-\rangle\langle y_+y_-| + |y_-y_+\rangle\langle y_-y_+| = \frac{\mathbb{I}\otimes\mathbb{I} - \sigma_y\sigma_y}{2}$$

$$|01\rangle\langle01| + |10\rangle\langle10| = \frac{\mathbb{I}\otimes\mathbb{I} - \sigma_z\sigma_z}{2},$$

$$|++\rangle\langle++| + |--\rangle\langle--| = \frac{\mathbb{I}\otimes\mathbb{I} + \sigma_x\sigma_x}{2}$$

$$|y_+y_+\rangle\langle y_+y_+| + |y_-y_-\rangle\langle y_-y_-| = \frac{\mathbb{I}\otimes\mathbb{I} + \sigma_y\sigma_y}{2}$$

$$|00\rangle\langle00| + |11\rangle\langle11| = \frac{\mathbb{I}\otimes\mathbb{I} + \sigma_z\sigma_z}{2}$$

(A.5)

A.2. Separable form

Now consider the Werner state

$$
\begin{aligned}
\rho_W &= \frac{4p}{3}\frac{\mathbb{I}_4}{4} + (1 - \frac{4p}{3})\,|\phi_-\rangle\langle\phi_-| \\
&= \frac{4p}{3}\frac{\mathbb{I}_4}{4} + (1 - \frac{4p}{3})\frac{\mathbb{I}_4 - \sigma_x\sigma_x - \sigma_y\sigma_y - \sigma_z\sigma_z}{4} \\
&= \frac{\mathbb{I}_4}{4}\left(\frac{4p}{3} - 2(1 - \frac{4p}{3})\right) + (1 - \frac{4p}{3})\left(\frac{\mathbb{I}_4 - \sigma_x\sigma_x}{4} + \frac{\mathbb{I}_4 - \sigma_y\sigma_y}{4} + \frac{\mathbb{I}_4 - \sigma_z\sigma_z}{4}\right) \\
&= (4p - 2)\frac{\mathbb{I}_4}{4} + (1 - \frac{4p}{3})\frac{1}{2}\left(\,|+-\rangle\langle+-| + |-+\rangle\langle-+| + |y_+y_-\rangle\langle y_+y_-| + |y_-y_+\rangle\langle y_-y_+|\right. \\
&\qquad \left. + |01\rangle\langle01| + |10\rangle\langle10|\,\right) \\
&= (4p - 2)\frac{\mathbb{I}_4}{4} + \frac{3 - 4p}{6}\left(\,|+-\rangle\langle+-| + |-+\rangle\langle-+| + |y_+y_-\rangle\langle y_+y_-| + |y_-y_+\rangle\langle y_-y_+|\right. \\
&\qquad \left. + |01\rangle\langle01| + |10\rangle\langle10|\,\right)
\end{aligned}
$$

$$(A.6)$$

The last line is a decomposition of ρ_W in terms of separable pure state. This decomposition corresponds to a physical realization if and only if $p \geq 1/2$ and $p \leq 3/4$. It results that $\rho_W(p)$ is separable $\forall p \in [\frac{1}{2}, \frac{3}{4}]$.

We can also write

$$
\begin{aligned}
\rho_W =&\, \frac{4p}{3}\frac{\mathbb{I}_4}{4} + (1 - \frac{4p}{3})\,|\phi_-\rangle\,\langle\phi_-| \\
=&\, \frac{p}{3}\,|\psi_+\rangle\,\langle\psi_+| + \frac{p}{3}\,|\psi_-\rangle\,\langle\psi_-| + \frac{p}{3}\,|\phi_+\rangle\,\langle\phi_+| + (1-p)\,|\phi_-\rangle\,\langle\phi_-| \\
=&\, \frac{p}{3}\Big(\frac{1}{4}(\mathbb{I}_4 + \sigma_x\sigma_x - \sigma_y\sigma_y + \sigma_z\sigma_z) + \frac{1}{4}(\mathbb{I}_4 - \sigma_x\sigma_x + \sigma_y\sigma_y + \sigma_z\sigma_z) \\
& + \frac{1}{4}(\mathbb{I}_4 + \sigma_x\sigma_x + \sigma_y\sigma_y - \sigma_z\sigma_z)\Big) + (1-p)\frac{1}{4}(\mathbb{I}_4 - \sigma_x\sigma_x - \sigma_y\sigma_y - \sigma_z\sigma_z) \\
=&\, \frac{1}{4}\Big(\mathbb{I}_4 + \frac{p}{3}(\sigma_x\sigma_x + \sigma_y\sigma_y + \sigma_z\sigma_z) + (1-p)(-\sigma_x\sigma_x - \sigma_y\sigma_y - \sigma_z\sigma_z)\Big) \\
=&\, \frac{1}{4}\Big(\mathbb{I}_4 + (\frac{4p}{3} - 1)(\sigma_x\sigma_x + \sigma_y\sigma_y + \sigma_z\sigma_z)\Big) \\
=&\, \frac{1}{4}\Big(\mathbb{I}_4\big(1 - 3(\frac{4p}{3} - 1)\big) + (\frac{4p}{3} - 1)\big((\mathbb{I}_4 + \sigma_x\sigma_x) + (\mathbb{I}_4 + \sigma_y\sigma_y) + (\mathbb{I}_4 + \sigma_z\sigma_z)\big)\Big) \\
=&\, 4(1-p)\frac{\mathbb{I}_4}{4} + (\frac{2p}{3} - \frac{1}{2})\Big(\frac{\mathbb{I}_4 + \sigma_x\sigma_x}{2} + \frac{\mathbb{I}_4 + \sigma_y\sigma_y}{2} + \frac{\mathbb{I}_4 + \sigma_z\sigma_z}{2}\Big) \\
=&\, 4(1-p)\frac{\mathbb{I}_4}{4} + \frac{4p-3}{6}\Big(|{+}{+}\rangle\,\langle{+}{+}| + |{-}{-}\rangle\,\langle{-}{-}| + |y_+ y_+\rangle\,\langle y_+ y_+| + |y_- y_-\rangle\,\langle y_- y_-| \\
& + |00\rangle\,\langle00| + |11\rangle\,\langle11|\Big)
\end{aligned}
\tag{A.7}
$$

This last decomposition corresponds to a physical realization if and only if $p \geq 3/4$. It results that $\rho_W(p)$ is also separable in this region.

Hence, $\rho_W(p)$ is separable for $p \geq 1/2$.

A.3. Regularization

One can see from (A.6) and (A.7) that the separable forms of the Werner state are not, in general, classical: their substates are not orthogonal. Hence, from Definition 2, it is clear that a measure of quantum correlations like the QCD would give non-zero values even in the separable region. One hence needs to apply the regularization procedure (3.15). Consider the regularized Werner state:

$$
\begin{aligned}
\tilde{\rho}_W &= p\Big(\frac{1}{3}U_1\,|\psi_+\rangle\,\langle\psi_+|\,U_1^\dagger + \frac{1}{3}U_2\,|\psi_-\rangle\,\langle\psi_-|\,U_2^\dagger + \frac{1}{3}U_3\,|\phi_+\rangle\,\langle\phi_+|\,U_3^\dagger\Big) + (1-p)\,|\phi_-\rangle\,\langle\phi_-| \\
&= p\rho_U^{BD} + (1-p)\,|\phi_-\rangle\,\langle\phi_-|,
\end{aligned}
\tag{A.8}
$$

where ρ_U^{BD} is the regularization of a Bell-diagonal (BD) state (i.e. a mixture of Bell states). We refer the reader to [45, 69, 70] for definition of the BD states and the convention linking the coefficients c_i and the spectrum of these states.

A. Separable Form of Werner States

The Werner state is invariant with respect with qubit permutations; the operators U_j realizing the minimization of E are hence joint identical local unitaries, i.e. of the form $U_j = U_j^A(\boldsymbol{n}, \theta) \otimes U_j^B(\boldsymbol{n}, \theta)$. Such unitaries send the original BD state of the above equation to any other BD state. We hence can write

$$\widetilde{\rho}_W = p\frac{1}{4}\Big(\mathbb{I} + c_x\sigma_x\sigma_x + c_y\sigma_y\sigma_y + c_z\sigma_z\sigma_z\Big) + (1-p)\frac{1}{4}\Big(\mathbb{I} - \sigma_x\sigma_x - \sigma_y\sigma_y - \sigma_z\sigma_z\Big)$$
$$= \frac{1}{4}\Big(\mathbb{I} + (p(c_x+1)-1)\sigma_x\sigma_x + (p(c_y+1)-1)\sigma_y\sigma_y + (p(c_z+1)-1)\sigma_z\sigma_z\Big) \tag{A.9}$$

The regularization procedure can now be performed by tuning the c_i's; one possible choice is to set, for some i, $p(c_i+1)-1 = -1$ and $\forall j \neq i$, $p(c_j+1)-1 = 0$, so that

$$\widetilde{\rho}_W = \frac{1}{4}\Big(\mathbb{I} - \sigma_i\sigma_i\Big), \tag{A.10}$$

which is classical. We hence have $c_i = -1$ and $c_{j\neq i} = \frac{1}{p}-1$. Arbitrarily setting $i = z$, we now consider the eigenvalues of a Bell-diagonal state; they can be expressed in terms of the coefficients c_i, using the formula $\lambda_{ab} = \frac{1}{4}\Big(1 + (-1)^a c_x - (-1)^{a+b}c_y + (-1)^b c_z\Big)$. In our case, we get

$$\lambda_{00} = \lambda_{10} = 0$$
$$\lambda_{01} = \frac{1}{2p} \tag{A.11}$$
$$\lambda_{11} = 1 - \frac{1}{2p}$$

which corresponds to a physical BD state (so is realizable by ρ_U^{BD}) if and only if $p \geq \frac{1}{2}$. In this range of p, it is hence possible to regularize ρ_W towards a fully classical state, of null QC measure.

B. Supplementary Figures of Bicluster

Below are shown the dynamics of $\boldsymbol{M}$ in Cartesian coordinates, along with the corresponding distributions $\mathcal{P}(\phi)$, from different simulations. The histograms are derived from samples of values retrieved in the time interval $t \in [10000, 11000]$, while the dynamics are bounded by the time interval $t \in [10000, 10100]$. We used the time step $\Delta t = 0.05$.

The upper figures display the dynamics directly retrieved from simulations, while the lower ones show the same views of a vector $\boldsymbol{v}$ defined using Eq. (6.9). The frequencies $\omega_\pm$ are drawn from measurements of M_2, $v_\pm = \max(M_{x,y})$ (with $\boldsymbol{M}$ rotated of $-\phi_2/2$), and we finally rotate $\boldsymbol{v}$ of $\phi_2/2$, as suggested by Eq. (6.8).

Visibly, the discrepancy between the real dynamics and our analytical formula is higher for less well-formed biclusters. This is due to the fact that, as mentioned is Section 6.4, in this regime, the amplitudes $M_\pm$ are fluctuating, whereas our parameters $v_\pm$ are constant.
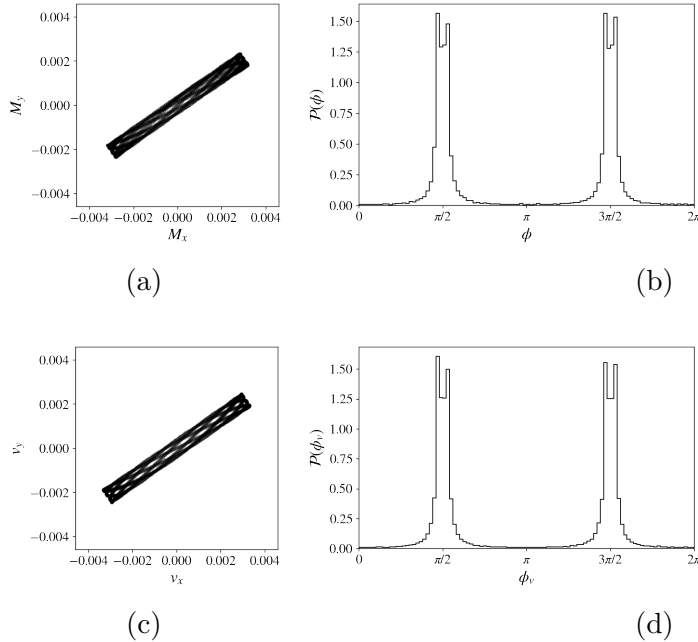

Figure B.1.: $\gamma_0 = 1$, $M_2 = 0.51$, $\Delta = -0.98$, long-time behaviour shown in Fig. 6.3b
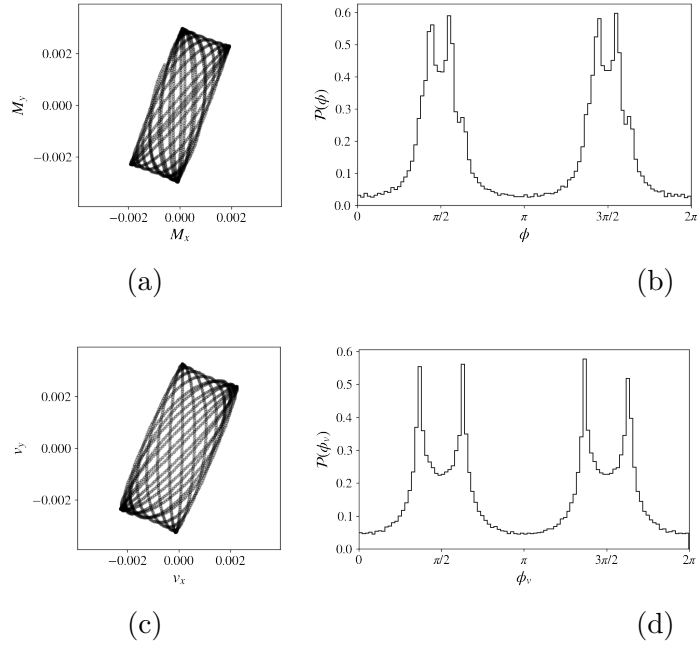
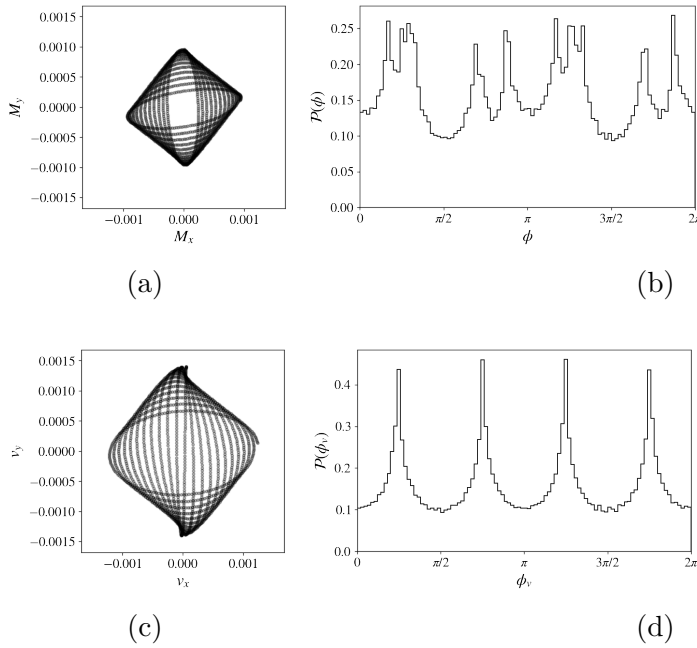Figure B.2.: $\gamma_0 = 0.46$, $M_2 = 0.06$, $\Delta = -0.94$, long-time behaviour shown in Fig. 6.3c

Figure B.3.: $\gamma_0 = 0.05$, $M_2 = 0.03$, $\Delta = -0.11$, long-time behaviour shown in Fig. 6.3d

C. Monte Carlo method

Simulating glass formers is a notoriously complex task. The main reason is that, in the glass phase, these systems exhibit a large number of energy minima, and tend to remain trapped in the surrounding potential wells. Therefore, gathering a representative set of data points, i.e performing an importance sampling of the energy surface, requires the use of numerous tricks and techniques.

The simulation scheme we developed belong to the class of Monte Carlo algorithm, which are among the most commonly employed in simulations of systems at equilibrium. In principle, Monte Carlo algorithms are ergodic: relying on random displacements of the system rather than to its exact dynamics, they do not get stuck as easily in potential wells and thus sample state space much more effectively.

Also, in contrast with molecular dynamics simulations, Monte Carlo algorithms do not require the integration of the equations of motion at each time step, but a mere update of the energy, which yields a considerable computational speedup.

C.1. Quick introduction to Monte Carlo algorithms

Monte Carlo algorithms form a class of numerical methods based on stochastic procedures. The principle is to exploit the probabilistic properties of a mathematical or physical object, in order to achieve calculations with precision strongly linked to the number of iterations; this is, of course, due to the law of large numbers, insuring that the outcome would converge to the exact result with the number of iterations.

One should note that Monte Carlo methods can be applied as well to systems of a stochastic nature as to totally deterministic systems, or to find mathematical constants.

It is very much adapted to the study of random systems as statistical physics models, since they come with well-defined probabilistic features.

Simulations of N-body systems are best achieve with Markov Chain Monte Carlo methods (MCMC), through thermalization. Namely, in a MCMC, the system evolves from state to state with some transition probability that is determined by statistical constraints, converging to the equilibrium distribution.

The following introduction to Monte Carlo methods is mainly drawn from the excellent manual [159].

The canonical ensemble average $\langle O \rangle_{can}$ of an observable O can be computed

analytically by integration over the whole state-space Σ, weighted by the Boltzmann distribution: $p(\mathbf{\Gamma}) = \frac{e^{-\beta E(\mathbf{\Gamma})}}{Z(\beta)}$, with $\mathbf{\Gamma} = \{\boldsymbol{q}_i\}_i$ the instantaneous configuration of the system (i.e. a *microstate*), $\boldsymbol{q}_i$ being the 3-dimensional position vector of the ith particle, and $Z(\beta) = \int_\Sigma d\mathbf{\Gamma} e^{-\beta E(\mathbf{\Gamma})}$ is the partition function. In practice, the latter is for some systems impossible to compute analytically, and very hard to compute numerically in a reasonable time (except for systems of a very small size). The goal of an MCMC algorithm is to allow the computation of $\langle O \rangle$ without any knowledge of Z; namely, instead of integrating over Σ, we sum up measurement of O taken on a discrete sample $\sigma \subset \Sigma$. Provided that the sample σ is representative enough of Σ, the average thus obtained converges to the canonical one $\langle O \rangle_{can}$.

In order to do this without directly computing the equilibrium distribution $p(x)$, we consider the *detailed balance condition*, necessary and sufficient condition for a Markov process to converge to $p(x)$:

$$p(\mathbf{\Gamma}_\mu)P(\mathbf{\Gamma}_\mu \longrightarrow \mathbf{\Gamma}_\nu) = p(\mathbf{\Gamma}_\nu)P(\mathbf{\Gamma}_\nu \longrightarrow \mathbf{\Gamma}_\mu), \tag{C.1}$$

where $\mathbf{\Gamma}_\mu$ and $\mathbf{\Gamma}_\nu$ denote two distinct microstates.

Now, as the following will make clearer, it is often meaningful to decompose the transition probability P into a selection probability g and an *acceptance rate A*, namely $P(\mathbf{\Gamma}_\mu \to \mathbf{\Gamma}_\nu) = A(\mathbf{\Gamma}_\mu \to \mathbf{\Gamma}_\nu)g(\mathbf{\Gamma}_\mu \to \mathbf{\Gamma}_\nu)$. The acceptance rate represents, once the spin has been chosen, the probability that the algorithm accepts the transition and actually update the state.

For our purpose, and as it is often the case, the selection probability is taken to be a constant (no given state is more likely to be selected than another).

From Eq. (C.1) we obtain

$$\frac{A(\mathbf{\Gamma}_\mu \to \mathbf{\Gamma}_\nu)g(\mathbf{\Gamma}_\mu \to \mathbf{\Gamma}_\nu)}{A(\mathbf{\Gamma}_\nu \to \mathbf{\Gamma}_\mu)g(\mathbf{\Gamma}_\nu \to \mathbf{\Gamma}_\mu)} = \frac{A(\mathbf{\Gamma}_\mu \to \mathbf{\Gamma}_\nu)}{A(\mathbf{\Gamma}_\nu \to \mathbf{\Gamma}_\mu)} = \frac{p(\mathbf{\Gamma}_\nu)}{p(\mathbf{\Gamma}_\mu)}. \tag{C.2}$$

Any Markov chain satisfying this condition, provided that ergodicity is insured (in practice, this just means that every state must be accessible), converges to the equilibrium distribution.

In the above formula, it is already clear that the partition function Z, entering in the definition of $p(\mathbf{\Gamma})$, cancels out as desired.

This leaves us with a great freedom in the construction of an algorithm. One should always exploit this freedom to make the algorithm the most efficient possible, by which we mean that the system should evolve as fast as possible, and avoid wasting computation time because of too rare transitions. To this end, the optimal choice is to set the largest of the two acceptance rates to 1 (the maximal possible value), and deduce the smallest accordingly. That choice can be expressed through

the formula

$$A(\mathbf{\Gamma}_\mu \to \mathbf{\Gamma}_\nu) = \min\left\{1, \frac{p(\mathbf{\Gamma}_\mu)}{p(\mathbf{\Gamma}_\nu)}\right\} \tag{C.3}$$

For instance, in the case of a Boltzmann equilibrium distribution, we have $p(\mathbf{\Gamma}_\mu) = e^{-\beta\phi_\mu}/Z$, where β is the inverse temperature and we abbreviated $\phi(\mathbf{\Gamma}_\mu) := \phi_\mu$ the potential energy of the system in the microstate $\mathbf{\Gamma}_\mu$. The optimal choice for the acceptance rate is therefore

$$p(\mu \to \nu) = \min\left\{1, e^{-\beta(\phi_\nu - \phi_\mu)}\right\} \tag{C.4}$$

Remark that, as is made clear by the above equation, canonical Monte Carlo algorithms use β as the control parameter. Even if the system possesses a kinetic energy $K = \sum_i p_i^2/2$, the momenta p_i are hence usually not considered in the algorithm, as implied by the kinetic definition of the temperature $T = 3NK/2$.

C.2. Microcanonical Monte Carlo

Yet the microcanonical case is sensibly less common in the literature, and somewhat less straightforward in its implementation. This is due to the fact that, in such a framework, the system is strictly constrained to a surface of constant energy, hence evolves in a subspace of null measure in Σ.

A possible workaround is to exploit independence of momenta and position, namely the separability of the partition function. As, at equilibrium, momenta are known to trivially follow the Boltzmann distribution, it is not necessary to implement random momentum changes at each step of the algorithm. Not investigating these degrees of freedom leaves the kinetic energy available as a free parameter, that we can use to maintain the total energy of the system at the desired value, by compensating the energy change coming from the change in configuration.

The microcanonical probability density for a given microstate μ at energy E is given by [148, 160, 161]

$$p_E(\mu) \propto \Theta\left(E - \phi_\mu\right)\left[E - \phi_\mu\right]^{(3N/2-1)}. \tag{C.5}$$

Let us now consider a transition $\mu \to \nu$. For any physically relevant initial state, we must have $E \geq \phi_\mu$, hence $\Theta\left(E - \phi_\mu\right) = 1$. Eq. (C.3) becomes

$$A(\mu \to \nu) = \min\left\{1, \Theta\left(E - \phi_\nu\right)\left[\frac{E - \phi_\nu}{E - \phi_\mu}\right]^{(3N/2-1)}\right\} \tag{C.6}$$

C.3. Particle exchange and parallel tempering

As stated before, simulating the vitreous phase raises great challenges, as the system tends to be stuck in potential wells for extensive amounts of time, preventing us from efficiently sampling the configuration space Σ.

Overcoming this difficulty requires to fully take advantage of the Monte Carlo framework, which allows us to perform updates of the system that do not follow the conventional dynamics, provided that detailed balance is fulfilled. In fact, the power of MCMC comes from the fact that any kind of move is allowed in principle, and that the validity of the results is guaranteed by the sole choice of acceptance rate.

A first method that we put in place to overcome the problem of potential barriers is the particle swapping move, first proposed in [151]. At each MC step, with a probability that we (arbitrarily) set to $p = 0.1$, one particle of each species is chosen at random, both their positions are swapped and displaced according to the usual random displacement rule; with probability $(1 - p)$, a conventional MC step is performed. Afterwards, the move is accepted according to the usual acceptance rate (C.6)."

Another well-known and very elegant workaround is the method coined as *parallel tempering* (PT), or sometimes *replica exchange*. We thereafter use the term PT, to stick with the conventional terminology, even if it is somehow misleading, given that the control parameter of our simulations is energy rather than temperature.

Using multiprocessing, we simulate M instances of the system (the so-called replicas) in parallel, each at a different energy $E_0 < E_1 < \ldots < E_{M-2} < E_{M-1}$. Above the transition, the system does not exhibit these potential wells, and is hence much less constrained, rapidly exploring a variety of regions of Σ. The main idea of PT is to exploit that fact by periodically attempt to exchange replicas of neighbouring energies E_i, E_{i+1}, with an acceptance rate satisfying Eq. (C.2), insuring convergence to the equilibrium distribution. Doing so, the low energy replica can effectively jump out of potential wells, allowing a more thorough sampling.[1]

The probability of a microstate being a function of its associated potential energy, it is clear that the average acceptance rate for the exchanges of two given replicas depends on the overlap of their potential energy distributions $p_E(U)$. It results that, the closer are the energies of the two replicas, the more likely in average are their exchanges. In this context, the number M of replicas is thus a parameter of critical importance. Furthermore, as we increase the system size N, the distributions $p_E(U)$ become narrower, and an efficient algorithm would hence need neighbouring energies to be even closer to one another, and M to be larger.

---

[1]The experimental equivalent of this technique is to simply melt and vitrify the sample many times, performing the measurements of interest at each cycle. Doing so, one is able to capture a great variety of configurations allowed in the vitreous phase.

It is straightforward to apply the same reasoning, relying on the detailed balance condition (C.1), as in the previous section, to compute the acceptance rate of the exchanges.

Consider an initial state where a replica i of energy E_i is in the configuration μ, and a replica $i+1$ of energy E_{i+1} is in the configuration ν. As before, assuming this initial state physically relevant, we have $E_i > \phi_\mu$ and $E_{i+1} > E_\nu$; since $E_{i+1} > E_i$, this also implies $E_{i+1} > \phi_\mu$. This remark will conveniently allow us to discard three Heaviside functions among four.

We denote $A_{i,i+1}(\phi_\mu, \phi_\nu \to \phi_\nu, \phi_\mu)$ the acceptance rate for the exchange of the configurations of these two replicas. The probabilities $p(\mu)$ in Eq. (C.1), (C.2) and (C.3) should now be replaced by joint probabilities for the replica i to be in the microstate ϕ_μ and the replica $i+1$ to be in the microstate ϕ_ν, namely: $p_{i,i+1}(\phi_\mu, \phi_\nu) = p_i(\phi_\mu) p_{i+1}(\phi_\nu)$.

Eq. (C.3) then becomes

$$
\begin{aligned}
A_{i,i+1}(\phi_\mu, \phi_\nu \to \phi_\nu, \phi_\mu) &= \min\left\{1, \frac{p_i(\mu) p_{i+1}(\nu)}{p_i(\nu) p_{i+1}(\mu)}\right\} \\
&= \min\left\{1, \Theta\left(E_i - \phi_\nu\right) \left[\frac{(E_i - \phi_\nu)(E_{i+1} - \phi_\mu)}{(E_i - \phi_\mu)(E_{i+1} - \phi_\nu)}\right]^{(3N/2-1)}\right\}
\end{aligned}
$$
$$(C.7)$$

The latter expression is scales exponentially with the system size N. Thus, even if the system sizes are very far from the Avogadro number, the behaviour of this acceptance rate in the thermodynamic limit is quite relevant to our understanding of the performance of our PT scheme. It simply writes

$$
\begin{aligned}
\lim_{N\to\infty} A_{i,i+1}(\phi_\mu, \phi_\nu \to \phi_\nu, \phi_\mu) &= \Theta\left(E_i - \phi_\nu\right) \Theta\left((E_i - \phi_\nu)(E_{i+1} - \phi_\mu) - (E_i - \phi_\mu)(E_{i+1} - \phi_\nu)\right) \\
&= \Theta\left(E_i - \phi_\nu\right) \Theta\left(-E_i\phi_\mu - \phi_\nu E_{i+1} + E_i\phi_\nu + \phi_\mu E_{i+1})\right) \\
&= \Theta\left(E_i - \phi_\nu\right) \Theta\left((E_{i+1} - E_i)(\phi_\mu - \phi_\nu)\right) \\
&= \Theta\left(E_i - \phi_\nu\right) \Theta\left(\phi_\mu - \phi_\nu\right) \\
&= \Theta\left(\phi_\mu - \phi_\nu\right),
\end{aligned}
$$
$$(C.8)$$

where we used the fact that $E_{i+1} - E_i > 0$, and that $E_i > \phi_\mu$ hence $\phi_\mu > \phi_\nu$ implies $E_i > \phi_\nu$.

C.4. Choice of energy arrays

As stated before, the choice of an array of energies $\{E_i\}_{i=0,\dots,M-1}$ is of great importance, as it should roughly optimize the replica exchange rate, within the limitation of the accessible number of processors (CPU). Note that this choice only affects

efficiency, as the convergence of the Monte Carlo algorithm toward equilibrium distributions is already insured by our choices of acceptance rates satisfying the detailed balance condition (C.2).

In a first simulation, with a system of relatively modest size (i.e. $N = 216$) we found that it was a good enough choice of an energy array to simply define a power law:

$$E_i = E_{min} \left(\frac{E_{max}}{E_{min}} \right)^{\frac{i}{M-1}}, \qquad (C.9)$$

with $i = 0, \dots, M - 1$.

Yet, as soon as we start tackling a larger system (i.e. $N = 512$), the replica exchange rate becomes much lower. The first, obvious solution we set up was to simulate a larger array of energies, namely 2×60 different energies: as the work station we were working on only has 64 CPUs, we simulate 60 energies, then 60 others, before attempting the replica exchanges. Yet we found that this wasn't enough, as some energies behaved as bottlenecks, through which replicas couldn't diffuse efficiently enough.

We hence resorted to a simple algorithm, described in Refs. [162, 163], in the context of canonical ensemble simulations; the adaptation to the microcanonical case is however straightforward. Given two fixed extremal energies E_0, E_M and the number M of replicas we wish to simulate, it consists in finding the $M - 2$ intermediate energies such that the exchange rate between adjacent replicas is uniform. In other words, we look convergence towards the fixed point

$$\langle A_{i,i+1} \rangle = \langle A_{i,i-1} \rangle, \ \forall i = 0, \dots, M. \qquad (C.10)$$

In principle, the closest we are to these fixed point (C.10), the more efficient is the replica exchange algorithm in average.

Remark that, in contrast with Refs. [162, 163], we require equality of the average acceptance rates rather than the equality of the acceptance rates, given the average potential energy. This change is in fact necessary because we have in general $\langle \phi \rangle (E_i) < \langle \phi \rangle (E_i + 1)$; yet, considering Eq. (C.8), it is clear that using average potential energies will lead to vanishing or very small acceptance rates.

To get around this issue, we simply take into account the overlap of potential energy distributions instead of the mere average, that is

$$\langle A_{i,i+1} \rangle = \int_{-\infty}^{E_{i+1}} d\phi' \int_{-\infty}^{E_i} d\phi \, p_{E_i} (\phi) \, p_{E_{i+1}} (\phi') \, A_{i,i+1} (\phi, \phi' \to \phi', \phi). \qquad (C.11)$$

We further use the approximation (C.8), which greatly accelerate the algorithm, as it avoids many exponentiation and reduces the interval on which the above

integral in computed. We end up with

$$
\begin{aligned}
\langle A_{i,i+1} \rangle &\approx \int_{-\infty}^{E_{i+1}} d\phi' \int_{-\infty}^{E_i} d\phi \, p_{E_i}(\phi) \, p_{E_{i+1}}(\phi') \, \Theta(\phi - \phi') \\
&= \int_{-\infty}^{E_{i+1}} d\phi' \int_{\phi'}^{E_i} d\phi \, p_{E_i}(\phi) \, p_{E_{i+1}}(\phi') .
\end{aligned}
\tag{C.12}
$$

We set an initial array of energies using Eq.(C.9), and run Monte Carlo simulations until we obtain a reasonable energy-temperature dependence. We then compute and interpolate the average $\mu_\phi(E)$ and standard deviation $\sigma_\phi(E)$ of ϕ as functions of E, so that we are able to estimate the corresponding Gaussian probability distributions $p_E(\phi)$ for any E. The integrals (C.12) are computed numerically, using a discrete set of 10^3 potential energies in the range $\mu_\phi(E_i) - 2\sigma_\phi(E_i) \leq \phi \leq \mu_\phi(E_{i+1}) + 2\sigma_\phi(E_{i+1})$.

Algorithm 1: E-range optimization through U-overlap method

Data: Initialize $\{E_i\}_{i=0,\ldots,M-1}$;
Interpolate $\mu_\phi(E)$ from data;
Interpolate $\sigma_\phi(E)$ from data;
Set the number of iterations n_{max} ;
Initialize the number of repeats $n = 1$;
repeat
    for $i_0 = 0, 1$ **do**
        $i \leftarrow i_0$;
        while $i < M$ **do**
            $f(E_i) \leftarrow \langle A_{i,i+1} \rangle (E_i) - \langle A_{i-1,i} \rangle (E_i)$;
            $E_i \leftarrow (E_i + f^{-1}(0))/2$;
            $i \leftarrow i + 1$;
        end
    end
until $n = n_{max}$;

C.5. Initial configuration, periodic boundary conditions and cutoff

The system is simulated in a cubic box of volume L^3.

As we are working in the microcanonical ensemble, our control parameter is the internal energy $E = K + \Phi$. We tune it by an appropriate choice of initial configuration, which determines the value of the potential energy Φ, and the subsequent setting of a positive value for the kinetic energy K.

C. Monte Carlo method

The system we investigate is governed by the continuous potential (7.1), depending on negative powers of the interatomic distances r_{ij} and repulsive at short range. When some r_{ij} become to small, the energy thus diverges. Since our simulations are performed at high density ($\rho > 1$), totally random initial configurations typically result in very high energies, which cannot be corrected by the choice of K, since the latter is a positive quantity.

To get around this issue and have a sufficient control over the initial ϕ, we were thus obligated to implement initial conditions with a high degree of symmetry.

Namely, we initially arranged the particles in a cubic lattice configuration, where each particle's first neighbours are of the other species. Then we randomly replaced particles of species 1 by particles of species 2, until we reach the desired species ratio.

To avoid undesired boundary effects, we implemented, as is it customary, periodic boundary conditions (PBC). Namely, $\forall i, j = 1, \ldots, N$, the interatomic distance along an axis $\gamma = x, y, z$ is redefined as

$$\Delta \gamma_{ij} = \begin{cases} (\gamma_i - \gamma_j) & \text{if } -L/2 \leq (\gamma_i - \gamma_j) \leq L/2. \\ (\gamma_i - \gamma_j) + L & \text{if } (\gamma_i - \gamma_j) < -L/2. \\ (\gamma_i - \gamma_j) - L & \text{if } (\gamma_i - \gamma_j) > L/2. \end{cases} \tag{C.13}$$

Remark that the PBC entails a periodic pattern in the particles' spatial distribution.

Smooth cutoffs must therefore be implemented, not only for performance purposes, but also to avoid this unwanted symmetry introduced by the PBC. Since we aim at computing quantities derived from both the gradient and the Hessian of $\phi(\mathbf{\Gamma})$, we accordingly need cutoffs that is continuous up to the second order.

The non-monotonic, interspecies potential of Eq. (7.1) is redefined as

$$\begin{cases} \phi_{12}(r) = 4\epsilon_{12} \left(\sigma_{12}^{12} r^{-12} - \sigma_{12}^6 r^{-6} \right) & , \ 0 < r \leq r_c^{(12)} \\ \phi_{12}(r) = C(r - r_m^{(12)})^4 + D(r - r_m^{(12)})^3 & , \ r_c^{(12)} < r \leq r_m^{(12)} \\ \phi_{12}(r) = 0 & , \ r_m^{(12)} < r, \end{cases} \tag{C.14}$$

On the other hand, the monotonic, intra-species potentials are redefined as

$$\begin{cases} \phi_{\alpha\alpha}(r) = 4\epsilon_{\alpha\alpha} \sigma_{\alpha\alpha}^{12} r^{-12} + A_\alpha & , \ 0 < r \leq r_c^{(\alpha\alpha)} \\ \phi_{\alpha\alpha}(r) = B_\alpha (r - r_m^{(\alpha\alpha)})^3 & , \ r_c^{(\alpha\alpha)} < r \leq r_m \\ \phi_{\alpha\alpha}(r) = 0 & , \ r_m^{(\alpha\alpha)} < r, \end{cases} \tag{C.15}$$

where $\alpha = 1, 2$.

Following [164], we set $r_c^{(12)} = \left(\dfrac{7}{26} \right)^{1/6} \sigma_{12}$, i.e. the distance such that $\phi_{12}''(r_c^{(12)}) = 0$. Though this condition becomes meaningless for the monotonic potentials, we

also, arbitrarily, chose $r_c^{(\alpha\alpha)} = \left(\dfrac{7}{26}\right)^{1/6} \sigma_{\alpha\alpha}$.

From there, requiring the continuity, up to the second derivative, of these potential functions at the first cutoff distance r_c, straightforwardly implies the values of the other constants of Eqs. (C.14) and (C.15).